



**PROCEEDINGS OF THE 24TH
INTERNATIONAL APPLIED GEOCHEMISTRY SYMPOSIUM
FREDERICTON, NEW BRUNSWICK, CANADA**



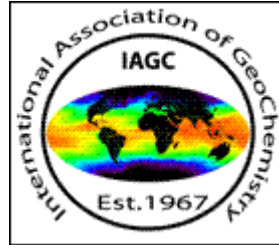
JUNE 1ST-4TH, 2009

EDITED BY

DAVID R. LENTZ, KATHLEEN G. THORNE, & KRISTY-LEE BEAL



VOLUME I



All rights reserved.
This publication may not be reproduced in whole or in part, stored in a retrieval system or transmitted in any form or by any means without permission from the publisher.

ISBN 978-1-55131-136-4

©2009 AAG

**PROCEEDINGS OF THE 24TH
INTERNATIONAL APPLIED GEOCHEMISTRY SYMPOSIUM
FREDERICTON, NEW BRUNSWICK
CANADA
JUNE 1ST-4TH, 2009**

EDITED BY

**DAVID R. LENTZ
KATHLEEN G. THORNE
KRISTY-LEE BEAL**

VOLUME I

Lithogeochemical halos and vectors for ores in volcanic arcs and sedimentary basins	59
<i>Ross R. Large</i>	59
Groundwaters in mineral exploration.....	63
<i>Matthew I. Leybourne¹ & Eion M. Cameron²</i>	63
Soluble ionic gold in soils.....	67
<i>Melvyn J. Lintern¹, Chris G. Ryan², & Robert M. Hough¹</i>	67
Gold in pedogenic carbonate revealed	71
<i>Melvyn J. Lintern^{1,2}, Chris G. Ryan³ & Robert M. Hough¹</i>	71
Till indicator mineral and geochemical signatures of magmatic Ni-Cu deposits, Thompson Nickel Belt, central Canada	75
<i>M.B. McClenaghan¹, S.A. Averill², I.M. Kjarsgaard³, D. Layton-Matthews⁴, & G. Matile⁵</i>	75
Lithogeochemical exploration vectors for Au-rich volcanogenic massive sulfide deposits: Examples from the world-class Doyon-Bousquet-LaRonde mining camp, Abitibi Greenstone Belt, Canada..	79
<i>Patrick Mercier-Langevin¹, Benoît Dubé¹, & Mark D. Hannington²</i>	79
Application of field-portable x-ray fluorescence spectrometers in mineral exploration, with examples from the Abitibi Greenstone Belt	83
<i>Jan M. Peter¹, Patrick Mercier-Langevin², & John B. Chapman¹</i>	83
Exploration for Zn-rich mineralisation in semi-arid environments: an example from the Cobar region, NSW, Australia.....	87
<i>Keith M. Scott¹ & Angela N. Lorrigan²,</i>	87
Soil micro-layer, airborne particles, and pH: the Govett connection	91
<i>Barry W. Smee</i>	91
Robust 'organic' geochemistry identifies and vectors to deeply buried exploration targets.....	97
<i>D. A. Sutherland¹</i>	97
ORE-FORMING SYSTEMS: A GEOCHEMICAL PERSPECTIVE	101
Siderophile elements in the zonal structure of ore geochemical systems: exploration aspects	103
<i>G. Abramson¹</i>	103
Cassiterite-sulfide mineralization revealed by dispersion flows in Belaya Sopka Mountain (northeastern Russia).....	107
<i>Anna D. Ananchenko^{†1} & Svetlana R. Tikhomirova^{†1}</i>	107
Geochemical characterization of humic substances isolated from phosphatic pellets and their surrounding matrix, Ras-Draâ, Tunisia	111
<i>Aida Ben Hassen¹, Jean Trichet¹, Jean-Robert Disnar¹, & Habib Belayouni²</i>	111
Petrogenesis of dykes related to Cu-Au & base-metal Au-Ag occurrences, Mt. Freegold area, Dawson Range, Yukon Territory, Canada	115
<i>Thierry Bineli Betsi¹ & David R. Lentz¹</i>	115
The primacy of magma compositions in determining the Re and W contents of molybdenite.....	119
<i>Phillip L. Blevin¹</i>	119
RE minerals in Esfordi apatite- magnetite deposit, Central Iran	123
<i>Mohammad Boomeri¹, Kazuo Nakashima², & David R. Lentz³</i>	123
Numerical simulation of the sill-driven convective ore-forming system at Matagami, Quebec: implications for metal leach zones	127
<i>Patrick M. Carr¹, Lawrence M. Cathles III², & C. Tucker Barrie³</i>	127

Minerals exploration and supply: a worldwide perspective	131
<i>William X. Chávez, Jr.</i>	131
Mineralogical host phases for the PGE in magmatic Ni-Cu-PGE deposits at the Creighton Mine, Sudbury, Canada	135
<i>Sarah A.S. Dare¹, Sarah-Jane Barnes¹, Hazel M. Prichard², & Peter C. Fisher²</i>	135
Late Mesoproterozoic S-type Sargipali granite and tungsten-mineralization: Singhbhum-Orissa craton, India	139
<i>Sangita Chowdhury¹, David R. Lentz², & Saumitra Misra³</i>	139
Bimodal post-collision volcano-plutonic complex in the southern rim of the eastern flank of the Mongol-Okhotsk orogenic belt	143
<i>I.M. Derbeko¹, V.A. Ponomarchuk², D.L. Vyunov³, & S.K. Kozyrev³</i>	143
Petrographic characterization of propylitic alteration associated with porphyry Cu–Mo deposits in the Collahuasi District, Northern Chile: implications for mineral exploration	147
<i>Merline Djouka-Fonkwé¹, Kurt Kyser¹, H. Alan Clark¹, J. Christopher Oates², & Christian Ihlenfeld²</i>	147
Petrologic, geochemical characteristics, and age of skarn-related granitoids at the Mactung Tungsten Deposit, Yukon, Canada.....	151
<i>Ayalew. L. Gebru¹ & David R. Lentz¹</i>	151
Use of micro-XRF in the characterization of hydrothermal alteration: application to the subaqueous felsic dome-flow complex of the Cap d’Ours segment of the Glenwood rhyolite, Rouyn-Noranda, Québec	157
<i>Dominique Genna^{1,2}, Damien Gaboury^{1,2}, Lyndsay Moore¹, & Wulf Mueller¹</i>	157
Regional rock geochemistry of the Leninogorsk and Zyryanovsk VMS region (Rudny Altay Kazakhstan) - implications for genesis and exploration.....	161
<i>I. Goldberg¹, G. Abramson¹, V. Los², V. Nazarov³, & C. Haslam⁴</i>	161
Geochemistry and tectonics as an exploration tool for Circum-Pacific porphyry copper, gold, and molybdenum deposits: evidence from the Baguio District, Philippines	165
<i>Pete Hollings¹ & David R. Cooke²</i>	165
Metals distribution and correlations in polymetallic veins from Pingüino Indium-bearing deposit, Deseado Massif, Patagonia, Argentina	169
<i>Sebastián Jovic^{1,2}, Paula Liñan¹, Diego Guido^{1,2}, Gerardo Páez^{1,2}, Remigio Ruiz¹, & Isidoro Schalamuk^{1,2}</i>	169
Chemical compositions of carbonate minerals from Chehelkureh ore deposit, Iran: implications for evolution of base-metal mineralization	173
<i>Mohammad Maanijou¹, David R. Lentz², & Iraj Rasa³</i>	173
Rare earth element variations in volcanogenic massive sulfides, Bathurst Mining Camp, New Brunswick: evidence from laser-ablation ICPMS analyses of phosphate accessory phases	177
<i>Sean H. McClenaghan¹, David R. Lentz², & Wilfredo G. Diegor³</i>	177
Controls and consequences of intrusion-related Au deposition at the Morila Au Mine, SW Mali .	181
<i>Christopher R.M. McFarlane¹, Karen Grey¹, & David Lentz¹</i>	181
Syenite, lamprophyre, and carbonatite dykes of the Moose Creek Valley, Ice River Alkaline Complex, southeastern British Columbia, Canada: implications for REE potential	185
<i>Thomas R. Mumford¹, Dave R. Lentz¹, & Cliff S.J. Shaw¹</i>	185

Morphology of gold nanoparticles synthesised from gold chloride and gold cyanide complexes under evaporative conditions	189
<i>Ryan R. P. Noble¹, Elizabeth M. Grenik^{1,2}, Robert M. Hough¹, Melvyn J. Lintern¹, David J. Gray¹, Rob Hart², Peta Clode³, & John Murphy³</i>	189
Coupled Micro-XRF elemental mapping and LA-ICP-MS geochemistry of pyrites to decipher the cause of gold precipitation in quartz-sulfide gold-bearing veins, Poderosa-Pataz district, Peru.....	193
<i>Carlos Oré Sanchez¹ & Damien Gaboury^{1,2}</i>	193
IPGE (Os, Ir, Ru) are not in chromite	197
<i>Philippe Pagé¹, Sarah-Jane Barnes¹, Michael L. Zientek², Hazel M. Prichard³, & Peter C. Fisher³</i>	197
Aplitic dykes at the world-class Cantung tungsten skarn deposit: indicators of fluid flow and mineralizing processes	201
<i>Kirsten L. Rasmussen¹, David Lentz², & Hendrik Falck³</i>	201
Geochemistry and genesis of a mafic-ultramafic hosted VMS occurrence, Marathon, Ontario	205
<i>Marc L. Rinne¹, Peter N. Hollings¹, & Aubrey J. Eveleigh²</i>	205
The Middle River Gold deposit, NE New Brunswick, Canada: an example of an orogenic style gold system in the Brunswick Subduction Complex.....	209
<i>Sabine Schwarz¹, David Lentz¹, & James Walker²</i>	209
Gold mineralization in the Kakagi-Rowan Lake greenstone belt: a study of the Angel Hill Gold Zone	213
<i>Scott Secord¹ & Pete Hollings¹</i>	213
Rhenium in Canadian mineral deposits.....	217
<i>W. David Sinclair¹, Ian R. Jonasson¹, Rod V. Kirkham², & Art E. Soregaroli³</i>	217
Getting the scale right: links between metallogenesis, planetary degassing and the redox state of Earth's oceans?	221
<i>John L. Walshe¹</i>	221
⁴⁰ Ar- ³⁹ Ar geochronological constraints of the ore-bearing ductile shear zones at Hukeng tungsten deposit, Jiangxi Province	225
<i>Zhang Wei¹, Chen Maohong^{1,2}, Ye Huishou², & Yang Zongxi¹</i>	225
USING ISOTOPE GEOCHEMISTRY TO EXPLORE FOR RESOURCES	229
Isotopic studies and comparison of marbles in the Sambagawa metamorphic belt, central Shikoku, Japan and marbles from the Kumdy-Kol area of Kokchetav Massif, North Kazakhstan.....	231
<i>Zaure Bekmukhametova¹</i>	231
Cu Isotope Study of the Silver Bell Porphyry Cu Mine.....	235
<i>Molly Dendas¹, Ryan Mathur¹, & Spencer Titley²</i>	235
A geochronological based approach to characterize the setting of the Buffalo Head Hills kimberlite field, northern Alberta, Canada.....	239
<i>D. Roy Eccles¹, Art R. Sweet², Rob A. Creaser³, & Larry M. Heaman³</i>	239
Nature of $\delta^{18}\text{O}_{\text{quartz}}$ variation in a Slate-belt – hosted orogenic gold province, Nova Scotia, Canada: evidence for fluid: rock interaction	243
<i>Daniel J. Kontak¹, T. Kurt Kyser², & Rick J. Horne³</i>	243

TECHNICAL EDITORS
(Listed in alphabetical order)

Mark Arundell
U. Aswathanarayana
Roger Beckie
Chris Benn
Robert Howell
Charles Butt
Bill Coker
Hugh deSouza
Sara Fortner
David Gladwell
Wayne Goodfellow
Eric Grunsky
William Gunter
Gwendy Hall
Jacob Hanley
Russell Harmon
David Heberlein
Brian Hitchon
Andrew Kerr
Dan Kontak
Kurt Kyser

David Lentz
Ray Lett
Matthew Leybourne
Steven McCutcheon
Beth McClenaghan
Nancy McMillan
Paul Morris
Lee Ann Munk
Dogan Paktunc
Roger Paulen
Ernie Perkins
David Quirt
Andy Rencz
David Smith
Cliff Stanley
Gerry Stanley
Nick Susak
Bruce Taylor
Ed Van Hees
James Walker
Lawrence Winter

ORE-FORMING SYSTEMS: A GEOCHEMICAL PERSPECTIVE

EDITED BY:

**JACOB HANLEY
DAN KONTAK
PETE HOLLINGS**

Siderophile elements in the zonal structure of ore geochemical systems: exploration aspects

G. Abramson ¹

¹*Iteresources Pty Ptd, Level 2, 49-51 York st., Sydney, NSW, 2000 AUSTRALIA
(e-mail: gabramson@ionex.com.au)*

ABSTRACT: The elements of the iron group (Co, Ni, Mn, Cr, Ti, V, and Sc) have specific features of distribution in ores and wall rock as follows:

- These elements are localized mainly in the outer zones of the nuclear parts of ore geochemical systems of different ranks (ore bodies, ore deposits, ore regions), frequently forming sub-annular structures.
- Within the limits of the positive anomalies of the ore-forming elements the siderophile elements are in the anomalously lowered (sometimes in the sub-background) concentrations.
- These regularities are fractal, i.e. occur at all scales of ore objects - from the regional to the local.
- In the barren anomalies (in zones with dispersal mineralization) the regular distribution of iron group elements is not observed.

Detailed mineralogical studies have shown that pyrite of different generations is the main form containing siderophile elements, and their zonal distribution is connected both to the position of wall rock pyritization zones and to the concentration changes of these elements within the pyrites.

The presentation on sections, plans and 3-D models provides examples of the distribution of siderophile element.

KEYWORDS: *exploration, geochemical, system, siderophile, anomaly*

INTRODUCTION

A model of an ore geochemical system has been developed (Goldberg et al, 2003), which can be applied to ore entities of various categories: ore bodies, deposits and ore regions. The nuclear section of the system contains a zone of accumulation of the principal ore and associated elements. The peripheral areas contain zones of depletion of ore-forming elements. Anomalies of siderophile elements (Ni, Co, Mn, Ti, V, Cr), which are the subject of this paper, are located on the periphery of the nuclear sections of these systems.

In areas of accumulation of ore-forming elements the siderophile elements, as a rule, form zones of lower concentrations relative to the background concentration. Experience shows that these zones most probably contain ore bodies and deposits

of commercial significance. Examples are given below which illustrate the behaviour of siderophile elements in ore objects of various ranks and types of mineralisation.

MAYSKOE AU-AS DEPOSIT (RUSSIA)

This deposit is located in the north-east of Russia and belongs to a gold-arsenic type of low-sulphide formation (Abramson et al, 1980). It lies within a carbonaceous terrigenous rock of Triassic age and is associated with a dome-shaped uplift in a node of intersecting faults of various directions. The ore bodies consist of zones of silicification and kaolinization with veinlet-disseminated sulphide mineralisation. Gold is present in the form of finely-dispersed dissemination in arsenopyrite and pyrite. As an example, Figure 1 illustrates the distribution of Au and Mn in connection with commercial ore

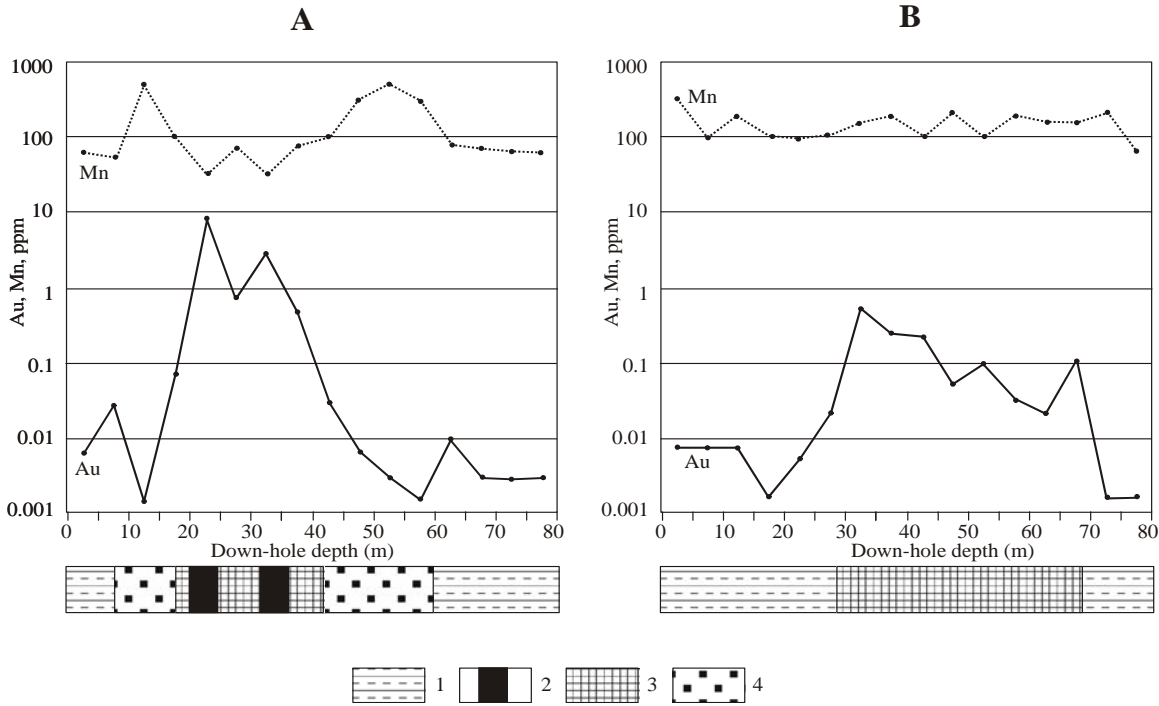


Fig.1. Distribution of Au and Mn in haloes of commercial ore bodies (A) and in a zone of barren disseminated mineralisation (B). Mayskoe deposit. Russia. 1. Black shale. 2. Ore body. 3. Zone of mineralisation. 4. Zone of pyritization

bodies (A) and a zone of disseminated mineralisation (B). Clear differences can be seen in the distribution of Mn in these two cases. In the first case (Fig. 1A) manganese comprises relatively low concentrations in the ore-bearing zone and ore bodies, while accumulating in the external pyritization zones. The distribution curve for gold shows the level of accumulation of this metal in the ores and haloes. The zone of disseminated mineralisation (Fig. 1B) is marked by elevated concentrations of gold and weak, undifferentiated haloes of Mn. A similar pattern of distribution can be seen in the case of Co and Ni (Abramson & Zhabin 1991).

BENDIGO GOLD FIELD (AUSTRALIA)

Bendigo is a classic example of a low-sulphide gold-quartz deposit located in a folded sequence of sandstone and shale of the Cambrian-Ordovician age (Ramsay *et al.* 1998; Goldberg *et al.* 2007). Regional soil geochemistry covers an area of ~4,000 km². Sampling Grid 5x5 km. 134 samples were collected as can be seen in Fig. 2, titanium anomalies form sub-

annular structures. Moreover, in the zone of the Bendigo deposit titanium forms areas with relatively low concentrations (depletion zones) and accumulates in its peripheral sections at a considerable distance from the centre of commercial mineralisation.

PROMEZHUTOCHNOE AU-AG DEPOSIT (RUSSIA)

This example shows possible mineral forms of occurrence of siderophile elements in ores and ore-surrounding zones.

The deposit is located in north-eastern Russia and belongs to a gold-silver type of sulphide-deficient formation (Abramson *et al.* 1993). It lies within a black-shale rock mass of the Upper Triassic. They consist of quartz breccias and veins of quartz of a colomorphic texture. Ore mineralisation includes low-grade gold, electrum and a small quantity of sulphides (< 0.1%). The average gold content in the ore bodies is 10 ppm, Ag >100 ppm. In the lateral sections of the ore bodies and at some distance from them there are zones of pyritization. The geochemical features of

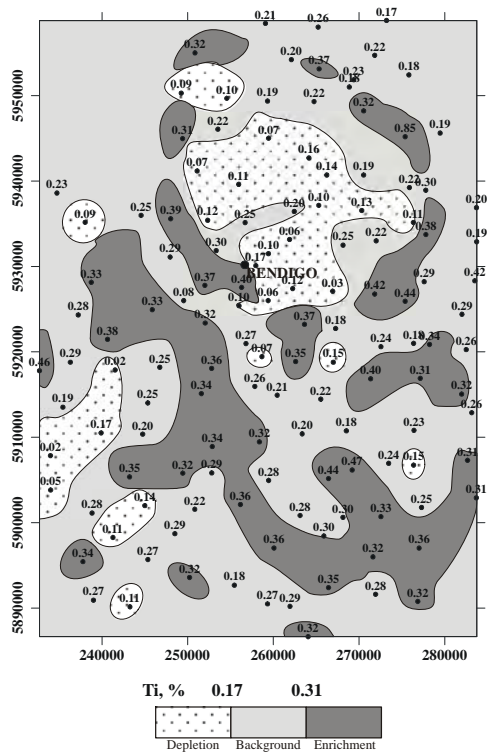


Fig.2. Distribution of Ti in rock. Bendigo Gold Field, Victoria. Australia.

the deposit were studied on the basis of geochemical sampling of trench walls and deep bore cores. The vertical zonality of the ore bodies is characterised by rapid petering out of gold as the depth increases, and an accumulation of tungsten and tin. An important part is played by elements of the siderophile group: Co, Ni and Mn. Their distribution is characterised by low (relative to background levels) concentrations at the ore level of the ore-bearing structures and a constant increase in concentration in relation to depth and on the flanks of the ore bodies. Because the ore bodies crop out at the surface, the distribution of elements in the upper sections is not discussed here.

An investigation of mineral fractions in ores and ore-adjacent areas carried out jointly with I.M. Shulgina (Abramson *et al.* 1993) has shown that pyrite of various generations is the main concentrator of Co, Ni and Mn (Table 1). The distribution of these elements is linked mainly with the quantity of pyrite concentration in ores and

Table 1. Concentration of Co, Ni and Mn in minerals and pyritization zones (ppm) of the Promezhutochnoe deposit.

Minerals	Ni	Co	Mn
Pyrite	160	70	1650
Limonite	70	45	650
Antimonite	10	none	300
Miargyrite	10	none	240
Pyritization zones	170	60	2100

Table 2. Distribution of main ore minerals in the Promezhutochnoe deposit (% , ppm).

Zones	Minerals (%)			
	Pyrite	Limo-nite	Antimo-nite	Miargy-rite
Upper-middle	0.03	1.2	3	0.07
Middle	~1	-	0.7	-
Bottom	7	-	-	-

ore-adjacent areas (Table 2).

CONCLUSIONS

The material obtained from this investigation shows:

- (1) Despite the individual features of formation of the deposits and differences in ore composition and morphology, a general pattern of distribution of elements of the siderophile group can be observed. They accumulate in the peripheral areas of ore objects (the nuclear parts of ore geochemical systems) of different categories, often forming a picture of concentric zonality.
- (2) Pyrite of various generations is the main mineral form of occurrence of the siderophile elements.
- (3) Siderophile elements can serve as a reliable indicator for determining the commercial significance of an anomaly and its spatial location within commercial ore mineralisation.

ACKNOWLEDGEMENTS

I should like to express my gratitude to Issai Goldberg, who provided very useful advice to me in the preparation of this paper.

REFERENCES

ABRAMSON, G.J., GRIGORIAN, S.V., & GRIGOROV, S.A. 1980. Results of an investigation of the geochemical halos at one Au deposit. *Lithochemical method of exploration of*

- endogenetic deposits*. Moscow, IMGRE, 16-22 (In Russian).
- ABRAMSON, G.J. & ZHABIN A.G. 1991. Recommendations for the use of geochemical methods in exploration for gold deposits. Moscow, IMGRE. (In Russian).
- ABRAMSON, G.J., KASUSHKIN, A.V., & SHULGINA, I.M. 1993. A geological and geochemical model as a reflection of structure of the anomaly field of an ore object. *Applied aspects of geochemical research*. Moscow, IMGRE, 29-50 (In Russian).
- GOLDBERG, I.S., ABRAMSON, G.J., HASLAM, C.O., & LOS, V.L. 2003. Depletion and enrichment of primary haloes: their importance in the genesis of and exploration for mineral deposits. *Geochemistry: Exploration, Environment, Analysis*, **3**, 281-293.
- GOLDBERG, I.S., ABRAMSON, G.J., HASLAM, C.O., & LOS, V.L. 2007. Depletion and enrichment zones in the Bendigo gold field: a possible source of gold and implications for exploration. *Economic Geology*, **102**, 745-753.
- RAMSAY, W.R.H., BIERLEIN, F., PARNE, D.C., & VANDERBERG, A.H.M. 1998. A review of turbidite-hosted gold deposits, central Victoria. Regional setting, styles of mineralisation and genetic constraints. *Ore Geology Reviews*, **13**, 131-151.

Cassiterite-sulfide mineralization revealed by dispersion flows in Belaya Sopka Mountain (northeastern Russia)

Anna D. Ananchenko^{†1} & Svetlana R. Tikhomirova^{†1}

¹ Federal State Unitary Scientific-Production Enterprise Aerogeologia
(<http://www.aerogeologia.ru/>; s.tikhomirova@g-to-g.com)
2/8, Academician Volgin Street, Moscow, 117071 RUSSIAN FEDERATION
† Deceased

ABSTRACT: Lithochemical mapping on *dispersion flows* in northeastern Russia (4000 km²) established precious metal, cassiterite-sulfide, polymetallic, lead-zinc, copper-molybdenum, and other types of mineralization. Spectral assays of the *dispersion flows* identified complex point, linear, and areal geochemical anomalies that required systematization. The assays underwent statistical processing to calculate the local geochemical background and make a quantitative estimate of the mineral potential throughout the studied territory based on *dispersion flow productivity*. The high *total dispersion flow productivity* led to the selection of several sites for detailed study. Geological examination confirmed the geochemist presence of numerous types of mineralization, including cassiterite-sulfide ore within Belaya Sopka Mt. (White Hill Mt., 100 km²), where, besides a high tin concentration, the potential also exists for mineable contents of lead, zinc, copper. Plots, portrayed on a space image, of *total dispersion flows productivity* and *secondary halo productivity* revealed the importance of superimposition of linear and ring structures which may aid in selection of target areas for exploration and setting a high priority for field studies in few areas of 3 km².

KEYWORDS: *dispersion flows, cassiterite-sulfide, Belaya Sopka Mt., northeastern Russia*

INTRODUCTION

In 1974–1982 geochemical mapping on *dispersion flows* throughout an area of 4000 km² in northeastern Russia (Fig. 1) was conducted by a team of the Aerogeologia Expedition. The supervisor of the geochemical investigations, Anna D. Ananchenko, was at that time a senior geochemist of Aerogeologia and PhD researcher at the Chair of Geochemistry at the Moscow State University.

The theoretical basis for the development of geochemical methods in Russian exploration practice was the 1909 work by V. I. Vernadsky on the universal *dispersion, migration, and concentration* of chemical elements and the teaching of *mineral deposit field dispersion* in conjunction with the *quantitative interpretation of geochemical anomalies* in the basic practical works of N.I. Safronov (1936, 1957), who was a geophysicist and geochemist who experienced Soviet government repression.

TECTONICS AND METALLOGENY

The studied area is part of the Okhotsk-Chukotka Volcanogenic Belt (OChVB). The OChVB is an elongated structure on the border between two folded provinces: Verhoyan-Chukotka (Mesozoic) and Koryak-Kamchatka (Cenozoic). The metallogeny of the Penzhinsky sector of the OChVB is characterized by three main types of mineralization: plutonic (gold-sulfide-quartz, gold-rare-metal, lead-zinc), volcanic (copper-molybdenum, polymetallic, gold-quartz), and telethermal (mercury, mercury-antimony). The main metallogenic feature of the OChVB was its high prospectiveness for precious metal deposits (Shilo & Babkin 1978; and others). Prospecting practice has determined that epithermal deposits, which formed in hydrothermal systems related to volcanic activity, are characterized by fine-grained gold (0.05–0.2 mm) and cassiterite. Minerals may be encountered in samples removed from a local source larger than 100 km² (Lugov

Makeev *et al.* 1972). The gold dust fraction lost during panning ranged up to 150–200 grains, a possible loss of 25–100% (Krutous 1976). Mineral search on dispersion flows proved to be an effective exploration method in poorly studied northeastern Russia.

Eastern and Western Projects

At several stages of the geochemical mapping (1:50,000) spectral assays on dispersion flows within the Eastern and Western Project areas (Fig. 1) revealed numerous occurrences. Below is an example of the mineralization discovered during the Western Project (Fig. 2). *Dispersion flow* samples were collected from clay-sand stream sediments. Sampling followed a grid that provided an observation density of 2–4 geochemical samples per km² (Solovov 1965). *Secondary dispersion halos* in sites were sampled by taking fine fractions from eluvial or diluvial deposits 15–20 cm beneath the surface. Depending on the features of the promising areas, testing was carried out on a 200/250 x 40/50 m or 100 x 20 m grid. Field processing of the samples consisted of drying and screening the sampled material through a sieve (–1 mm). The final weight of one dried sample was about 100–150 g.

Geochemical Halos of Western Project

During the Western Project, a total of 3000 grab samples were assayed by using the rapid spectral method to determine 32 elements and chemical adsorption to determine gold. Spectral assay data were processed in order to determine the distribution of 24 elements. Background (C_i) values were calculated using Lognormal Statistics software.

Anomalous concentrations of associated elements were established for five local areas (Fig. 3a). Revealed within the 100-km² Belaya Sopka Mt. area was a combined anomaly with up to 2 g/t Ag, 0.6 g/t Au, 0.1% Pb, 0.2% Zn, 0.003% Sn, 0.002% Bi, and 0.015% As.

Twenty three catchment basins were identified by dividing each elementary stream into several intervals containing

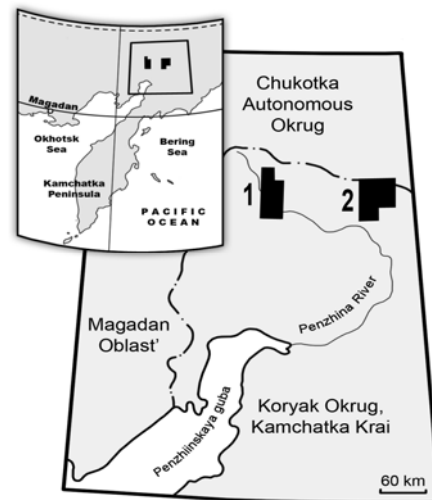


Fig. 1. Eastern (1) and Western (2) Project areas, Koryak Okrug, Kamchatka Krai (North), northeastern Russia.

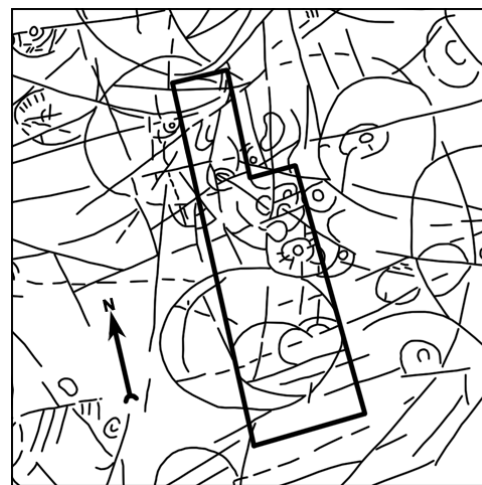


Fig. 2. Western Project limit (1600 km²) on interpreted satellite image (1:1,200,000), Penzhina River sector of the OChVB.

sample points. The position of the initial points (R_0) was clearly defined in almost all cases. Location of finite points (R) for some cases required a correction (λ'), which depends on the local slope effect (α) and the ratio between the size of the catchment area at the initial (S_R) and final (S_R) points. The required corrections were made using productivity diagrams and equations from Solovov & Shvarov (1980).

Equations (Solovov 1965) calculated the *dispersion flow productivity* (P'_x) and the *total dispersion flow productivity* (P'_Σ).

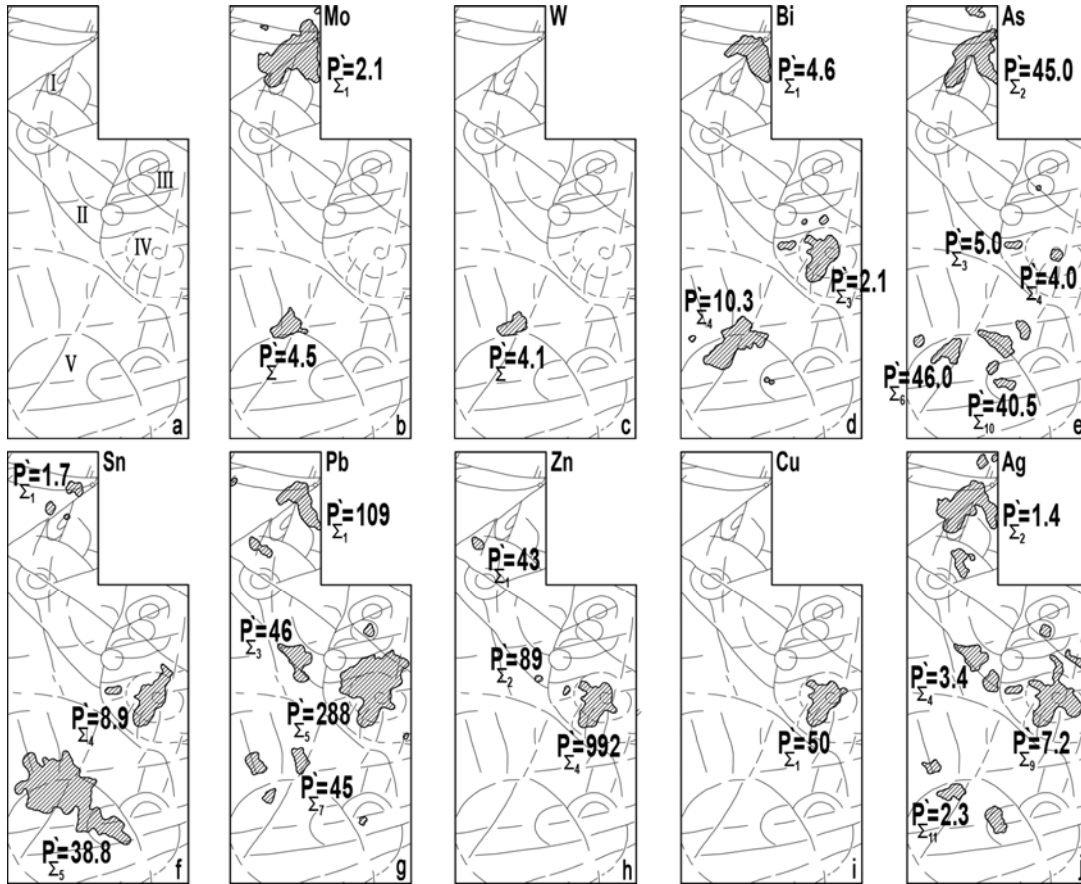


Fig. 3. Mineralization linked to the ring structures: I – Urkuveem (Mo with Ag and Bi, greisen type), II – Keyukveem (polymetallic), III – Kitivelgin (Au, arsenic-antimony association), IV - Belaya Sopka (Sn, cassiterite-sulfide association), V – Shestakovka (Sn with Ag and Bi, cassiterite-silicate association). *Total productivities* (P_{Σ} , $m^2\%$) for more promising catchment areas (outlined) and/or linear and ring structures are numbered.

High *productivity of dispersion flows* (P'_x) for the major associated elements (Sn, Pb, Zn, Cu) that are typical for cassiterite-sulfide mineralization have been established for the Belaya Sopka Volcano-Plutonic Structure that made the like-named mountain range a high, first-priority target (Ananchenko 1982).

Geological Confirmation

Calculation of P'_x showed that Sn has the highest productivity in three catchment basins. This fact has allowed definition of a site (2.5 km^2) for detailed investigation. Examination was accompanied by control grab, chip, channel, and technological sampling. Testing in a grid of $200 \times 40 \text{ m}$ identified anomalies with the following

maximum concentrations: 0.1% Pb ($C'_i = 0.03\%$), 0.2% Zn ($C'_i = 0.007$), 10 g/t Ag ($C'_i = 0.6 \text{ g/t}$), 0.08% Sn ($C'_i = 0.001\%$).

Mineralization was represented by quartz-chlorite-carbonate-sulfide veins with visible chalcopyrite, galena, sphalerite, pyrrhotite, cobaltite, limonite and malachite. Fractures filled by veins are identified on aerial photos as one submeridional zone up to 20 m thick and 500 m long. The northeastern linear system represented by a shear zone containing veinlets with arsenopyrite, bismuthine, gold and silver sulfosalts. Twelve veins that differ in extent and intensity of mineralization were discovered, with some veins yielding 3 wt. % Sn, 3 wt. % Cu, and up to 250 g/t Ag.

CONCLUSIONS

The geochemical investigations have taken on a far greater significance due to the discovery of numerous deposits in inaccessible Koryak Okrug. The Serebryany and Bich Au-Ag occurrences were discovered in 1975-1976. Panning and geochemical mapping revealed the Chuvanka and Os'minog (Au-Ag, Cu-Mo) occurrences. The Left Urkuveem Pb-Zn occurrence was established in 1978 and the Burnyi (Sn-Cu-Ag) and Sulfidnyi (Cu-Ag) occurrences were evaluated in the early 1980s.

ACKNOWLEDGEMENTS

Many people contributed to sampling and initial processing of a vast amount of dispersion flow data: Lazareva Z.A., Meretskov S.G., Shavurin S.A., Kotov S.Yu., Kuks K.R., Kuks K.A., Kuznetsova T.G., Pavlova V.E., and Shmakov S.G.† Valuable comments were given by Kostenko N.P., Plyashkevich L.N., Yakymenko E.L., and others. Sonin, I.I.†, who was chief of the team at Aerogeologia and Solovov A.P.† gave invaluable help. Thanks to all who assisted. The second author participated in works in 1981-1983.

REFERENCES

ANANCHENKO, A.D. 1982. *Geochemical investigations during the group geological mapping of 1: 50 000 scale in the North-East of the U.S.S.R. Methodology and results.* PhD dissertation. Chair of Geochemistry, Moscow State University, Moscow, 256

- KRUTOUS, V.I. 1976. Study of the shapes, numbers, and terms of the fine gold concentrations in the Yano-Kolyma gold bearing belt. *Magadan*, 250.
- LUGOV, S.F., MAKEEV, B.F., & POTAPOVA, T.M. 1972. Mechanism of development and location of the North-East USSR tin-ore deposits. Moscow, *Nedra*, 360.
- SAFRONOV, N.I. 1936. On the question of "dispersing halos" of mineral deposits and their using during the search and exploration. *Problems of Soviet Geology*, **4**, 302-323
- SAFRONOV, N.I. 1957. The form of the state of dispersed elements in nature and their searching importance. In: *Geochemical search for ore deposits.* Moscow, Gosgeoltekhizdat, 52-61.
- SHILO, N.A., BABKIN, N.B., & BELYI, V.F. 1978. East-Asian system of marginal volcanic belts, features of the structure, magmatism and metallogeny. In: *Proceedings of the Academy of Sciences of the U.S.S.R., Geological Series*, **2**, 24-31.
- SOLOVOV, A.P. 1952. On the question of estimation of mineralization on the results of the metallometric surveys. *Subsoil Exploration*, **4**, 48-50.
- SOLOVOV, A.P. 1965. Lithochemical methods of searching on the secondary dispersion halos and dispersion flows. In: *Instruction on the geochemical methods for searching of ore deposits.* Moscow, Nedra, 43-95.
- SOLOVOV, A.P. & SHVAROV Y.V. 1980. Estimation of mineralization on the lithochemical dispersion flows. *Exploration and Protection of Subsoil*, 25-30

Geochemical characterization of humic substances isolated from phosphatic pellets and their surrounding matrix, Ras-Draâ, Tunisia

Aida Ben Hassen¹, Jean Trichet¹, Jean-Robert Disnar¹, & Habib Belayouni²

¹ ISTO, Institut des Sciences de la Terre d'Orléans, Rue de Saint-Amand, Bâtiment Géosciences, BP 6759, 45067 Orléans Cedex 2 (email: aidabenhassen@yahoo.fr)

² Département des Sciences de la Terre, Faculté des Sciences de Tunis, Université Tunis El Manar, 1060, Tunis TUNISIE

ABSTRACT: Humic substances (HS) were extracted from pellets (phosphatic grains 10-500 µm size) and their surrounding matrices (< 50 µm), collected from Ras-Draâ deposit (Tunisia). Before, extraction, TOC content was measured using Rock-Eval pyrolysis. The HS were characterized by various geochemical analyses: CHONS elemental analysis, Fourier-transformed infrared spectroscopy (FTIR) and solid-state ¹³C CPMAS NMR. The chemical extraction of the HS from both fractions according to the IHSS (International Humic Substances Society) procedure, indicates a higher abundance of extractable humic compounds within pellets (~70% of TOC) and a variable but lower extraction yield in matrices (~18% of TOC). The elemental composition of extracted HS shows high H/C and S/C ratios in both fractions indicating that these HS originated from marine aliphatic OM. This planktonic origin was confirmed by spectroscopic analyses of HS (FTIR and solid-state ¹³C CPMAS NMR) that show a predominance of aliphatic structures and O-containing functional groups. The Rock-Eval pyrolysis applied to total OM confirms the marine planktonic origin of the phosphatic OM but it exposes its low degree of diagenetic evolution. Despite the homogeneity in their origin, pelletal and matricial OM give critical differences which are indicators of allochthonous origin of these pellets - faecal pellets - within their related sediments.

KEYWORDS: *humic, phosphatic, extraction, pyrolysis, pellets*

INTRODUCTION

Several investigators of the organic matter (OM) associated to sedimentary phosphatic deposits (Sandstrom 1982; Belayouni 1983; Belayouni & Trichet 1983; Nathan 1990; Ben Hassen 2003, 2007) have already highlighted the importance of studying this organic content within phosphorites for understanding the phosphatogenesis.

These Early works, mainly for ca. thirty years ago, provided information about the nature and the origin (mainly marine planktonic) and the low degree of diagenetic evolution of this OM. Moreover, all these studies concluded the quantitative importance of extractable HC in the OM associated to phosphorites. But these works were performed on bulk phosphorites. Thus, it seems to us that a comparative study of the specific composition and properties of the OM of pellets and of their surrounding sediments

separately, can help to understand the mechanisms of phosphatogenesis. Our study aimed to carry geochemical characterization of OM in both fractions and to draw some relevant conclusions on the genesis of the Ras-Draâ ore pellets.

GEOLOGICAL SETTING

The Ras-Draâ ore mine is located between Tozeur and Nefta, in southern Tunisia. This deposit is a natural continuity of the great Gafsa-Metlaoui phosphatic basin (Fig. 1).

During the paleocene, the phosphatized basin was a marine gulf open to the sea on both sides of an emerging land mass, the Kasserine island (Cayeux 1896, 1941; Sassi 1974).

The phosphatic series, about ~ 50 m thick, and of Paleocene-Eocene age, consists of ten phosphatic layers (Sassi 1974) interbedded with non- or poorly phosphatized strata with various facies

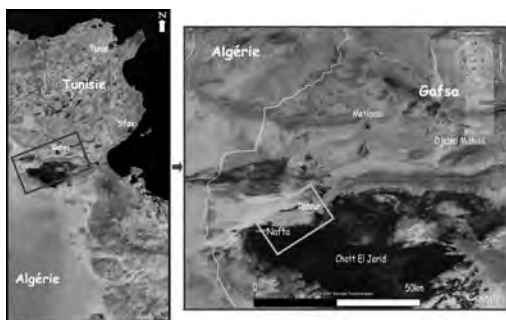


Fig. 1. Location map of the Ras-Draâ phosphate ore deposit in the Gafsa-Mélaoui basin, Tunisia (source: www.earth.google. fr).

(shales, marls, cherts, limestones).

EXPERIMENTAL

The studied samples were collected from the Ras-Draâ mine. The phosphatic grains (pellets) were separated from their exogangue (matrix) by granulometric fractionation after hand-processing the bulk samples under water.

For the analysis we selected pellets whose size lie between 100 and 500 µm (with 28 to 38% of P₂O₅) and matrix samples defined by a grain size < 50µm (less phosphatized with P₂O₅ ~ 7%).

Humic (HA) and fulvic acids (FA) and Humin (HU) were isolated utilizing the standard method recommended by the International Humic Substances Society (IHSS). Their amounts were obtained by quantifying carbon in each fraction and in each step of the fractionation procedure.

The study of HS extracted from both fractions (pellets and matrices) was performed by various geochemical analyses: CHONS elemental analysis, Fourier-transformed infrared spectroscopy (FTIR) and solid-state ¹³C CPMAS NMR.

RESULTS AND DISCUSSION

The main results of the quantitative extraction of HS and of geochemical analyses of extracted organic fractions are:

- (1) The Total Organic Carbon (TOC) content (Table 1), given by the Rock-Eval pyrolysis, varies between 0.30 % and 1.62 % in phosphatic pellets and between 1.22 % and 4.05 % in their adjacent matrices.
- (2) The characterization of the OM

Table 1. HS yields and Rock-Eval pyrolysis data on pellets and matrices from the CI à CVIII layers of the Ras-Draâ deposit. ns : non significant values.

	AF (%)	AH (%)	HU (%)	TOC (%)	Tmax (°C)
CI Pellets	13,59	50,45	35,96	1,26	ns
CII Pellets	12,92	68,58	18,50	1,48	ns
CIII Pellets	7,67	73,62	18,70	0,40	421
CIV Pellets	16,21	73,39	10,40	0,30	427
CV Pellets	5,34	79,07	15,59	0,49	427
CVI Pellets	6,17	85,57	8,26	0,68	422
CVII Pellets	11,84	68,12	20,03	0,57	421
CVIII Pellets	17,03	55,82	27,15	1,62	ns
CI Matrice	2,48	4,46	93,06	2,41	ns
CII Matrice	4,23	6,46	89,31	2,14	ns
CIII Matrice	6,52	32,03	61,45	1,22	410
CIV Matrice	8,87	14,85	76,27	3,24	419
CV Matrice	2,00	23,23	74,77	3,10	413
CVI Matrice	1,90	10,81	87,29	3,82	419
CVII Matrice	2,78	7,08	90,14	4,00	417
CVIII Matrice	7,07	4,42	88,51	2,57	ns

contained in the two fractions (pellets and matrices) by RE pyrolysis concludes, on one hand, to the planktonic origin of the OM (Type II), in both fractions, and, on the other hand, to a low degree of maturity of the pelletal and matricial OM (RE Tmax < 430 °C) (Table 1).

(3) The HS yields from the pelletal and matricial OM (Table 1) shows a high content of humic compounds isolated from pellets (humic carbon up to 75% of TOC) and a lower one in adjacent sediments (humic carbon less than 21% of TOC), along with the higher content of HU (low mature kerogen) in surrounding sediments and the lowest in the pellets.

(4) The OM appears to be essentially of marine planktonic origin, as deduced from: (i) elemental analysis (the atomic ratios O/C and H/C values of 0.15 and 1.29 % in HA and 0.40 and 1.55% in FA, respectively, indicate that these humic compounds originated from marine aliphatic organic matter); (ii) FTIR analysis of humic materials (Fig. 2. spectra obtained for HA show these humics are rich with aliphatic structures which is

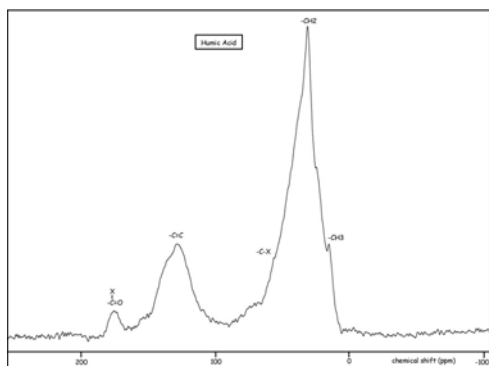


Fig. 2. ¹³C solid state NMR spectrum of a HA extracted from phosphatic pellets collected from Ras-Draâ phosphatic sediments.

typical of algal material); (iii) solid-state ¹³C CPMAS NMR (Figure 3 spectra obtained for HA show a strong aliphatic carbon peak at 0-50 ppm, indicating abundant oxygen-bearing aliphatic structures within these organic components).

CONCLUSIONS

This comparative study of OM in phosphatic pellets and their surrounding matrix provided information about the origin (essentially planktonic) and the low degree of diagenetic evolution of this OM in both fractions. Moreover, this study confirms the abundance of extractable humic compounds in the OM associated to phosphatized samples. The bulk OM within the pellets is essentially humic whereas the OM within the matrix of these pellets is different: it is not humic but a low mature kerogen. With regards to the age of the pellets, such high concentrations of HS in Ypresian phosphatic sediments imply an excellent preservation of the OM within the phosphatic grains. In contrast, the matricial OM differ by the nature of the diagenetic evolution that it has undergone. The nature of this matricial OM is quite usual for an ypresian age, epicontinental, never buried over a maximum of 150 m depth, sedimentary layer.

One explanation can be given for these differences: pellets though to be foreign bodies whose diagenetic story has been quite different, and independent, of that of their embedding sediment. These bodies

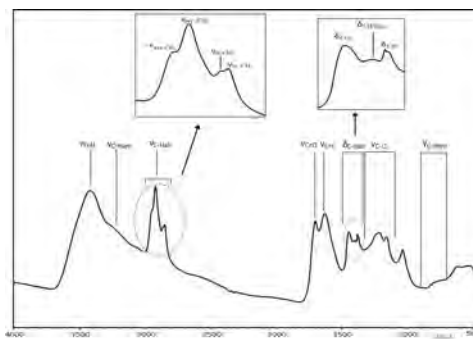


Fig. 3. FTIR spectrum of a HA extracted from phosphatic pellets collected from Ras-Draâ phosphatic sediments.

have been demonstrated to have derived from fish feces (Ben Hassen 2007) and their OM has been ingested by planktivorous fishes.

REFERENCES

- BELAYOUNI, H. 1983. Etude de la matière organique dans la série phosphatée du bassin de Gafsa-Métlaoui (Tunisie). *Application à la compréhension des mécanismes de la phosphatogenèse*. Thèse de Doctorat es-Sciences, Université d'Orléans. France.
- BELAYOUNI, H. & TRICHET, J. 1983. Preliminary Data On The Origin And Diagenesis Of The Organic Matter In The Phosphate Basin Of Gafsa (Tunisia), In: BJØROY *et al.* (eds.), *Advances In Organic Geochemistry 1981*. John Wiley And Sons, 328-335.
- BEN HASSEN, A. 2003. *Etude Pétrographique Et Minéralogique Préliminaire D'une Série Phosphatée Tunisienne*. Rapport Diplôme d'Etudes Approfondies, Université d'Orléans. France.
- BEN HASSEN, A. 2007. *Données Nouvelles Sur La Matière Organique Associée Aux Séries Du Bassin Phosphaté Du Sud-Tunisien (Gisement De Ras-Draâ) Et Sur La Phosphatogenèse*. Thèse De Doctorat, Université d'Orléans. France.
- CAYEUX L. 1896. Note Préliminaire Sur La Constitution Des Phosphates De Chaux Du Sénonien Du Sud De La Tunisie. *Comptes Rendus De l'Académie Des Sciences, Paris*, 273-276.
- CAYEUX L. 1941. Les Phosphates De Chaux Sédimentaires De France (France Métropolitaine Et d'Outre-Mer). **Tome I**. Imprimerie Nationale, Paris.
- NATHAN, Y. 1990. Humic substances in phosphorites: occurrence, characterization and significance. In: NOTHOLT, A.J.G. &

- JARVIS, I. (eds.), *Phosphorite Research and Development*, Geological Society Special Publications, **52**, 49-58.
- SANDSTROM, M.W. 1982. *Organic Geochemistry Of Phosphorites And Associated Sediments*. Phd Thesis, Australian National University, Canberra.
- SASSI, S. 1974. *La sédimentation phosphatée au Paléocène dans le sud et le centre-ouest de la Tunisie*. Thèse de Doctorat es-Sciences, Université de Paris-Orsay, France.

Petrogenesis of dykes related to Cu-Au & base-metal Au-Ag occurrences, Mt. Freegold area, Dawson Range, Yukon Territory, Canada

Thierry Bineli Betsi¹ & David R. Lentz¹

¹Department of Geology, University of New Brunswick, 2 Bailey Drive, Fredericton NB, E3B 5A3 CANADA
(e-mail: dlentz@unb.ca)

ABSTRACT: Dykes spatially associated with porphyry-like Cu and base-metal Au-Ag occurrences in the Mt. Freegold area (northern Canadian Cordillera) range from mafic (basaltic andesite) to felsic (rhyolite) units. Major and trace elements, as well as O and H isotope data, are consistent with magmas from both the crust and the mantle that evolved through crystal fractionation, crustal assimilation, and mixing processes. Dykes typically display much lower HREE relative to LREE, i.e., high La/Yb and high Sr/Y, which may at the first glance suggest an adakite-like signature. However assessments on other parameters such as Mg#, Na₂O, and Cr contents do not attest their adakitic affinity. The plagioclase-hornblende association and the lack of pyroxene are indicative of a water-rich source magma and support the high pressures (1.95 & 3.4-3.7 kb) derived from hornblende geobarometry. Zircon ²⁰⁶Pb/²³⁸U weighted ages reveal that dykes were emplaced from Jurassic (188 Ma) through to Middle Cretaceous (104-109 Ma) and Late Cretaceous (75.2 Ma). This suggests that mineralization may also have occurred at different times.

KEYWORDS: Cordillera, fractionation, mixing, calc alkaline, adakite

INTRODUCTION

The Dawson Range in the Canadian Cordillera hosts several deposit types that belong to the Dawson Range Au-Cu-(Mo) Belt portion of the Tintina Au Province. The geology of the area (Fig. 1) consists of the Devonian-Permian Yukon-Tanana Terrane intruded by the Upper Triassic to Early Jurassic Big Creek Metaplutonic Suite and Granite Batholith, as well as the Early Cretaceous Dawson Range Batholith. This terrane also hosts Middle to Late Cretaceous volcanic rocks and related dykes of the Mount Nansen and Carmacks groups, respectively (Carlson 1987). Mineralization is thought to be spatially and genetically associated with these dykes. The goal of this study is to provide a complete petrologic and geochemical data set to enable a better understanding of the petrogenesis of different dyke sets found in the area, referred to as the Northern Freegold Resources (NFR) Freegold Mountain project, and establish a petrologic link between them.

PETROLOGY

Dykes of the Dawson Range range from mafic to felsic aplitic and porphyritic bodies, which include: basaltic andesite, latite, andesite, trachyte, dacite, and rhyolite. Aplitic bodies are fine-grained, equigranular to sub-equigranular, whereas porphyritic dykes display phenocrysts of variable size in either a sugary or intergranular groundmass. Major minerals

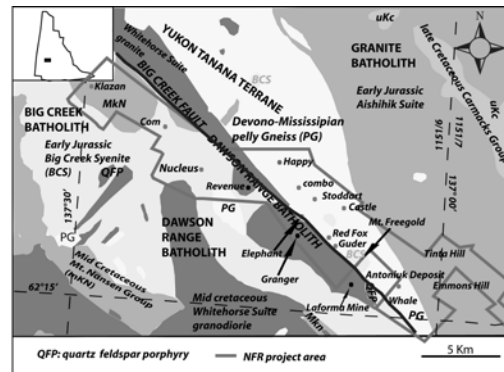


Fig.1. Location and geology of the Dawson Range, Yukon, and NFR claim boundaries (after Pautler 2006).

may be consistent with a magma mixing process. In the Rb versus Y+ Nb diagram (Fig. 4), dykes plot in the upper part of the I-type volcanic arc field overlapping into the syn-collisional. The position in the upper part of the volcanic arc field is consistent with mature arc rocks derived from the mantle, whereas the overlapping in the syn-collision field portrays once again the melting of crustal pelitic rocks or their incorporation in the melting process. Dykes are depleted in Rb, Th, and U, but slightly enriched in Cs. The depletion in Rb may suggest little or no crustal contribution during magma genesis and evolution, whereas the Cs content that is out of range of mantle values, testifies to the assimilation of crustal rocks. The $\delta^{18}\text{O}$ values from quartz grains and wall rock samples range from 6 to 10 ‰ (VSMOW) and are characteristic of igneous rocks with both mantle and crustal contribution. Wall rocks are depleted in D and δD values range from - 166 to -122 ‰ (VSMOW), which are beyond the range of magmatic isotopic values. These δD values may largely be a result of post-crystallization exchange between the rocks and heated meteoric ground water.

Chondrite-normalized REE patterns show that all types of dykes are depleted in HREE relative to LREE (Fig. 5). Also dykes display high Sr/Y (ave. 86 ppm) and La/ Yb (up to 80 ppm) ratios.

These characteristics may suggest geochemical characteristics similar to adakites and may also infer garnet-bearing and plagioclase-free sources. (Drummond & Defant 1990). However, others parameters such as the Mg# (ave. < 0.3), Na₂O < 3.5 wt.%, and Cr < 30 ppm are not consistent with an adakitic affinity. As pointed out by Richards & Kerrich (2007), other processes, likely fractionation of minerals that preferentially partition Y and HREE, may have contributed to high Sr/Y and La/Yb ratios. Hornblende, as well as zircon, apatite, and titanite are able to fractionate HREE relative to LREE and probably accounted for the observed pattern. Geobarometry of

hornblende in accordance with the calibration of Hammarstrom & Zen (1986) yielded pressures of 1.95, 3.4, & 3.6 to

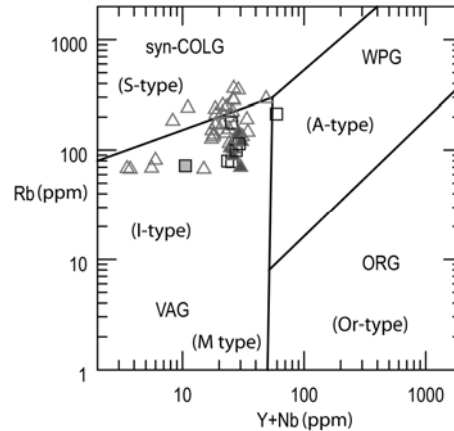


Fig. 4. Y+Nb vs. Rb (ppm) plot showing that dykes are mature arc rocks derived from the mantle, and from melting of crustal pelitic rocks or their incorporation in the melting process.

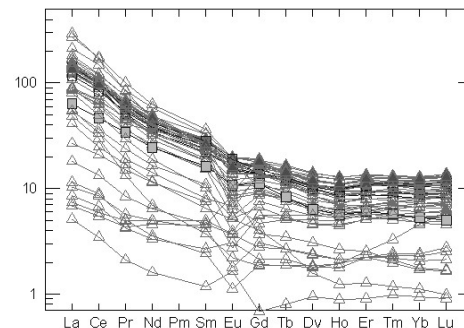


Fig. 5. C1 chondrite-normalized REE patterns showing the low HREE relative to LREE, suggesting a garnet-bearing and plagioclase-free source, as well as an adakitic-geochemical composition.

3.7kb. This is indicative of two magma chambers feeding the dykes, with one dacitic dyke deriving from the shallow chamber whereas, latitic, andesitic, and another dacitic dyke were derived from the deep chamber. Thermal ionisation mass spectrometry (TIMS) zircon U-Pb ages from mineralized quartz-feldspar rhyolitic dykes and those closely associated to the mineralization reveal that dykes range in age from Lower Jurassic (188 Ma) to Early Cretaceous (75.2 Ma) with most of them displaying Middle Cretaceous ages (104-109 Ma).

CONCLUSIONS

This study shows that:

- (1) Dawson Range's dykes were derived from both mantle and crustal sources. Melting of the rock sources gave rise to water-rich magmas that consequently crystallized over significant depths;
- (2) Dawson Range's dykes are a calc-alkaline suite that may have evolved through AFC and mixing processes, giving rise to a few samples that only partially fit the adakitic criteria;
- (3) While it has been thought that felsic dykes are only associated with the Middle Cretaceous Mount Nansen magmatic event in the Dawson Range, it appears that the Late Cretaceous Carmack's event also generated felsic dykes;
- (4) The Jurassic, Middle Cretaceous, and Late Cretaceous ages of dykes spatially associated with the mineralization suggests that the mineralization age may be extended beyond the unique Late Cretaceous age assigned to mineralization (Smuk *et al.* 1999).

ACKNOWLEDGEMENTS

We thank Yukon Geological Survey (YGS), Northern Freegold Resources (NFR), and NSERC for funding & logistical support.

REFERENCES

- ANNEN, C., BLUNDY, J.D., & SPARKS, R.S.J. 2006. The genesis of intermediate and silicic magmas in deep crustal hot zones. *Journal of Petrology*, **47**, 505-539.
- CARLSON, G.G. 1987. Geology of Mount Nansen (115-1/3) and Stoddart Creek (115-1/6) map areas Dawson Range, Central Yukon. *Indian and Northern Affairs Canada, Northern Affairs, Yukon Region, Open File 1987-2*.
- DRUMMOND, M.S. & DEFANT, M.J. 1990. A model for trondhjemite-tonalite-dacite genesis and crustal growth via slab melting: Archean to modern comparison. *Journal of Geophysical Research*, **95**, 21503-21521.
- HAMMARSTROM, J.M. & ZEN, E. 1986. Aluminum in hornblende: an empirical igneous geobarometer. *American Mineralogist*, **71**, 1297-1313.
- MOORE, G.M. & CARMICHAEL, I.S.E. 1998. The hydrous phase equilibria (to 3kbar) of an andesite and basaltic andesite from western Mexico: constraints on water content and conditions of phenocrysts growth. *Contributions to Mineralogy and Petrology*, **130**, 304-319.
- PAUTLER, J. 2006. *Evaluation Report on the Freegold Project, NTS 115/3, 6 & 7, Latitude 62°18'N, Longitude 137°12'W, Whitehorse Mining District, Yukon*, 108p.
- PETFORD, N. 2003. Rheology of granitic magmas during ascent and emplacement. *Annual Review of Earth and Planetary Sciences*, **31**, 399-427.
- RICHARDS, J.P. & KERRICH, R. 2007. Adakite - like rocks; their diverse origins and questionable role in metallogenesis. *Economic Geology*, **102**, 537-576.
- SMUK, K.A., WILLIAMS-JONES, A.E., & FRANCIS, D. 1997. The Carmacks hydrothermal event: an alteration study in the southern in the southern Dawson Range, In: *Yukon Geology 1996, Exploration and Geological Services Division, Yukon Region, Indian and Northern Affairs, Canada*, 92-106.

The primacy of magma compositions in determining the Re and W contents of molybdenite

Phillip L. Blevin¹

¹NSW Department of Primary Industries, PO Box 344, Hunter Regional Mail Centre, 2320, NSW, AUSTRALIA.
(e-mail: phillip.blevin@dpi.nsw.gov.au)

ABSTRACT: The Re contents of molybdenites from intrusion related ore deposits in eastern Australia are strongly negatively correlated with the degree of compositional evolution of the associated granitoids. Conversely, the tungsten content and Se/Te ratio of molybdenites (as analysed by LAM-ICP-MS) are positively correlated, indicating that the composition of the magmatic sources is a primary control on the abundance of these elements in molybdenite. In this regard, the siderophile/lithophile trace element geochemistry of the molybdenites parallel the broader gradation from Cu dominated to Sn-Mo-W dominated mineralization with increasing magmatic compositional evolution. Reconnaissance studies indicate that relative oxidation state of the Mo- versus Sn-mineralised magmatic suites do not affect these relationships. While whole rock analytical data indicates that Mo behaves incompatibly in oxidised intermediate to felsic magmas and compatibly in reduced magmas, the behaviour of Re appears compatible in both cases. These results have applications for exploration, ore genesis and Re-Os dating.

KEYWORDS: molybdenite, rhenium, granite, ore deposit, fractionation

INTRODUCTION

Molybdenite is the only common concentrator and economic source of Re. This is because MoS₂-ReS₂ effectively comprises a solid solution. The association of Re with Mo in this manner suggests that Mo and Re may also behave similarly during magmatic processes.

The Re content of unaltered hydrothermal molybdenites range from fractions of parts per million to percent values although a range of atomic Re/Mo values between 10⁻³ to 10⁻⁶ is most common (Terada *et al.* 1971; Newberry 1979a; Ishihara 1988). Numerous studies have dealt with aspects of Re in molybdenite including the documentation of Re contents in natural samples; correlation of Re content with conditions of molybdenite formation such as *f*S₂ and T (Terada *et al.* 1971); inter- and intra-deposit and inter-regional comparative studies (Morgan *et al.* 1968; Terada *et al.* 1971; Giles & Schilling 1972; Ishihara 1988); the relationship between Re contents and polytypism in molybdenite (Ayres 1974; Newberry 1979b); the effects

of post-crystallisation alteration (Newberry 1979a; McCandless *et al.* 1993); and even as evidence for metamorphic origin for low Re molybdenite (Stein 2006). A common conclusion of many earlier studies was that the Re/Mo ratio in molybdenites was a function of crystallisation temperature (Terada *et al.* 1971).

Giles and Schilling (1972) showed that the Re contents of molybdenite from porphyry Cu deposits was significantly higher (mean = 720 ppm) than those from porphyry Mo systems (mean = 50 ppm) while Re contents of molybdenites from greisens and pegmatites tended to be relatively low (Morgan *et al.* 1968). Newberry (1979a) noted that a strong inverse relationship existed between Re content (of molybdenites) and the Cu grade in several ore deposits. Despite the number of these studies little attention has been paid to the possibility that primary magmatic compositional controls, such as those which influence the ore element ratios (Cu:Mo:Sn:W etc.) observed in these deposits may also be an important control on the Re content of molybdenites.

MOLYBDENITES IN EASTERN AUSTRALIA

Molybdenite is a widespread and common mineral in hundreds of small deposits, disseminations and showings associated with the Palaeozoic granites of eastern Australia. Data exists on the geology of these deposits (Weber *et al.* 1978); the Re content of molybdenites (Riley 1967; Morgan *et al.* 1968; Blevin & Jackson 1998); the distribution of molybdenite polytypes (Ayres 1974), and the chemistry of Mo-mineralized granites (Blevin & Chappell 1992). Molybdenite occurs in veins, pipes, skarn and greisen style Mo, W-Mo±Bi and Cu-Mo deposits, as an accessory in Cu and/or Au deposits, and in trace amounts in Sn deposits. In eastern Australia molybdenite is mainly associated with oxidized, medium- to high-K I-type granites (Blevin & Chappell 1992) in addition to porphyry Cu-Au systems. Molybdenum dominant deposits are generally small and are not generally overprinted by high temperature potassic alteration, or lower temperature supergene overprints. Phyllic alteration is commonly present. Post crystallisation alteration of molybdenite, where present, is usually represented by ferrimolybdate.

METHODS AND RESULTS

Analytical Procedures

Rhenium contents of molybdenites have been derived from two sources: the literature (see above) where most Re concentration data was obtained by solution analysis and neutron activation; and by *insitu* LAM-ICP-MS (Blevin & Jackson 1998). In the later study molybdenites were analysed in 100 micrometer thick sections using a UV laser ablation microprobe at Macquarie University. In the absence of suitable sulfide reference materials, standardisation was performed using the silicate reference material NIST SRM 610. Differences in ablation yields were corrected by internal standardisation using Mo. The elements analysed were Si, Ti, Cr, Fe, Ni, Cu, Zn, As, Se, Zr, Nb, Mo, Pd, Ag, Sn, Sb, Te, W, Re, Au, Pb, and Bi. The elements Re, W, Se, and Te were found to be highly correlated with Mo. In

some cases Bi and Sn showed good correlations although most Bi was located in inclusions of galenobismutite, cosalite, and ikunolite that were common in most molybdenites analysed. The high degree of correlation of Re, W, Se, and Te strongly suggested that they comprise substitutions within the molybdenite lattice, rather than inclusions. Calculated Re concentrations using this method agreed well with previous analytical work on other molybdenites from these deposits, and with electron microprobe microanalysis of the laser analysed crystals.

Results

The relative degree of fractionation undergone by the medium- to high-K granite magmas of eastern Australia can be monitored by the concentration of Rb, which is incompatible in granitic magmas during fractionation, and by the ratios Rb/Sr and K/Rb. This relationship holds also for low-K granites which have low Rb contents and high K/Rb values (>300). Atomic Re/Mo ratios of molybdenites and the degree of fractionation of the related granites are strongly negatively correlated. The highest atomic Re/Mo value was from the Mt Morgan, Cadia and Yeoval Cu-Au deposits while lower Re/Mo molybdenites are associated with Mo-dominant or Sn-dominant mineralizing systems which are related to chemically more evolved granites. Molybdenite from scheelite skarn deposits occupies an intermediate position between Cu- and Mo-dominant granites both in terms of the Re/Mo ratio of the molybdenite and the degree of evolution of the related granite (at least in terms of Rb/Sr). Tungsten contents in the molybdenites are correlated in exactly the opposite way to that of Re. The Se/Te ratio increases from Cu-dominated to Mo and Sn dominated mineral systems.

DISCUSSION

Rhenium contents are low in molybdenites associated with reduced Sn-mineralized granites, and in molybdenites associated with the ilmenite-series granites of Japan. Ilmenite-series granites obtained their

reduced character through incorporation of crustal carbon either via assimilation of reduced sediments or mixing with magmas derived at least in part from those sources containing reduced sediment (Ishihara 1981). The average Re content of reducing marine sediments is ~50 ppb (with a range of 2 - 127 ppb; Koide *et al.* 1986) which is significantly above crustal and mantle averages. If ilmenite-series granites have attained their reduced character through the incorporation of reduced sedimentary materials, then it may be speculated that molybdenites related to these rocks could be expected to have higher Re contents than those related to granites derived from more purely igneous protoliths. The ilmenite-series granites of Japan tend to have lower K/Rb than magnetite-series granites, and are generally more felsic (Ishihara & Terashima 1992). In this regard, the difference observed in Re contents between molybdenites of the magnetite and ilmenite-series may alternatively be reconciled with the degree of compositional evolution of the associated magmas rather than to their relative oxidation states. The observed regional variation in Re contents of molybdenites in eastern Australia (e.g. between Tasmania and the mainland) can also simply be explained by the Tasmanian granites being generally more felsic and compositionally evolved.

Behaviour of other elements in molybdenite are highly consistent with ore element ratios in associated mineral deposits and strongly suggest that their control is dominantly that of their availability in the associated magmas at the time of hydrothermal fluid exsolution and transport.

Implications for Re-Os dating

The comparison of the Re content of a molybdenite with its structural polytype has been proposed as a method for assessing the viability of samples for Re-Os dating. "3R" molybdenite has been assumed to grow via a screw dislocation mechanism triggered by the incorporation of Re during crystallisation. Low Re "3R"

molybdenites are assumed to have lost Re during post crystallisation processes and are thus unviable for Re-Os dating. The results of this study have shown that W and probably Bi and Sn can substitute in significant amounts into molybdenite. The structural mismatch between these elements and the molybdenite lattice is much higher than that for Re suggesting that these elements may also be responsible for the triggering of the 3R polytype formation.

CONCLUSIONS

- (1) Re contents of unaltered molybdenites are primarily a function of the composition of the related ore magma.
- (2) LAM-ICP-MS studies indicate that other elements, in particular W, can substitute into the molybdenite lattice and can also be interpreted in terms of magma composition.
- (3) Re/W and Se/Te ratios in molybdenites are sensitive indicators of the ore element assemblages of the associated mineral deposits, and of the degree of compositional evolution of the associated magma.
- (4) Low Re molybdenite in granite related Sn-W-Mo mineral systems are not the result of post crystallisation leaching of Re, nor are they evidence for a metamorphic origin (cf. Stein 2006).

ACKNOWLEDGEMENTS

Published with the permission of the Director, Geological Survey of New South Wales, NSW Department of Primary Industries.

REFERENCES

- AYRES, D. 1974. Distribution and occurrence of some naturally-occurring polytypes of molybdenite in Australia and Papua New Guinea. *Journal of the Geological Society of Australia*, **21**, 273-278.
- BLEVIN, P.L. & CHAPPELL, B.W. 1992. The role of magma sources, oxidation states and fractionation in determining the granite metallogeny of eastern Australia. *Transactions of the Royal Society of Edinburgh*, **83**, 305-316.
- BLEVIN, P.L. & JACKSON, S. 1998. Potential Applications of LAM-ICP-MS technology in

- economic geology: a preliminary study of molybdenite and pyrite. *Geological Society of Australia Abstracts*, **49**, 44.
- GILES, D.L. & SCHILLING, J.H. 1972. Variation in rhenium content of molybdenite. 24th *International Geological Congress*, **10**, 145-152.
- ISHIHARA, S. 1981. The granite series and mineralization. *Economic Geology 75th Anniversary Volume*, 458-484.
- ISHIHARA, S. 1988. Rhenium contents of molybdenites in granitoid-series rocks in Japan. *Economic Geology*, **83**, 1047-1051.
- ISHIHARA, S. & TERASHIMA, S. 1992. K/Rb ratio of two contrasting magma series of the neogene plutonic belts in Japan. In: GUANGZHI, T (ed.), *Petrogenesis and mineralization of granitoids*. Science Press, Beijing, 23-33.
- KOIDE, M., HODGE, V. F., YANG, J., STALLARD, M., GOLDBERG, E., CALHOUN, J., & BERTINE, K. 1986. Some comparative marine chemistries of rhenium, gold, silver and molybdenum. *Applied Geochemistry*, **1**, 705-714.
- MCCANDLESS, T.E., RUIZ, J. & CAMPBELL, A.R. 1993. Rhenium behaviour in molybdenite in hypogene and near surface environments: Implications for Re-Os geochronometry. *Geochimica et Cosmochimica Acta*, **57**, 889-905.
- MORGAN, J.W., LOVERING, J.F., & FORD, R.J. 1968. Rhenium and non-radiogenic osmium in Australian molybdenites and other sulphide minerals by neutron activation analysis, *Journal of the Geological Society of Australia*, **15**, 189-194.
- NEWBERRY, R.J.J. 1979a. Polytypism in molybdenite (II): relationship between polytypism, ore deposition, alteration stages and rhenium contents. *American Mineralogist*, **64**, 768-775.
- NEWBERRY, R.J.J. 1979b. Polytypism in molybdenite (I): a non-equilibrium impurity-induced phenomenon. *American Mineralogist*, **64**, 758-767.
- RILEY, G.H. 1967. Rhenium concentration in Australian molybdenites by stable isotope dilution. *Geochimica et Cosmochimica Acta*, **31**, 1489-1497.
- STEIN, H.J. 2005. Low-rhenium molybdenite by metamorphism in northern Sweden: Recognition, genesis, and global implications. *Lithos*, **87**, 300-327.
- TERADA, K., OSAKI, S., ISHIHARA, S., & KIBA, T. 1971. Distribution of rhenium in molybdenites from Japan. *Geochemical Journal*, **4**, 123-141.
- WEBER, C.R., PATERSON, I.B.L., & TOWNSEND, D.J. 1978. Molybdenum in New South Wales. Geological Survey of New South Wales. *Mineral Resource Series* 43

RE minerals in Esfordi apatite- magnetite deposit, Central Iran

Mohammad Boomeri¹, Kazuo Nakashima², & David R. Lentz³

¹Geology Department, University of Sistan and Baluchestan, Zahedan IRAN

(e-mail: boomeri@hamoon.usb.ac.ir)

²Department of Earth and Environmental Sciences, Faculty of Science, Yamagata University, Yamagata JAPAN.

³Department of Geology, University of New Brunswick, PO Box 4400, Fredericton, NB, E3B5A3 CANADA

ABSTRACT: The stratabound Esfordi REE-P iron deposit is located in an Upper Precambrian volcanogenic complex. It is one of the more than 45 iron deposits in the Bafq area. The deposit has been petrologically investigated for textural relations, mineralogy, and mineral composition. This deposit is highly P-rich with local pegmatitic apatite veins. The main mineral assemblage in the Esfordi deposit is magnetite and apatite that is associated with Fe-Mg calcic pyroxene and actinolite. RE-bearing minerals are mainly apatite, monazite, allanite, and parisite. F.g. pink apatite occurs interstitial to granular apatite and magnetite crystals. Huge euhedral pyramidal and prismatic crystals of apatite are also abundant. Analysis shows these are fluor-apatite with F contents between 2.68 and 4.87 wt%. RE minerals were mainly formed along apatite grain boundaries and within veinlets. RE minerals are very rich in light REE (Ce, La, Nd, & Pr).

The deposit has similarities to Kiruna-type deposits. The Kiruna-type deposits are thought to have crystallized from volatile-rich iron oxide magmas derived by immiscibility in calc-alkaline to slightly alkaline parental magmas. The skarn assemblage, one head crystals of apatite, late RE minerals and veining around the Esfordi deposit indicate that hydrothermal process were definitely active at a later stage.

KEYWORDS: *Central Iran, Esfordi, apatite-magnetite, RE minerals*

INTRODUCTION

Esfordi apatite-magnetite deposit is located in 35 km northeast of Bafq city, in Central Iran. The Bafq is an important mining district and hosts several Iron deposit (about 2000 million tonnes) and a few Zn-Pb, U, Mn, and REE anomalies. The Esfordi deposit is the most rare-earth elements (REE)-rich and most P-rich member of these iron deposits. Choghart (200 million tonnes) and Chadormalu (400 million tonnes) iron deposits are now operating for iron, while Esfordi deposit (17 million tonnes with 30 % Fe oxide, 14 wt% P₂O₅, and about 2 wt% REE) is now operating for P. In addition, economic grade for REE is quite high relative to other rare elements, because their extraction as pure elements requires a higher technology than for other elements (Mariano 1989). Although, the Esfordi deposit is not comparable to giant REE deposits, such as Bayan Obo (China) and Mountain Pass (USA) carbonatite deposits (Kanazawa & Kamitani 2006) with respect

to the size and grade, but it appears to be a valuable REE deposit, because the mining is by inexpensive open-pit methods.

This paper identifies the RE minerals and presents preliminary information on mineral composition and geological and mineralogical features of the deposit. Chemical composition of minerals was determined by a wave length dispersive electron probe microanalyzer (EPMA), an automated JEOL JXA-8600 Superprobe, at Yamagata University.

GEOLOGICAL SETTING

The mineralized district is restricted by two main strike-slip faults of Kubanan to the east and Posht e Bdam to the west (Fig. 1a). The host rocks are a thick sequence of Upper Precambrian-Cambrian rhyolite, tuff, alkali granite, syenite, mafic dykes, magnetite, dolomite, gypsum, limestone, black shale, and sandstone. The Upper Precambrian-Cambrian sequence is overlain unconformably by Mesozoic and

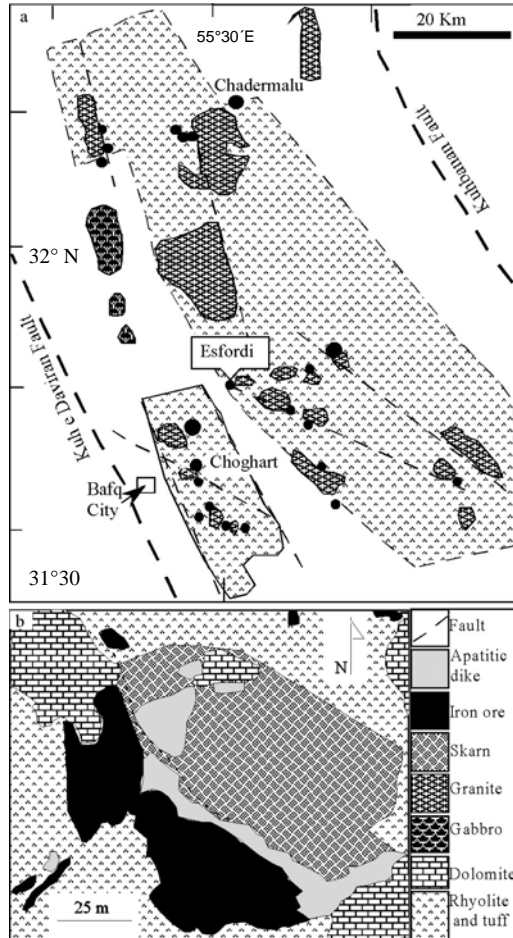


Fig. 1. a) Upper Precambrian-Cambrian Bafq metallogenic province in Central Iran (modified from NISCO 1980. b) a simple geology map of the Esfordi P mine (modified after Jami *et al.* 2007).

younger formations. The felsic igneous rocks are calc-alkaline and alkaline series magmas. The nature of the volcanism in the area can be interpreted as a signature of extensional tectonic setting such as arc/back-arc basin complexes. On the other hand, black shale and thick sequence of limestone and dolomite are similar as those of formed in intracontinental and passive continental margins. Ramezani & Tucker (2003) reported that the granitic intrusions and felsic volcanic rocks were formed in an active continental margin.

DISCUSSION & CONCLUSIONS

The ores appear to be a part of a thick

dolomitic layer that occurs on top a thick volcanic sequence dominated by acid pyroclastic rocks (Fig. 1b). The mine area is spherical in shape with a diameter of 500 metres, depth of 100 metres and spread across 20 hectares. It comprises of iron ore and phosphatic rocks of igneous type associated with actinolite, diopsidic pyroxene, quartz, feldspar, and carbonates. The ore can be divide into magnetite-rich, apatite-rich, apatite dyke, actinolite-rich and felsic pyroclastic horizons (Fig. 1b). Apatite occurs as microcrystalline red rocks with more than 90 wt % apatite, euhedral pyramidal and prismatic crystals of apatite (up to 15 cm length and 10 cm diameter) and pink powder interstitial to magnetite and granular apatite crystals. The analyzed apatites are fluor-apatites with F contents between 2.68 and 4.87 wt%. Amphibole occurs as long tabular and fibrous crystals and it is the most abundant skarn mineral. The analyzed amphibole classify as actinolite with Mg/(Mg +Fe) between 0.63 to 0.82. Calcic pyroxene occurs as tabular and prismatic long crystals. This mineral appears to be an earlier phase, because it was cut by amphiboles. It is diopsidic in composition, with the hedenbergite component ranging from 23 to 26 %. Garnet occurs as euhedral isotropic minerals and it is associated with apatite in actinolite-rich horizon. Although actinolite and diopsidic pyroxene are the most common silicates found in the deposit, garnet is a rare phase. Garnet classify as pure andradite (andradite end member is > 90 %). Common RE minerals in Esfordi are monazite, allanite, and parasite (Table 1). There are also other phases with briotholite composition. RE minerals were mainly formed along apatite and actinolite grain boundaries and within fractures (Fig. 2). Large size RE minerals (mainly as allanite) are associated with apatite-actinolite assemblage (Fig. 2b), whereas f.g. RE minerals (mainly as monazite) are associated with pure apatite samples (Fig. 2c). RE minerals are highly enriched in light REE such as Ce, La, Nd and Pr (Table 1). Apatite contains a few

Table 1. EPMA of RE minerals from the Esfordi deposit, Bafq, Iran.

Minerals	Allanite		Monazite		Parisite	
	Max	Min	Max	Min	Max	Min
SiO ₂ wt%	33.29	31.29	28.17	26.92	3.34	0.00
TiO ₂	0.82	0.23	0.00	0.00	0.06	0.00
Al ₂ O ₃	9.90	7.54	0.02	0.00	0.50	0.00
Fe ₂ O ₃	23.98	20.85	0.30	0.00	1.86	0.37
MnO	0.21	0.12	0.07	0.03	0.07	0.00
MgO	0.67	0.28	0.01	0.00	0.62	0.00
CaO	10.78	9.60	0.98	0.30	18.23	17.36
P ₂ O ₅	0.00	0.00	0.00	0.00	1.56	0.06
Ce ₂ O ₃	13.86	9.84	36.93	36.42	26.05	22.78
La ₂ O ₃	6.31	4.59	16.87	12.55	8.78	8.28
Pr ₂ O ₃	2.20	0.92	5.43	4.11	3.64	3.14
Nd ₂ O ₃	3.54	1.80	11.74	7.27	9.43	8.42
Gd ₂ O ₃	0.86	0.55	3.01	2.60	2.99	2.67
F	0.18	0.10	0.70	0.53	3.17	2.21
Sm ₂ O ₃	0.43	0.01	1.56	0.03	1.20	0.93
Eu ₂ O ₃	0.21	0.07	0.71	0.05	0.67	0.43
Dy ₂ O ₃	0.14	0.00	0.09	0.00	0.83	0.18
ThO ₂	0.13	0.00	1.48	0.00	0.22	0.05
Total	98.5	95.3	101.0	98.1	76.9	69.2
Si	3.29	3.16	0.96	0.94		
Ti	0.06	0.02	0.00	0.00		
Al	1.15	0.89	0.00	0.00		
Fe	1.81	1.58	0.01	0.00		
Mn	0.02	0.01	0.00	0.00		
Mg	0.10	0.04	0.00	0.00		
Ca	1.14	1.04	0.04	0.01		
Ce	0.51	0.36	0.55	0.54		
La	0.23	0.17	0.25	0.19		
Pr	0.08	0.03	0.08	0.06		
Nd	0.13	0.06	0.17	0.11		
Gd	0.03	0.02	0.04	0.04		
F	0.03	0.02	0.05	0.04		
Sm	0.02	0.00	0.02	0.00		
Eu	0.01	0.00	0.01	0.00		
Dy	0.00	0.00	0.00	0.00		
Th	0.01	0.00	0.03	0.00		

percent REE in its composition. However, the main part of REE may be from apatite as it is main mineral of the deposit and apatite-rich horizons contain high-grade REE ore.

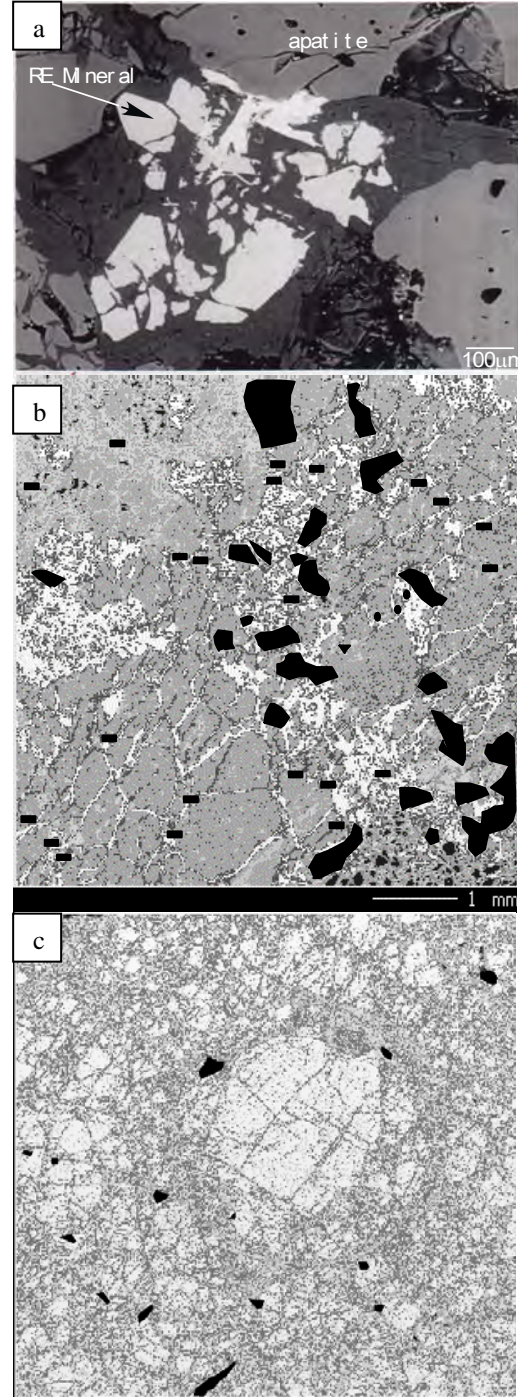


Fig. 2. SEM-BSE image and EPMA maps from Esfordi deposit. a) White crystals in fractures are REE minerals. b). RE minerals (sketched by black colour) are interstitial to actinolite (gray parts). c) RE minerals (black) and apatite (white) EPMA map.

REE ores are mainly associated with

carbonatite, alkaline, and pegmatitic rocks, associated hydrothermal systems, and placer environments. The Esfordi deposit is a Kiruna-type deposit. Several hypotheses have been examined to explain the origin of Kiruna-type deposits. The idea of an iron-oxide melt solidified into ore was first introduced by Geijer (1910). The Kiruna-type iron ores also introduced as hydrothermal deposits by Sillitoe & Burrows (2002). Recently, most REE mineralization associated with Kiruna-type systems is interpreted to be hydrothermal in origin. The skarn assemblage, one head crystals of apatite, late REE-rich minerals and veining around the Esfordi deposit indicate that hydrothermal process were definitely active at a late stage. Fluid inclusion studies on the Esfordi deposit by Jami *et al.* (2007) indicate three types of hydrothermal fluids. The hydrothermal fluids have probably remobilized REE from apatite and formed LE minerals at these late stages.

REFERENCES

- GEIJER, P. 1910. Igneous rocks and iron ores at Kiirunavaara, Lausavaara, and Toulluvaara, Sweden. *Economic Geology*, **5**, 699-718.
- JAMI, M., DUNLOP, A.C., & COHEN D.R. 2007. Fluid inclusion and stable isotope study of the Esfordi apatite-magnetite deposit, Central Iran. *Economic Geology*, **102**, 1111-1128.
- KANAZAWA, Y. & KAMITANI, M. 2006. Rare earth minerals and resources in the world. *Journal of alloys and compounds*, **408-412**, 1339-1343.
- MARIANO, A.N. 1989. Economic geology of Rare earth elements. In: LIPIN, B.R., & MCKAY, G.A. (eds.), *Geochemistry and mineralogy of rare earth elements*. Reviews in Mineralogy, **21**, 309-337.
- NISCO (National Iranian Steel Corporation), 1980. Report on result of search and evaluation works at magnetic anomalies of the Bafq iron ore region during 1976-1979. *Unpublished internal report*, 260 p.
- RAMEZANI, J. & TUCKER R.D. 2003. The Saghand region, Central Iran: U-Pb geochronology, petrogenesis and implications for Gondwana tectonics. *American Journal of Science*, **303**, 622-665.
- SILLITOE, R.H. & BURROWS. D.R. 2002. New field evidence bearing on the origin of the EL Laco magnetite deposit, northern Chile. *Economic Geology*, **97**, 1101-1109.

Numerical simulation of the sill-driven convective ore-forming system at Matagami, Quebec: implications for metal leach zones

Patrick M. Carr¹, Lawrence M. Cathles III², & C. Tucker Barrie³

¹Xstrata Exploration, 500, boulevard Industriel, Matagami, QC, J0Y 2A0 CANADA
(e-mail: pcarr@xstratazinc.ca)

²Cornell University, Ithaca, NY, 14853 USA

³C.T. Barrie and Associates, 29 Euclid Avenue, Ottawa, ON, K1S 2W2 CANADA

ABSTRACT: VMS districts are typically ~40 km in diameter and contain about a dozen regularly spaced Cu-Zn orebodies; in these districts, typically one or two of the deposits contain more than half of the district's resources. We numerically investigate this deposit size and spatial distribution through two-dimensional finite element modeling of the convection above the Bell River sill in the Matagami district, Quebec, Canada. The zinc transport across the seafloor is dominated by those hydrothermal plumes driven by the strong horizontal gradient in temperature alongside the vertical portion of the retreating 350°C isotherm of the edges of the cooling intrusion. Convection occurs both above the sill and along its underside, and metal is extracted from both sides of the cooling sill.

KEYWORDS: VMS deposits, sill-driven convection, numerical models, metal depletion, thermal mixing zones

INTRODUCTION

In most VMS districts, one or two large deposits dominate a camp full of smaller deposits (e.g., Horne Mine, Noranda; Matsumine, Kuroko; Mattagami Lake Mine, Matagami). We use finite element simulation of hydrothermal convection and associated chemical processes in attempt to explain this spatial distribution.

Thermally-driven convection in porous media has been simulated since Lapwood (1948) and has become increasingly complex and realistic. No models to our knowledge have systematically investigated the number and size of deposits that might form above a sill, nor have any modeled a system that would permit significant flow on the side and under the intrusive heat source.

MODEL BASICS

We simulate these systems using standard finite element techniques (e.g., Baker 1983) for solutions to the porous media conservation equations of mass, momentum, and energy on a rectilinear mesh using a code called BasinLab (Manning *et al.* 1987).

We deliberately keep the simulations as

simple as possible, and many assumptions and simplifications are included. Of particular note, rock permeability is taken to be a constant, modified only as a function of temperature in which it is elevated between 275 and 375°C and depressed at higher temperatures. This simulates thermal cracking (Lister 1974) and reproduces observed seafloor vent temperatures (Von Damm *et al.* 1983; Kelley *et al.* 2002).

Simulation results are shown here in terms of zinc metal vented into the ocean by hydrothermal fluid saturated with respect to zinc sulfide, the concentration of which increases exponentially with temperature (capped at 14.5 ppm at 400°C). The specific relation is similar to the one given by Large (1992), and is calibrated to end-member concentrations derived from seafloor observations (Seyfried *et al.* 2003). Details of the calculations are outlined in Carr *et al.* (2008).

MATAGAMI MODEL

The Matagami VMS district is located in western Quebec in the Archaean Abitibi green-stone belt and comprises primarily

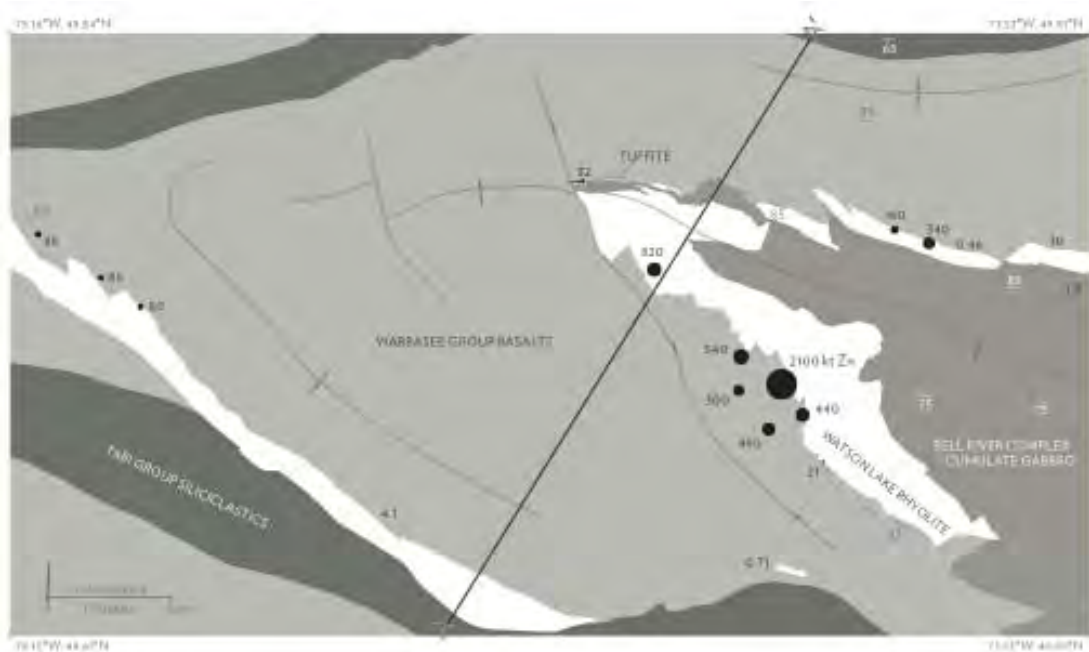


Fig. 1. Regional geology of the Matagami area (after Sharpe 1968) showing the tonnage of zinc metal at known deposits. Cross section A–A' is shown in Fig. 2

tholeiitic volcanics and intrusions formed in a back arc or continental rift zone. The regional geology is shown in Figures 1 (map) and 2 (cross-section A–A').

Most of the deposits are conformable with the Key Tuffite, a silicified tuff with a thickness ranging from 0.3 to 20 m, and traceable throughout the camp.

The footwall units below the ore horizon include the Watson Lake Rhyolite and the Bell River Complex intrusion. Both have U–Pb dates of ~2724 Ma (Mortensen 1993), and the Bell River Complex is considered to be the heat source which drove the hydrothermal circulation that created the ore deposits.

The hanging wall is composed of intermediate to mafic volcanics, beginning with the Wabasse Group basalts. Upsection are some interfingered rhyolites and small tuffaceous units, followed by hundreds of meters of massive basalt.

For the simulation, we reconstruct cross section A–A' to the time of ore deposition assuming conservation of rock volume and a sharp anticlinal postmineralization fold. The reconstructed sill has a thickness of 6.5 km at its centre thinning to a feather

edge over 30 km and a flat top. At the simulation of intrusion, the top of the calculation domain is the Watson Lake Rhyolite; 50,000 years after intrusion 100-m-thick strata at 2°C are added at 10,000 year intervals. All strata have a base permeability of 10^{-15} m^2 (1 millidarcy).

Figure 3 shows the metal transported across the numerical seafloor folded back onto cross section A–A'. Figure 4 shows zinc addition and depletion in the domain.

The evolution of the simulation (Carr *et al.* 2008, their Figure 12) shows that the vent site farthest from the cell center develops first, at 700 years after intrusion. Weak convection cells develop over the center of the sill, but most of the high-temperature venting occurs where the circulation is driven by the edge of the cooling sill. Venting of 300°C fluid continues for 135,000 years.

DISCUSSION

One of the most interesting aspects of the simulations is the way in which the convection cell that forms at the edge of the sill subsequently induces the formation of convection cells above the sill. Although

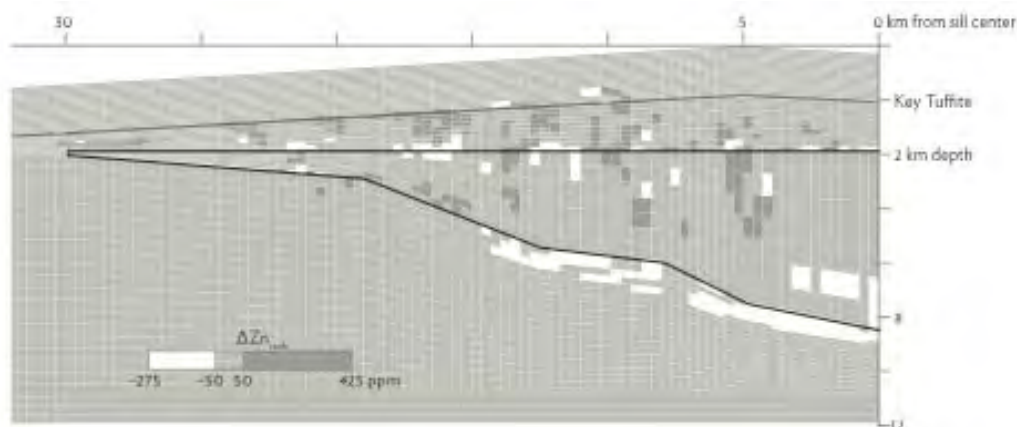


Fig. 3. Cumulative extraction and deposition of zinc at the end of the simulation. The algorithm assumes local chemical equilibrium.

of the Royal Astronomical Society, **39**, 465-509.

MANNING, R.A., MANHARDT, P.D., ORZECOWSKI, J.A., CATHLES, L.M., & BAKER, A.J. 1993. A parallel 3-D geologic basin modeling code. *Technical Report for the SIAM Conference on Mathematical and Computational Issues in the Geosciences, Knoxville*.

SEYFRIED, W.E., JR., SEEWALD, J.S., BERNDT, M.E., DING, K., & FOUSTOUKOS, D.I. 2003. Chemistry of hydrothermal vent fluids from the Main Endeavor Field, northern Juan de

Fuca Ridge: geochemical controls in the aftermath of June 1999 seismic events. *Journal of Geophysical Research*, **108**, 2429-2452.

VON DAMM, K.L., GRANT, B., & EDMOND, J.M. 1983. Preliminary report on the chemistry of hydrothermal solutions at 20°N, East Pacific Rise. In: RONA, P.A., BOSTROM, K., & SMITH, K.L., JR. (eds.) *Hydrothermal Processes at Seafloor Spreading Centers*. Plenum, New York, 369-389.

Minerals exploration and supply: a worldwide perspective

William X. Chávez, Jr.

*Minerals Engineering Department, New México School of Mines, Socorro, New México U.S.A.
(email: wxchavez@nmt.edu)*

Abstract: The current economic “downturn” in the consumption of mineral commodities has changed the manner in which companies and countries attempt to guarantee a secure supply of mineral resources. Although minerals exploration as yet comprises traditional, greenfield-style ore search, many companies now emphasize brownfield exploration efforts because the economics of expanding current mine operations is generally much more advantageous than developing a start-up mine.

Current stockpiles of base metals, aluminum, and ferrous products indicate that mine production has not yet been restricted enough so as to allow consumption of metals to reach an equilibrium with mine production. Even given this observation, some companies and countries are increasing metals production from mines so as to exert greater influence on the economics of a particular metals commodity; this is true for major and intermediate mining companies, and countries with substantial base metal or ferrous mineral resources.

Property acquisitions represent an alternative to the risks associated with traditional exploration, and available to companies and countries with sufficient cash-on-hand or with joint-venture partners. Because many mineral properties are substantially undervalued, acquisitions represent an economically-favorable manner of securing future mineral resources, allowing companies and state entities to prepare for the next upswing in mineral commodity demand; in addition, acquiring future resources provides some measure of economic security in that a source of minerals commodities is essentially guaranteed.

Although future minerals exploration will continue to involve high-risk frontier and novel geographic regions, the conservative nature of the mining and minerals supply businesses dictates that more traditional and pragmatic methods will be applied to ore search.

Keywords: *mineral exploration, supply, mine start-up*

BACKGROUND

Although worldwide exploration for ferrous, base-, and strategic metals has slowed substantially, the production of these metals has not slowed concomitantly; exploration for, and in some regions, production of, base- and precious metals is presently increasing. Because the consumption – and hence, production – of ferrous-, base-, and many strategic metals has been limited by economic considerations in the greatest consuming nations, most notably China, India, Russia, and the United States, metal stockpiles continue to increase or have stalled at a metastable equilibrium, pushing producers into mine closures or restriction of mine production, with important exceptions.

Current stockpiles of base- and ferrous metals are so great as to require that

mines slow significantly their metals production if an equilibrium between metals supply and consumption demand is to be established. World copper stockpiles, for example, contain so much refined metal that they represent the annual production from several world-class copper mines; in this case, the equivalent of the current annual copper production from the combined Collahuasi-Quebrada Blanca Districts of northern Chile, representing about one-seventh of the total copper production from Chile. Similarly, zinc stockpiles represent nearly a year of metal production from the Cloncurry District of northern Australia - as well as a substantial amount of primary lead production. The fact that stockpiles continue to grow or are just reaching a quasi- equilibrium state, even with mine closures and production decreases,

means that mine production has yet to adjust substantially to worldwide base metals demand.

Restriction of metals production by operating mines will likely be necessary for several years as consumption from current metal stockpiles catches up with stockpiled inventories and mine production. Even recent copper purchases by China have only slightly drawn down stockpiles, and are reflected in modest increases in short-term copper prices. The obvious global crisis has also stemmed demand, although precious metal markets are moving ahead, albeit sluggishly.

PRODUCTION & EXPLORATION VS. ACQUISITION CONSIDERATIONS

Counter to the necessity of temporarily decreasing base metals production are new mine openings that have been undertaken because some producers expect to gain financial advantage by having new mines ready to replace closed or reduced-output mines, to supply to local metals markets, or to keep prices depressed so as to place an economic *force majeure* on struggling producers. For example, CODELCO, the Chilean state mining company, continues to mine as-usual with the hope of maintaining a significant advantage in overall costs for copper production; MMC Norilsk Nickel, the world's leading nickel and PGE producer, also expects to maintain nickel production, but only in its mines in Russia, having closed all of its nickel mines in Australia and limiting production from other non-Russian mines. This action has had ramifications for other nickel producers, who can not compete with the greater grades and lower labour costs of Russian mines. Precious metal mines, especially those of gold, have generally fared better than base metals as consumers purchase gold as a hedge commodity.

The decreased value of holdings in minerals properties has meant that even large mining companies are considered to be available as potential sources of metal resources – via takeover - by both well-funded companies and as-yet well-funded

nations. This means that it is more expedient with respect to economies of investment and of time to purchase mineral resources – and the companies that hold them – than to engage in the laborious, expensive, and risky ventures of minerals exploration. Consequently, many mineral properties that might otherwise languish due to insufficient financing (or interest) on behalf of mining companies may now see some re-activation of exploration as they are taken-over by entities with capital to spend on property evaluation. Another benefit of this practice is that some marginal properties may receive greater exploration attention, with the idea of establishing better or new resource models for future metal mines.

Besides the observation that some countries and companies that have available cash are preparing for the next demand-driven upswing in required minerals production by acquiring mineral properties, there is also the opportunity by money-flush organizations to negotiate commitments from local to national governments for minerals supplies in exchange for development of infrastructure. This is a barter-style agreement that is of particular interest to commodity-rich or potentially-rich developing nations, whose own economies can not support development of necessary infrastructure, and whose technical support and labor pools may not have the background to design and construct significant development projects. The upside here is that countries receive needed infrastructure, often designed and built by the resource-requiring company or country. Downsides to this type of minerals-for-development swap is that in many cases the infrastructure is provided only in those mineral-rich geographic regions that are of direct interest to the mineral-receiving beneficiary (for example, as has happened in the past in Bolivia, México, the D.R.C., Zambia, Botswana), and that such development projects may be postponed or delayed indefinitely if economic conditions and the value of a particular commodity warrant such. As an example, the agreement between various

Chinese metals companies and the Democratic Republic of the Congo, involving development of infrastructure in return for commitments of significant quantities of base metals, has been put in abeyance until base metal values improve to the point where development of mines and their associated infrastructure is economically more advantageous than simply buying base metals from available providers.

Because so many mineral properties are currently undervalued, property acquisition represents a very favorable avenue of insuring future metals supply; this option is available only to those companies or countries with substantial cash reserves or those willing to engage in joint-venture arrangements in order to share risks and benefits. China, Russia, and India have each shown the initiative of acquiring either specific mineral properties or a specific commodity in order to satisfy national interests. For example, China has acquired properties or companies that would help assure supplies of copper, nickel, tantalum-niobium, and iron; Russia continues to seek expansion of its nickel and PGE reserves through the purchase of foreign assets, and India has attempted to acquire copper resources through a tender for ASARCO. Forward actions such as these allow countries to gain greater control on certain commodities supplies to greater extents than otherwise permitted through domestic-only production, as well as securing and satisfying domestic requirements of metals.

It is apparent that the need for a secure supply of mineral commodities is currently driving some countries, and forward-thinking companies, to continue to acquire, prospect for, evaluate, and enter into feasibility studies of, potential near-term mining properties. In some cases, properties are being prepared for immediate production by either completing construction of mining infrastructure or by expansion of existing mine and mill capacities. The idea is to have a property ready to increase production or to be put into production when commodity prices rebound, and to do so more quickly than

care-and-maintenance mines. Although quite risky, the current undervalued nature of such acquisitions represents a substantial potential for economic and security-of-supply gains by the investing countries and companies.

FUTURE EXPLORATION

Future exploration efforts, necessary to maintain detailed knowledge of the location, size, and concentrations of metals resources, will necessarily emphasize under-explored and frontier regions. Exploration in geologically-, geographically-, and socially-challenging areas will consume substantial amounts of time and money in defining potentially productive metallogenic regions; for example, targets being considered include: epithermal precious metal systems in shallow waters of the southwest Pacific; base- and precious metal occurrences in the Himalaya regions, notably large (and to-date, low-grade) porphyry systems; extensions of known metallogenic belts into the northern Andes, notably Colombia; highly prospective areas within conflict regions (for example, Tethys Belt countries). Some very prospective areas may be deemed too risky because of state-imposed taxes/royalties or inconsistent legal bases (e.g., Mongolia, the D.R.C., central Asia, Bolivia, Venezuela) or continued social-economic or security difficulties (e.g., East African Rift region, some Latin America countries, Himalaya – Tethys region). As such, and given the conservative nature of minerals exploration and mining companies, the overall exploration picture will almost certainly result in companies investing the bulk of their resources in and around known districts, retreat prospects, and relatively safe greenfield terrains rather than in novel frontier regions.

Mineralogical host phases for the PGE in magmatic Ni-Cu-PGE deposits at the Creighton Mine, Sudbury, Canada

Sarah A.S. Dare¹, Sarah-Jane Barnes¹, Hazel M. Prichard², & Peter C. Fisher²

¹Canadian Research Chair in Magmatic Metallogeny, Science de la Terre, Université du Québec à Chicoutimi, 555 Bld. de l'Université, Saguenay, PQ, G7H 2B1 CANADA (e-mail: sasdare@hotmail.com)

²School of Earth and Ocean Sciences, Cardiff University, Main Building, Park Place, Cardiff, CF10 3YE UK

ABSTRACT: Magmatic Ni-Cu sulfide ores may contain platinum-group elements (PGE) that are recoverable as by-products of mining these ores. It is of interest to understand which minerals host the PGE for two reasons: 1) to efficiently extract the PGE; 2) to understand the petrogenesis of the ores. The distribution of PGE from magmatic Ni-Cu-PGE deposits at the Creighton Mine, Sudbury, Canada has been investigated. A PGE mass balance has been carried out by comparing whole rock PGE concentrations to the sum of solid solution concentrations of PGE in base metal sulfides (BMS) and the associated PGM. Calculations show that the BMS host the majority of Ru and Pd (80-95%) and Os (65%), but Ir, Rh, Pt and Au are absent from the BMS. In contrast, Ir, Rh and Pt are hosted by sulfarsenide-bearing PGM within the BMS. These comprise irarsite (IrAsS)-hollingworthite (RhAsS) cores, containing some Pt, Os and Ru, and Ni-cobaltite (NiCoAsS) rims. Pentlandite is the main host for Pd because Pd diffuses from nearby Cu-rich phases into early-forming coarse-grained pentlandite. Pd-bearing PGM (michenerite PdBiTe), Pt-bearing PGM (sperrylite PtAs₂) and Au (electrum AuAg) are present but rare.

KEYWORDS: Ni-Cu-PGE deposit, sulfides, Sudbury, Laser-Ablation ICPMS, PGM

INTRODUCTION

It is well known that magmatic sulfides collect PGE and can form magmatic ore deposits (e.g., Merensky Reef, Bushveld, Republic of South Africa; Noril'sk, northern Siberia, Russia; Sudbury, Ontario Canada). It is necessary to determine which mineral phases host the PGE in order to: 1) efficiently extract the PGE and 2) better understand the petrogenesis of the ores. A number of processes may control the distribution the PGE in a magmatic sulfide ore deposit, including fractional crystallization of monosulfide solid solution (mss) from a base metal-rich sulfide liquid, direct crystallization of PGM from fractionated sulfide liquid, exsolution of PGM during sulfide cooling, and remobilization of PGE by reworking of the sulfides by late magmatic and/or hydrothermal fluids, deformation and metamorphism (see Barnes *et al.* 2008 for references).

Earlier studies of PGE distribution in magmatic sulfides have used microprobe, SIMS and micro-PIXE (e.g. Cabri *et al.*

2003). However, for many of the PGE, the concentrations in ores from Ni-Cu-PGE deposits were less than detection limit. laser ablation ICPMS (LA-ICPMS) offers three advantages over these techniques, namely: 1) lower detection limits (ppb level), 2) accessibility, and 3) time-resolved analysis.

LA-ICPMS has been used to determine the *in-situ* PGE content of base metal sulfides from PGE-rich reefs (e.g., Ballhaus *et al.* 2001; Holwell *et al.* 2007; Godel *et al.* 2008; Barnes *et al.* 2008). These studies demonstrate that all of the PGE, except Pt together with Au, are predominantly hosted by sulfides in solid solution and that pentlandite is a major carrier for Pd. The distribution of PGE in Ni-Cu-rich PGE deposits is less well-known. Huminicki *et al.* (2005) lasered sulfides from Copper Cliff Mine, Sudbury and calculated that the sulfides carried very little PGE and thus PGE were hosted mainly by PGM. We are furthering the study of Sudbury by investigating the distribution of PGE from Creighton Mine.

GEOLOGICAL SETTING AND SAMPLES

Ni-Cu-PGE mineralization at Sudbury is zoned with respect to Cu and PGE as a result of fractional crystallization from a base metal sulfide liquid, but metamorphism, fluids and deformation also affected these ore deposits (e.g., Farrow & Lightfoot 2002 and authors therein). The two main styles of mineralization are: 1) Fe-Ni-rich pyrrhotite ores (with minor pentlandite and chalcopyrite) in embayments along the base of the complex in noritic/gabbro-noritic (contact ores) and 2) Cu-Pt-Pd-Au-rich chalcopyrite ores (with minor pentlandite, pyrrhotite and PGM) forming veins and stockworks in the country rock below the complex (footwall ores). Creighton Mine, on the southern margin of the complex, is one of the largest contact-style deposits.

We have analysed 14 samples of contact-style ore from Creighton Mine comprising disseminated ores (< 30% sulfides), inclusion-bearing ores (containing fragments of the norite) and massive ores (> 80% sulfides). The ores contain on average 75% pyrrhotite, 17% pentlandite and 8% chalcopyrite. Chalcopyrite content varies from 0-25%.

ANALYTICAL METHODS

Whole rock and LA-ICPMS analyses were carried out at Université du Québec à Chicoutimi (UQAC). Sulfur was determined by combustion and IR analysis. Ni and Cu were determined by atomic absorption spectrophotometry after aqua regia digestion. Gold and PGE were determined by Ni-sulfide fire assay followed by Te co-precipitation followed by ICPMS.

We used a Thermo X7 ICPMS coupled to a New Wave Research 213 nm UV laser to determine the PGE and Au in the sulfides. Other chalcophile metals (Ag, As, Bi, Cd, Co, Cu, Fe, Ni, Pb, Re, Sb, Se, Sn, Te and Zn) were also monitored. Analytical conditions were: beam size of 80 µm; laser pulse rate of 10 Hz; laser output power of 0.3 mJ/pulse to ablate the sulfide for 60s after a 20s gas blank was collected. Sulfide standards were used to

calibrate analyte sensitivities and to monitor data quality. Detection limits were: 3-10 ppb for Os, Ir, Rh, Pt and Au and 20-30 ppb for Ru and Pd. A typical time-resolved spectrum for LA-ICPMS analysis is shown in Figure 1. The PGM were located on a Zeiss SMT S360 SEM at Cardiff University using a magnification of x50. PGM were qualitatively analyzed with INCA ENERGY EDX system.

PGE MASS BALANCE

In order to establish which base metal sulfide minerals host the PGE at the Creighton Mine we calculated a mass balance following the method of Barnes *et al.* (2008). We used the whole rock PGE content, the concentration of PGE in each sulfide and the mass fraction of each sulfide phase in the ore to determine the proportion (wt. %) of each PGE hosted by the sulfides in solid solution.

At the Creighton Mine, the sulfides host the majority of Ru and Pd (80-95%) and Os (65%) but Ir, Rh, Pt and Au are not hosted by the sulfides. Pyrrhotite and

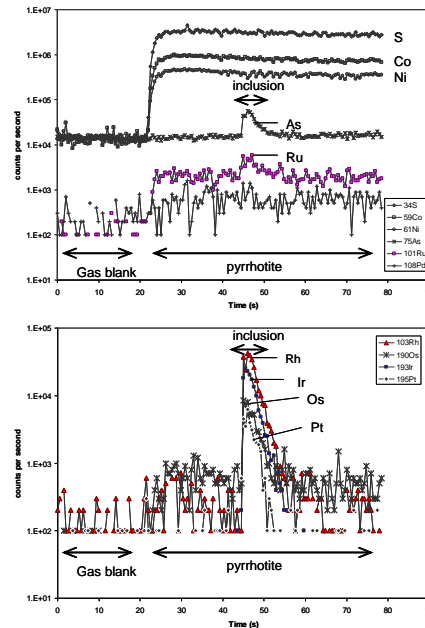


Fig. 1. Time-resolved spectrum for the LA-ICP-MS analysis of PGE in pyrrhotite. After 20s of gas blank the laser is turned on for 60s. Pyrrhotite contains only Os-Ru but a peak in the signal for Ir-Rh-Pt (Os) and As occurs where a PGM inclusion is encountered.

pentlandite host Ru and Os in equal proportions. Pentlandite is the main host of Pd (1 ppm) but chalcopyrite also contains some Pd (0.6 ppm); in contrast, pyrrhotite contains none. This indicates pentlandite exsolved from an Os-Ru rich mss, together with pyrrhotite. The origin of Pd in pentlandite is discussed below.

PGM

The PGM study reveals that sulfarsenide minerals are very common in the ores. They account for the Ir, Rh and Pt 'missing' from our calculated sulfide mass balance. These sulfarsenide minerals are euhedral and zoned in PGE (Fig. 2). They have an irarsite (IrAsS) surrounded by hollingworthite (RhAsS) core and a Ni-cobaltite (CoAsS) rim that contains some Rh (3 wt. %). The PGM cores also contain minor amounts of Pt (6 wt. %) and Os-Ru (1 wt%).

The sulfarsenides are small (5-20 μm) and the PGM cores are typically 1 – 5 μm . They are hosted almost entirely within the base metal sulfides, mainly in pyrrhotite and pentlandite but also in chalcopyrite. We estimate that the cobaltite equilibrated at 550-600°C. The PGM cores either crystallized from the sulfide melt or exsolved > 550°C from the sulfides during cooling.

Sperrylite (PtAs₂), electrum (AuAg) and michenerite (PdBiTe) are rare. Michenerite was observed to infill fractures in amphibole indicating that some Pd can be remobilized during metamorphism and deformation.

TEXTURAL LA-ICPMS STUDY OF Pd IN PENTLANDITE

In order to investigate why pentlandite is enriched in Pd compared to pyrrhotite we used the LA-ICP-MS to measure Pd in three different textures of pentlandite shown in Figure 3.

In all cases, the amount to Pd in pentlandite decreases from coarse grained (0.5 – 2.5 ppm) to veinlets (0.2 – 1 ppm) to flames (< 0.2 ppm). Also, coarse-grained pentlandite in chalcopyrite-rich ores (10 – 25% Ccp) are richer in Pd (1 – 2.5 ppm) than those (0.5 ppm Pd) in

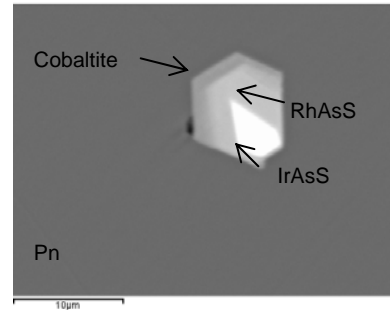


Fig. 2. Back-scattered electron image of a euhedral, zoned sulfarsenide hosted in pentlandite (Pn). Inner core (white) is irarsite (IrAsS), outer core (pale grey) is hollingworthite (RhAsS), rim (dark grey) is Rh-bearing Ni-cobaltite.

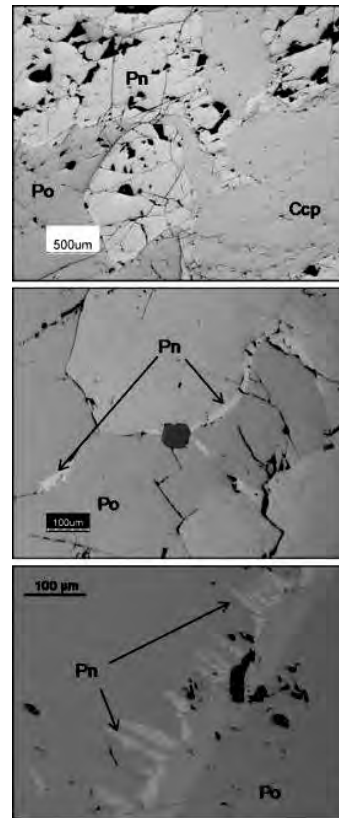


Fig. 3. Coarse grained pentlandite (Pn), often associated with chalcopyrite (Ccp), b) fine to medium-grained pentlandite aligned in veinlets along the pyrrhotite (Po) grain boundaries and c) exsolution flames of pentlandite in pyrrhotite.

chalcopyrite-poor ores (< 10% Ccp).

We propose that Pd diffuses from trapped Cu-rich phases into pentlandite during/after its exsolution from mss.

Chalcopyrite-rich pyrrhotite ores provided more Pd to diffuse into pentlandite than chalcopyrite-poor ores because Pd partitions into the Cu-rich liquid during sulfide fractionation. Most of the diffusion occurred early, when the coarse grained pentlandite formed, before the pentlandite veinlets and flames exsolved from mss.

CONCLUSIONS

- (1) Base-metal sulfides host the majority of Ru, Pd and Os in solid solution but contain no Ir, Rh and Pt.
- (2) Pyrrhotite and pentlandite exsolve from mss with equal proportions of Os and Ru.
- (3) Pyrrhotite does not contain Pd whereas pentlandite is enriched in Pd (up to 2.5 ppm).
- (4) Pd diffuses from Cu-rich phases into nearby pentlandite that formed early (i.e. coarse grained).
- (5) Sulfarsenide-bearing PGM are zoned with respect to Ir, Rh, Pt, Co, Ni and As (irarsite, hollingworthite, Rh-bearing cobaltite) and probably exsolved from the base-metal sulfides during cooling.
- (6) Only a minor amount of Pd is remobilized into PGM (michenerite) during deformation and metamorphism.

ACKNOWLEDGEMENTS

We thank Vale-Inco for partially funding the project and with thanks to the technical support from Creighton Mine and the Exploration groups from Vale and Vale-Inco. We also thank D. Savard and R. Cox for their support with whole rock and LA-ICPMS analyses. This work was partially funded by the Canadian Research Chair in Magmatic Metallogeny.

REFERENCES

- BALLHAUS, C. & SYLVESTER, P. 2001. Nobel metal enrichment processes in the Merenkys Reef, Bushveld Complex. *Journal of Petrology*, **41**, 545-561.
- BARNES, S.J., PRICHARD, H.P., COX, R.A., FISHER, P.C., & GODEL, B. 2008. The location of the chalcophile and siderophile elements in platinum-group elements ore deposits (a textural, microbeam and whole rock geochemical study): Implication for the formation of ore deposits. *Chemical Geology*, **248**, 295-317.
- CABRI, L.J., SYLVESTER, P., TUBRETT, M., PEREGOEDOVA, A., TUBRETT, M., & LAFLAMME, J.H.G. 2003. Comparison of LAM-ICP-MS and micro-PIXE results for palladium and rhodium in selected samples of Noril'sk and Talnakh sulfides. *The Canadian Mineralogist*, **41**, 321-329.
- FARROW, C.E.G. & LIGHTFOOT, P.C. 2002. Sudbury PGE revisited: Toward an integrated model. In: CABRI, L.J. (ed.), *The geology, geochemistry, mineralogy and mineral beneficiation of platinum group element 2002*. Canadian Institute of Mining, Metallurgy and Petroleum, Special Volume, **54**, 273-297.
- GODEL, B., BARNES, S.J., & MAIER, W.D. 2008. Platinum-group elements in sulphide minerals, platinum-group minerals, and whole-rocks of the Merenkys Reef (Bushveld Complex, South Africa). *Journal of Petrology*, **48**, 1569-1604.
- HOLWELL, D.A. & McDONALD, I. 2007. Distribution of platinum-group elements in the Platreef at Overysel, northern Bushveld Complex: a combined PGM and LA-ICP-MS study. *Contributions to Mineralogy and Petrology*, **154**, 171-190.
- HUMINICKI, M.A.E., SYLVESTER, P.J., CABRI, L.J., LESHER, C.M., & TUBRETT, M. 2005. Quantitative mass balance of platinum-group elements in the Kelly Lake Ni-Cu-PGE deposit, Copper Cliff Offset, Sudbury. *Economic Geology*, **100**, 1631-1646.

Late Mesoproterozoic S-type Sargipali granite and tungsten-mineralization: Singhbhum-Orissa craton, India

Sangita Chowdhury¹, David R. Lentz², & Saumitra Misra³

¹Department of Geology, University of Calcutta, Kolkata-700019, INDIA
(e-mail: sanggeol@live.in)

²Department of Geology, University of New Brunswick, Fredericton, NB, E3B 5A3 CANADA

³Indian Institute of Geomagnetism, New Panvel, Navi Mumbai- 410 218, INDIA

ABSTRACT: The Sargipali granitoid pluton, intrusive into the western part of Singhbhum Group of metasediments lying at the northern, eastern, and western margins of the Singhbhum-Orissa craton, eastern India, is spatially and temporally associated with co-genetic tungsten-bearing calc-silicate skarn. Geochemical features imply that the granites are highly evolved. Petrographic and geochemical considerations point towards a monazite and Zr fractionated low temperature S-type granite that was emplaced at ~0.96 Ga (CHIME monazite age) post-dating the sedimentation of Gangpur Group of rocks at ~1.7 Ga and syngenetic Pb-Cu sulfide mineralization in this area at ~1.69 Ga. The emplacement of the pluton was age equivalent to the final phase of deformation and metamorphism of the area. The REE data suggest that the foliated variety of the pluton might have generated by partial melting process whereas the composition of the main massive variety was mostly dominated by variable source rock composition.

KEYWORDS: *Singhbhum-Orissa craton, Singhbhum Group supracrustals, Peraluminous S-type granite, Geochemistry, Monazite age*

INTRODUCTION

The Singhbhum-Orissa craton of the eastern Indian shield, a granite-greenstone terrain of Archaean age (~3.6-3.1 Ga) having an areal extent of ~ 40,000 sq. km., is unconformably overlain by a supracrustal sequence of Mesoarchaean age (~3.12-3.09 Ga), known as the Singhbhum Group along the northern, western and eastern margins of the craton (Saha 1994; Misra 2006). This supracrustal cover, also described as Singhbhum Mobile Belt, is intruded by a number of small younger granitoid plutons of various ages. Among them a less known granitoid body that is intrusive into the mobile belt metasediments to the west in and around Sargipali, Sundergarh District, Orissa, is economically important because it is spatially and temporally associated with the tungsten-bearing calc-silicate skarn. The granitoid pluton also has intruded a Pb-Cu ore body (Fig.1), but shows no genetic relationship with the sulfide ores.

A considerable amount of work has

been undertaken in this region mostly aimed at the economic aspects of the Pb-Cu deposits (Sarkar, 1974; Chowdhury 2002). Although most primary tungsten deposits in the world are spatially and genetically related to granitoids, the granitoids and tungsten-bearing calc-silicate skarns of Sargipali area have received little recognition so far. It is, therefore, clear that the necessity exists to investigate the granitoid in more detail to gain better evaluation on the possible chemical properties of the magma that perhaps gave rise to the associated W-bearing skarns. Also no attempt had been made to establish age data of the granites. Therefore, the petrology, mineralogy, geochemistry, and a new monazite U-Th-total Pb age data of the Sargipali granitoid body were obtained, in an attempt to evaluate the genesis and tectonic setting of evolution of this pluton, and its possible relationship to W.

GEOLOGICAL SETTING

The Sargipali granitoid pluton occurs

within a metasedimentary assemblage of pelitic, psammitic, and calc-silicate units of the Gangpur Group.

The regional structure of the Gangpur Group is represented by an easterly plunging reclined fold (F_1), which co-axially refolded into an antiform (F_2). A later generation gentle F_3 fold with N-S trending vertical axial planes, however, has overprinted these F_1 and F_2 folds. The present study area lies on the southern limb of the regional fold. The granitoid pluton intruded along the fold axis of the late generation cross fold (F_3) (Fig. 1).

The granitoid pluton is mostly massive, with some isolated off-shoots of the pluton in the east show foliation in the NW-SE direction with moderate dips towards SW (Fig.1), which is parallel to the schistosity of the country-rock metapelites. Pegmatites and pegmatitic quartz veins occur in metasediments, spatially associated with the granites.

PETROLOGY & GEOCHEMISTRY

The underformed massive variety of granitoid pluton is leucocratic, white, very coarse to medium grained showing hypidiomorphic granular texture. A pink coloured, coarse porphyritic granitoid variety is also recognized locally. A white-coloured granitoid material locally occurs in fractures of the porphyritic variety of the pluton indicating a late phase of granitic activity. Both the massive and foliated varieties of the granitoid pluton consist predominantly of quartz, K-feldspar, and plagioclase (An_8 to An_{10}) with muscovite, tourmaline, biotite, chlorite, garnet, monazite, zircon, apatite, titanite fluorite, scheelite, galena, chalcopryrite, and ilmenite as common accessories. Secondary minerals formed via alteration are epidote and sericite.

In the CIPW normative Ab-An-Or diagram, the Sargipali granitoid is a 'granite' (Fig. 2a). This granite is characterized by high normative corundum (avg. 4%), therefore is strongly peraluminous (Fig. 2b).

The Harker variation plots do not show any significant correlations of oxides such as Al_2O_3 , Na_2O , CaO , MgO , P_2O_5 , and FeO^T with SiO_2 , only K_2O shows

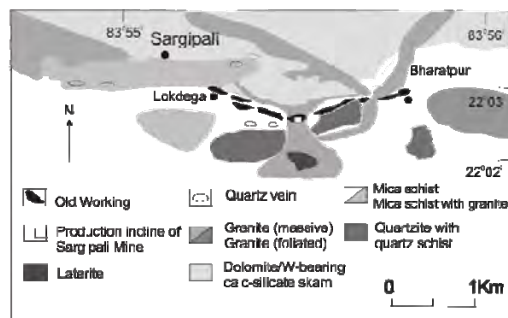


Fig. 1. Geological map of the area around Sargipali (modified after Ghosh *et al.* 1999)

decreasing trend with increasing SiO_2 . The SiO_2 content (>74 wt%), molar A/CNK ratios (>1.2), K_2O/Na_2O ratios (~ 2), and presence of accessory minerals like muscovite, biotite, garnet and ilmenite in the pluton suggest that the Sargipali granite is S-type in nature. In the Rb – (Y+Nb) (Fig. 3a), Nb–Y, Ta–Yb, and Rb–(Yb+Ta) trace-element discrimination diagrams, all varieties of Sargipali granites plot mostly in the syn-collision granite (syn-COLG) field after Pearce (1996), which is consistent with S-type granite characteristics.

The granite as a whole are rich in incompatible elements (Rb, Y, Nb, Ga), but poor in compatible elements (Sr, Cr, V). The rocks are remarkably rich in Rb (>300 ppm) and depleted in Sr (~ 35 ppm). This readily defines them as being highly evolved. However, increasing of SiO_2 , and decreasing of TiO_2 , FeO^T , K_2O , Th, Zr and LREE from foliated to massive variety indicate that foliated granite may represent a higher degree of partial melting, and considerably less evolved than massive granite (cf. Bogaerts *et al.* 2003). Low Zr (4-90 ppm) is indicative of low temperature of this highly silicic felsic magma (Lentz & Suzuki 2000). The positive correlation of Zr with TiO_2 probably imply that Zr fractionated from the initial melt with time.

In C1 chondrite-normalised REE plots (Fig. 3b), the foliated granites ($\sum REE \sim 200$ ppm) show strongly fractionated LREE and flat HREE with $(Ce/Yb)_N \sim 50$. The massive granites are relatively very low in REE (9 to 34 ppm), showing relatively flat to highly variable LREE and

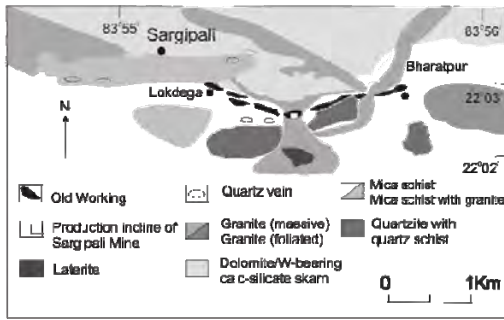


Fig. 1. Geological map of the area around Sargipali (modified after Ghosh *et al.* 1999)

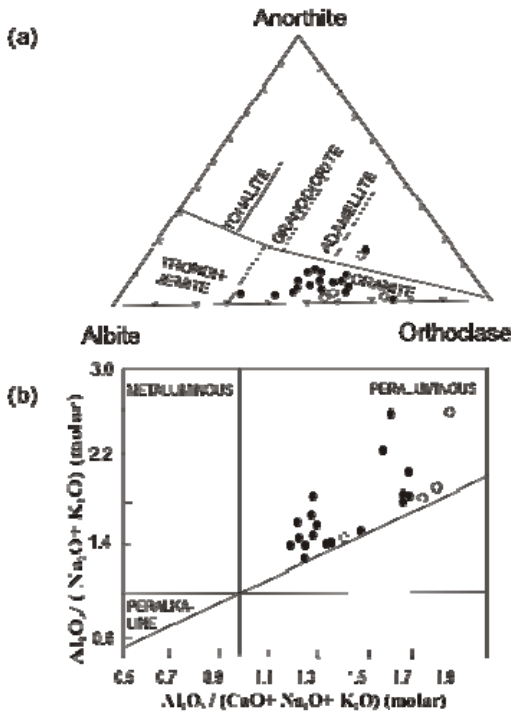


Fig. 2. Plot of Sargipali granitoid in (a) CIPW normative Ab-Or-An diagram (after Barker 1979), and (b) Shand's classification of granites, based on Al-saturation index. Symbols: filled circles - massive granite, open circles - foliated granite.

relative enrichment of HREE. The $(Ce/Yb)_N$ ratios of this granite is ~ 5 . The fractionated LREE and flat HREE pattern of the foliated granites perhaps indicate low T partial melting dominating chemistry of this granite or extensive low T fractionation. The REE pattern of the massive granite is heterogeneous and perhaps suggestive of source-dominated chemistry of these granites. The low REE may be due to the fractionation of LREE-

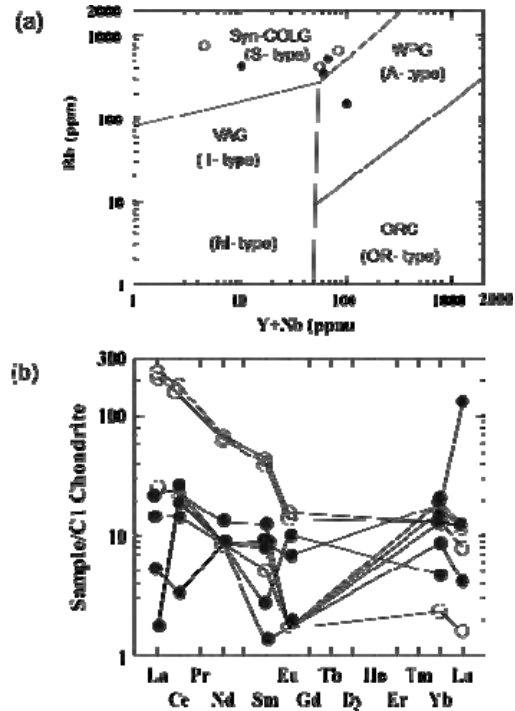


Fig. 3. Sargipali granitoid showing (a) updated Rb vs Y+Nb discrimination plots (after Pearce 1996) and (b) CN REE systematics. Symbols are same as in Figure 2

enriched accessory minerals like monazite and HREE enriched zircon and apatite that take up all the REEs.

Broad correlation between igneous composition, skarn type, spatial association, and respective metal contents indicates that the granite is associated with W skarns. Both the varieties of granite are W-bearing. The concentration of W (avg. 500 ppm) in granite is very high compare to the associated skarns (W \sim 300 ppm). In terms of major- and trace-element chemistry, the Sargipali granite is comparable to averages of world S-type granitoids associated with W skarns. Like many other W-bearing granites, the Rb/Sr ratio of Sargipali granite is high (> 4), while unlike other W-Sn deposit related granites, W is concentrated in both early and late intrusive stages.

GEOCHRONOLOGY

The monazite U-Th-Pb CHIME ages of massive and foliated granites (one sample each) were calculated from microprobe data (after Montel *et al.* 1996). The

foliated and massive granite yield Th-U total Pb weighted mean age of 974 ± 6 Ma and 959 ± 6 Ma, respectively. These age data indicate that the Sargipali granite has post-dated the sedimentation of the host Gangpur Group of rocks at ~ 1.70 Ga (Sarkar 1980) and syngenetic Pb-Cu sulfide mineralization at ~ 1.69 Ga (Ghosh *et al.* 1999). This pluton is time correlative with the last phase of deformation of the present area, and final phase of shearing along the Singhbhum Shear zone that is situated mostly along the boundary of the Singhbhum-Orissa craton to the south and the Singhbhum Group of metasediments in the north, and related to metamorphism at ~ 1.0 Ga.

CONCLUSIONS

- (1) The granite pluton, which intruded the Singhbhum Group of metasediments to the west near the Sargipali area, is of two broad types, i.e., an undeformed massive granite and pegmatite system in the west and foliated granite along the east margin.
- (2) Both of these granite phases are highly evolved, strongly peraluminous muscovite-, garnet-, monazite-, zircon-, and ilmenite- bearing low T S-type syncollisional granites. The massive variety is more evolved than the foliated one.
- (3) Both the massive and foliated granites are spatially and temporally associated with the tungsten-bearing calc-silicate skarn, which is likely formed by this evolved pluton.
- (4) Monazite dating suggests that the Sargipali granite pluton is ~ 0.96 - 0.97 Ga, post dating the sedimentation of the host Gangpur Group of rocks (~ 1.70 Ga) and syngenetic Pb-Cu sulfide mineralization (~ 1.69 Ga). It is time equivalent to the final phase of deformation in the Sargipali area as well as the movement along the Singhbhum Shear Zone, and related metamorphism at ~ 1.0 Ga.

ACKNOWLEDGEMENTS

Financial support for this research was provided by NSERC Discovery grant (DL).

Douglas Hall supervised monazite age analyses at UNB, Canada.

REFERENCES

- BARKER, F. 1979. Trondhjemite: definition, environment and hypothesis of origin, in Trondhjemites, Dacites and related rocks. F. BARKER (ed.). Elsevier Scientific Publishing Co., 1-12.
- BOGAERTS, M., SCAILLET, B., LIEGEOIS, J.P., & VANDER A.J. 2003. Petrology and geochemistry of the Lyngdal granodiorite (Southern Norway) and role of fractional crystallisation in the genesis of Proterozoic ferro-potassic A-type granites. *Precambrian Research*, **124**, 149-184.
- CHOWDHURY, S. 2002. The Sargipali sulfide deposit of Orissa, India: its atypical lead-high character and genesis. *Journal Nepal Geological Cong. Society*, **27** (Special Issue), 11-24.
- GHOSH, S., THORPE, R.I., & GHOSH, A.K. 1999. Lead and sulphur isotope geochemistry of galena from Sargipali sulphide deposit, Sundergarh, Orissa –Implications for ore genesis. *Indian Journal of Earth Science*, **26**, 1-12.
- LENTZ, D.R. & SUZUKI, K. 2000. A low F pegmatite-related Mo skarn from the southwestern Grenville Province, Ontario, Canada: Phase equilibria and petrogenetic implications. *Economic Geology*, **95**, 1319-1337.
- MISRA, S. 2006. Precambrian chrono-stratigraphic growth of Singhbhum-Orissa craton, eastern Indian shield: An alternative model. *Journal Geological Society of India*, **67**, 356-378.
- MONTEL, J.M., FORET, S., VESCHAMBRE, M., NICOLLET, C. & PROVOST, A. 1996. Electron microprobe dating of monazite. *Chemical Geology*, **131**, 37-53.
- PEARCE, J.A. 1996. Sources and settings of granitic rocks. *Episodes*, **19**, 120-125.
- SAHA, A.K. 1994. Crustal evolution of Singhbhum-North Orissa, eastern India. *Geological Society of India memoir*, **27**, 341p.
- SARKAR, S.C. 1974. Sulfide mineralization at Sargipali, Orissa. *India. Economic Geology*, **69**, 206-217.
- SARKAR, S.N. 1980. Precambrian stratigraphy and geochronology of Peninsular India. A review. *Indian journal of Earth Science*, **7**, 12-26.

Bimodal post-collision volcano-plutonic complex in the southern rim of the eastern flank of the Mongol-Okhotsk orogenic belt

I.M. Derbeko¹, V.A. Ponomarchuk², D.L. Vyunov³, & S.K. Kozyrev³

¹ Institute of Geology and Nature Management, Far East Division, Russian Academy of Sciences, 1, Relochniy, Blagoveshchensk, 675000 RUSSIA (e-mail: derbeko@mail.ru)

² Institute of Geology and Mineralogy, Siberian Division, Russian Academy of Sciences, 3, Akademika Koptyuga, Novosibirsk, 630090 RUSSIA

³ "Amurgeologia" open joint-stock company, 15, Chudinovsky, Blagoveshchensk, 675014 RUSSIA

ABSTRACT: In the southern rim of the eastern flank of the Mongol-Okhotsk orogenic belt a bimodal volcano-plutonic complex of trachybasalt-rhyolite composition was being formed 119-97 Ma ago. The occurrence of the rocks of the complex is bounded by the structures of the Anikinsky "threshold" (120 meridians) in the west of the area and by the Bureya-Jiamusi terrane in the east. The rocks are enriched in Ba, Sr and Pb at low Ta, Nb, Ti concentrations and a high value of Zr/Hf (34-52) ratio. They are characterized by quite a narrow range of isotope compositions of ⁸⁷Sr/⁸⁶Sr (0.7057-0.7065) at T_{Nd}(DM-2st)=975-1047 Ma and this may be indicative of a substantial homogeneity of a melting substratum and a crustal component of the beginning of the Late Riphean. Such characteristics bring those rocks closer to the Late Paleozoic-Early Mesozoic bimodal associations of the Central-Asian rift system. There is an assumption that the formation of the rocks is related to collision processes that resulted in the closure of the eastern flank of the Mongol-Okhotsk basin and there was also an effect of the plume source.

KEYWORDS: *bimodal complex, collision, orogenic belt*

INTRODUCTION

By the present time the models of geodynamic settings for a number of regions of the North-Asian continent combining the action of deep plumes and riftogenesis have been worked out (see. Magma types 2006). A significant part in formation of magmatic complexes accompanying riftogenesis belongs to the sources of different nature and to characteristics of the continental crust contaminated by those complexes. These very data accounted for the formation of a contrasting volcanism which is widely developed in the zone of the Central-Asian fold belt. The paper considers a bimodal volcano-plutonic complex of the end of the Late Cretaceous. It is spatially located within the continuation of the formations with similar composition which compose the Central-Asian fold belt.

GEOLOGICAL SETTING

Along the southern margin of the Mongol-Okhotsk orogenic belt (the north-western

flank of the Amur continent) the bimodal occurrences form separate volcanic fields from 2 to 180 km² (Fig. 1) within the area extended for 600 km with the width from 50 to 300 km. In the south their extent is actually bounded by the river Amur valley (Zhang Hong *et al.* 2000) and in the east by the structures of the Bureya-Jiamusi terrane. In the west they disappear at the point of the belt wedging (120 meridians) and subsequently reappear in the rim of the western branch of the Mongol-Okhotsk belt with the age of the Early MZ and older (Magma types 2006). The origin of the bimodal rock complexes in the rim of the western branch of the Mongol-Okhotsk belt is attributed to collision between the North-Asian and Sino-Korean continents (Magma types 2006).

Collision processes in this region involving large-scale intraplate processes have been completed by the beginning of the Early Cretaceous (190 Ma) by the closure of the Paleoasian ocean and a significant western part the Mongol-Okhotsk basin (Magma types 2006). In

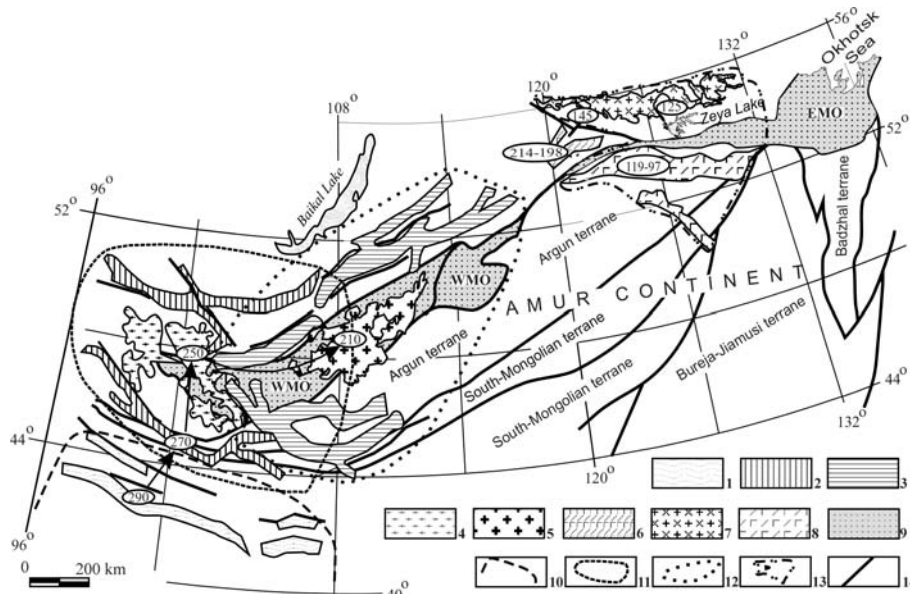


Fig.1. Structural-tectonic sketch map of volcano-plutonic complex and plutonic complex of the Late Paleozoic-Mesozoic within the rim of the Mongol-Okhotsk orogenic belt. Central Asian rift system to the west from 120° meridian, modified from Yarmolyuk et al, 2002: bimodal and alkaline-granitic rocks of the Late Carboniferous – Early Permian -1, Permian -2; bimodal basalt-comendite and alkaline granites -3; granitoids: Permian -4, Early Mesozoic -5. Collisional alkaline – moderately alkaline volcano-plutonic complexes -6. Subalkaline – normal granitoids Late Mesozoic -7. Field spread of bimodal volcano-plutonic complex of the end of the Early Cretaceous -8. Mongol-Okhotsk orogenic belt (Parfenov *et al.* 1999) -MO. Boundaries of the Mongolian Plume's projection in time: Late Carboniferous–Early Permian -10, Permian -11, Early Mesozoic -12 (from Magma types 2006), towards the end of the Early Cretaceous by authors' data -13. Tectonic contacts -14.

that time in the east within the Mongol-Okhotsk basin terrigenous rocks continued to accumulate. About 130 Ma ago continental volcano-plutonic complexes began to form: at the beginning calc-alkali andesite complexes and, then, bimodal trachybasalt – rhyolite ones in the belt's rim. A sequence of the formation of the bimodal complex's cover facies is as follows (from the bottom to the top): trachyandesite basalts, trachyandesites, tuffogenic-sedimentary rocks; rhyolites, rhyodacites, trachyrhyolites, perlites, tuffs and ignimbrites, interlayers of trachyandesites and tuffogenic sedimentary rocks; trachyandesites, andesites. The total thickness is up to 500 m. The complex comprises the bodies of the subvolcanic and vent fennel facies, and comagmatic plutonic rocks: subalkaline granites – leucogranites, granodiorites, quartz diorites, quartz monzonites.

Age

According to geochronological data obtained by Rb-Sr, U-Pb, ⁴⁰Ar/³⁹Ar methods the following sequence is revealed: trachyandesite basalts, trachyandesites -119, 115, 100, 97 Ma; rhyolites -117, 115 Ma; andesites -105.9 Ma. The age of subalkaline granites of the complex is 118 Ma (⁴⁰Ar/³⁹Ar, Sorokin & Ponomarchuk 2002). It can be said that magmatic activity (119-97 Ma) extinguished in the very beginning of the Late Cretaceous. The bimodal composition of the complex's rocks is accounted for two ranges of SiO₂ concentration: I – 52-67 wt.% - trachyandesite basalts, trachyandesites, andesites. Their high alkalinity is related to the presence of potassic feldspar, red-brown biotite in matrix and sanidine in phenocrysts. These are moderately low magnesia, moderately low titaniferous rocks with Al₂O₃=16.0-17.3 wt.% of the high potassic calc-alkali series. II - 72-78

wt.% - rhyolites, trachyrhyolites, perlites with normal, rarely, moderate alkalinity, $Al_2O_3=11.1-13.9$ wt.%, low magnesia, low titaniferous belong to the high potassic calc-alkaline series. All the varieties are enriched in LREE. In $(La/Yb)_n$ ratio the values 10-20 predominante, $(La/Sm)_n=2.9-6.0$, and the fractionation level of heavy lanthanoids is lower: $(Gd/Yb)_n=0.6-3.4$. Eu minimum in basic-medium rocks is not distinct ($Eu/Eu^*=0.70-0.86$) but in acid rocks it is deeper ($Eu/Eu^*=0.33-0.70$). By the bimodal character, A-type granitoids development and a number of geochemical features (sharp Nb, Ta, Ti minimums, and the maximums in Ba, Rb, Th, K concentrations) and also by the ratio of $Zr/Hf=34-52$ in basic and medium varieties the rocks of the complex are close to some occurrences in the western flank of the Mongol-Okhotsk orogenic belt which form a part of the North-Mongolian – West-Transbaikalian rift zone (Vorontsov *et al.* 2007). The rocks of the complex under consideration are characterized by quite a narrow range of isotope compositions at rather slight variations of $^{87}Rb/^{86}Sr$ (0.7057-0.7065) that may be indicative of an affinity of the source for petrochemically different occurrences. A relatively wide is the range of values of $\gamma_{Nd}(T)=(-0.6)-(-3.3)$ at $T_{Nd}(DM-2\sigma)=975-1047$. These data indicate that there is a substantial affinity between substratum of melting and crustal component of the beginning of the Late Riphean. It is mentioned above that there is similarity between some geochemical features of the rocks of the complex under study and that of the Late Paleozoic-Mezozoic Central-Asian rift system. On $^{87}Rb/^{86}Sr - \gamma_{Nd}(T)$ diagram the field of figurative points of this complex fits in the composition fields of the Early- Late Mesozoic intraplate magmatic rocks of the Central Asia (Fig. 2).

But still there are some differences between those rocks: the presence of rocks with normal alkalinity (they predominate in a group of acid rock varieties) in the described complex, low

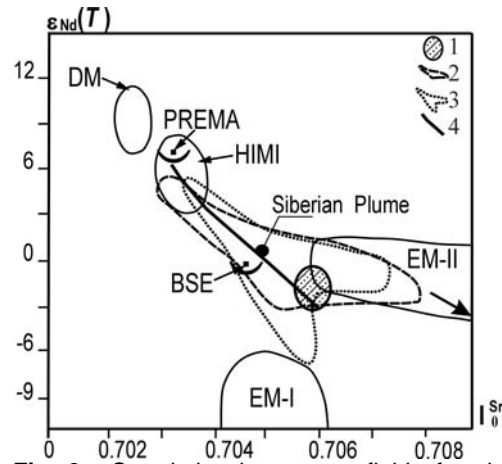


Fig. 2. Correlation between a field of rocks' compositions of the bimodal complex and the fields of intraplate magmatic rocks in the Central Asia and typical magma sources by primary isotope compositions of Sr and Nd. Fields of rocks: explore bimodal complex -1, Early Mesozoic -2 and Late Mesozoic -3 of Central Asia. Correlation trend of basalt composition of the bimodal series of the Early Mesozoic Mongol – Transbaikalian region (Yarmolyuk *et al.* 2002) -4. At drawing of the diagram we used the data from the work (Magma types, 2006). PREMA and BSE values (Zindler & Hart 1986), Siberian plume (Sharma *et al.* 1992).

concentrations of highly-charged elements such as Nb, Ta, Zr, Hf. Such features bring them closer to the products of subduction origin. The studied structures are confined to the zones of the rocks with the age of (130-120 Ma) that are compared with the products formed under subduction conditions (Gordienko *et al.* 2000). Taking into account a proximity of their ages we presume that the rocks of the bimodal complex intruded into continental crust warmed up by subduction processes and this resulted in partial mixing and inheritance of the subduction rocks' features by the occurrences of the bimodal complex.

Geodynamic model

In the west of the Mongol-Okhotsk belt the rocks of a bimodal series constitute a part of the Early Mesozoic North-Mongolian – West-Transbaikalian rift zone. For this zone a quite precise geodynamic model has been worked out (Magma types

2006). It lies in the parallel existing conditions of collisional compression and in a plume impact on a site being under the conditions of collisional compression. On the discrimination rocks of the complex in question is plotted at a direct proximity from the points determining a position of those characteristics for the Siberian plume (Sharma 1992). It is also combined with the fields of the Late Mesozoic intraplate magmatic occurrences, of the Central Asia and overlaps the lower part of a correlation trend of basalts of the bimodal series of the Late Mesozoic Mongol–Transbaikalian Region.

On the diagrams showing tectonic settings (Pearce 1996) the figurative points of acid rocks are concentrated within the fields of post-collision (syn-collision) or at the boundary of collision – intraplate conditions. For the rocks of acid - medium composition the field of the Island arcs' basalts with a shift and their partial location in the field of the continental rift basalts is determined. To establish a probability of a plume impact on the Late Mesozoic magmatic process in the region the following calculation was used (Fitton *et al.* 1997): $\epsilon_{\text{Nb}} = 1.74 + \log(\text{Nb}/\text{Y}) - \log(\text{Zr}/\text{Y})$. Positive ϵ_{Nb} values indicating an impact of the plume source are characteristic of basic-medium rocks. For the acid rock varieties ϵ_{Nb} value is (-1.4) - (1.5). The diagnostic features are also: a moderate enrichment of the rocks in LREE; ratios of $(\text{La}/\text{Sm})_n > 1.8$ and $(\text{Ce}/\text{Yb})_n > 7$ (Schilling *et al.*, 1983; LeRoe *et al.*, 1983), being 2.9-5.7 and 11.6-25.5 for basic – medium rocks, respectively.

CONCLUSIONS

119-97 Ma ago, along the south margin of the eastern flank of the Mongol-Okhotsk orogenic belt a bimodal volcano-plutonic complex of subalkaline – normal petrochemical series was being formed. At the present stage of its study one may presume that the petrochemical and geochemical characteristics of rocks are the evidence that its formation was going on under the collisional conditions at the impact of a plume source. Its impact manifested itself stronger at forming of

basic-medium rocks while at the formation of acid rocks a leading part belonged to the crustal melt sources.

REFERENCES

- FITTON, J.G. *et al.* 1997. Thermal and chemical structure of the Iceland plume. *Earth and Planetary Science Letters*, **153**, 197-208.
- GORDIENKO, I.V. *et al.* 2000. Upper Amur volcano-plutonic belt East Asia. *Geology & Geophysics*, **41**, 1655-1669.
- LE ROEX, A. P. *et al.* 1982. Ferrobasalts from the Spiess Ridge segment of the Southwest Indian Ridge. *Earth and Planetary Science Letters*, **60**, 437-451.
- Magma types and their sources in the Earth's history. 2006. Moscow: IGEM RAS.
- PARFENOV, L.M., POPEKO, L.I., & TOMURTOGOO, O. 1999. Problems of tectonics of Mongol-Okhotsk orogenic belt. *Geology of the Pacific Ocean*, **18**, 24-43.
- PEARCE, J. 1996. Sources and settings of granitic rocks. *Episodes*, **24**, 956-983.
- SCHILLING, J.-K. *et al.* 1983. Petrologic variations along the Mid-Atlantic Ridge from 29°N to 73°N. *American Journal of Science*, **283**, 510-586.
- SHARMA, M., BASU, A.R., & NESTERENKO, G.V. 1992. Temporal, Sr-, Nd- and Pb-isotopic variations in the Siberian flood basalts: implications for the plume-source characteristics. *Earth and Planetary Science Letters*, **113**, 365-381.
- SOROKIN, A.A. & PONOMARCHUK, V.A. 2002. Umlekan-Ogodzha Early Cretaceous magmatic belt: duration of magmatism. *Geochimica et Cosmochimica Acta*, **66**, 15^a, A728.
- VORONTSOV, A.A. *et al.* 2007. Sources of magmatism and geodynamics of formation of the Early Mesozoic North-Mongolian – West-Transbaikalian rift zone. *Petrology*, **15**, 37-60.
- YARMOLYUK, V.V. *et al.* 2002. Tectono-magmatic zoning, sources of magmatic rocks and geodynamics of the Early Mesozoic Mongol-Transbaikalian region. *Geotectonics*, **4**, 42-63.
- ZHANG HONG *et al.* 2000. The dynamic background of Mesozoic volcanic activity in northern part of Daxing'anling Mts. (China). *Geology of the Pacific ocean*, **19**, 109-117.
- ZINDLER, A. & HARRIS, S. 1986. Chemical geodynamics. *Annual Reviews of Earth and Planetary Science*, **14**, 493-571.

Petrographic characterization of propylitic alteration associated with porphyry Cu–Mo deposits in the Collahuasi District, Northern Chile: implications for mineral exploration

Merline Djouka-Fonkwé¹, Kurt Kyser¹, H. Alan Clark¹, J. Christopher Oates², & Christian Ihlenfeld²

¹*Department of Geological Sciences and Geological Engineering, Queen's University, Kingston, ON, K7L 3N6 CANADA (email: merlinefonkwe@geol.queensu.ca)*

²*Geochemistry Division, Anglo American plc, 20 Carlton House Terrace, London, SW1Y 5AN UNITED KINGDOM*

ABSTRACT: The Collahuasi district is a major porphyry Cu–Mo sub-province in northern Chile. Late Eocene-early Oligocene mineralization in the district involved hydrothermal alteration of the Permo-Triassic Collahuasi Group granodiorites, diorites, andesites, dacites and voluminous rhyolites, which had previously experienced regional sub-greenschist metamorphism. Hydrothermal alteration mapping represents an indispensable and effective technique in prospecting for hydrothermal deposits, but in low-grade metamorphic terrains, recognition of key minerals, particularly those associated with subtle propylitic alteration, is hampered by their resemblance to metamorphic mineral assemblages (the “green rock” dilemma). Distinguishing propylitic alteration from “background” metamorphism is also a challenge using geochemistry because petrographic criteria for recognizing subtle propylitic alteration, particularly in felsic rocks, are poorly defined. However, specific features of the petrography of outcrop mafic and felsic samples from the Collahuasi district do distinguish rocks with varying degrees of propylitic alteration, the latter representing a key boundary of the mineralizing system in porphyry Cu–Mo deposits, from background rocks that resemble propylitically altered rocks in outcrop. The mineralogical criteria, which differ for each rock type, are useful in refining the geochemical changes associated with propylitic alteration, aid in defining the location and extent of porphyry Cu–Mo systems in similar terrains.

KEYWORDS: *Collahuasi District, porphyry Cu–Mo deposit, petrography, propylitic alteration, sub-greenschist metamorphism*

INTRODUCTION

Porphyry Cu–Mo deposits and other hydrothermal deposits are commonly associated with characteristic hydrothermal alteration patterns (Lowell & Guilbert 1970) that may be far more extensive than the ore zone, thereby providing a much larger target for exploration. Consequently, identification and mapping of hydrothermal alteration have become important techniques in exploring for porphyry Cu–Mo deposits at both regional and local scales.

Mineralization-related alteration processes induce changes in mineralogical compositions as well as textural and chemical changes of the host-rocks in the environs of ore deposits, including those at depth. Distal to the deposits, the impact on the host-rocks is

subtle, and identification of the chemical changes and alteration minerals is difficult, due to their typically fine-grained nature. Moreover, in many terrains, alteration is further obscured because similar mineral assemblages may form as products of regional low-grade metamorphic processes. Methodologies that identify hydrothermally altered-rocks associated with mineralization include multispectral remote sensing (Sabins 1999) and litho-geochemistry (Urqueta *et al.* 2005). However, these methods rarely differentiate subtle hydrothermal effects, such as propylitic alteration that marks the outer boundary of the system, from regional low-grade metamorphic mineral assemblages.

This study uses microscopic observations to discriminate propylitic

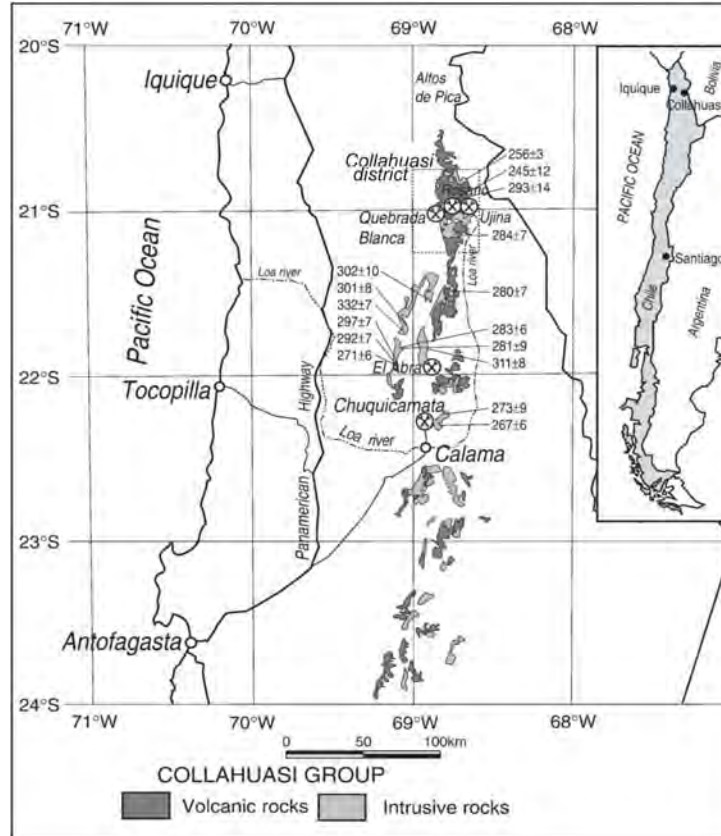


Fig. 1. Location map of the Collahuasi district (outlined) and geographic distribution of the outcrops of main igneous units of the Collahuasi Group in northern Chile. Ages for granitoids from the region are also shown (from Munizaga *et al.* 2008 and references therein).

alteration minerals from assemblages characteristic of regional very low-grade metamorphism in the porphyry Cu–Mo deposit-rich Collahuasi district of northern Chile. Propylitic alteration is normally directly associated with potassic alteration that accompanies Cu mineralization. Proper identification of propylitically-altered rocks relative to “background” regional rocks that appear to be the same in the field is therefore of value delineating of potentially fertile areas. The aim of this study is to evaluate the usefulness of petrography as an effective tool to refine exploration strategies for porphyry Cu–Mo deposits in the Collahuasi district.

GEOLOGY OF THE COLLAHUASI DISTRICT

The Collahuasi district occupies an area of 1250 km² in the Andes of northern Chile, between 20°45’S–21°07’S, 68°75’W–

68°20’W (Fig. 1). It belongs to the most important porphyry Cu–Mo belt in Chile (Maksaev *et al.* 2007). The porphyry Cu–Mo deposits are associated mainly with granodiorite to quartz monzonite plutons of late Eocene-early Oligocene age, which intruded igneous, volcanic and sedimentary rocks of the Permo-Triassic Collahuasi Group (Masterman 2003; Munizaga *et al.* 2008). The north-trending Domeyko and Loa faults bound the rocks of the Collahuasi Group. To the west, Jurassic sedimentary rocks of the Quehuita Formation and Cretaceous volcanic and sedimentary rocks of the Cerro Empexa Formation unconformably overlie the rocks of the Collahuasi Group. Voluminous Neogene ignimbrites and lavas occur in the eastern part of the district.

Prior to the hydrothermal alteration associated with mineralization in the

Collahuasi district, regional low-grade metamorphism affected most parts of northern Chile. To the west of the Collahuasi district, in the Coastal Cordillera, regional metamorphism is interpreted to be prehnite–pumpellyite to lower greenschist facies and is characterized by the epidote–chlorite–actinolite–titanite–K-feldspar–quartz–calcite–prehnite–pumpellyite association (Fuentes *et al.* 2005; Oliveros *et al.* 2006)

PETROGRAPHIC OBSERVATIONS

Petrographic observations were made on polished thin sections, for 313 outcrop samples. Average sample spacing was one sample per 1 km² within a radius of 15 km or less from the known porphyry Cu–Mo deposits, and one sample per 2 km² outside this area. Five rock types are distinguished in the district: andesites, diorites, granodiorites, dacites, rhyolites and sandstones. Rhyolites and dacites dominate in the zone of known porphyry Cu–Mo deposits. Sandstones are much less common and were not studied.

Low-Grade Regional Metamorphism

The low-grade regional metamorphism is interpreted to be sub-greenschist facies, according to the metamorphic facies definition of Turner (1981). This metamorphism is non-destructive, with preservation of primary textures. Characteristic metamorphic minerals in diorites, granodiorites and andesites are chlorite, epidote and sericite. Chlorite has a dark-green colour and replaces hornblende and biotite along grain margins. Epidote, colourless to pale-yellow, alters hornblende. Plagioclase is moderately sericitized. Calcite is observed in rare cases, mainly as veinlets. In rhyolites and dacites, the effects of greenschist metamorphism are much more subtle, with limited modification of original minerals. Sericite selectively replaces feldspars and is found as disseminations in the groundmass.

Propylitic Alteration

In diorite, granodiorite and andesites, propylitic alteration is characterized by

abundant epidote, chlorite, carbonates and albite. This propylitic assemblage is similar to the original definition of propylitic alteration, which was described in intermediate to mafic rocks (Coats 1940; Creasey 1959; Rose & Burt 1979) and propylitic alteration minerals in some key porphyry Cu deposits (e.g., Creasey 1966; Lowell & Guilbert 1970; Norman *et al.* 1991). In contrast to greenschist metamorphism in the Collahuasi district, propylitic alteration has a pervasive character wherein alteration minerals are distributed throughout the rocks with partial or total destruction of original textures. Plagioclase, are altered to aggregates of calcite, chlorite, epidote, and minor albite and sericite. Chlorite, epidote and calcite also replace hornblende and biotite, but the chlorite is light- to medium- green and the epidote pinkish- to greenish- yellow.

Propylitically-altered rhyolites and dacites are characterized by widespread aggregates of calcite disseminated in the groundmass and replacing feldspars, leading to partial to complete destruction of the rock textures. Scarce albite is also observed. In ferromagnesian deficient rocks (felsic rocks), calcite and albite are most likely to form as products of propylitic alteration, as chlorite and epidote need an Fe- and Mg-rich environment to develop. Propylitic alteration is attributed to H₂O- and CO₂-rich, low temperature (200-350°C) fluids (Reed 1997), which cannot transport the Fe and Mg necessary for the formation of chlorite and epidote when reacting with felsic rocks. Thus, the mineral assemblages of propylitic alteration are strongly related to the lithology and original mineralogical composition of the rock.

CONCLUSIONS

The diagnostic mineralogy of sub-greenschist metamorphism and propylitic alteration of altered plutonic and volcanic rocks associated with porphyry Cu–Mo deposits in the Collahuasi district is summarized in Table 1. Chlorite and epidote originating from regional meta-

Table 1. Diagnostic mineralogy of greenschist metamorphism and propylitic alteration of associated with porphyry Cu–Mo deposits in Collahuasi district.

		Diagnostic minerals for propylitic alteration	Diagnostic minerals for sub-greenschist metamorphism
Rock type	Granodiorites Diorites Andesites	Chlorite, Epidote, Carbonates, Albite	Chlorite, Epidote, Sericite, Rare carbonate veinlets
	Rhyolites Dacites	Carbonate, Albite	No carbonates Minor sericite
Mode of occurrence of the alteration minerals		Abundant and disseminated in the rock with destruction of original textures	Incipient depending on the mineral, preservation of the primary igneous textures

morphism versus propylitic alteration display different habits and colours that relate to their distinct chemical compositions. For felsic rocks in which mafic minerals are absent or rare, the mineral assemblage calcite and albite is considered as typical for propylitic alteration. The habit of carbonates, widespread and disseminated in the groundmass, is diagnostic of propylitic versus “background” alteration with the former originating from the addition of magmatic CO₂.

REFERENCES

COATS, R. 1940. Propylitization and related types of alteration on the Comstock Lode. *Economic Geology*, **35**, 1-16

CREASEY, S. C. 1959. Some phase relations in hydrothermally altered rocks of porphyry copper deposits. *Economic Geology*, **54**, 351-373.

FUENTES, F., FÉRAUD, G. AGUIRE, L., & MORATA, D. 2005. ⁴⁰Ar/³⁹Ar dating of volcanism and subsequent very low-grade metamorphism in a subsiding basin: example of the Cretaceous lava series from central Chile. *Chemical Geology*, **214**, 15-177.

LOWELL, J.D., & GUILBERT, J.M. 1970. Lateral and vertical alteration–mineralization zoning in porphyry ore deposits. *Economic Geology*, **65**, 373-408.

MAKSAEV, V., TOWNLEY, B., PALACIOS, C., &

CAMUS, F. 2007. Metallic ore deposits. In: MORENO T. & GIBBONS W. (eds.), *The Geology of Chile*. The Geological Society, London, 179-199.

MASTERMAN, G.J. 2003. *Structural and geochemical evolution of the Rosario Cu-Mo porphyry deposit and related Cu-Ag veins, Collahuasi district, northern Chile*. PhD thesis, University of Tasmania, Tasmania, Australia.

MUNIZAGA, F., MAKSAEV, V., FANNING, C.M., GIGLIO, S., YAXLEY, G., & TASSINARI, C.C.G. 2008. Late Paleozoic–Early Triassic magmatism on the western margin of Gondwana: Collahuasi area, Northern Chile. *Gondwana Research*, **13**, 407-427.

NORMAN, D.K., PARRY, W.T., & BOWMAN, J.R. 1991. Petrology and Geochemistry of Propylitic Alteration at Southwest Tintic, Utah. *Economic Geology*, **86**, 13-28.

OLIVEROS, V., FÉRAUD, G. AGUIRE, L., FORNARI, M., & MORATA, D. 2006. The Early Andean Magmatic Province (EAMP): ⁴⁰Ar/³⁹Ar dating on Mesozoic volcanic and plutonic rocks from the Coastal Cordillera, northern Chile. *Journal of Volcanology and Geothermal Research*, **157**, 31-330.

REED, M. H. 1997. Hydrothermal alteration and its relationship to ore fluid composition. In: BARNES, H.L. (ed.), *Geochemistry of hydrothermal ore deposits*, 3rd ed., J. Wiley & Sons, Inc., New York, 173-235.

ROSE, A.W. & BURT, D.M. 1979. Hydrothermal alteration. In: BARNES, H.L. (ed.), *Geochemistry of hydrothermal ore deposits*, 2nd ed., J. Wiley & Sons, Inc., New York, 173-235.

SABINS F.F. 1999. Remote sensing for mineral exploration. *Ore Geology Reviews*, **14**, 157-183.

TURNER, F.J. 1981. *Metamorphic petrology: mineralogical, field, and tectonic aspects*, 2nd ed., Hemisphere Publishing Corporation Washington New York London.

URQUETA, E., KYSER, K., CLARK, A., STANLEY, C., & OATES, C. 2005. Rosario & District Mineralization, Alteration and Geochemistry: Vectors to Ore. *22nd International Geochemical Exploration Symposium* September 19-23, 2005, Perth, Australia.

Petrologic, geochemical characteristics, and age of skarn-related granitoids at the Mactung Tungsten Deposit, Yukon, Canada

Ayalew. L. Gebru¹ & David R. Lentz¹

¹Dept. of Geology, University of New Brunswick, Fredericton, NB, E3B 5A3 CANADA (email: d835v@unb.ca)

ABSTRACT: Three granitic rocks types occur adjacent to the Mactung pyroxene skarn-related tungsten mineralization hosted by metamorphosed calcareous rocks. All the granitic rocks are peraluminous with ASI ranging from 1.05 to 1.6. Trace elements, such as Ba, Rb, Th, Sr, Ce, Zr, Nd, Pb, Rb, and La, strongly differentiate the three groups of intrusions. The biotite granite and the plagiogranite appear to have an arc-like affinity. The leucogranite depicts both S- and crustal A-type affinity. However, due to their low content of Zr, REE, and Na/Ka, and higher Rb, they may be classified as fractionated S-type granites. Ar-Ar dating of micas and U-Pb dating of zircons indicate at least two magmatic episodes at Mactung, at about 92.1 and 97.6 Ma for the younger leucogranite and the older biotite granite, respectively. The oldest and deepest intrusive phase is most intimately associated with the main stage W (Cu-Bi-Au) mineralization.

KEYWORDS: *Yukon, Mactung, Geochemistry, Geochronology, Granitoids,*

INTRODUCTION

Mactung is located in the Yukon Territory, in northwestern Canada, NE of Whitehorse, the capital of Yukon. The area is known for its large tungsten skarn deposit (33 Mt at 0.9% WO₃, using 0.5% cut-off grade). The deposit lies near the border of the Yukon and NWT, and is centred at about 63° 17' N latitude and 130° 10' W longitude.

There is general agreement on the magmatic origin of the deposit, although the role of the adjacent granite pluton in mineralization processes has been disputed. For instance, Atkinson *et al.* (1986) stated the circular Mactung leucogranitic pluton's proximity to the skarn is accidental. Selby *et al.* (2003) determined that the Mactung intrusion is a late granite (92.1± 0.2 Ma), based on dating of zircon by U-Pb methods, compared to a mineralization age of 97.5 ±0.5 Ma (Re-Os isochron age of molybdenite in quartz veins).

GEOLOGICAL SETTING

All rocks of the area belong to the sedimentary sequence of the Selwyn basin of late Proterozoic to Mississippian age (Abbott *et al.* 1986), and are on a

major NW-SE facies boundary. The sedimentary rocks have undergone low-grade regional metamorphism prior to contact metamorphism.

Supracrustal rocks at Mactung may be grouped into three major types: Upper, Middle, and Lower Metasedimentary rocks (Fig. 1). The Upper Metasedimentary rocks consist of dark limestone, chert, black shale, and conglomerate and are correlated to the Devonian-Mississippian Earn Group. The Middle Metasedimentary rocks consist of calcareous black shale, graptolitic black shale, and pelite belonging to the Due Lake Fm; dolostone (now talc-tremolite rock) and calcareous-pelites belonging to the Rabbitkettle Fm; pelites belonging to the Hess River Fm, and carbonate-rich layers belonging to the Sekwi Fm. The Lower Metasedimentary rocks belong to the Vampire Fm and are comprised of biotite schist and biotite-chlorite-muscovite schist. Tungsten ore, skarn, and calc-silicate alteration are associated with the lower carbonate layer overlying the Vampire Fm., and in an upper calcareous pelite belonging to the Rabbitkettle Fm, separated from each other by a barren 100m thick strongly hornfelsed pelite belonging to the Hess

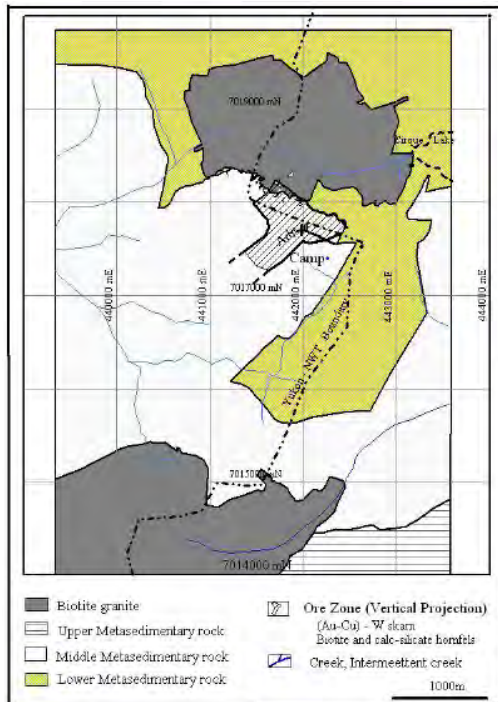


Fig. 1. Local Mactung Geology (Yukon-NWT). further south, a number of prominent aplitic dykes occur. Porphyritic granites similar in colour to that of the biotite granite, and leucogranite were intersected in drill holes. In places, these granites become richer in calcic plagioclase with lower amounts of biotite giving the rocks a lighter colour.

River Fm.

Two biotite granite stocks occur south and north of the Mactung tungsten deposit. The northern granite is porphyritic, composed of quartz, feldspar, biotite, muscovite, and tourmaline. Accessory minerals are apatite, epidote, rutile, titanite, and zircon. It is cut by a late generation of quartz veins that are typically molybdenite bearing. Quartz veinlets of 0.2-1.2cm, similar to those found in the ore zone biotite hornfels, were found in partially assimilated biotite hornfels xenoliths, near the southern contact zone of the northern granite. These xenoliths are hornfelsed and the veins in them do not cross the granite-hornfels boundary and hence are considered to be of an early generation. The southern granite is medium grained and equigranular in texture and is

mineralogically similar to the northern stock. Leucocratic granite, composed of feldspars, quartz, muscovite, tourmaline, garnet, apatite, epidote, and rare dark biotite, occurs as a smaller intrusion within the porphyritic biotite granite, dominating the peripheral part. Granitic dykes that are similar in composition to the leucocratic granite crop out to the north. In the southern part of the area, in the valley south of the camp and

GEOCHEMICAL COMPOSITION

All of the samples from the three rock types have SiO₂ greater than 68%; the highest values occurring in leucogranite (72-75%). Using the Middlemost's classification diagram, the plagiogranite plots within the granodiorite field, and the remaining intrusions plot in the granite field. Selected trace-element plots are presented in Figure 2. These plots show a scattered relationship between the leucogranite and the biotite granite and do not define coherent trends, implying they are not cogenetic. The leucogranite shows variability in the trace-element contents, possibly due to local magma interaction with host rocks, and subsequent chemical modification. Increasing muscovite and tourmaline contents close to host rocks may support this suggestion. The composition of biotite granite appears homogeneous suggesting either that there was little interaction with host rocks during emplacement or that the primary magma interacted with the country rocks, but had homogenized well prior to final emplacement and solidification.

All the rocks are peraluminous with ASI in the range of 1.05-1.1 for plagiogranite; 1.1-1.2 for porphyritic biotite granite, and 1.2-1.6 for leucogranite.

The biotite granite and the plagiogranite appear to have an arc-like I-type affinity. The leucogranite depicts both S- and crustal A-type affinity (Fig. 3a, b). However, the leucogranite has low values of Zr, REE, and Na/K, and higher Rb. Such features are characteristic of very fractionated S-type granites. Based on the Whalen *et al.* (1987) discrimination

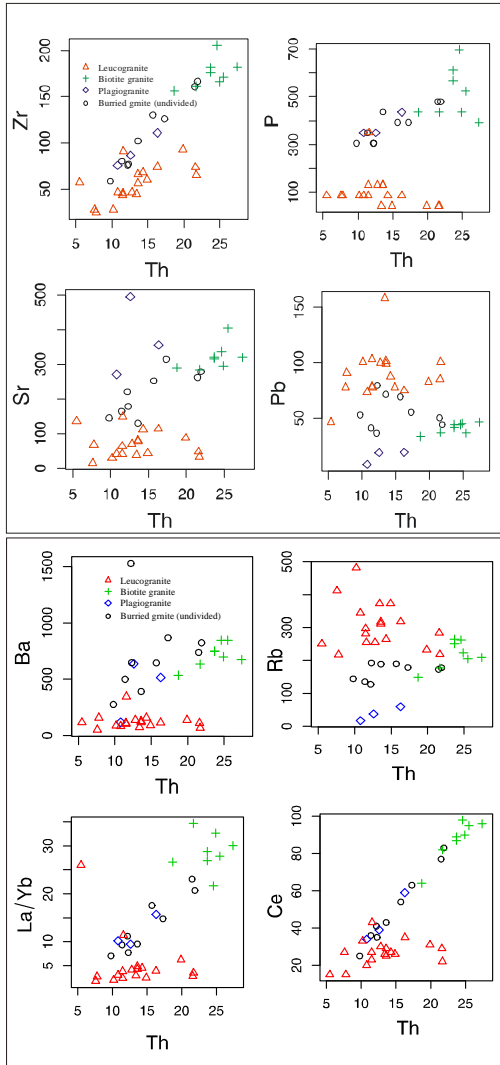


Fig. 2. Thorium variation diagram (ppm) versus selected trace-elements (ppm).

diagram (Fig. 4c, d), plots of the leucogranite entirely fall within the "I+S" field, strengthening the S-type classification of the leucogranite. The petrogenetic difference between the biotite granite and the leucogranite is also reflected in their REE composition. The average La, Ce, Nd, Sm, Eu, Tb, Yb, Lu, and Σ REE content of the leucogranite is 12.8, 26.8, 5.2, 3.2, 0.6, 0.7, 3.6, 0.6, 53.4, and that of the biotite granite is 49.5, 87.6, 25.3, 5.0, 1.3, 0.5, 1.8, 0.3, 171.1, respectively. The REE values in 0.6, 0.5, 2.0, 0.3, and 86.2 in the order plagiogranites are 23.8, 44.0, 12.0, 2.9,

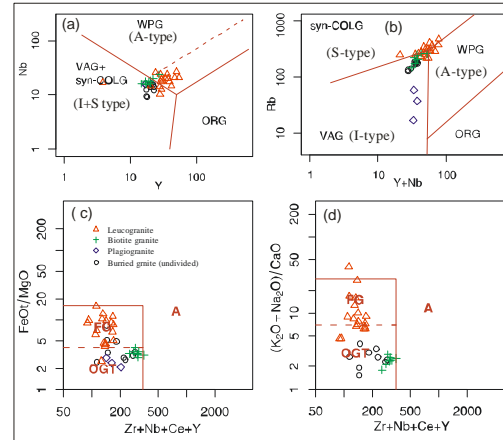


Fig. 3. Empirical geotectonic discrimination diagrams: (a, b) after Pearce *et al.* (1984); (c, d) after Whalen *et al.* (1987)

above. REE values of the biotite granite suggest a possible continental crust magma derivation.

Based on zircon saturation geothermometry, the plagiogranite formed near a liquidus of about 740°C; porphyritic biotite granite from a melt of 800°C, and leucogranite from a melt of 720°C. Pressure for the emplacement of granitoids of Mactung maybe deduced from the skarn minerals. Analysis of sphalerite co-existing with pyrrhotite and pyrite using SEM-EDS for S, Cd, Mn, Fe and Zn at the UNB laboratory gave 33.26, 1, 0.54, 10.3, and 54.32 %, respectively. This amounts to about 18.04 mole% FeS in sphalerite yielding a pressure estimate of about 2kb.

GEOCHRONOLOGY

Mineral grains of biotite and muscovite were separated from ten samples representing biotite granite, leucogranite, aplitic dyke, granite dyke, biotite hornfels, amphibole-pyroxene skarn, and biotite schist (Vampire Fm), lower ore zone biotite, and pyrrhotite-bearing skarn. They were age dated using the Ar-Ar method at the University of Toronto. Five granitic samples were later dated using U-Pb on zircons at University of British Columbia.. Summary of the estimated ages are given in Table 1.

Interaction between late-stage alteration processes, possibly related to the

Table 1. Ar-Ar and U-Pb age dates for Mactung granitoids

Lithology	Easting (m)	Northing (m)	Ar-Ar age (Ma)	U-Pb age (Ma)
Aplitic dyke	441501	7015976	94.0±0.5Ma (bt)	97.2 ± 0.2
Granitic dike	442733	7017826	92.9±0.4 Ma (mu) 95.3±0.4Ma (mu)	97.1 ± 0.3
Biotite granite	440026	7015106	-	97.2 ± 0.2
Biotite granite	442806	7018033	95.6 ±0.3Ma (mu) 94.0±0.3Ma (bt) 91.8±0.4 Ma (bt)	97.1 ± 0.1
Leucogranite	442806	7018033	93.3±1.2Ma (mu)	*92.1 ± 0.2
Biotite granite (near skarn)	441839	7018089	98.1±2 Ma (mu) 95.1 ±0.8 Ma (bt)	97.6 ± 0.2
Biotite hornfels	441889	7018110	97.1±1.9Ma (bi)	-
Amph-Pxn skarn	441910	7018082	127±20 Ma (Amph with pxn core)	127.1 20
Biotite schist (Vampire Fm):	441979	7017724	95.7±0.4 Ma (bt)	-
Biotite bearing skarn (Ore zone)	442117	7017731	90.7±3.1 Ma (bt)	-

* Interpreted from Selby *et al.* (2003)

leucogranite magmatic episode, and biotite granite is evident from occurrence of distinct plateaus of at least two important ages; for instance in felsic granitic dyke (MAC-165), based on muscovite grains step heating, two plateaus of low and high temperatures, representing corresponding ages of 92.9 ± 0.4 Ma and 95.3 ± 0.4 Ma, are recognized. This sample was seen to contain biotite richer portions in the field. U-Pb age dating on zircons also revealed an older age attributable to biotite granite. Overprinting of similar younger age is seen in biotite crystals from biotite granite, where a lower age of 91.8 ± 0.4 Ma indicates resetting until the cessation of plutonism. Another observable feature of the Ar-Ar dating is the closeness between biotite ages of biotite granite and biotite hornfels. Zircon grains separated from two samples of the biotite granite near the contact and away from the contact gave U-Pb dates of 97.6 ± 0.2 and 97.1 ± 0.1 Ma, respectively.

CONCLUSIONS

(1) Based on the geochemistry and age dating of the granitoids, at least two episodes of magmatism of different sources are evident at Mactung: the first episode, possibly from the melting of the crust, formed the biotite granite – the main

intrusion near the skarn and further south. The second episode resulted in the emplacement of leucogranite peripheral to the biotite granite and probably originated from the fusion of sediments followed by extensive crystal fractionation.

(2) The biotite granite is similar in age and composition to those of the Tungsten suite intrusions of the Nahanni area, including that of the Cantung Granite, the causative intrusion for tungsten mineralization at Cantung. The leucogranite is similar in age to those of the youngest part of the Tombstone suite, lying northwest of Mactung and those occurring all the way into Alaska. These granite types are known for porphyry-type gold (W-Mo).

(3) Based on these new results, the U-Pb ages of 92.1 ± 0.2 Ma determined by Selby *et al.* (2003) represents the latest magmatic episode (leucogranite) instead of the main ore-forming magmatic episode (biotite granite). The 97.5 ± 0.5 Ma Re-Os age dates on molybdenite determined by Selby *et al.* (2003) are identical to our U-Pb age dating on zircon crystals of porphyritic biotite granite, which is the main intrusion phase at Mactung, linked to W (Cu-Bi-Au) skarn. However, mineralizing fluids began separating during emplacement of this deeper coarsely porphyritic granite, based on the mineralized breccia fragments locally hosted by this granite and associated dykes.

ACKNOWLEDGEMENTS

We thank NA Tungsten Corp. for covering field work expenses, and for permission to carry out this research on its property. Argon-Argon dating of biotite and U-Pb dating of zircons were possible through the generous grants of the Geological Surveys of the Yukon and North West Territories.

REFERENCES

ABBOT J.G., GORDEY, S.P., & Templeman-Kluit, D.J. 1986. Setting of stratiform, sediment hosted lead zinc deposits in Yukon and northeastern British Columbia, In: MORIN, J.A. (ed.), *Mineral Deposits of the Northern Cordillera*. Canadian Institute of Mining and

- Metallurgy Special Volume **37**, 1-18.
- ATKINSON, D. & BAKER, D.J. 1986. Recent developments in the geologic understanding of Mactung, In: MORIN, J.A. (ed.), *Mineral Deposits of the Northern Cordillera*. Canadian Institute of Mining and Metallurgy Special **37**, 234-244.
- PEARCE, J., HARRIS, N.B.W., & TINDLE, A.D. 1984. Trace element discrimination diagrams for the tectonic interpretation of granitic rocks. *Journal of Petrology*, **25**, 956-983.
- SELBY, D., CREASER, R.A., HEAMAN, L.M., & HART, C.J.R. 2003. Re-Os and U-Pb Geochronology of the Clear Creek, Dublin Gulch, and Mactung Deposits, Tombstone Gold Belt, Yukon, Canada: absolute timing relationships between plutonism and mineralization. *Canadian Journal of Earth Science*, **40**, 1839-1852.
- WHALEN, J.B., CURRIE, K.L., & CHAPPELL, B.W. 1987. A-type granites: geochemical characteristics, discrimination and petrogenesis. *Contributions to Mineralogy and Petrology*, **95**, 407-419.

Use of micro-XRF in the characterization of hydrothermal alteration: application to the subaqueous felsic dome-flow complex of the Cap d'Ours segment of the Glenwood rhyolite, Rouyn-Noranda, Québec

Dominique Genna^{1,2}, Damien Gaboury^{1,2}, Lyndsay Moore¹, & Wulf Mueller¹

¹ Université du Québec à Chicoutimi (UQAC), ² Laboratoire de métallogénie expérimentale et quantitative (LAMEQ) 555, boul. de l'Université, Chicoutimi, QC, G7H 2B1 CANADA (e-mail: dominique.genna@uqac.ca)

ABSTRACT: Hydrothermal alteration is important in the vectoring of mineralization in volcanic terrains. However, geochemical analyses of these alterations are often based on bulk rock analyses and are unrepresentative. For example, in the context of a subaqueous felsic dome-flow complex such as those found in the Abitibi greenstone belt, the breccia facies is omnipresent and the glassy matrix, more porous than the fragments, better records the passage of hydrothermal fluids. The development of a new analytical methodology using micro-XRF enables separate studies of alteration of the matrix versus the fragments with respect to major element composition. Twelve elements are mapped on windows considered sufficiently homogenous and representative of each sample. An average is then calculated for the analyzed area and yields a nearly complete analysis (with the exception of loss on ignition). In the field, a sufficiently uniform sampling mesh allows the determination of spatial distribution of alteration. The application of this method has been tested successfully on samples from the Cap d'Ours complex of the Glenwood rhyolite in the Rouyn-Noranda region of Québec. The use of micro-XRF offers new perspectives in the treatment of hydrothermal alteration such as variations of chemical elements in minerals, calculation of normative minerals on homogeneous areas and mapping of compositional zonation in minerals.

KEYWORDS: *hydrothermal alteration, Micro-XRF, volcanogenic mineralization, felsic complex, Blake River Group*

INTRODUCTION

The study of hydrothermal alteration is of major interest in the understanding and subsequent exploration of volcanogenic mineralizing systems and, therefore, is relatively well documented (Franklin *et al.* 2005). Bulk analytical methods to characterize the alteration, such as X-ray fluorescence, are fairly effective for homogeneous rock samples. However, in volcanic complexes where alteration is heterogeneous (such as volcanic breccias), it becomes important to analyze fragments and matrix separately because of differing porosities. This is especially problematic in subaqueous felsic dome-flow complexes, which have a strong economic potential for volcanogenic massive sulphide deposits, where brecciated facies are omnipresent. It is to account for such problems that the proposed method was developed.

GEOLOGICAL PARAMETERS

Regional Geology

The field area selected for the development of this methodology was the Cap d'Ours segment of the Glenwood rhyolite, located in the Blake River Group (BRG) in the Abitibi greenstone belt. Pearson & Daigneault (2009) interpret the BRG as the result of a large complex of nested and sequential calderas, which correspond to the successive collapses of the Misema, New Senator and Noranda calderas (Fig. 1).

Local Geology

The Cap d'Ours is largely composed of fragmentary Filla rhyolitic lavas and forms the eastern boundary of the Glenwood rhyolite at the south-eastern margin of the New Senator caldera (Fig. 1). Field work conducted during the summer of 2008 led to the interpretation of the Cap d'Ours as remnants of a subaqueous felsic dome-

flow complex (Fig. 2). The abundance of brecciated facies, the favourability of type FIIIa rhyolites for VMS mineralization (Gaboury & Pearson 2009), disseminated mineralization (fine pyrite replacement +/- chalcopyrite and trace gold), hydrothermal alteration and the low degree of deformation and metamorphism (sub-greenschist) of the study area provide an ideal environment to conduct this newly proposed analytical technique on hydrothermally altered volcanic rocks.

METHODOLOGY

Hydrothermal alteration of the Cap d'Ours is typified by silica, chlorite, sericite, epidote and carbonate phases. In order to quantify the intensity of alteration within the volcanic edifice, a new approach was adopted for both sampling and analyses.

The increased porosity of the matrix of the brecciated facies facilitated circulation of hydrothermal fluids and recorded a much better expression of hydrothermal alteration, necessitating separate analyses of both matrix and fragments for each sample. The composition of the rhyolitic fragments is relatively constant for both major and trace elements and is the least altered material. Sampling at 50 m intervals provided a mesh sufficiently uniform to be representative. Fragments and matrix were collected for all breccias sampled.

Geochemical analyses were conducted on unpolished thin sections 30 μm thick using micro-XRF – EDAC Eagle III mapping at the l'Université du Québec à Chicoutimi (UQAC). Use of the micro-XRF permits analyses of major element compositions with a relatively fast, non-destructive, *in situ* method through points or maps. The parameters (Table 1) were selected in order to optimize the speed and quality of the results on the basis of micro-probe analyses of chlorite.

Over 160 analyses were conducted using 58 thin sections. Twelve elements were mapped on a minimum of three areas per thin section. The windows of analysis correspond to areas of 64 x 50 pixels (1.7 x 1.3 mm) and were considered sufficiently homogeneous to be representative of the sample. The composition was determined using a time analysis of 800 ms per pixel and an average was calculated using the area analyzed. The method provides a nearly complete chemical analysis, with the exception of loss on ignition.

Table 1. Micro-XRF analysis parameters.	
Map size	64 x 50 pixels (1.7 x 1.3 mm)
Limit - kV	20
μA	200
Dwell (time/point)	800

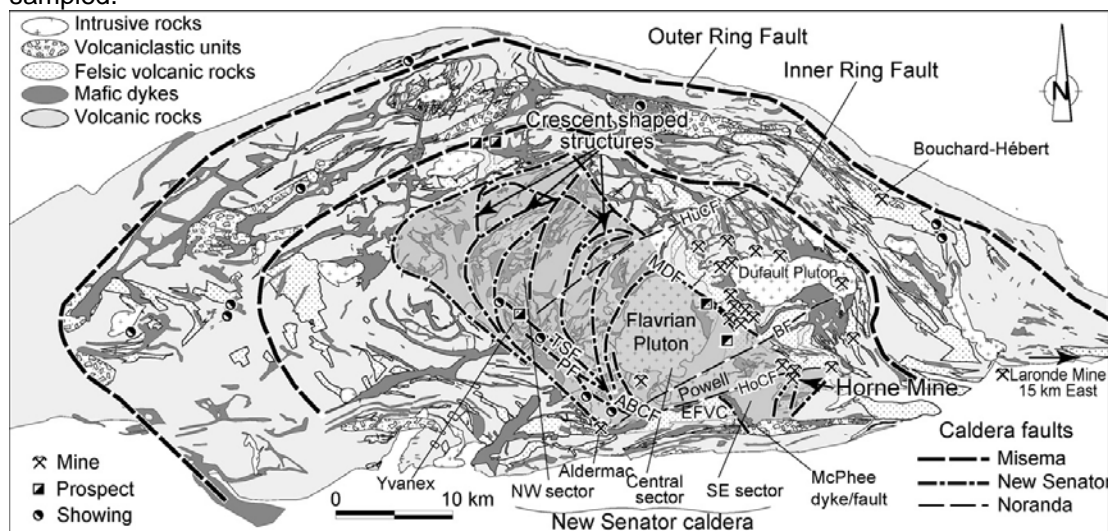


Fig. 1. Structure and geometry of the Blake River megacaldera complex (modified from Pearson & Daigneault 2009). The Cap d'Ours area is located 2km south of the VMS Horne Mine.

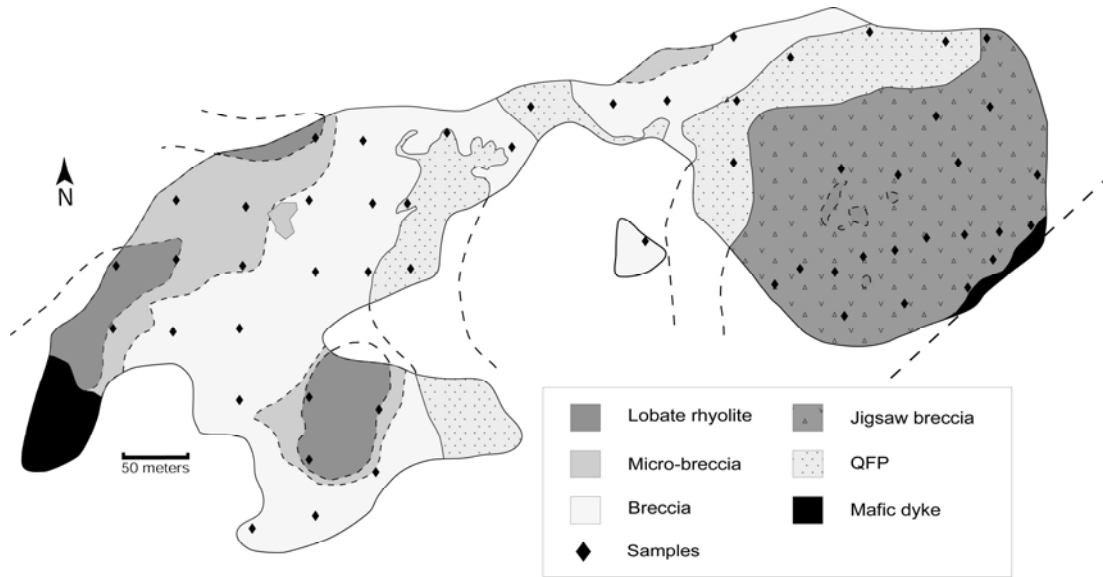


Fig. 2. Interpretative volcanic facies mapping of the Cap d'Ours segment of the Glenwood rhyolite (Genna & Moore 2008).

RESULTS

Sampling at 50 m intervals provided a sufficiently uniform mesh to represent the spatial zonation of the hydrothermal alteration of the Cap d'Ours. The mass balance calculations (not presented here) are used to highlight a leaching of MgO, Na₂O and SiO₂ in the eastern part of the complex, while the west is more enriched in these elements. Figure 5 illustrates the distribution of SiO₂ and shows a significant silicification of the glassy matrix in the west part of the outcrop, proximal to the inferred vent of the complex. An increase in alteration can also be correlated with proximity to mineralized zones.

In addition to micro-XRF analyses, 13 samples were analyzed by X-Ray Fluorescence (XRF) (ALS Chemex) to compare major element results. Although some discrepancies were observed, the difference between XRF and micro-XRF was relatively consistent and it is therefore possible to establish a correction factor for each element.

The range of possible uses for micro-XRF in application to the analysis of hydrothermal alteration is significant: elemental variations in minerals (e.g., Fe and Mg in chlorite), calculation of

normative minerals in a homogeneous area, mapping the compositional zonation of minerals, etc.

CONCLUSIONS: ADVANTAGES AND LIMITS

Application of this method within the Cap d'Ours segment of the Glenwood rhyolite has identified distinct distributions of alteration associated with a low-temperature hydrothermal system. The ability of this method to detect diffuse alteration will make micro-XRF analyses a powerful tool in exploration.

Advantages: 1) consistent and valid results despite a semi-quantitative

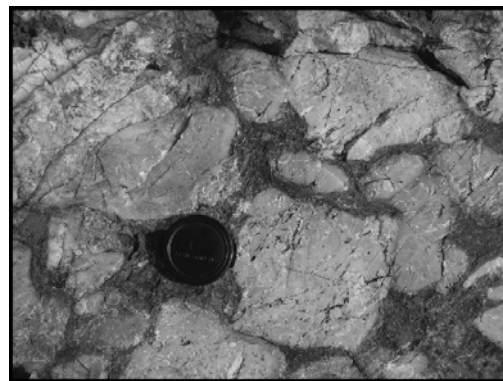


Fig. 3. Photograph of brecciated facies of the Cap d'Ours (lens cap is 43 mm).

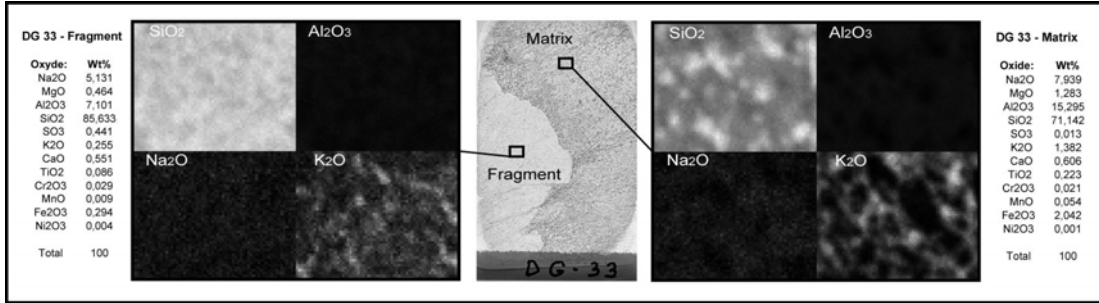


Fig. 4. Example of elemental mapping of both fragments and matrix with average composition of analyzed areas at left and right margins, respectively.

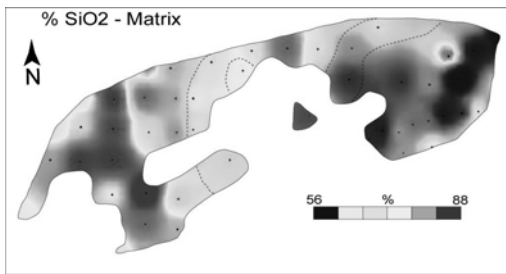


Fig. 5. Distribution of SiO₂ in glassy matrix.

method; 2) direct link between mineralogy, texture and chemical composition; 3) fast acquisition and data processing with low-cost analysis.

Limitations: 1) uniformity and representativeness of the analyzed area; 2) quantification of light elements (e.g. Mg); and 3) inability to obtain levels of

volatiles. These limitations can be overcome easily by dedicated calibrations, optimization of the analytical window size and normative mineral calculations for volatile estimation.

REFERENCES

- FRANKLIN, J.M., GIBSON, H.L., JONASSON, I.R., & GALLEY, A.G. 2005. Volcanic Massive Sulfide Deposits. *Society of Economic Geology – 100th Anniversary Volume*, 523-560.
- GABOURY, D. & PEARSON, V. 2008. Rhyolite geochemical signatures and association with volcanogenic massive sulfide deposits: Examples from the Abitibi belt, Canada. *Economic Geology*, **103**, 1531-1562.
- PEARSON, V. & DAIGNEAULT, R. 2009. An Archean megacaldera complex: The Blake River Group, Abitibi greenstone belt. *Precambrian Research*, **168**, 66-82.

Regional rock geochemistry of the Leninogorsk and Zyryanovsk VMS region (Rudny Altay Kazakhstan) - implications for genesis and exploration

I. Goldberg¹, G. Abramson¹, V. Los², V. Nazarov³, & C. Haslam⁴

¹Interresources Pty Ltd, Level 2, 49-51 York Street, Sydney, NSW 2000 AUSTRALIA
(e-mail: igoldberg@allegiance-mining.com.au)

²Academy of Mineral Resources, Nazyrbaya Batyra, 146/11, Almaty KAZAKHSTAN
³JSC "Kazzinc", Promyshlennaya, 1, Ust-Kamenogorsk KAZAKHSTAN

⁴Trident Energy Ltd, Suite 3, Level 15 Wawkner Centre, 449 St. Kilda Rd Vic 3004

ABSTRACT: The Rudny Altay VMS province extends over 500 km along the north-eastern border of Kazakhstan. The deposits are now largely depleted and this aim, the "Kazzinc" has commenced exploration work based on IONEX technology, which involves mapping of polar geochemical systems. The work is being conducted in several stages, the first stage include 20,000 km² a regional geochemical survey (5 x 5 km) in Leninogorsk and Zyryanovsk ore regions, which are content the main resources in Rudny Altay. Geochemical survey has shown, that all deposits are localised into enrichment zones of ore forming elements (nuclear systems). Depletion zones of these metals have been identified on the periphery of the enrichment zones. The sizes of the Leninogorsk geochemical system constitutes 8000 km², and Zyryanovsk system – 6000 km². Titanium is formed enrichment zones on the external boundaries of the nuclei of these systems. The formation of such systems is associated with the huge-scale mobilization metals from rocks. These studies have shown that, with IONEX technology, indentifying and then appraising geochemical systems is a first step in regional mineral exploration. In the case of the Leninogorsk and Zyryanovsk regions this technology has enabled to reduce the area for further exploration by about 80%

KEYWORDS: *geochemistry, Rudny Altai, depletion, enrichment, anomaly*

INTRODUCTION

The Rudny Altay pyrite-polymetallic province (VMS deposits) which includes the Leninogorsk and Zyryanovsk ore regions, located along the north-eastern border of Kazakhstan (Fig 1). Total reserves Zn, Pb and Cu in of the Leninogorsk and Zyryanovsk ore regions sums to 43 million tonnes of metals. The deposits are now largely depleted and this aim, the "Kazzinc" has commenced exploration work in the Leninogorsk and Zyryanovsk ore regions using IONEX technology. (Goldberg et al., 2003, Goldberg et al., 2007). The work is being conducted in several stages. The first stage included a regional geochemical survey on area of 20 000 km², scale - 1:500,000 (5X5 km) with sampling, including 800 rock samples. It is the first time that a geochemical survey has been carried out in Rudny Altay on such a

scale. Based on these data, the following aspects are discussed: geochemical pattern of zinc and titanium distribution, the source of the metals, and the criteria of evaluation of potential areas.

THE GENERAL GEOLOGICAL SETTING

The Rudny-Altay volcanic arc is a Devonian bimodal suite of volcanic rocks. The Rudny Altay Block is separated by the Irtysh dip-sited shear zone on the west from Kalba and the North-Eastern shear zone on the East from Gorny Altay (Fig1). Down to a depth of about ten kilometres the territory of the region has a distinct two-layer structure. The lower layer (S₂-D₁) consists of highly dislocated and metamorphosed sandstones and greenschist rocks. Higher up lie the rocks of the upper layer. It is presented volcanogenic-sedimentary formation (D₁-D₃). The main deposits are linked spatially

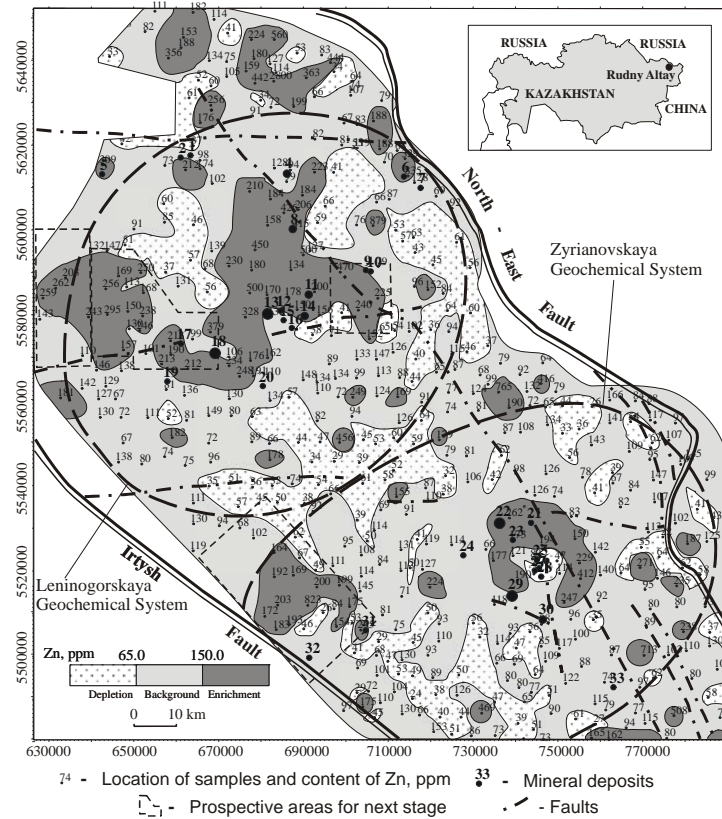


Fig. 1. Distribution of Zn in rock in in Leninogorsk and Zyryanovsk regions.

to this formation. The youngest rocks consist of carbonate-terrigenous deposits (D_3-C_1), rocks of gabbro-granodiorite-granite formation (C_2-C_3) and granites (P_1). The total area formed by granites is approximately 30%. Quaternary deposits cover approximately one third of the area.

THE GEOCHEMICAL SYSTEMS OF THE LENINOGORSH AND ZYRYANOVSK ORE REGIONS

The analysis of rock samples was conducted in the chemical laboratory in Ust-Kamenogorsk, Kazakhstan. by inductively coupled plasma mass spectrometry, and the equipment used was an ELAN-6100 (US) mass spectrometer. In the present abstract the distribution of two elements: zinc (as the basic ore-forming element) and titanium (of the siderophile element) is examined. The sensitivity of the analysis is 5 ppm for Zn and 0.05% for Ti. The analytical results for Zn and Ti are presented on contoured

maps at scale of 1:500,000. The contour intervals used for each element were based on the statistical cumulative graphs of distribution (Figs. 1 and 2).

Distribution of Zn, (Fig.1)

The distribution of zinc over the area is characterised by considerable heterogeneity. Anomalous concentrations of Zn (enrichment and depletion zones) cover approximately 35% of the study area.

Enrichment zones: within the study area there are several enrichment zones: two, Leninogorsk and Zyryanovsk, contain most of the know VMS deposits. Both are proximal to intersection of major regional fault. In Leninogorsk ore region the total area of the enrichment zone is approximately 2,400 km². In the Zyryanovsk region area of enrichment is approximately 1,300 km².

Depletion zones: In the Leninogorsk region the depletion zones are located

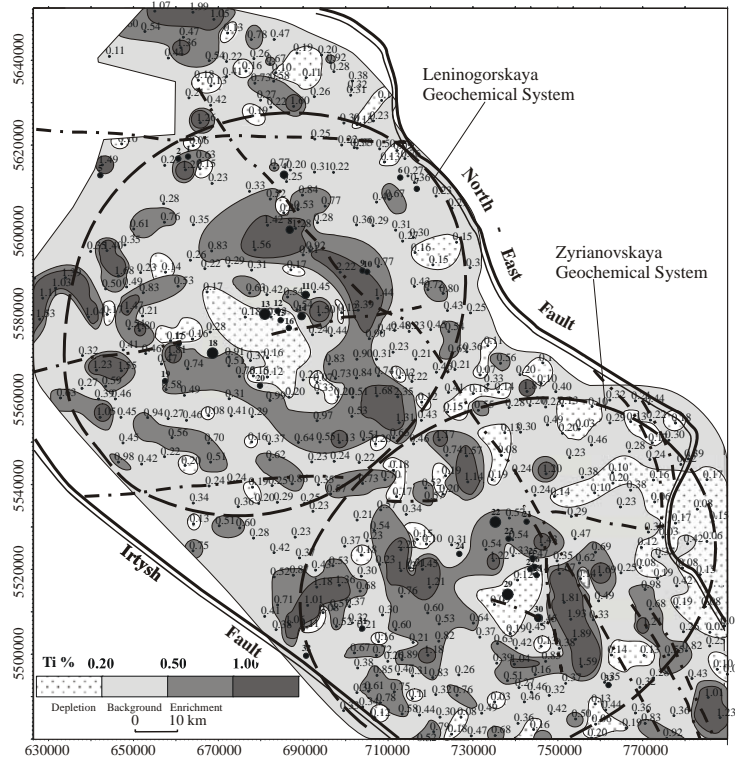


Fig. 2. Distribution of Ti. in rock in in Leninogorsk and Zyryanovsk regions (see Fig.1).

around the enrichment zones. To the north and north-east they are immediately contiguous, while to the south-east and south they are situated at a distance of 10-20 km, forming a semicircle around the central enrichment zone. The total area of depletion in this region is approximately 2,400 km².

In the Zyryanovsk region the depletion zones are located primarily in the form of individual anomalous areas 10-20 km wide surrounding the enrichment zone to the south-west and north-east. They are situated at a distance of approximately 10 km from the enrichment zone, essentially forming a ring-like structure. The total area of depletion is 1,300 km².

Distribution of Ti (Fig. 2)

In the Leninogorsk ore region the main titanium enrichment zone forms a horsehoe-shaped anomaly around the zinc enrichment zones. The size of the internal area is about 900 km². At its centre there is a depletion zone of 450

km². The majority of deposits are inside this zone or on its periphery.

The diameter of this external ring-like structure centered round the main group of deposits of the Leninogorsk region is 80-90 km.

To the west of this ring-like structure, on the boundary of the area, there are several enrichment local anomalies of Ti around enrichment zones of Zn and Pb. In the Zyryanovsk region all the main deposits, are surrounded by a ring-shaped zone of Ti enrichment of 5-10 km in width. The internal part of the area of the ring-like anomaly mainly comprises a depletion zone of about 150 km².

CONCLUSIONS

1. Implication for ore genesis

This regional-scale geochemical survey has defined two main polar geochemical systems: the Leninogorsk and Zyryanovsk. The main VMS deposits are localised in zones of enrichment of the ore-forming elements. The depletion zones of the ore-forming elements

surround the enrichment zones. The geochemical ore systems have a shape close to isometric. The area of the Leninogorsk system is approximately of 8000 km² and the Zyryanovsk system - about 6000 km². The enrichment zones of Ti define the external borders of the nuclei of these systems.

The geochemical data shows that: 1. The main enrichment zones coincide with rocks of the volcanogenic-sedimentary sequence (D₁-D₃) which are the host all of the VMS deposits. However, the enrichment zone of ore forming elements also represented in younger rocks, including P₁. 2. An enormous redistribution of the ore forming elements throughout the regional rock mass, including post-Devonian rock.

2. Implication for exploration

These studies have shown that, with IONEX technology, indentifying and then appraising geochemical systems is a natural first step in regional mineral exploration. If a number of geochemical systems are defined, the quantum of metal depletion in the depletion zones is the key parameter in allocating priority among those geochemical systems. In second phase of exploration a closer

sample spacing is employed over only the enrichment zone of the selected geochemical system, as such systems are fractal.

In the case of the Leninogorsk and Zyryanovsk regions this technology has enabled the client to reduce the area for further exploration by about 80%

REFERENCES

- GOLDBERG, I.S., ABRAMSON, G.J., & LOS, V.L. 2003. Depletion and enrichment of primary haloes: their importance in the genesis of and exploration for mineral deposits: *Geochemistry, Exploration, Environment, Analysis*, **3**, 281-293.
- GOLDBERG, I.S., ABRAMSON, G.J., HASLAM C.O., & LOS, V.L. 2007. Depletion and enrichment zones in the Bendigo Gold Field: a possible source of gold and implications for exploration. *Economic Geology*, **102**, 745-753.
- POPOV V.V., STUCHEVSKY N.I., & DEMIN, U.I. 1995. *Polymetallic ore deposits of Rudny Altai, Moscow*, 420 p. (In Russian).
- SHERBA, G.N. 1983. Polymetallic massive sulfide deposits of Rudny Altai. In: IVANOV, S.N. (ed.), *Massive sulphide deposits of the USSR*: Moscow, Nauka Publishing House, 87-148 (In Russian).
- SMIRNOV V.I. (edited). 1977, *Ore Deposits of the USSR*, **2**, Pitman Publishing, London, San Francisco.

Geochemistry and tectonics as an exploration tool for Circum-Pacific porphyry copper, gold, and molybdenum deposits: evidence from the Baguio District, Philippines

Pete Hollings¹ & David R. Cooke²

¹Geology Department, Lakehead University, 955 Oliver Rd, Thunder Bay, ON, P7B 5E1 CANADA
(e-mail: peter.hollings@lakeheadu.ca)

²CODES, The Australian Research Council's Centre for Excellence in Ore Deposits, University of Tasmania, Private Bag 79, Hobart, 7001, Tasmania AUSTRALIA

ABSTRACT: Pliocene and Pleistocene magmatic rocks of the Baguio District, Philippines, that are spatially and temporally associated with mineralisation can be broadly subdivided into an intermediate to felsic suite of mineralised low- to medium-K intrusions, some of which have adakitic affinities, and a suite of mafic to intermediate, medium-K to shoshonitic hornblende-phyric dykes. The geochemical and isotopic characteristics of the dykes are consistent with primitive mantle-derived melts that underwent minimal crustal contamination as they ascended through the arc crust. In contrast, the intermediate to felsic suite has been contaminated by young arc crust, suggesting ponding and fractionation within shallow-crustal magma chambers. Eastward-directed subduction of the Scarborough Ridge along the Manila Trench is associated with flattening of the downgoing slab. Magmas generated from the downgoing ridge can account for the isotopic recharge of the Pliocene sub-arc mantle, as well as the generation of the primitive melts and adakitic rocks found within the Baguio District. The interaction between primitive mafic melts and the more felsic calc alkaline rocks has generated fertile magmas that were highly productive for porphyry copper and epithermal gold mineralization.

KEYWORDS: *Porphyry Cu-Au, Philippines, Ridge subduction, adakites*

INTRODUCTION

The circum-Pacific region hosts spectacular examples of porphyry Cu-Au, Cu-Mo, and related epithermal Au-Ag deposits. The Andean margin of South America contains some of the world's largest porphyry Cu-Mo deposits, and also some significant Cu-Au systems. Giant Cu-Mo systems also characterise SW USA and NW Mexico. The SW Pacific region is well-endowed with porphyry Cu-Au deposits. Tertiary or Quaternary oceanic island arcs host porphyry systems in the Philippines, Indonesia, and PNG. Significant Cu-Au porphyries also occur in Alaska, Canada, and Central America. Some segments of the Pacific rim are poorly endowed with porphyry deposits (e.g., New Zealand, Japan), but do contain important epithermal gold deposits. The ore deposits are most commonly associated with calc-alkalic magmatism. Cu-Au porphyry intrusions can be low-K (e.g., Batu Hijau, Indonesia),

medium-K (e.g., Baguio, Philippines), high-K (e.g., Grasberg, Indonesia) or alkalic in composition (e.g., Galore Creek, British Columbia).

Most of the youngest porphyries in the circum-Pacific region (e.g., Baguio and Mankayan districts, Philippines; Ok Tedi and Grasberg, New Guinea; El Teniente and Rio Blanco, Chile) have been exposed in arc segments that have undergone rapid uplift and exhumation. It has also been demonstrated that in the last 20 m.y., the formation of giant porphyry copper-molybdenum and copper-gold deposits in the circum-Pacific region has been closely associated with subduction of aseismic ridges and seamount chains, and (or) collision with oceanic plateaus beneath oceanic island and continental arcs (e.g., porphyry Cu-Mo deposits in central Chile, Cu-Au porphyries and giant high sulfidation deposits in northern Peru and Central America; porphyry and epithermal

deposits in northern Philippines; Cooke *et al.* 2005).

Studies of the host rocks to giant porphyry copper deposits in Central and Northern Chile have shown that there are recognizable changes in the geochemistry of the volcanic rocks prior to mineralizing events (Skewes & Stern 1995; Kay *et al.* 1999; Hollings *et al.* 2005). These include abrupt increases in the La/Yb ratios of volcanic rocks associated with mineralization, which have been interpreted to indicate a rapid change in the tectonic environment, likely associated with the subduction of an aseismic ridge. This study investigates those relationships in the island arc system of the Philippines.

THE BAGUIO DISTRICT

The Baguio District of the Philippines represents a complex tectonic setting sandwiched between two oppositely dipping subduction zones and associated with the subduction of the Scarborough Ridge (Fig. 1). The district is located in the Central Cordillera of Luzon within the Western Luzon arc. It records the evolution from Cretaceous - Eocene marginal basin sedimentation and volcanism, to shallow marine sedimentation, followed by construction of a calc-alkaline magmatic arc above the Manila Trench in the Middle Miocene. The Northern Luzon segment of the archipelago has experienced seamount subduction/obduction, collision, arc-flipping and ophiolite emplacement since the Cretaceous. The district represents one of the world's premier mineral provinces with >35 million ounces of gold and 2.7 million tonnes of copper contained in epithermal (e.g., Antamok; Sawkins *et al.*, 1979; Acupan, Cooke *et al.*, 1996), porphyry (e.g., Santo Tomas II; Imai 2001) and skarn resources (e.g., Thanksgiving; Callow 1967). The Mankayan district, approximately 70 km to the north, contains an additional 37 million ounces of Au and 8 Mt Cu in porphyry and epithermal deposits that formed at the same time as those in the Baguio district (Chang *et al.* submitted), highlighting the extraordinary fertility of this part of northern Luzon.

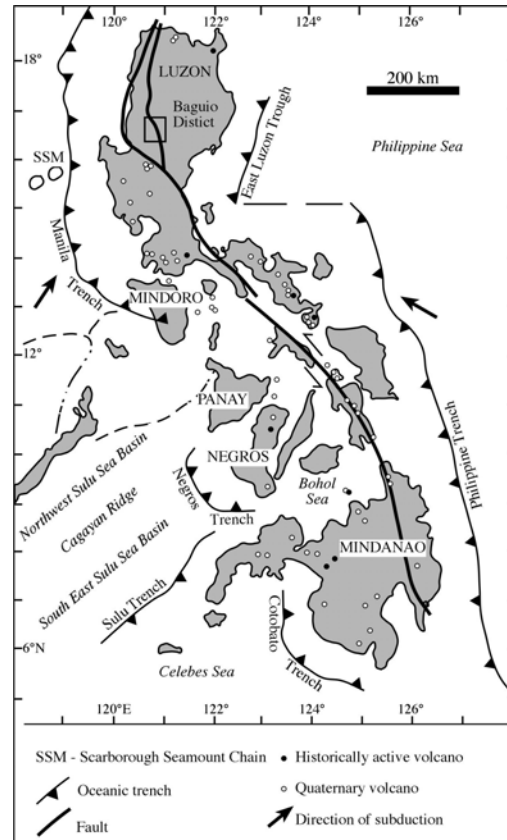


Fig. 1. Map of the Philippines showing submarine trenches, Philippine Fault and relative motion of Philippine and Eurasian plates (arrow). Solid circle = historically active volcano, open circle = Quaternary volcano. Modified after Mitchell and Leach (1991).

The Miocene stratigraphy in the Baguio District has been intruded by a series of Pliocene rocks. The hornblende-phyrlic Mafic Dike Complex intruded the central part of the Baguio District at 4.5 – 4 Ma (Waters *et al.* submitted). The complex is characterized by dense clusters of coarsely hornblende phenocrystic dikes with evidence for multiple injections. Several Pliocene to Pleistocene dioritic intrusive complexes are associated with porphyry copper-gold mineralization in the Baguio district. The Black Mountain Intrusive Complex includes the Black Mountain quartz diorite and the Mexico Diorite, as well as andesite dykes that have yielded ages of between 3.14 and 2.78 Ma (Waters *et al.* submitted; Sweet *et al.* 2008). Other Pliocene intrusive rocks

include the ~2 Ma Santo Tomas II-Bumolo-Clifton Cluster and the ~1 Ma Ampucao-Hartwell-Balatoc Cluster (Waters *et al.* submitted).

The dyke complex forms a coherent suite of basaltic through to evolved andesitic compositions, plot on a calc-alkaline to high-K calc-alkaline trend and show a narrow range of La/Sm_n ratios (1.4-3.1; Fig. 2). Younger Pliocene samples typically have higher La_n/Sm_n ratios with a peak in values around 3 Ma. Similarly the SiO₂ contents show a slight increase in younger samples, but also a spike at around 3 Ma. The trend to more felsic samples implies either a change in the nature of the mantle source or simply progressive fractionation of the same relatively shallow level magma chamber.

CONCLUSIONS

Unlike Central Chile, the tectonic complexity and gaps in the igneous record between 17 and 5 Ma obscures the signal of igneous fertility in the Baguio District. However, La/Yb ratios do show an increase in host rocks that predate and are coeval with mineralization. Published data for igneous rocks associated with porphyry mineralization in the Batu Hijau district also shows an increase in La/Yb ratios at the time of mineralization with ratios increasing to levels comparable to those in the Baguio district (Garwin 2000). This implies that in oceanic arc systems changes in the tectonic setting resulting in crustal thickening appear to be associated with mineralization events. The thinner crust beneath island arcs compared to that below continental arcs results in more subdued geochemical signatures of crustal thickening. Radiogenic isotopic data from rocks coeval with mineralization in the Baguio District can be interpreted to indicate that more primitive magmas were emplaced immediately prior to mineralization and may have acted as a heat or metal source. The data implies that in oceanic arc systems changes in the tectonic setting resulting in crustal thickening appear to be associated with mineralization events.

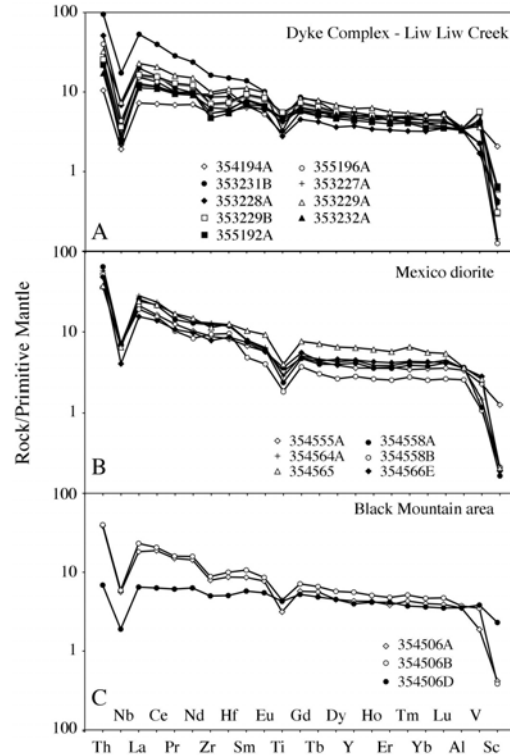


Fig. 2. Representative primitive mantle-normalized diagrams for samples from the Baguio District. Normalising values of Sun and MacDonough (1989).

ACKNOWLEDGEMENTS

This study was undertaken as part of Australian Mineral Industry Research Association (AMIRA) project P765—“Geochemical and Geological Halos in Green Rocks and Lithocaps”. Additional financial support was provided by a Natural Sciences and Engineering Research Council (NSERC) Discovery Grant to Hollings. The authors gratefully acknowledge logistical support from Anglo American personnel in the Philippines.

REFERENCES

CALLOW, K.J. 1967. The geology of the Thanksgiving mine, Baguio district, Mountain Province, Philippines. *Economic Geology*, **60**, 251-268.

CHANG, Z., HEDENQUIST, J., WHITE, N *et al.* Exploration tools for linked porphyry and epithermal deposits: Example from the Mankayan intrusion-centered Cu-Au district, Luzon, Philippines. *Economic Geology*, in review.

- COOKE, D.R., HOLLINGS, P., & WALSH, J. 2005. Giant porphyry deposits – characteristics, distribution and tectonic controls. *Economic Geology*, **100**, 801-818.
- COOKE, D.R., MCPHAIL, D.C., & BLOOM, M.S., 1996. Epithermal gold mineralization, Acupan, Baguio district, Philippines: geology, mineralization, alteration and the thermochemical environment of ore deposition. *Economic Geology*, **91**, 243-272.
- GARWIN, S.L. 2000. *The setting, geometry and timing of intrusion-related hydrothermal systems in the vicinity of the Batu Hijau porphyry copper-gold deposit, Sumbawa, Indonesia*. Unpublished PhD thesis, University of Western Australia, Perth, Australia.
- HOLLINGS, P., COOKE, D.R., & CLARK, A. 2005. Regional geochemistry of Tertiary volcanic rocks in Central Chile: implications for tectonic setting and ore deposit genesis. *Economic Geology*, **100**, 887-904.
- KAY, S.M., MPODOZIS, C., & COIRA, B. 1999. Neogene magmatism, tectonism and mineral deposits of the central Andes. In: SKINNER, B.J. (ed), *Geology and ore deposits of the Central Andes*. Society of Economic Geologists Special Publication, **7**, 27-59.
- MITCHELL, A.H.G. & LEACH, T. M. 1991. *Epithermal gold in the Philippines. island arc metallogenesis, geothermal systems and geology*. Academic Press Geology Series, London.
- SAWKINS, F.J., O'NEILL, J.R., & THOMPSON, J.M. 1979. Fluid inclusion and geochemical studies of vein gold deposits, Baguio District, Philippines. *Economic Geology*, **74**, 1420-1434.
- SKEWES, M.A. & STERN, C.R. 1994. Tectonic trigger for the formation of late Miocene Curich breccia deposits in the Andes of central Chile. *Geology*, **22**, 551-554.
- SUN, S.-s. & McDONOUGH, W.F. 1989. Chemical and isotopic systematics of oceanic basalts: implications for mantle composition and processes. In: SAUNDERS, A.D. & NORR, A.J. (eds.), *Magmatism in the ocean basins*. Geological Society, Special Publication **42**, 313-345.
- SWEET, G., WATERS, P., BAKER, M., HOLLINGS, P., & COOKE, D.R. 2008. The Black Mountain porphyry Cu-Au deposit, Baguio, Philippines. *Australasian Institute of Mining and Metallurgy, PACRIM Congress 2008, The Pacific Rim: Mineral Endowment, Discoveries & Exploration Frontiers*, Gold Coast, 451-456.
- WATERS, P.J., GONZALES, R.I., & COOKE, D.R. Geological setting and mineral deposits of the Baguio Mineral District. *Economic Geology*, in review.

Metals distribution and correlations in polymetallic veins from Pingüino Indium-bearing deposit, Deseado Massif, Patagonia, Argentina

Sebastián Jovic¹⁻², Paula Liñan¹, Diego Guido¹⁻², Gerardo Páez¹⁻²,
Remigio Ruiz¹, & Isidoro Schalamuk¹⁻²

¹Instituto de Recursos Minerales-Universidad Nacional de La Plata, La Plata ARGENTINA

²CONICET (e-mail: sebastianjovic@yahoo.com.ar)

ABSTRACT: The Pingüino deposit is characterized by the presence of In-rich polymetallic vein mineralization that represents an atypical epithermal occurrence for the low sulfidation epithermal mineralization from the Deseado Massif, Patagonia, Argentina. Polymetallic veins display high In, Zn, Pb, Ag, Cd, Au, As, Cu, Sn, W, and Bi values that are represented by complex sulfide mineralogy. This mineralization is developed in two main stages: an early Cu-Au-In-As-Sn-W-Bi stage, where indium is associated mainly with Sn mineralogy (ferrokesterite, stannite and cassiterite), and a late Zn-Pb-Ag-In-Cd-Sb stage with highest indium values related mainly with Zn (Fe-rich sphalerite).

KEYWORDS: *metals distribution, indium, Deseado Massif, Argentina*

INTRODUCTION

The Deseado Massif (DM) is located in the Santa Cruz province of the southern Argentinean Patagonia (Fig. 1). It is characterized by the presence of low sulfidation (LS) epithermal deposits that are genetically related to a complex long-lived (30 Ma) Jurassic bimodal magmatic event associated with tectonic extension. The DM is an important Au-Ag producer with four mines (Cerro Vanguardia, Martha, San José and Manantial Espejo) and it is the subject of intense prospecting activities. Mineralization consists of quartz veins, vein stockworks and hydrothermal breccias mainly hosted in Jurassic volcanic rocks. Metalliferous minerals in the quartz veins are commonly less than 1% in volume, mainly pyrite, native gold, electrum, argentite, native silver, Ag-sulfosalts, hematite, sphalerite, galena and chalcopryrite. The geochemical signature is characterized by anomalous precious metals, Au-Ag (Guido *et al.* 2005).

In recent years, some atypical epithermal occurrences (different to LS type) have been found in the DM. Mina Martha for example, is a Ag-rich deposit with a Ag:Au ratio of 1000:1 and high contents of base metals, and has been

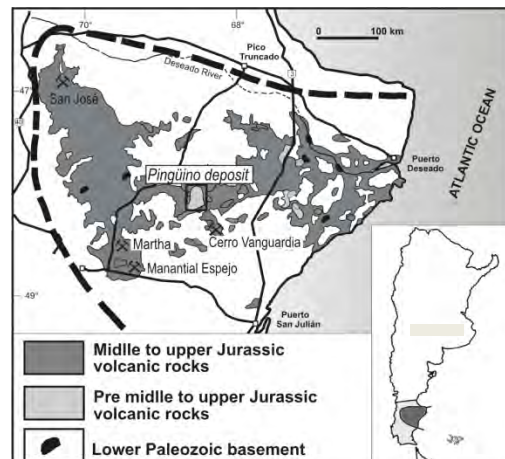


Fig 1. Deseado Massif geological map with Pingüino deposit location. (Guido *et al.* 2005).

defined as a intermediate sulfidation (IS) deposit (Gonzalez Guillot *et al.* 2004). The Pingüino deposit is another atypical epithermal deposit in the DM (Guido *et al.* 2005). It is located in the central part of the province, 40 km northwest from Cerro Vanguardia mine (Fig. 1) and is characterized by the presence of two vein types, early polymetallic sulfide-rich veins and late quartz-rich Ag-Au veins. The polymetallic veins show anomalous contents of Zn, Pb, Ag, In, Au, Cu, Cd, Sn,

Table 1. Summary of geochemistry analyses of polymetallic sulfide veins from Pingüino deposit.

Stage	Values	In	Au	Ag	Cu	Pb	Zn	Sn	Bi	Cd	As	Sb	W
PS ₁		ppm	ppm	ppm	wt.%	wt.%	wt.%	ppm	ppm	ppm	wt.%	ppm	ppm
Ivonne vein	Ave.	49.6	2.77	45.5	0.41	0.13	1.27	1267	93.9	61.7	1.00	66.5	55.2
n = 45	Max.	159.4	8.07	237.0	2.47	0.30	6.10	5961	390.8	338.2	4.41	509.1	740.0
	Min.	3.4	0.01	2.6	0.01	0.01	0.02	7	0.8	3.6	0.02	1.4	0.2
PS ₂													
M. Centro vein	Ave.	161.8	0.74	156.3	0.14	3.65	10.81	153	5.3	848.5	0.40	87.0	2.4
n = 100	Max.	1184	1.34	684.0	5.99	19.30	32.95	564	30.1	14900	1.28	634.8	25.2
	Min.	5.25	0.10	14.5	0.01	0.16	0.08	23	0.1	6.0	0.07	5.0	0.1

Sb, As, W, and Bi, classifying it as an indium-bearing polymetallic deposit.

The occurrence of indium-minerals is very rare in general, and indium substitutes in base metal sulfide minerals for elements with similar ionic radii. The most common In-bearing minerals are: sphalerite where In is substituting for Zn and Fe, stannite, kesterite and cassiterite where In is replacing Sn and Fe (Shwarz-Schampera & Herzig 2002).

The aim of this contribution is study the metals distribution, and specifically the indium distribution into the polymetallic mineralization stages from the Pingüino deposit sulfide veins.

PINGUINO DEPOSIT

The Pingüino veins, occupy more than 30 fault controlled structures. They have a NW and ENE strike and are hosted in Triassic continental sedimentary rocks and lower Jurassic epiclastic and volcanoclastic rocks, and are spatially related to lower Jurassic subvolcanic dioritic intrusions, basaltic sills and andesitic porphyries (Jovic *et al.* 2005).

Polymetallic Mineralization

The polymetallic veins are poorly exposed at surface and are characterized by the presence of gossans with remnants of breccias with quartz matrix and oxidized sulfide clasts. Hypogene polymetallic mineralization is characterized by the presence of massive and banded sulfide veins and sulfide breccias up to 13 m thick. This mineralization is developed in

two main stages. The early stage (Ps₁) is characterized by a complex paragenesis composed of pyrite, arsenopyrite, chalcopyrite, cassiterite, stannite, ferrokesterite, and minor sphalerite, galena, wolframite, bournonite, tetrahedrite, freibergite, argentotenantite, Ag-Pb-Bi sulfosalts (aramayoite, owyheeite, giesenita, ourayita), lillongite, enargite, and quartz, that is best represented in the Ivonne vein. During the second stage (Ps₂), Ps₁ minerals were replaced by Fe-rich sphalerite, galena, ferrokesterite, Ag-Pb sulfosalts and minor chalcopyrite, pirrotine, marcasite and tetrahedrite. The Ps₂ is best developed in the Marta Centro vein (Jovic *et al.* 2005; Crespi 2006).

Sampling and Geochemical Analysis

Hypogene veins zones between -30m to -120m depth from the Ivonne and Marta Centro veins were studied. These veins are 1000m and 700m in length and average 3m and 7m in thickness respectively and were drilled up to -400m. Representative samples were analyzed at Acme Analytical Laboratories (Chile-Canada) by instrumental neutron activation analyses (INAA), inductively coupled plasma-optical emission spectroscopy (ICP-OES), and inductively coupled plasma-mass spectrometry (ICP-MS). The studied Ps₁ samples are from the Ivonne vein (n=45) and Ps₂ from the Marta Centro vein (n=100). The average, maximum and minimum values of major (Zn, Pb, Cu, As), and trace element

Table 2. Correlation matrix for metals in Ps₁ from polymetallic sulfide veins at Pingüino deposit.

	In	Au	Ag	Cu	Pb	Zn	Sn	Bi	Cd	As	Sb
Au	0.67										
Ag	0.70	0.69									
Cu	0.67	0.66	0.84								
Pb	0.67	0.59	0.77	0.64							
Zn	0.40	-0.08	0.35	0.18	0.48						
Sn	0.77	0.82	0.64	0.54	0.63	-0.03					
Bi	0.67	0.69	0.83	0.63	0.50	0.22	0.52				
Cd	0.60	0.33	0.57	0.38	0.83	0.71	0.49	0.27			
As	0.31	0.61	0.50	0.24	0.34	0.02	0.34	0.59	0.23		
Sb	0.77	0.80	0.81	0.72	0.62	0.07	0.76	0.74	0.38	0.48	
W	0.50	0.71	0.41	0.47	0.52	-0.17	0.82	0.34	0.26	0.08	0.67

contents (Au, Ag, Sb, Bi, Sn, In, Cd, W) are listed in Table 1.

Ore Geochemistry

The ore geochemistry indicates the presence of high values of Cu, Au, As, Sn, W, Bi, Zn, Pb, Ag, In, Cd, and Sb in the polymetallic veins. Major and minor element associations reflect the two different mineralogical assemblages: the Ps₁ assemblage is characterized by anomalous values of Au, Cu, Sn, Bi, As and W, whereas the highest values of Zn, Pb, In, Ag, Cd and Sb are present in Ps₂ (Table 1). Ps₁ shows high correlations between Ag-Pb-Bi-Sb, Ag-Cu-Sb, Au-Sn-Sb-W and In-Sn-Sb (Table 2) while in Ps₂ the highest correlations are between In-Zn-Cd, In-Sn and Ag-Pb-Sb (Table 3).

DISCUSSION

Anomalous values of Au, Cu, Sn, Bi, As, and W in the Ps₁ indicate the precipitation of high temperatures minerals and metals that are represented by a complex mineralogy. The correlation between Ag-Pb-Bi-Sb suggests the presence of different Ag-Pb-Bi sulfosalts; correlation between Ag-Cu-Sb is associated with freibergite, argentotenantite, and tetrahedrite, while Sn-W is related to wolframite and cassiterite, and In-Sn-Sb with ferrokesterite, stannite and cassiterite. In Ps₂ the In and Cd, are present in the Fe-rich sphalerite (Crespi 2006) showing a high correlation between In-Zn-Cd; the correlation between In-Sn is associated with ferrokesterite. The presence of Ag-Pb sulfosalts is

responsible for the high correlation between these elements.

Indium concentrations in the polymetallic veins show a wide range (3.4 to 1184ppm In, Table 1). Based on the correlation coefficients of ore geochemistry, significant Indium (up to 1184 ppm) is related to the Ps₂ mineralization stage and closely associated with Fe-rich sphalerite, but also with ferrokesterite. There are important In anomalies in Ps₁ (up to 159.4 ppm) that are related to the Sn minerals, cassiterite, ferrokesterite and stannite (Crespi 2006).

CONCLUSIONS

The presence of high values of Cu, Au, As, Sn, W, Bi, Zn, Pb, Ag, In, Cd and Sb in the polymetallic veins from the Pingüinodeposit, represents an atypical geochemical signature for the epithermal deposits from the DM.

The distribution of the metals in the veins is represented by two mineralization stages: an early Ps₁ characterized by the presence Sn sulfides, Ag-Pb-Bi sulfosalts, Ag-Cu sulfosalts with the highest concentration of Cu, Au, As, Sn, W and Bi, and a late Ps₂ that shows the highest values of Zn, Pb, Ag, In, Cd and Sb with Fe-rich sphalerite, galena and Ag-Pb sulfosalts.

Indium is associated with both stages, but is concentrated in Ps₂ related mainly with Zn (Fe-rich sphalerite) and minor association with Sn (ferrokesterite). For Ps₁, Indium is associated with Sn, present

Table 3. Correlation matrix for metals in Ps₂ from polymetallic sulfide veins at Pingüino deposit.

	In	Au	Ag	Cu	Pb	Zn	Sn	Bi	Cd	As	Sb
Au	0.06										
Ag	0.19	0.21									
Cu	-0.07	0.00	-0.02								
Pb	0.17	-0.03	0.74	-0.09							
Zn	0.77	0.21	0.27	-0.16	0.39						
Sn	0.71	-0.03	0.46	-0.03	0.35	0.58					
Bi	0.56	0.06	0.09	0.39	-0.01	0.35	0.36				
Cd	0.80	0.26	0.23	-0.09	0.22	0.82	0.67	0.44			
As	0.05	-0.08	0.22	-0.09	0.37	0.17	0.10	0.01	0.11		
Sb	0.07	-0.02	0.81	-0.10	0.89	0.27	0.33	-0.09	0.16	0.37	
W	0.28	-0.03	0.07	0.38	-0.01	0.10	0.25	0.31	0.12	0.03	-0.01

in the Sn sulfides and oxides (ferrokesterite, stannite and cassiterite).

REFERENCES

- CRESPI, A. 2006. Estudi mineralògic dels dipòsits del massís de el Deseado (Argentina). *Universidad de Barcelona. Barcelona, España*
- GONZALEZ GUILLOT, M., DE BARRIO, R., & GANEM, F. 2004. Mina Martha, un yacimiento epitermal en el Macizodel Deseado, provincia de Santa Cruz. *VII Congreso de Mineralogía y Metalogenia, Córdoba, 1*, 199-204.
- GUIDO, D., JOVIC, S., & SCHALAMUK, I. 2005. A new metallogenic association (Sn-Cd-In-Zn-Ag-Au) in the Deseado Auroargentiferous province, Deseado Massif, Patagonia, Argentina. *Mineral Deposit Research: Meeting the Global Challenge. Beijing, China, 2*, 965-968.
- JOVIC, S., GUIDO, D., SCHALAMUK, I., MELGAREJO, J., & PROENZA, J. 2005. Mineralogía de veta Ivonne, deposito Cerro León: ¿Paragénesis de alta temperatura en la Provincia Auroargentífera del Deseado? *XVI Congreso Geológico Argentino, La Plata, 2*, 257-262.
- SCHWARZ-SCHAMPERA, U. & HERZIG, P. 2002. *Indium. Geology, Mineralogy, and Economics*. Springer-Verlag, Berlin, 257 p.

Chemical compositions of carbonate minerals from Chehelkureh ore deposit, Iran: implications for evolution of base-metal mineralization

Mohammad Maanijou¹, David R. Lentz², & Iraj Rasa³

¹Dept. of Geology, Faculty of Science, Bu-Ali Sina University, Hamedan IRAN (e-mail: mohammad@basu.ac.ir)

²Dept. of Geology, University of New Brunswick, P.O.Box 4400, Fredericton, NB E3B 5A3 CANADA

³Dept. of Geology, Faculty of Earth Sciences, Shahid Beheshti University, Tehran IRAN

ABSTRACT: The Chehelkureh Cu deposit is located NW of Zahedan (SE of Iran). Several stocks and dykes with granodiorite to quartz monzodiorite composition intruded the Eocene turbidites, and locally converted them to hornfels. Hypogene alteration consists of chloritization, carbonatization, silicification, kaolinization, sulfidization, and sericitization. Electron microprobe (EPMA) data show that carbonate compositions in the Chehelkureh deposit range from dolomite to ankerite, siderite, and magnesite. Replacement textures are present and oscillatory zoning apparently occurred during crystal growth in response to changes in temperature and composition of hydrothermal fluids. Temperatures derived from the ankerite-siderite geothermometer are 450° to 250°C and generally consistent with those from fluid inclusions and oxygen isotopes. The MnO and SrO contents of carbonate minerals in samples are up to 5.4 wt% and 0.2 wt%, which indicate at least parts of these carbonates were from hydrothermal fluids with an igneous origin, consistent with carbon isotopes results.

KEYWORDS: *chemical composition, carbonates, EPMA, Chehelkureh Ore Deposit, Iran*

INTRODUCTION

Chehelkureh is an ancient copper mine in Kuh-e-Lunka area, located 120 km NW of Zahedan (SE of Iran) at the longitude of 060°07'28.8" E and latitude of 30°14'9.3" N. The Kuh-e-Lunka area is in the eastern part of Dasht-e-Lut, located near the border with Pakistan and Afghanistan (Maanijou 2007). The Chehelkureh ore field consists of numerous lenses and veins with irregular shapes. In spite of high contents of base metals, with an average of 4.1% Cu+Zn+Pb, and Ag (average 22 ppm), they are poor in Au (average 0.14 ppm in 45 samples).

Carbonate mineralization is present in many hydrothermal deposits including base-metal veins and mesothermal gold deposits. In the Chehelkureh deposit, carbonate minerals occur in all host, altered and mineralized rocks. The ubiquitous occurrence of these minerals makes them potential indicators of changes in physical and chemical parameters during the evolution of the hydrothermal system. In this study we use chemical compositions of carbonates to

investigate the evolution of mineralization in Chehelkureh ore deposit.

GEOLOGICAL SETTING

The area is underlain by a sequence of Eocene intercalated greywackes, siltstones, and shales that host the ore deposit, and is bordered to the west by Cretaceous ophiolitic mélangé and to the east by Middle Eocene limestones (Valeh & Saeedi 1989). The Chehelkureh ore field is of complex shape with numerous, irregular lenses and veins. The ore field has an overall strike of N23°W and is displaced by faults striking roughly E-W (Maanijou *et al.* 2006). Several stocks and dykes of granodiorite to quartz monzodiorite and granite have intruded the sedimentary sequence of the area; they are oriented parallel to the major NW-SE fault set (Fig. 1).

The fault-fill mineralization includes quartz, dolomite, ankerite, siderite, calcite, molybdenite, pyrrhotite, arsenopyrite, pyrite, chalcopyrite, sphalerite, galena, selenian galena, marcasite, ilmenite, and rutile (Maanijou 2007).

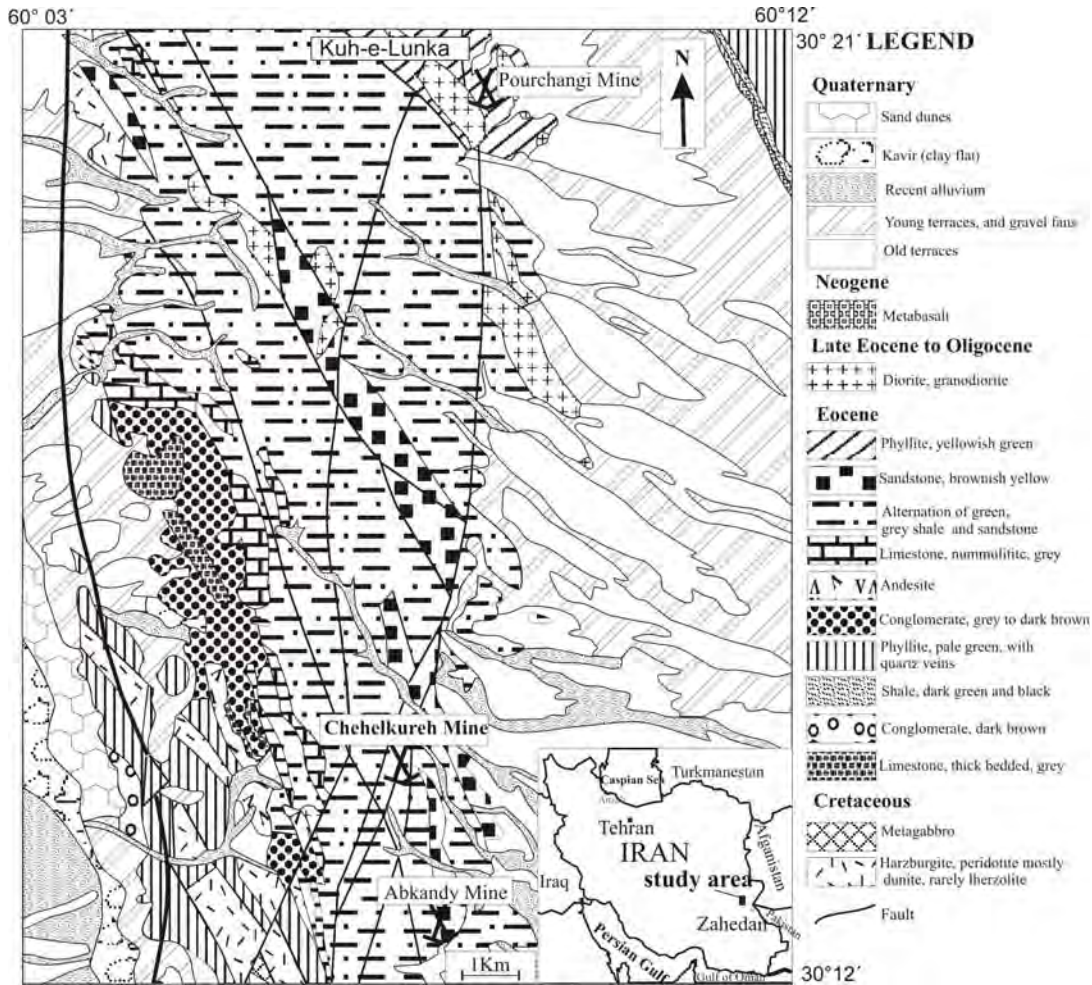


Fig. 1. Regional geological map of Chehelkureh polymetallic ore deposit (modified from Valeh & Saeedi 1989).

ANALYTICAL METHODS

One hundred samples were collected from drillholes, consisting of different lithologies, alteration, and mineralization. Polished thin sections were made from 70 samples of Chehelkureh rocks. Carbonates were analyzed for K, Na, Ca, Mg, Fe, Mn, Pb, Zn, Y and Sr using a JEOL-733 electron microprobe at the University of New Brunswick. An accelerating voltage of 15 kV with a beam current of 30 nA was applied (1µm beam) for a maximum count-time of 30 seconds.

CARBONATE OCCURRENCE AND PARAGENESIS

The carbonates typically occur as fine

grains disseminated throughout the matrix of greywackes and shales (turbidites), and as veins and veinlets. Veins and veinlets consist of coarser anhedral to subhedral carbonates with subordinate quartz in the center. Carbonate minerals also occur as complex intergrowths of siderite, magnesite, ankerite, and dolomite that contain abundant inclusions of quartz, chlorite, rutile, and pyrite. Most of the siderite and some of the ankerite were apparently consumed by sulfidation to pyrite, chalcopyrite, and other sulfides. There is also zoning in carbonates, which can be seen in veins and (or) at the scale of an isolated grain.

Oscillatory zoning apparently occurred during crystal growth in response to

changes in hydrothermal fluids (Fig. 2). Ca, Mg, and Fe mapping show the relative distribution of these elements in the grain. This compositional variation is attributed to episodic fluctuation in the temperature and composition of fluids in the Chehelkureh deposit.

CHEMICAL COMPOSITION OF CARBONATES AND CONCLUSIONS

The most important feature of mineral chemistry in carbonates of Chehelkureh deposit is the large range in the $\text{FeCO}_3:\text{MgCO}_3$ ratio which can indicate large variations in chemistry of hydrothermal fluids. Compositions extend along the magnesite-siderite join, from 22 to 72 mole% FeCO_3 (Fig. 3). Dolomite and ankerite compositions extend between 0 to 27 mole% FeCO_3 .

The major components CaO and MgO in dolomite have a minimal range indicative of very small variation in $\text{Ca}/(\text{Ca}+\text{Mg}+\text{Fe})$ ratios, whereas the minor elements such as SrO and MnO have a wide variation. Therefore trace components in carbonate minerals can be used as discriminant parameters to determine the origin of the carbonate rocks (cf. Yang & LeBas 2004). Compositional variation of carbonate minerals from Chehelkureh on the basis of MnO or SrO (wt%) versus $[\text{Ca}/(\text{Ca}+\text{Mg}+\text{Fe})]$ (atoms per formula unit, a.f.u.) diagrams (Fig. 4) show that the MnO and SrO contents in dolomite-ankerite are higher than those in siderite-magnesite and accessory calcite.

Calcite, ankerite, and dolomite in carbonates formed by hydrothermal fluids from mantle devolatilization usually contain higher MnO than SrO, indicating that Mn activity is relatively higher in the fluids (Yang & Le Bas 2004). Carbonates in veins and disseminated grains from Chehelkureh contain up to 5.4 wt% MnO and up to 0.2 wt% SrO, which suggests an igneous origin. Anovitz & Essene (1987) calibrated an ankerite-siderite geothermometer by fitting the Fe-Mg distribution constant (K_D) data for natural assemblages. Temperatures derived from the ankerite-siderite composition geothermometer in Chehelkureh deposit are generally consistent with those from fluid inclusions and oxygen stable isotope and are 450° to 250°C.

Ion microprobe analyses of *in situ*

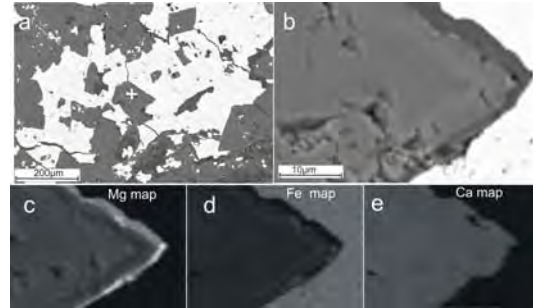


Fig. 2. EPMA back-scattered electron images of a polished section from Chehelkureh deposit. a) carbonate in a mineralized vein with chalcopyrite; b) larger image of carbonate grain marked by + in previous image, c), d) and e) are in turn compositional Mg, Fe and Ca images of that grain.

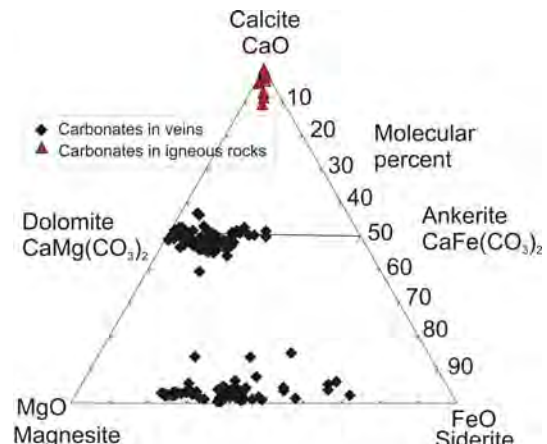


Fig. 3. Ternary plot of carbonate composition (EMP, mol%) in the Chehelkureh ore deposit.

accessory calcite grains in granites indicate relatively low Sr (120 to 660 ppm), negligible Rb and $^{87}\text{Sr}/^{86}\text{Sr}$ ratios equal to or higher than those of coexisting plagioclase (White *et al.* 2005). Sr content in the calcite of the Chehelkureh granitoids is relatively low. The ubiquitous nature of accessory calcite documented in this study implies late-magmatic growth or subsolidus replacement of igneous phases.

Mineral chemistry of carbonates of mineralized veins in the Chehelkureh ore deposit show that at least some of these carbonates were deposited from hydrothermal fluids of igneous origin, which is consistent with carbon isotopes results (Maanijou 2007).

REFERENCES

- ANOVITZ, L.M. & ESSENE, E.J. 1987. Phase equilibria in the system $\text{CaCO}_3\text{-MgCO}_3\text{-FeCO}_3$. *Journal of Petrology*, **28**, 389-414.

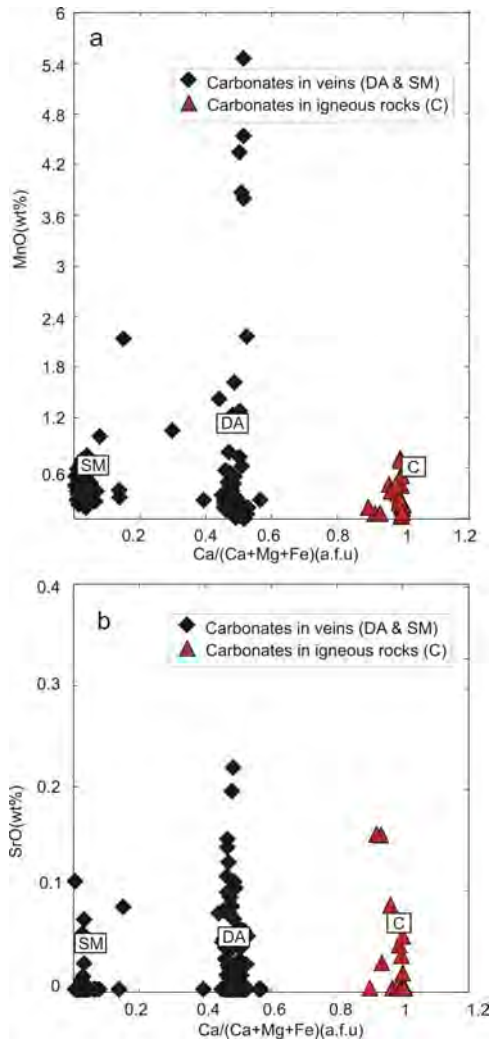


Fig. 4. Compositional variation of carbonate minerals from Chehelkureh on the basis of a) MnO (wt%) versus $[Ca/(Ca+Mg+Fe)]$ (atoms per formula unit, a.f.u.) diagram and b) SrO (wt%) versus $[Ca/(Ca+Mg+Fe)]$ a.f.u. diagram showed that there are three main groups: dolomite-ankerite (DA), siderite-magnesite (SM), and accessory calcite in igneous rocks (C).

MAANIJOU, M. 2007. *Geochemistry, origin of ore fluids, and formation of Chehelkureh copper deposit (NW of Zahedan)*. Ph.D. Thesis, Shahid Beheshti University, Tehran (in farsi with english abstract).

MAANIJOU, M., LENTZ, D., RASA, I., & ALETAHA, B. 2006. Petrography, Geochemistry and Geotectonic Environment of Arc-Related Granitoids in the Chehelkureh area, Southeast Iran: Implications for the Formation of the Polymetallic Ore Deposit in the Region. *12th IAGOD, Moscow*, 4 p.

VALEH, N. & SAEEDI, A. 1989. Geological map of Chehel Kureh. *Geological Society of Iran*, Sheet **8050**.

YANG, X.M. & LE BAS, M.J. 2004. Chemical composition of carbonate minerals from Bayan Obo, Inner Mongolia, China, implications for petrogenesis. *Lithos*, **72**, 97-116.

WHITE, A.F., SCHULZ, M.S., LOWENSTERN, J.B., VIVIT, D.V., & BULLEN, T.D. 2005. The ubiquitous nature of accessory calcite in granitoid rocks: Implications for petrogenesis. *Geochimica et Cosmochimica Acta*, **69**, 1455-1471.

Rare earth element variations in volcanogenic massive sulfides, Bathurst Mining Camp, New Brunswick: evidence from laser-ablation ICPMS analyses of phosphate accessory phases

Sean H. McClenaghan¹, David R. Lentz², & Wilfredo G. Diegor³

¹Geological Surveys Branch, New Brunswick Department of Natural Resources, P.O. Box 50, Bathurst, NB, E2A 3Z1 CANADA (e-mail: Sean.McClenaghan@gnb.ca)

²Department of Geology, University of New Brunswick, Fredericton, NB, E3B 5A3 CANADA

³Department of Earth Sciences, Memorial University of Newfoundland, St. John's, NF, A1B 3X5 CANADA

ABSTRACT: Chondrite-normalized REE profiles for massive sulfides exhibit a prominent positive Eu anomaly, with $(Eu/Eu^*)_N$ averaging 4.7, that correlates positively with Sn, Se, In, Co, Sc, and $(La/Lu)_N$, suggesting a hydrothermal influence on the enrichment of LREE and Eu. *In situ* analyses (n=112) of apatite, reveal elevated contents of Y, Sr, and REE with Σ REE contents averaging 1549 ppm. REE profiles for apatite display a prominent enrichment in Eu, with anomalies averaging 19 (as high as 222), that correlates with Sr and ratios of U/Th. REE profiles for xenotime (n=58) exhibit small positive Eu anomalies, averaging 3.4, broadly consistent with hydrothermal and diagenetic varieties of xenotime. Monazite analyses (n=140) exhibit enrichment in LREE and a prominent negative Eu anomaly, with $(Eu/Eu^*)_N$ averaging 0.52, consistent with a detrital signature that may mask hydrothermal components in massive sulfides of the Bathurst Mining Camp.

KEYWORDS: Rare-Earth-Elements, Phosphate, Bathurst Mining Camp, Volcanogenic Massive Sulfide, Laser Ablation ICP-MS

INTRODUCTION

The potential application of rare-earth elements (REE) as a hydrothermal tracer was originally investigated by Graf (1977), who first reported positive Eu anomalies in Algoma-type iron formation associated with volcanogenic massive sulfides (VMS) of the Bathurst Mining Camp (BMC), New Brunswick, Canada. It was also known that some REE, in particular Eu and the light rare earth elements (LREE), could be enriched in massive sulfides (Fig. 1), as well as their cogenetic stockwork sulfide complexes. Since then, similar REE variations have been reported in many ancient VMS deposits. Furthermore, measurements on hydrothermal fluids emanating from modern VMS systems on the seafloor have shown positive Eu anomalies, as well as LREE enrichment (Michard 1989).

Recent work (Peter & Goodfellow 2003) has documented the distribution of REE in iron formations of the BMC. Despite what is currently known of trace-element behaviour in exhalative sedimentary

systems (Gale *et al.* 1999; Spry *et al.* 2000) and footwall alteration zones (Lentz & Goodfellow 1996), there are few REE studies on massive sulfides. Moreover, mineralogical controls on REE distribution in zone-refined VMS deposits remain enigmatic. Elucidation of controls on REE distribution may enhance base-metal exploration in volcanic terrains.

GEOLOGICAL SETTING

VMS deposits of the BMC occur within a Middle-Ordovician bimodal volcanic and sedimentary sequence in the northern Appalachians of New Brunswick, Canada (Goodfellow & McCutcheon 2003). Volcanic rocks were emplaced between 472 and 455 Ma within an intra-continental back-arc basin (the Tetagouche-Exploits basin) at the eastern margin of the proto-Atlantic (Iapetus) Ocean (van Staal *et al.* 2003).

Syngenetic massive sulfides are largely concentrated along several prominent horizons corresponding to discrete breaks in volcanism, which are marked by the

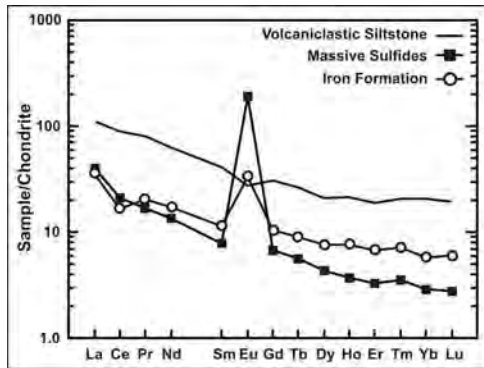


Fig. 1. Chondrite-normalized REE profiles for massive sulfides in the BMC.

accumulation of tuffaceous sedimentary rocks and locally Algoma-type iron formation (Peter & Goodfellow 2003).

Closure of the Tetagouche–Exploits basin by northwest-directed subduction from the Late Ordovician to Silurian led to incorporation of the back-arc terrain into the Brunswick subduction complex, accompanied by polyphase deformation and dominantly greenschist facies metamorphism (van Staal *et al.* 2003).

BULK GEOCHEMISTRY

Massive sulfides generally contain small quantities of REE compared to volcanic and sedimentary lithotypes; Σ REE contents average 33 ppm ranging from 0.93 to 263 ppm. Overall, Σ REE contents are strongly controlled by volcaniclastic material incorporated in massive sulfides during seafloor sedimentation. Consequently, there is a strong Σ REE correlation with Al_2O_3 ($r'=0.83$), TiO_2 ($r'=0.76$), Nb ($r'=0.82$), Th ($r'=0.87$), Y ($r'=0.86$), and Zr ($r'=0.73$).

Chondrite-normalized REE profiles (Fig. 1) for massive sulfides exhibit a prominent enrichment in LREE and Eu. The enrichment of LREE over the HREE is substantiated by strong positive Σ REE correlations with La, Ce, Pr, Nd and Sm, and a $(\text{La}/\text{Lu})_N$ ranging widely from 0.15 to 387. Europium anomalies are distinctly positive with $(\text{Eu}/\text{Eu}^*)_N$ averaging 4.7, but vary widely, ranging from 0.21 to 36. Minor negative Eu anomalies occur in semi-massive sulfides, due to dilution by volcaniclastic material. A positive

correlation of $(\text{Eu}/\text{Eu}^*)_N$ with Sn ($r'=0.43$), Se ($r'=0.32$), In ($r'=0.35$), Co ($r'=0.33$), and La/Lu ($r'=0.47$) suggests a degree of hydrothermal enrichment of LREE and Eu. Furthermore, a correlation between Σ REE and P_2O_5 ($r'=0.63$) indicates that hydrothermal REE signatures are strongly controlled by phosphate accessory phases.

MINERAL CHEMISTRY

Monazite

Monazite occurs as anhedral to subhedral masses associated with phyllosilicate-rich domains in massive sulfides. Masses display simple concentric zoning, a primary core, and commonly show fracturing and healing involving later generations of monazite growth that are likely a product of metamorphism (Fig. 2a).

Monazite has an average formula, $(\text{REE}_{0.89}\text{Y}_{0.03}\text{Th}_{0.03}\text{Ca}_{0.02}\text{Si}_{0.01})\text{P}_{1.01}\text{O}_4$ with REE dominated by La, Ce, and Nd, and notable contents of Y (1.5% Y_2O_3), Th (3.3% ThO_2) and U (0.19% UO_2). Chondrite-normalized REE profiles (Fig. 3) display a distinct enrichment in LREE with prominent negative Eu anomalies, which are broadly consistent with known profiles of monazite in metamorphosed terrains (Spear & Pyle 2002). The LREE contents of monazite have fairly restricted compositions dominated by Ce averaging 29.8% Ce_2O_3 and behaving sympathetically with contiguous LREE, exhibiting a positive correlation with La ($r'=0.61$), Nd ($r'=0.46$), and Pr ($r'=0.38$). Overall, Σ REE contents average 61.1%, ranging from 55.4 to 67.6% REE_2O_3 and display a negative correlation with Th ($r'=-0.86$), Ca ($r'=-0.85$), Y ($r'=-0.75$), and Pb ($r'=-0.54$). Trace-element contents of monazite masses are variable with primary cores that are depleted in LREE and enriched in Y and Th; whereas, late rims and healed fractures of monazite possess the higher contents of LREE. Raw count data for single spot laser-ablation ICP–MS analyses of monazite display sympathetic zoning of Th, U, and most REE, with Eu displaying sharp signal spikes corresponding with the ablation of monazite rims. The presence of distinctive

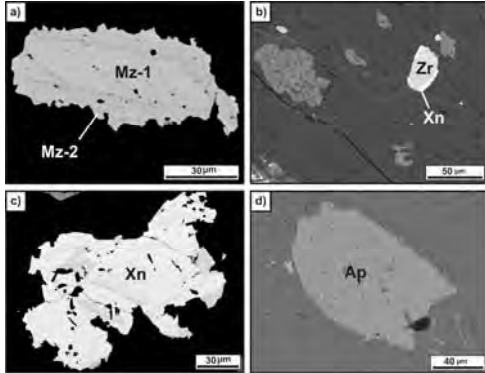


Fig. 2. SEM-BSE images of phosphate minerals in massive sulfides, (a) detrital monazite grain with a metamorphic rim, (b) detrital zircon grain with a xenotime rim, (c) complex zonation of a xenotime mass, and (d) apatite mass with a syntaxial overgrowth

spikes in Eu relative to LREE and HREE within monazite rims implies mobility of Eu during syn-metamorphic deformation.

Xenotime

Xenotime is the least abundant accessory mineral, occurring chiefly as small (<10 µm) overgrowths on detrital zircon grains (Fig. 2b). Zircon grains are likely detrital in origin based on their equant sub-rounded character and the deflection of a composite S_0/S_1 foliation, which is penetrative throughout the sulfide sections. Rare masses of xenotime can exhibit complex rhythmic (concentric) and irregular intergrowth zoning (Fig. 2c).

Analyses of xenotime provide an average formula, $(Y_{0.69}REE_{0.28})P_{1.01}O_4$ with contents of Y_2O_3 ranging from 34.5 to 42.6%; Y exhibits a positive correlation with Er ($r'=0.80$) and Yb ($r'=0.80$). Compositional zonation of xenotime varies as a function of REE content, with marked enrichment of MREE and Th in the core of xenotime masses and correspondingly higher $(Gd/Yb)_N$, averaging 2.3. In contrast, xenotime rims are enriched in Y and HREE, with lower ratios of $(Gd/Yb)_N$ averaging 1.0. Chondrite-normalized REE profiles (Fig. 3) display a characteristic “dogleg” pattern (Spear and Pyle, 2002) with enrichment in HREE relative to LREE and La, Ce, and Pr largely below the detection limits of the electron microprobe.

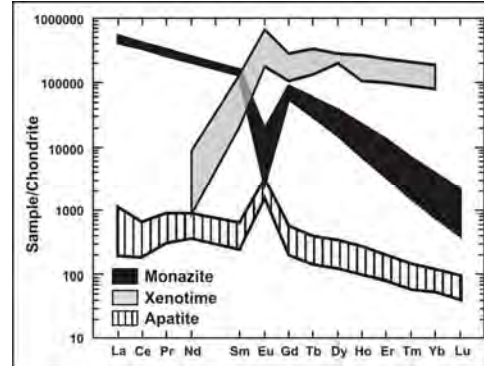


Fig. 3. Chondrite-normalized REE profiles for phosphate minerals in massive sulfides, BMC.

Profiles also exhibit small positive Eu anomalies, with values of $(Eu/Eu^*)_N$ averaging 3.4, and exhibiting a positive correlation with U ($r'=0.44$). Unlike monazite, xenotime has limited amounts of the actinide-series elements with ThO_2 averaging 0.33% and exhibiting a positive correlation with U ($r'=0.75$) and SiO_2 ($r'=0.61$). This suggests coupled substitution as thorite, $ThSiO_4$ or huttonite, $(Th,U)SiO_4$, which are isostructural with xenotime. Contents of REE, Th and U are broadly consistent with documented signatures for hydrothermal and diagenetic varieties of xenotime (Spear & Pyle 2002); whereas, igneous varieties typically possess much higher contents of U and Th, and prominent negative Eu anomalies.

Apatite

Apatite is the most abundant phosphate mineral in exhalative sedimentary rocks of the BMC (Peter & Goodfellow 2003). Apatite occurs as fine- to medium-grained anhedral masses (Fig. 2), commonly 50 to 100 µm in diameter with rare masses reaching 1 mm in size. A composite S_0/S_1 foliation is deflected around apatite grains with the development of phyllosilicate- and quartz-rich pressure shadows. Extensive solution transfer during D_1 has led to continuous growth of apatite masses, resulting in syntaxial overgrowths that truncate the S_0/S_1 foliation and pre-deformation grain boundaries marked by distinct inclusion trails (Fig. 2).

Analyses revealed a fluor-apatite composition with an average formula,

$\text{Ca}_{5.02}\text{P}_{2.94}\text{O}_{11.9}(\text{F}_{1.02},\text{Cl}_{0.002})$. Overall, Y and REE account for the largest amount of elemental substitution into fluor-apatite. Contents of Y average 510 ppm, exhibiting a positive correlation with ΣREE ($r'=0.65$), in particular Ho ($r'=0.92$). ΣREE contents in apatite average 1549 ppm with values as high as 24,038 ppm. Contents of Eu average 295 ppm (range from 7.8 ppm to 1554 ppm) and exhibit a positive correlation with Sr ($r'=0.50$) and to a lesser degree the MREE. Chondrite-normalized REE profiles display a prominent enrichment in Eu, with anomalies $(\text{Eu}/\text{Eu}^*)_{\text{N}}$ averaging 19.0 (as high as 222), suggesting high temperature ($>250^\circ\text{C}$) and/or low pH hydrothermal conditions. Chondrite-normalized HREE contents exhibit a consistent decrease in abundance with increasing atomic number producing a negative slope with $(\text{Gd}/\text{Yb})_{\text{N}}$ averaging 5.8 and ranging from 0.70 to 24.7. Chondrite-normalized LREE generally increase in abundance with atomic number with $(\text{La}/\text{Sm})_{\text{N}}$ averaging 0.64, but exhibit considerably higher variability, ranging from 0.02 to 3.5. REE profiles can also exhibit small negative $(\text{Ce}/\text{Ce}^*)_{\text{N}}$ anomalies likely imparted during the mixing of hydrothermal fluids with seawater at or near the seafloor.

CONCLUSIONS

Contents of REE in massive sulfides from the BMC are strongly controlled by the abundance of and REE concentrations in phosphate minerals, specifically apatite, xenotime and monazite. Strong positive Eu anomalies in apatite, account for the anomalous Eu signatures of exhalative sulfides; whereas REE in monazite masses are largely reflective of detrital sources and may mask hydrothermal signatures. Limited release of mobile trace elements (LREE and Eu) during greenschist facies metamorphism has partly modified REE profiles for VMS deposits of the BMC.

ACKNOWLEDGMENTS

Electron-microprobe analyses were conducted with the assistance of Douglas Hall (UNB). Laser-ablation ICP-MS

analyses were performed at MUN and facilitated by Paul Sylvester and Mike Tubrett. This project was funded by an NSERC-CRD grant to David Lentz and the NB Department of Natural Resources.

REFERENCES

- GALE, G.H., DABEK, L.B., & FEDIKOW, M.A.F. 1999. The application of rare earth element analyses in the exploration for volcanogenic massive sulfide type deposits. *Exploration and Mining Geology*, **6**, 233-252.
- GOODFELLOW, W.D. & MCCUTCHEON, S.R. 2003. Geologic and genetic attributes of volcanic sediment-hosted massive sulfide deposits of the Bathurst Mining Camp, northern New Brunswick – a synthesis. *Economic Geology Monograph*, **11**, 245-302.
- GRAF, J.L. 1977. Rare earth elements as hydrothermal tracers during the formation of massive sulfide deposits in volcanic rocks. *Economic Geology*, **72**, 527-548.
- LENTZ, D.R. & GOODFELLOW, W.D. 1996. Intense silicification of footwall sedimentary rocks in the stockwork alteration zone beneath the Brunswick No. 12 massive sulphide deposit, Bathurst, New Brunswick. *Canadian Journal of Earth Sciences*, **33**, 284-302.
- MICHARD, A. 1989. Rare earth element systematics in hydrothermal fluids. *Geochimica et Cosmochimica Acta*, **53**, 745-750.
- PETER, J.M. & GOODFELLOW, W.D. 2003. Hydrothermal sedimentary rocks of the Heath Steele Belt, Bathurst Mining Camp, New Brunswick: Part 3. Application of mineralogy, mineral chemistry and bulk compositions to massive sulfide exploration. *Economic Geology Monograph*, **11**, 417-434.
- SPEAR, F.S. & PYLE, J.M. 2002. Apatite, monazite and xenotime in metamorphic rocks. In: KOHN, M.J., RAKOVAN, J. & HUGHES, J.M. (eds.), *Phosphates – geochemical, geobiological, and materials importance*. *Reviews in Mineralogy & Geochemistry*, **48**, 293-335.
- SPRY, P.G., PETER, J.M., & SLACK, J.F. 2000. Meta-exhalites as exploration guides to ore. *Reviews in Economic Geology*, **11**, 163-201.
- VAN STAAL, C.R., WILSON, R.A., ROGERS, N., FYFFE, L.R., LANGTON, J.P., MCCUTCHEON, S.R., MCNICOLL, V., & RAVENHURST, C.E. 2003. Geology and tectonic history of the Bathurst Supergroup, Bathurst Mining Camp and its relationship to coeval rocks in southwestern New Brunswick and adjacent Maine – a synthesis. *Economic Geology Monograph*, **11**, 37-60.

Controls and consequences of intrusion-related Au deposition at the Morila Au Mine, SW Mali

Christopher R.M. McFarlane¹, Karen Grey¹, & David Lentz¹

¹Geology Department, University of New Brunswick, 2 Bailey Drive, Fredericton, NB, E3B 5A3 CANADA
(e-mail: crmm@unb.ca)

ABSTRACT: The Morila Au deposit, southern Mali, is interpreted as a Paleoproterozoic intrusion-related gold system. Morila is hosted by immature volcanoclastic rocks that contain abundant fine-grained hypabyssal mafic intrusions that appear to have served as the main chemical traps for subsequent Au mineralization. Early low-grade Au mineralization was synchronous with ductile shearing and biotitization of the host rocks. This package was subsequently tectonically imbricated and contact metamorphosed under low-pressure amphibolite facies conditions. The main pulse of Au mineralization occurred after peak contact metamorphism and is associated with albitisation and low-T K-metasomatism along a NE-trending brittle fracture zone. Scheelite, as well as Bi-Te, Au-Sb, and Au-Ag alloys accompany auriferous arsenopyrite. A model involving magmatic-hydrothermal fluids derived from variably contaminated magmas generated from re-melting of metasomatized sub-arc mantle lithosphere appears to best satisfy the temporal, petrological, and geochemical constraints on Au mineralization.

KEYWORDS: West Africa, intrusion-related, gold, Birimian, Mali

INTRODUCTION

The >7 Moz Morila Au deposit, Mali, is an enigmatic member of a continuum of Au deposits now described across the West African Craton (Fig. 1). In contrast to more traditional shear zone-hosted and stockwork deposits, hydrothermal alteration and brittle structures at Morila are cryptic and there are no apparent lithological controls on mineralization.

Through the integration of field, microscopic, geochemical, and isotopic datasets we have identified Morila as a paleoproterozoic example of an intrusion-related Au system (IRGS, e.g., Hart 2007).

GEOLOGICAL SETTING

The host rocks to Morila are regionally equivalent to the Mesoproterozoic Birrimian basin and belt sequences exposed across the West African craton in Senegal, Mali, Cote d'Ivoire, Ghana and Burkina (Feybesse *et al.* 2006).

Regional Geology

The metasedimentary (volcanoclastic) sequence hosting Morila was deposited between 2160 to 2135 Ma, based on the

provenance of inherited zircon grains in metasediments in the immediate hangingwall of the deposit (Armstrong 2006). Nd-isotope model ages of ca. 2300 Ma for the same rocks attest to the juvenile nature of the Birimian crust in the area. This syn-rift period of sedimentation was associated with coeval emplacement of locally porphyritic hypabyssal mafic to intermediate dykes and sills, and was broadly coincident with the appearance of a series of juvenile island arc terranes that were subsequently amalgamated during the short-lived Eburnean Orogeny (ca. 2105-2090 Ma).

Deformation during the Eburnean Orogeny was regionally extensive. Exhumed paragneisses in Ghana record an early (2130-2105 Ma) high-temperature flat-lying ductile D1 phase of Eburnean deformation and metamorphism followed by broadly northeast-southwest directed folding and thrusting during a poorly-constrained D2 event (~2100 Ma?).

The final D3 phase of deformation is associated with a change to a transpressional kinematic regime. Whereas structures associated with

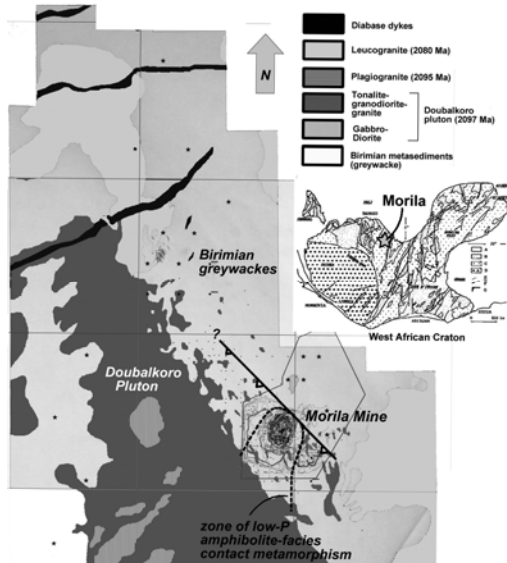


Fig. 1. Regional geology surrounding the Morila Au Mine, southern Mali. The deposit is hosted by immature Birimian metasediments and is proximal to a large composite post-Eburnean D2 pluton (Doubalkoro) and within a localized low-P contact aureole.

Eburnean D2 and D3 are well documented at Morila, evidence for early high-temperature ductile D1 deformation remains poorly documented.

In addition to the earliest syn-rift phase of hypabyssal magmatism, the host Birimian volcanoclastic rocks were intruded by a suite of syn- to post-Eburnean D2 plutons ranging in composition from diorite to granite. These magmas are calc-alkaline to alkaline (locally lamprophyric) and were emplaced as composite laccolithic plutons with associated dyke swarms. These composite plutons and dykes contain a variety of enclaves, xenoliths, and hybridized margins against host metasediments that record the effects of assimilation, contamination, and subsequent differentiation (AFC processes) of hybrid magmas.

A unique feature at Morila is the occurrence of locally abundant nebulous leucocratic veins that invade strongly foliated biotitized schists (Fig. 2).

Rather than partial melts derived from in-situ anatexis (i.e., leucosomes) these veins are trondhjemitic and represent distal magmatic injections from nearby

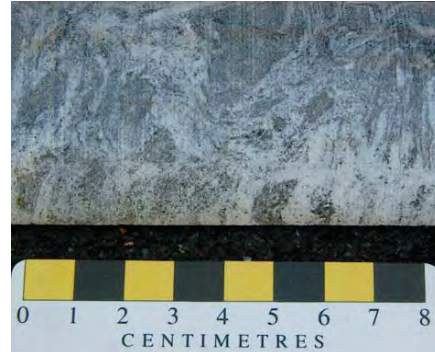


Fig. 2. Nebulous leucocratic veins representing magmatic-hydrothermal injections into hydrothermally-altered metasediments.

plutons.

Local Geology

A 10-20 m thick zone of low-grade disseminated Au mineralization (Fig. 3) broadly coincides with a sub-horizontal high-strain zone (Morila Shear Zone; MSZ) characterized by biotite schists with a sub-horizontal foliation that contains boudinaged and transposed milky white quartz veins, shallowly-plunging sheath folds, and translucent-grey quartz augen. The MSZ is locally proto-mylonitic to mylonitic as defined by elongate and rotated plagioclase porphyroclasts set in a very fine-grained matrix of dynamically recrystallized quartz and feldspar. Rather than a continuous through-going shear zone, the MSZ is now characterized by a network of anastomosing high-strain zones that may have been imbricated during Eburnean D2 or D3 deformation. Whereas biotite schists are the predominant lithology in the MSZ, dismembered, transposed, and metamorphosed enclaves of porphyritic mafic and intermediate intrusions are locally identifiable. Several lithochemical transects through the ore zone revealed elevated Cr, Ni, and V in ore zones suggesting a mafic protolith to the bulk of the mineralization.

The bulk of the Au mined at Morila was contained within a much narrower linear zone hosted within the MSZ. This north-northeast trending high-grade axis (HGA) was characterized by average Au grades >10 g/t with local intersections >100 g/t.

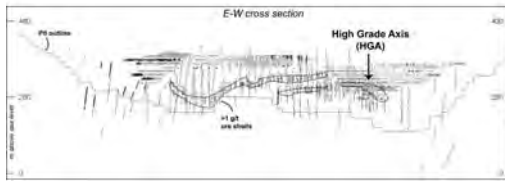


Fig. 3. E-W cross section through Morila showing the sub-horizontal attitude of the low-grade ore zones and the location of the HGA.

Mineralization along the HGA is contained primarily as Au blebs in post-D2 arsenopyrite porphyroblasts that overprint the main biotite foliation (MSZ, Fig. 4).

In addition to Au, a variety of Au-Sb, Au-Ag and Bi-Te alloys accompanied post-D2 arsenopyrite precipitation. Au and Bi-Te alloys are also locally concentrated in the biotite-rich margins of tonalite dykes that were contaminated by the host sediments. These alloys also appear to be concentrated within the HGA and are locally associated with disseminated scheelite and F-apatite. The latter also occur in late-stage veins that cross-cut weakly foliated granodiorite stocks that lie immediately beneath the HGA. A combination of BSE and CL imaging reveals that precipitation of these post-D2 sulfides and alloys occurred within a micro-porosity network that records dissolution-precipitation reactions involving quartz, plagioclase (albitised), and pyrrhotite (Fig. 5).

These textural observations suggest that the bulk of the mineralization at Morila was precipitated following low-P contact metamorphism and under relatively low fluid pressure conditions (i.e., no significant hydrofracturing).

CONCLUSIONS

The rocks at Morila record an intimate interplay between magmatism, contact metamorphism (and metasomatism), deformation, and mineralization. The spatial, temporal, and textural associations between contaminated post-D2 intrusions, contact metamorphism, and polymetallic post-D2 mineralization strongly suggests an intrusion-related origin for Morila. Other controls on Au mineralization include:

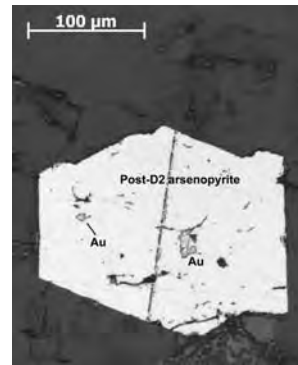


Fig. 4. Au blebs in post-tectonic arsenopyrite porphyroblast.

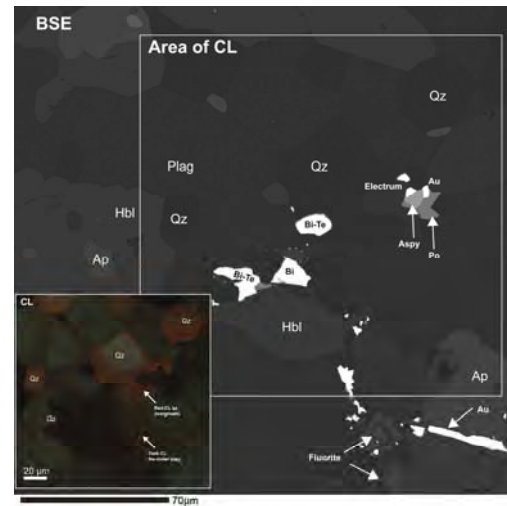


Fig. 5. SEM-BSE image showing Au, electrum, native Bi and BiTe alloys precipitated in an annealed amphibolite-facies metabasalt layer. The inset CL image reveals alloys and sulfides in contact with new generations of quartz (red) and plagioclase (dark) that records dissolution-precipitation reactions isolated along the grain boundaries of a previous annealed matrix.

- (1) Localization of Au precipitation in metabasaltic horizons.
- (2) Focusing of hydrothermal fluids below relatively impermeable greywacke hangingwall.
- (3) transfer of metals in high-T magmatic-hydrothermal veins.

Regionally, three magmatic processes are envisioned to have ultimately controlled mineralization at Morila: 1) re-melting of metasomatized lithospheric mantle during crustal-scale regional transpression; 2)

contamination and hybridization of magmas by relatively fertile immature rift-related sediments, and; 3) episodic magmatism and magma recharge over a ca. 10 Myr period following the waning phases of Eburnean D2.

ACKNOWLEDGEMENTS

We thank Paul Harbidge and Ken King (Randgold Resources Ltd), Tom Gell, and Sue Winkler (AngloGold Ashanti Ltd.), and the Government of Mali, for their support over the course of this project.

REFERENCES

ARMSTRONG, R. 2006. A Geochronological

Investigation of the Morila Gold Mine, Mali. PRISE (ANU, Research School of Earth Sciences) report #A03-220.

FEYBESSE, J.-L. *et al.* 2006. The paleoproterozoic Ghanaian province: Geodynamic model and ore controls, including regional stress modeling. *Precambrian Research*, **149**, 149-196.

HART, C.J.R. 2007. Reduced intrusion-related gold systems. In: Mineral deposits of Canada: A Synthesis of Major Deposit Types, District Metallogeny, the Evolution of Geological Provinces, and Exploration Methods. *Geological Association of Canada, Mineral Deposits Division, Special Publication No. 5*, 95-112.

Syenite, lamprophyre, and carbonatite dykes of the Moose Creek Valley, Ice River Alkaline Complex, southeastern British Columbia, Canada: implications for REE potential

Thomas R. Mumford¹, Dave R. Lentz¹, & Cliff S.J. Shaw¹

¹*Department of Geology, University of New Brunswick, PO Box 4400, Fredericton, NB, E3B 5A3 CANADA
(e-mail: thomas.mumford@unb.ca)*

ABSTRACT: The Ice River Alkaline Complex (IRAC) of southeastern BC is a well preserved bimodal Devonian-Carboniferous intrusion comprised of mafic-ultramafic and syenitic intrusive phases. Within the Moose Creek Valley there is an abundance of syenite, lamprophyre, and carbonatite dykes. The syenite dykes can be subdivided into three groups: nepheline syenite – nephelinolite group, syenite – monzodiorite group, and an alkali feldspar granite dyke. Two types of lamprophyres are present: sannaite and damtjernite, as well as calcio- and ferrocarnatites. Isotopic evidence suggests that the sannaite lamprophyres and syenite dykes are related to the partial melting of a depleted mantle source, the syenites are temporally related to the IRAC, and the ferrocarnatite displays an isotopically distinct signature.

KEYWORDS: *dykes, alkaline, carbonatite, syenite, lamprophyre*

INTRODUCTION

The Ice River Alkaline Complex (IRAC) in the western Main Ranges of the Canadian Rocky Mountains is a 29 km² J-shaped intrusion which comprises nepheline syenite and layered mafic sub-complexes intruded by a diverse swarm of dykes: syenitic, lamprophyric, and carbonatitic. Numerous geological investigations into the IRAC have resulted in a wide range of calculated ages, ranging from 165 to 459 Ma (Locock 1994). By focusing on the late dyke phases, it may be possible to constrain the age of the final period of magmatism associated with the IRAC, and provide insight into the parental source.

GEOLOGICAL SETTING

The IRAC is hosted in folded and faulted sedimentary rocks of Cambrian to lower Ordovician age (Currie 1975). These units are the slaty-limestone of the McKay Group (Cambro-Ordovician), massive limestone of the Ottertail Formation (Cambrian), and the sheared argillaceous rocks of the Cambrian Chancellor Formation (Allan 1914, Aitken & Norford 1967).

The IRAC was emplaced in a passive

margin setting, in the facies transition between shallow water carbonates and deeper water shales. During the Laramide orogeny (Cretaceous-Paleocene), the IRAC and host rocks were thrust approximately 200 km to the east, along a west-dipping décollement surface (Gabrielse 1991). During transport the IRAC acted as a relatively competent mass, whereas the host strata were mildly to strongly sheared (Currie 1975; Locock 1994). However, units near the margin of the IRAC, such as syenitic and lamprophyric dykes intruding the Ottertail Formation, are strongly deformed—often exhibiting boudinaged structures. The IRAC and host rocks have been regionally metamorphosed to prehnite-pumpellyite facies (Currie 1975).

Geology of the IRAC

The IRAC can be divided into four intrusive subunits, in order of emplacement these are: (1) an older feldspar-free layered mafic sub-complex (LMSC), (2) a large carbonatite lens, (3) a zoned nepheline syenite sub-complex (ZSSC), and (4) a dyke suite consisting of syenitic dykes, carbonatites, and alkaline

lamprophyres, as well as sodalite-bearing veins which cross-cut units of the complex and the host strata (Allan 1914; Currie 1975). The entire complex contains numerous veins, schlieren, and pegmatitic patches.

The feldspar-free LMSC consists of rhythmically layered sequences of: jacupirangite, ijolite, mela-ijolite, melanite ijolite, urtite, and wollastonite urtite (Currie 1975). These units are characterized by a lack of feldspar, and the presence of accessory primary calcite. Contacts between units are gradational, and grain size can vary widely within units.

The ZSSC consists of melano-leucocratic miaskitic nepheline syenite, with smaller quantities of sodalite syenite, peralkaline nepheline syenite pegmatites, zeolite syenite, and eudialyte syenite (Currie 1975; Locock 1994). The syenite sub-complex forms a roughly zoned, elliptical mass, which changes outwards from a pale green sodalite syenite core, to a leucocratic nepheline syenite, to a margin of melanocratic nepheline syenite.

Distribution of Dykes

The most pervasive late igneous feature in the eastern portion of the IRAC is the syenitic dyke swarm. The number of syenitic dykes is at least an order of magnitude greater than the lamprophyric dykes, and at least two orders of magnitude greater than the carbonatitic dykes. In its current orientation the syenitic dyke swarm displays a distinct NNW-trend, and the majority of the dykes dip southwest at moderate angles (35-65°), but shallow and near vertical dykes are observed. The dykes are typically light grey, fine-grained to pegmatitic, and range in width from 20 cm to >5 m. The exposed lateral extent of these dykes varies from a few metres to more than 200 m, where they typically either pinch out, or are covered in talus. Within the eastern portion of the IRAC, the syenitic dyke swarm cross-cuts the LMSC, ZSSC, and intrudes the Ottertail Formation. Within the dyke swarm, up to three different cross-cutting relationships have been observed

at a single outcrop, with contacts varying from sharp boundaries to diffuse margins.

Numerous aphanitic to fine-grained sannaite lamprophyres have been observed. They are dark grey to greenish, range in width from 15 cm to 3 m, and cross-cut the ZSSC, LMSC and Ottertail Formation. The lamprophyres all trend between ESE to WNW.

The contacts between lamprophyres and the IRAC range from planar to very irregular. The lamprophyres typically exhibit a chilled margin. However, at both the hand sample and thin-section scale, a sannaite lamprophyre sample exhibits a cusped boundary against a nepheline syenite dyke, indicative of two partially molten materials. Lamprophyre dykes cross-cutting syenitic dykes have also been observed.

Several carbonatite dykes/dykelets were observed; typically varying in width from 10 cm to 1.25 m, and from fine-grained to pegmatitic. The dykes generally have irregular contacts, and carbonatite dykes in the LMSC display evidence of a phlogopite-rich fenitization halo extending 1 to 5 m into the host rocks. There were no observed contacts between carbonatitic dykes and the syenitic dykes or lamprophyres, therefore no unambiguous order of relative emplacement can be determined for these units.

Petrography

Based on mineralogical and textural similarities (supported by geochemistry), the rocks of the syenitic dyke swarm can be subdivided into three groups: (1) nepheline syenite – nephelinolite group (NS-N), (2) syenite – monzodiorite group (SM), and (3) an alkali feldspar granite dyke.

The rocks of the NS-N dyke group range from nepheline syenite to sodalite-bearing nephelinolite. The primary phases in the NS-N dyke group are k-feldspar and nepheline, with variable abundances of amphibole, plagioclase, phlogopite, calcite, sodalite, titanite, cancrinite, apatite, clinopyroxene, zircon, chlorite, quartz, pyrochlore, and opaque phases.

The rocks of the SM dyke group range from mica syenite to mica rich nepheline-bearing monzodiorite. All observed SM dykes intrude the Ottertail Formation. The SM dyke group is characterized by a foliation (with exceptions) defined by the arrangement of kfs, pl, and white mica, also containing variable abundances of amp, ne, phl, cal, ttn, cpx, zrn, ep, qtz, and opaque phases.

All lamprophyres have been classified as sannaite lamprophyres, except an ultramafic damtjernite. The sannaite lamprophyres contain kfs, amp ± cal, cpx, phl, ap, pl, sodalite, ms, ttn, ep, white mica, chl, zrn, and opaque phases. The coarse-grained damtjernite consists of phenocrystic phlogopite, with groundmass calcite, alkali feldspar, and apatite.

Based on mineralogy the carbonatitic dykes have been classified as calciocarbonatites and ferrocarnatites; composed of cal ± kfs, phl, chl, ne, sodalite, and monazite.

Geochemistry

Overall the syenitic dykes are characterized by moderate silica contents (48 – 66 wt.%), CaO < Na₂O, low P₂O₅ (< 0.19 wt.%), TiO₂ (< 1.02 wt.%), MnO (< 0.3 wt.%), and a strong negative correlation between Al₂O₃ and MgO. Although generally enriched, the syenites have a wide range in ΣLREE (100–1970 ppm) and ΣHREE + Y (10–234 ppm) concentrations. The dykes range between peraluminous to peralkaline, with a subordinate number that are metaluminous. The dykes do not have strong europium anomalies; all Eu/Eu* values fall within 1.00±0.26. Relative to the SM group and alkali feldspar granite dyke, the NS-N group is characterized by lower silica contents (37–54 wt.%), enrichment in CaO, K₂O, Sr, and lower concentrations of Zr, Hf, U, Th, and Ta. The NS-N group is compositionally akin to the ZSSC, and are interpreted to be the result of periodic tapping of the ZSSC during formation.

The sannaite lamprophyric dykes are characterized by low silica (< 46 wt.%), CaO > Na₂O, low P₂O₅ (< 1.09 wt.%), and

strong negative correlation of MgO with SiO₂ and Al₂O₃. The ΣREE range between 337 – 507 ppm, and the (La/Yb)_{pm} values range between 22-32, indicating moderate LREE enrichment.

The carbonatites have a wide range in ΣLREE (150–25600 ppm) and ΣHREE + Y (60–1690 ppm) concentrations, and (La/Yb)_{pm} values range from 4 – 275, indicating weak to very strong LREE enrichment.

Sm-Nd and Rb-Sr isotopes

Sm-Nd isotopic data for the SM – NS-N syenite groups and sannaite lamprophyres are indistinguishable ($\epsilon_{Nd}=2.5$ to 4.0; based on an age of 368 Ma). Using the Rb-Sr data, the sannaite lamprophyres ($^{87}Sr/^{86}Sr_{368} = 0.70334 - 0.70392$) and NS-N dykes ($^{87}Sr/^{86}Sr_{368} = 0.70328 - 0.70431$) are also inseparable; however, the representative sample of the SM group is slightly lower ($^{87}Sr/^{86}Sr_{368} = 0.70291$).

As the sannaites have moderate to high Mg# (27-54), Nb/U (26-48), and no xenoliths (all consistent with minimal crustal contamination) they can be used to assess the nature of the mantle source. Regardless of the variation between groups, the low $^{87}Sr/^{86}Sr_{368Ma}$ values suggest that the sannaites (and syenites) were derived from partial melting in the mantle, and the ϵ_{Nd} values indicate that the mantle source was depleted relative to bulk earth.

The Sm-Nd data were used to create an isochron, which was used to derive and age (Fig. 1). The calculated age, 369±19 Ma, is in excellent agreement with the known age of the complex, 368±4 Ma (Parrish *et al.* 1987). This age is also consistent with our preliminary LA-ICP-MS zircon U-Pb dating of dykes in the SM and the NS-N groups.

Monazite crystals within the ferrocarnatite sample were dated using CHIME U-Th-Pb, and an age of 165±8 Ma was calculated. This age was used to evaluate the Sm-Nd ($\epsilon_{Nd} = -6.0$) and Rb-Sr ($^{87}Sr/^{86}Sr_{165} = 0.71061$) data; these values are considerably different than the syenites and the sannaites. The high initial $^{87}Sr/^{86}Sr$ and low ϵ_{Nd} indicate that the

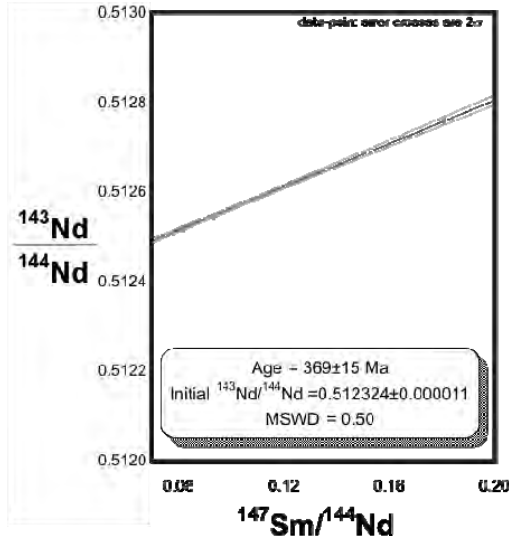


Fig. 1. Four point Sm-Nd isochron of the syenitic dykes (SM and NS-N groups).

carbonatite was derived from either a crustal source, or an enriched mantle source contaminated by crustal rocks, e.g., Ottetail Formation ($^{87}\text{Sr}/^{86}\text{Sr}_{165 \text{ Ma}} = 0.71206$, $\epsilon_{\text{Nd}} = -23$; Locock 1994).

CONCLUSIONS

- (1) The syenitic dyke swarm of the Moose Creek Valley can be subdivided based on mineralogy and geochemistry, into three groups: SM, NS-N, and an alkali feldspar granite dyke.
- (2) Isotopic data suggests that the sannaite lamprophyres and syenitic dykes are related to the same parental magma.
- (3) The SM and NS-N dykes are temporally related to the IRAC.
- (4) The ferrocarnatite is both isotopically and temporally distinct from the IRAC.
- (5) The carbonatites appear to have the

highest REE potential in the IRAC. However, as some REE-rich carbonatite dykes are related to separate magmatic event that occurred prior to the décollement, an undiscovered carbonatite body with REE potential may exist to the west.

ACKNOWLEDGEMENTS

We thank Eagle Plains Resources Ltd. for field area access, geochemical analyses, and financial support, specifically Jarrod Brown. Funding for this research was also provided by NSERC Discovery grants to D. Lentz and C. Shaw.

REFERENCES

- AITKEN, J.D. & NORFORD, B.S. 1976. Lower Ordovician Survey Peak and Outram Formations, southern Rocky Mountains of Alberta. *Bulletin of Canadian Petroleum Geology*, **15**, 150-207.
- ALLAN, J.A. 1914. Geology of field map-area, B.C. and Alberta. *Geological Survey of Canada, Memoir 55*, Ottawa, ON.
- CURRIE, K.L. 1975. The geology and petrology of the Ice River Alkaline Complex, British Columbia. *Geological Survey of Canada Bulletin 245*, Ottawa, ON.
- GABRIELSE, H. 1991. Structural Styles. In: GABRIELSE, H. & YORAT, C.J. (ed.), *Geology of the Cordilleran Orogen in Canada*. Geological Survey of Canada, Ottawa, ON, 81-98.
- LOCOCK, A.J. 1994. *Aspects of the geochemistry and mineralogy of the Ice River alkaline intrusive complex, Yoho National Park, British Columbia*. MSc thesis, University of Alberta, Edmonton, Alberta.
- PARRISH, R.R., HEINRICH, S., & ARCHIBALD, D. 1987. In: *Radiogenic Age and Isotopic Studies: Report 1*, Geological Survey of Canada, Paper **87-2**, 33-37.

Morphology of gold nanoparticles synthesised from gold chloride and gold cyanide complexes under evaporative conditions

Ryan R. P. Noble¹, Elizabeth M. Grenik^{1,2}, Robert M. Hough¹, Melvyn J. Lintern¹, David J. Gray¹, Rob Hart², Peta Clode³, & John Murphy³

¹CSIRO Exploration and Mining, 26 Dick Perry Avenue, Kensington, WA 6151 AUSTRALIA
(e-mail: ryan.noble@csiro.au)

²Centre for Materials Research, Curtin University of Technology, GPO Box U1987, Perth, WA 6845 AUSTRALIA

³Centre for Microscopy, Characterisation and Analysis, University of Western Australia, 35 Stirling Hwy, Crawley, WA 6009 AUSTRALIA

ABSTRACT: Single crystal, gold micro- and nano-particles were formed by evaporation of aqueous chloroauric acid and gold potassium cyanide. Gold crystal morphologies varied slightly with reaction time and temperature. In nearly all treatment combinations some micro and nano gold triangles and hexagons with face-centred cubic crystal system were present. Nanoparticles of Au were commonly observed in the 60-200 nm diameter size range. Characterization was conducted by UV-Vis spectroscopy, scanning electron microscopy with energy dispersive x-ray spectroscopy, transmission electron microscopy and confocal microscopy. The abundance of Au particles was low. However, the results of this work indicate that these morphologies are commonly and rapidly formed by evaporation, do not require bacteria, and have similar size distribution as those found naturally near a Au deposit in Western Australia. The results indicate that the formation of these natural crystals takes place very quickly (i.e., in a few hours or days). The inorganic process of groundwater evaporation is likely to be the major driving force for the formation of true secondary Au deposits in the vadose zone, particularly in arid and semi-arid regions of the world.

KEYWORDS: *gold, nano, particle, supergene, inorganic, Yilgarn Craton*

INTRODUCTION

Nano-particulate Au, with constrained morphology, has potential application in numerous fields. Bio-sensing, catalysis and optics (Shankar *et al.* 2004) are making use of nano-particulate noble metals.

Synthesis in solution of these nanoparticles has commonly used chloroauric acid, a reductant and a capping agent, with more recent developments utilizing organic ligands (Bi *et al.* 2008; Tan *et al.* 2003). The use of bacteria has also been associated with the formation of micro- and nano-particulate Au (Lengke *et al.* 2006; Southam & Beveridge 1994; Reith *et al.* 2006). Common gold crystal shapes (e.g., triangles and hexagons) have consistently been observed with these methods.

Recent work has identified populations of micro- and nano-particulate Au in natural supergene Au deposits (Hough *et*

al. 2008; Noble *et al.* in press). Natural supergene or secondary gold deposition occurs through weathering of the primary hypogene gold deposit and associated dissolution of the gold from the host quartz or sulfide primary minerals. The gold is remobilized in solution, transported and then redeposited via precipitation at a later stage.

Understanding the formation of micro- and nano-particulate gold may lead to a better understanding of supergene Au deposits, as well as the distance travelled and environmental conditions of mobilized Au (Noble *et al.* in press). This work has investigated the use of evaporation as the major process to form the Au morphologies observed. The influence of pH and ligand type on Au morphological variation has also been assessed.

MATERIALS AND METHODS

Experiments were conducted with

treatments varying in Au concentration, temperature of reaction, temperature of evaporation, time, organic additives and pH. The reagents used were: H₂AuCl₄ (Ajax); AuCl₃ (Alfa Aesar); KAuCN₂ (Johnson Matthey); millipore water (< 18 ohm); 0.1M HCl and 0.1M NaOH for pH adjustment of AuCl₃; 0.1M HNO₃, and 0.1M KOH for pH adjustment of KAuCN₂. In brief, 10 mL of Au-bearing solution was pipetted into a glass vial. The solution was then subjected to the various treatment parameters mentioned previously. Following this, 0.4 mL of the solution was pipetted onto glass slides (and carbon coated copper grids for Transmission Electron Microscopy - TEM) and left to evaporate at room temperature or on a hot plate at approx. 120°C in a fume hood. To confirm the absence of bacteria the slide was stained with SYTO[®] 9 green fluorescent nucleic acid stain.

UV-Vis absorbance of the solutions was measured on a Varian Cary 50 Spectrophotometer from 400-1000 nm at the initial introduction of solutions and at the end of the experiment.

Scanning electron microscopy (SEM; Philips XL-40) with an energy dispersive x-ray spectrometer (EDS) was used to obtain large scale images using the backscatter electron (BSE) detector and compositional data (EDS), operating at 30 kV. Field emission scanning electron microscopy (FESEM) images were collected on a model Zeiss 1555 VP-FESEM. An accelerating voltage of 3kV was used; this was adjusted to 1kV for some images to obtain true surface images during secondary electron imaging. For sample preparation the glass slides used previously, were subject to a thin carbon coating and were fixed on the edges using carbon tape.

TEM images were collected on a JEOL 2011 model at Curtin University Centre for Materials Research, Bentley, Australia.

SYTO[®] 9 stained fluorescence was imaged using a Leica TCS SP2 AOBS multiphoton confocal microscope.

RESULTS AND DISCUSSION

Single crystal, gold micro- and nano-

particles were formed by evaporation of aqueous chloroauric acid and gold potassium cyanide. Micro- and nano- gold triangles and hexagons with face centred cubic crystal morphology were observed. Nanoparticles of Au were commonly observed in the 60-200 nm diameter size range. Typical Au particles formed from AuCl₃ solutions are shown in Fig. 1. The experiments indicate that time in solution at a given temperature or pH condition did not greatly change the observed morphologies. Higher temperatures did result in fewer observed triangles.

In comparison to AuCN, AuCl₃ consistently produced greater numbers of Au triangles and hexagons. As expected, the more concentrated solutions produced greater numbers of Au particles. The dilute 5 ppm Au solutions were used for a more realistic comparison to natural solutions, although concentrations were still 2-3 orders of magnitude greater than those measured in the Golden Virgin pit, the site of naturally occurring particulate Au observed by Hough *et al* (2008).

The various experiments found populations of single crystal, Au particles. Sizes ranged from 20 µm to 60 nm. Numerous other Au-ligand salts were also present in varied morphologies.

The initial experiments conducted using H₂AuCl₄ and AuCN indicate that the particulate Au is not present in the solution, but is formed as a result of the concentration during evaporation. Later experiments with AuCl₃ solutions are similar to previous work in the area of materials science where nano-particles were shown to form in the solution as Au colloids formed with a resulting change in the solution colour as the reaction progresses, with colour controlled by the size of the colloidal Au (Shankar *et al.* 2004). Using evaporation as the mechanism of formation and the more acidified conditions similar to that of the southern Yilgarn groundwater environment, the absorption did not change during the experiments, indicating the Au is not colloidal during this time and formed after the solution was placed on the slide as a result of evaporation.

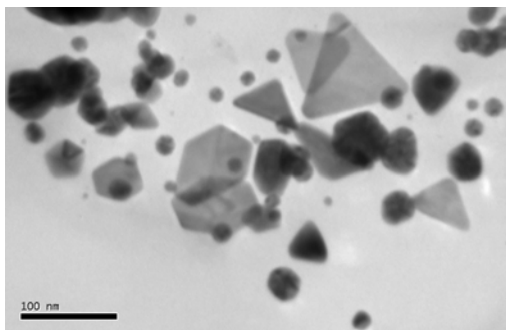


Fig. 1. Typical shapes of nanoparticulate gold formed from these experiments.

The size and nature of these Au populations is highly relevant to our understanding of partial extraction results of gold bearing regolith materials where interpretations of what Au is being extracted is key to the origin and exploration significance of the Au anomaly detected. It also supports a mechanism of colloidal transport of Au during supergene processes.

CONCLUSIONS

The results of this work indicate that triangular and hexagonal morphologies are commonly and rapidly formed by evaporation, do not require bacteria, and have similar size distribution as those found naturally near a Au deposit in Western Australia. The inorganic process of groundwater evaporation is potentially the driving force for the formation of transported Au deposits in the vadose zone, particularly in arid and semi-arid regions of the world.

ACKNOWLEDGEMENTS

Michael Verrall and Greg Hitchen (CSIRO) assisted in SEM work. The National Measurement Institute allowed use of the absorbance spectrophotometer. Western

Australia Centre for Microscopy for access to facilities. Funding for this work was provided by CRC LEME and CSIRO Minerals Down Under Flagship program.

REFERENCES

- BI, Y.P. & LU, G.X. 2008. Morphological controlled synthesis and catalytic activities of gold nanocrystals. *Materials Letters*, **62**, 2696-2699.
- HOUGH, R. M., NOBLE, R.R.P., HITCHEN, G.J. *et al.* 2008. Naturally occurring transparent gold nanoplates and particles. *Geology*, **36**, 571-574.
- KAMAT, P.V. 2002. Photophysical, photochemical and photocatalytic aspects of metal nanoparticles. *Journal of Physical Chemistry. B*, **106**, 7729-7744.
- LENGKE, M.F., FLEET, M.E., & SOUTHAM, G. 2006. Morphology of gold nanoparticles synthesised by filamentous cyanobacteria for gold(1)-thiosulfate and gold(III)-chloride complexes. *Langmuir*, **22**, 2780-2787.
- NOBLE, R.R.P., HOUGH, R.M., & GRENIK, E.M. *in press*. Natural and experimental clues to understand the transport and deposition of supergene gold in Western Australia. Explore.
- REITH, F., ROGERS, S. L., MCPHAIL, D. C., & WEBB, D. 2006. Biomineralization of Gold: *Biofilms on Bacterioform Gold*. *Science*, **313**, 233-236.
- SHANKAR, S.S., RAI, A., ANKAMWAR, B., SINGH, A., AHMAD, A., & SASTRY, M. 2004. Biological synthesis of triangular gold nanoparticles. *Nature Mater.* **3**, 482-488.
- SOUTHAM, G. & BEVERIDGE, T.J. 1994. The in-vitro formation of placer gold by bacteria. *Geochemica Cosmochemica Acta*, **58**, 4527-4530.
- TAN, Y., DAI, X., LI, Y., & ZHU, D. 2003. Preparation of gold, palladium and silver nanoparticles by the reduction of their salts with a weak reductant – potassium bitartrate. *Journal of Materials Chemistry*, **13**, 1069-1075.

Coupled Micro-XRF elemental mapping and LA-ICP-MS geochemistry of pyrites to decipher the cause of gold precipitation in quartz-sulfide gold-bearing veins, Poderosa-Pataz district, Peru

Carlos Oré Sanchez¹ & Damien Gaboury^{1, 2}

¹ Université du Québec à Chicoutimi (UQAC), ² Laboratoire de métallogénie expérimentale et quantitative (LAMEQ), 555, boul. de l'Université, Chicoutimi, G7H 2B1 CANADA (e-mail: carlos.ore@uqac.ca)

ABSTRACT: The geochemistry of pyrite associated with visible gold particles was studied by micro-XRF mapping and in situ LA-ICP-MS analysis to unravel metal enrichments and relationships in the quartz sulfide veins of the Poderosa-Pataz gold district in Peru. Element mapping in pyrite surrounding gold grains ranging from 0.01 to 0.15 mm revealed the systematic enrichment of As around or very close to visible gold accumulation. These As-enrichment zones define discordant rims and corridors overprinting pyrite grains. LA-ICP-MS spot analyses, performed in and outside the As-enrichment, indicate that As is enriched by factors up to 2000X in association with gold. In As-rich zones, Au, Ag, Hg and Sb are enriched 10X whereas Zn, Cu, Cd, In and Sn are depleted by the same factor. The electrochemical precipitation of gold is proposed as the main mechanism because of the intrinsic link between gold grains and As-enrichment in pyrites. Secondary pyrite transformation by hydrothermal fluids with elevated As and Au, Ag, Hg and Sb have induced change in semiconducting properties of the pyrite grains resulting in the precipitation of “invisible gold” and accumulation of gold particles during the last stage of the hydrothermal fluid circulation.

KEYWORDS: *Micro-XRF, LA-ICP-MS, pyrite, gold, Peru*

INTRODUCTION

The association between gold and pyrite is very common for most hydrothermal gold deposits. Gold can occur as “invisible gold” in arsenic-rich pyrite and arsenopyrite, as well as visible accumulations along the pyrite grain boundaries and as fracture filling and inclusions in pyrite. The cause of gold precipitation in association with pyrite has significant implications for ore genesis and mineral exploration. In this paper, we present the results of a detailed study of gold-pyrite relationships from various quartz sulfide gold-bearing veins from the Poderosa-Pataz district. This district, located in the Eastern Andean Cordillera of Northern Peru, produced > 6 M oz of gold in the past ~100 years from more than 30 veins hosted by the 330-327 Ma calc-alkaline granodiorite-diorite Pataz batholite (Haeberlin *et al.* 2004).

METHODOLOGY

Textural association between pyrite and

gold were studied in 96 polished sections from 20 different veins covering 2500 m of vertical elevation and 13 km laterally in the district. From these samples, 30 pyrite-gold relationships, on 17 polished sections were studied in detail using an EDAX Eagle III micro-XRF at UQAC. Detailed images of Mo, Ag, Sb, Cr, Fe, Co, Ni, Cu, As and Pb element distribution in pyrites with resolution of about 50 µm were produced over sample areas as large as 1 cm x 1 cm around visible gold grains (Fig. 1). The four most representative polished sections were studied by LA-ICP-MS at UQAC to obtain quantitative analyses of Ag, As, Au, Bi, Cd, Co, Cu, Ga, Ge, Hg, In, Mo, Ni, Pb, Sb, Se, Sn, Te, Th, Tl, W, U, and Zn. A total of 155 spot analyses, with spot diameter of 50 µm, were performed in pyrite grains close to visible gold particles. Analytical parameters and apparatus specifications are given in Gaboury & Graham (2004). The MASS-1 (Wilson *et al.* 2002; Tubrett *et al.* 2003) was used as a calibration standard for quantitative analyses. The data were

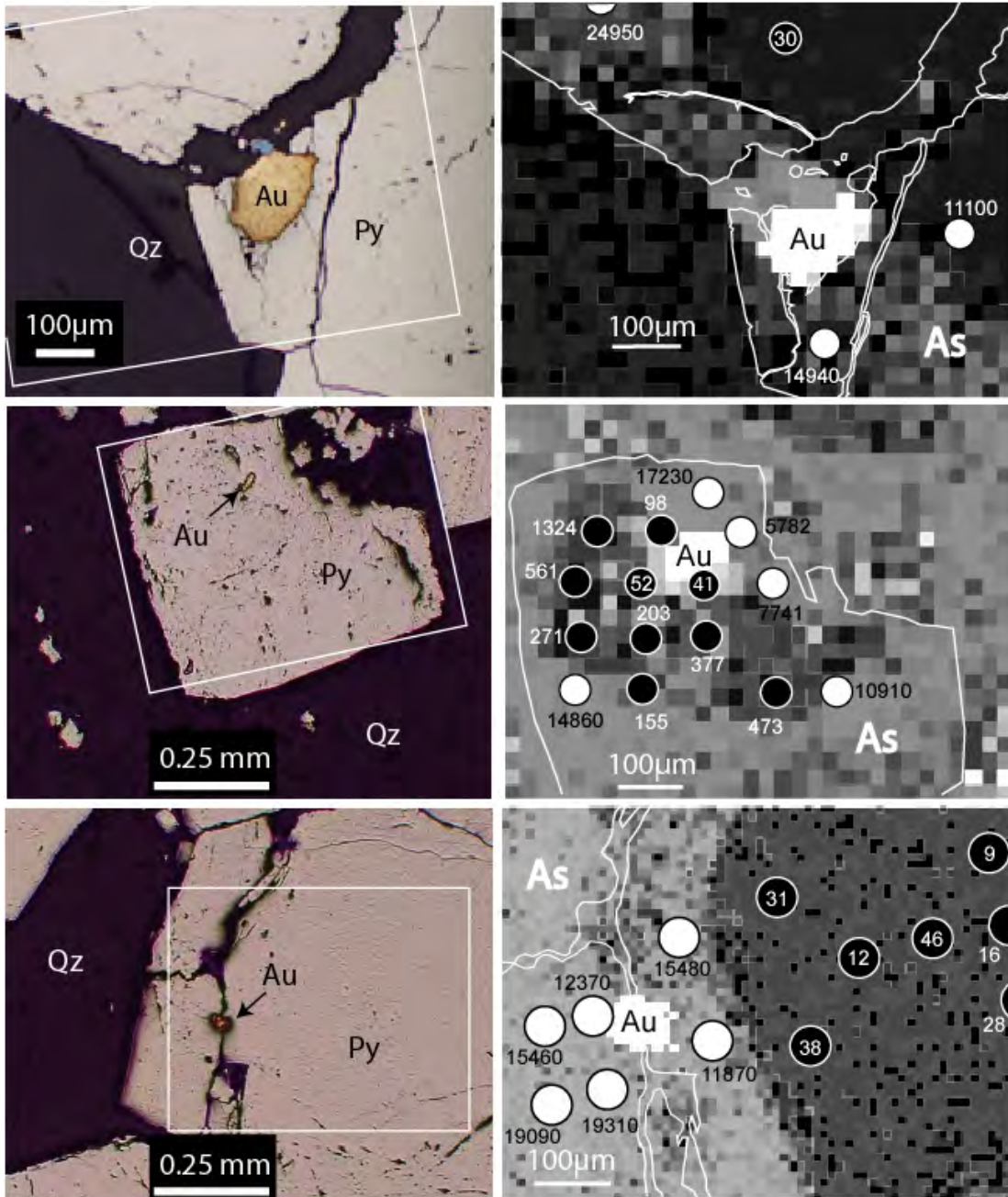


Fig. 1. Left side: microphotographs of visible gold occurrences in relation to pyrite crystals. Right side: related micro-XRF elemental mapping of As and spot location of LA-ICP-MS analyses with As values (ppm). The exact location of the micro-XRF map is indicated by the white square on the microphotographs (left side). On right side images, the light grey pixels indicate a relative enrichment of As in pyrites. For reference, the white contorted lines are the pyrite crystal borders. White and black spots are As-rich and As-poor portions of pyrites respectively. Note the discordant aspect of the As-enrichment corridors relative to the pyrite crystals and the sharp transition from As-poor and As-rich zones indicated by the LA-ICP-MS analytical As values.

reduced using the Thermo Plasmalab software version 2.5.5. Blank signal was

collected during 30s and ablation signal during 90s hence providing a time-

resolved signal. Calculation areas on the ablation signal were selected by considering consistency of As and Au signals. Sparks of Au-Ag signal related to inclusions were not included in the calculation. Analytical precision based on replicate analysis of the MASS-1 is better than 10%.

RESULTS

Under the microscope, gold forms visible particles ranging in size from 0.01 to 0.15 mm. Based on 839 observations of gold grains, it is established that visible gold occurs mostly 1) as fracture filling and inclusions in pyrite and at the interface between pyrite crystals (86%); 2) at the contact between pyrite and other sulfides (8%) such as arsenopyrite and chalcopyrite; and 3) in gangue minerals (6%).

The most striking outcome of the micro-XRF elemental mapping is the systematic association of visible gold with enrichment of As in pyrite (Fig. 1). Four dominant geometries are observed: 1) aureoles surrounding gold particles occurring as inclusions and along microfractures in pyrite; 2) rims developed at the interface along pyrite grains; 3) rims along boundaries of single pyrite crystals; and 4) as discordant corridors overprinting aggregated pyrite grains.

Quantitative LA-ICP-MS analyses were performed according to the subdivision between As-rich and As-poor portions of pyrite grains as revealed by micro-XRF maps. Suites of elements can be distinguished relative to As-enriched zones in pyrites (Fig. 2): 1) Au, Ag, Hg, and Sb are enriched by a factor of about 10 relative to As-poor zones; 2) Pb, Bi, and Co are slightly enriched; 3) Ni, Se, Mo, Ge, Te and Ga remain constant; and 4) Zn, Cu, Cd, In and Sn are depleted. Spatially, the transition from As-enriched to As-poor zones in pyrite is very sharp (Fig. 1). In these examples, the bimodal

distribution of As is clearly evidenced by factors of enrichment up to 2000 relative to the background levels in pyrite.

DISCUSSION

There is an intrinsic association between visible gold accumulation and zones of As-enrichment in pyrites. These spatial relationships may be explained by the electrochemical precipitation model of Moëller & Kersten (1994). The model implies that a small difference in electrical potential, due to As enrichment, induces electrochemical precipitation and accumulation of gold. Arsenic zoning in pyrite is well documented for gold deposits and commonly occurs as oscillatory concentric bands. They are interpreted as the result of fluctuation of fluid composition and physico-chemical conditions during pyrite growth (e.g., Belcher *et al.* 2004). In our case, the As-zoning clearly overprints pyrite crystals and aggregates and appears controlled by anisotropies such as fractures and grain boundaries. The precipitation of “visible gold” is hence related to a secondary change in pyrite composition induced by later hydrothermal fluids. These later fluids in addition to As, were also enriched in Au, Ag, Hg and Sb.

CONCLUSION

The electrochemical precipitation of gold is considered here the main mechanism for gold precipitation. Such a mechanism can be viewed as a filter to extract gold in solution, even in low concentration, during hydrothermal fluid flow in the veins. It can also be considered as independent of physico-chemical condition variations, hence accounting for the vertically and laterally extensive gold mineralization in the prolific Poderosa-Pataz district. The most important contribution of our study lies in the fact that the As enrichment is not a primary feature of pyrite growth but

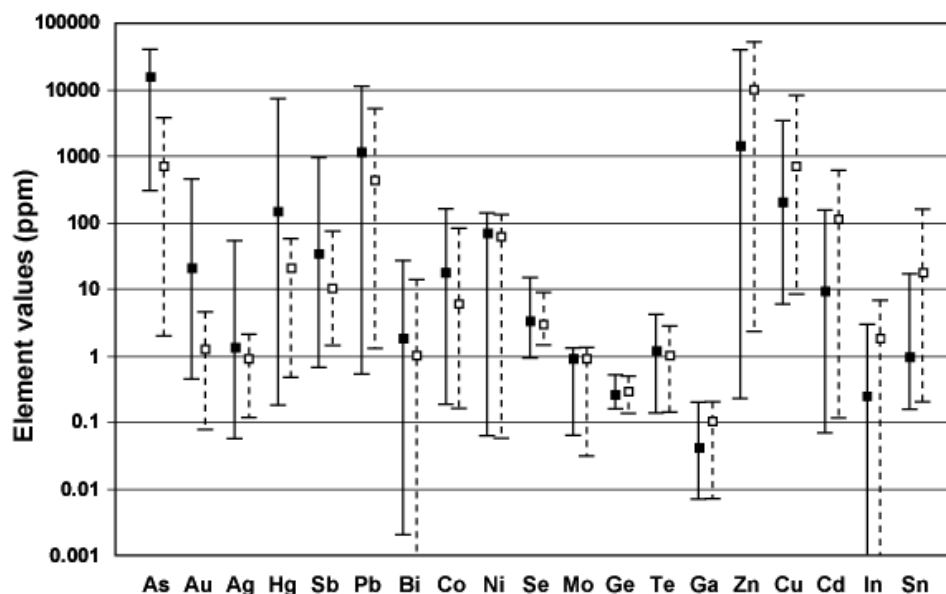


Fig. 2. Elemental range (line) and average (square dots) for LA-ICP-MS spot analyses in As-rich zones (black square: n = 96) and As-poor zones (open square and dashed line: n = 59) in pyrites. The order of elements follows the proposed suites of element behaviour relative to As enrichment (see text).

was rather induced by secondary fluid circulation. This conclusion highlights the critical role of arsenic for precipitating gold with pyrite even as a later overprint.

ACKNOWLEDGEMENTS

This is part of an ongoing PhD thesis by the first author. Funding is from Poderosa SA mining company (Peru) and NSERC grant to D. Gaboury. P. Bédard, R. Cox and D. Savard helped with the apparatus and data reduction.

REFERENCES

BELCHER, R.W., ROZENDAAL, A., & PRZYBYLOWICZ, W.J. 2004. Trace element zoning in pyrite determined by PIXE elemental mapping: evidence for varying ore-fluid composition and electrochemical precipitation of gold at the Spitskop deposit, Saldania Belt, South Africa. *X-Ray Spectrometry*, **33**, 174-180.

GABOURY, D. & GRAHAM, S. 2004. In-situ trace elements by LA-ICP-MS in metamorphosed pyrites as pathfinder for hydrothermal conditions. *Geochimica et Cosmochimica Acta*, Abstract of the 13th annual V.M.

Goldschmidt Conference Copenhagen, Denmark, June 5-11, 2004, A303.

HAEBERLIN, Y., MORITZ, R., FONBOTÉ, L., & COSCA, M. 2004. Carboniferous Orogenic Gold deposits at Pataz, Eastern Andean Cordillera, Peru: Geological and Structural Framework, Paragenesis, Alteration, and ⁴⁰Ar/³⁹Ar Geochronology. *Economic Geology*, **99**, 73-112.

MÖLLER, P. & KERSTEN, G. 1994. Electrochemical accumulation of visible gold on pyrite and arsenopyrites surfaces. *Mineralium Deposita*, **29**, 404-413.

TUBRETT, M., MIKOVA, J., SYLVESTER, P.J., & KOSLER, J. 2003. Trace element composition and homogeneity of MASS-1 sulfide calibration standard In: 5th International Conference on the Analysis of Geological and Environmental Materials, Rovaniemi. 9-11 June 2003 (<http://www.gsf.fi/geoanalysis2003/>)

WILSON, S.A., RIDLEY, W.I., & KOENIG, A.E. 2002. Development of sulfide calibration standards for the laser ablation inductively-coupled plasma mass spectrometry technique. *Journal of Analytical Atomic Spectrometry* **17**, 406-409.

IPGE (Os, Ir, Ru) are not in chromite

Philippe Pagé¹, Sarah-Jane Barnes¹, Michael L. Zientek²,
Hazel M. Prichard³, & Peter C. Fisher³

¹ Canadian Research Chair in Magmatic Metallogeny, Sciences de la Terre, Université du Québec à Chicoutimi (UQAC), 555 bld de l'Université, Saguenay, PQ, G7H 2B1 CANADA (e-mail: ppage@uqac.ca),

² U.S. Geological Survey, Spokane, Washington U.S.A

³ School of Earth and Ocean Sciences, Cardiff University, Main Building, Park Place, Cardiff, CF10 3YE UK

ABSTRACT: The correlation between Cr and IPGE (iridium-group platinum-group elements; Os, Ir, Ru, \pm Rh) and the similarity in the IPGE contents of chromitites from different settings suggest that the IPGE should partition into chromite. Experiments have shown that IPGE partition into spinel under oxidizing conditions. We have analyzed the IPGE in natural chromites using LA-ICPMS and can show that these elements are all below detection levels. Mass balance calculations show that chromite does not control the IPGE budget. Exsolution of IPGE from chromite in plutonic rocks is not a viable mechanism since we obtained similar results for chromite in lavas. IPGE are undetectable in chromite probably because they do not enter the chromite structure at geologically-realistic oxygen fugacities.

KEYWORDS: chromitite chromite, IPGE, PGM, oxygen fugacity, Laser-Ablation ICP-MS

INTRODUCTION

The well-known association between chromitite deposits and IPGE (Os, Ir, Ru, \pm Rh) enrichments (Page *et al.* 1982a, b; Stockman & Hlava 1984), as well as the similar IPGE contents between mantle chromitites and crustal chromitites (Fig. 1), have led researchers to suggest that IPGE partition into chromite. The fractionation of IPGE from Pt and Pd by chromite is used in petrogenetic modelling of stratiform PGE deposits.

This hypothesis has been reinforced by experimentalists who demonstrate that under oxidizing conditions ($fO_2 > FMQ+2$; FMQ: Fayalite-Magnetite-Quartz buffer) these elements can partition into spinel (Capobianco & Drake 1990; Capobianco *et al.* 1994; Richter *et al.* 2004; Homolova *et al.* 2008). However, laurite ([Ru, Os, Ir] S_2) and IPGE alloys are commonly present as small, discrete grains included within the chromites (Prichard *et al.* 1981; Stockman & Hlava 1984). Thus, there is some debate as to whether the IPGE enrichment of chromitites is due to partitioning of these elements into chromite or due to pre- to syngenetic laurite and/or alloys now included within chromite.

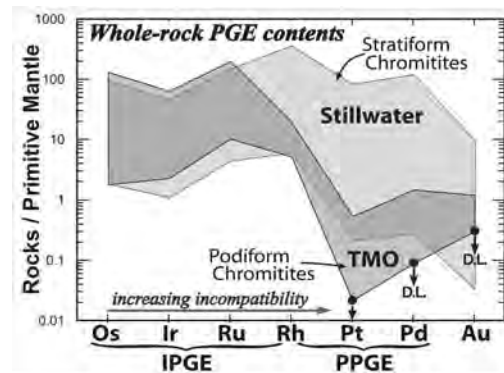


Fig. 1. Primitive mantle (PM) normalized whole rock PGE profiles for stratiform chromitites from the Stillwater Complex and for podiform chromitites from the mantle section of Theftord Mines Ophiolite (TMO). Note the similarity between IPGE contents of chromitites from these different tectonic settings. D.L.= detection limit.

The main purpose of this work is to determine the IPGE contents of chromites from mantle podiform chromitites, from crustal stratiform chromitites and from various types of lavas. The analyses have been carried out by laser ablation inductively coupled plasma mass spectrometer (LA-ICPMS) which allows *in-situ* determination of trace elements in chromite.

STUDIED SAMPLES

We analyzed chromites from 1) podiform chromitite deposits from the mantle section of the Thetford Mines Ophiolite (TMO), southern Québec Appalachians (Canada); 2) stratiform chromitite seams found within the Stillwater Complex, Montana (USA). In addition, we also analyzed chromite in lavas from different tectonic settings in order to: 1) verify whether the IPGE solubility in chromite could be related to geological setting and 2) eliminate recrystallization effects related to slow cooling which could be responsible for exsolution of the IPGE from chromite to form PGM (platinum-group minerals). The lavas we have analyzed to date are two boninites, (one from Bonin Island and the other from TMO), and a MORB from East Pacific Rise (Pagé 2001, 2006).

METHODOLOGY

Chromite major and minor element composition was determined by microprobe. The IPGE contents of chromite were determined at UQAC by a LA-ICPMS (Thermo X7 ICP-MS coupled to a New Wave Research 213 nm UV laser, 80 µm spot diameter, 10 Hz pulse rate, 0.3 mJ/pulse power). In addition to the IPGE other elements were monitored to control the nature of ablated material and the presence of included phases.

Whole rock Cr, Al, Mg, Fe, Co, Ni, Mn, V, Zn, and Sc of chromitites were determined by INAA; whole rock Ti and Ga were determined by XRF, and whole rock PGE were determined by Ni-sulfide fire assay followed by Te co-precipitation with ICP-MS finish.

RESULTS

Many inclusions of PGM were detected during ablation of chromite (Figs. 2 & 3). However, apart from the included PGM, the chromites do not contain any IPGE (detection limits for PGE: Os= 8.9 ppb, Ir= 3.0 ppb, Ru= 43.2 ppb, Rh= 15.9 ppb; Fig. 3).

A mass balance calculation was used to better understand the extent to which the IPGE are controlled by chromite. First, we

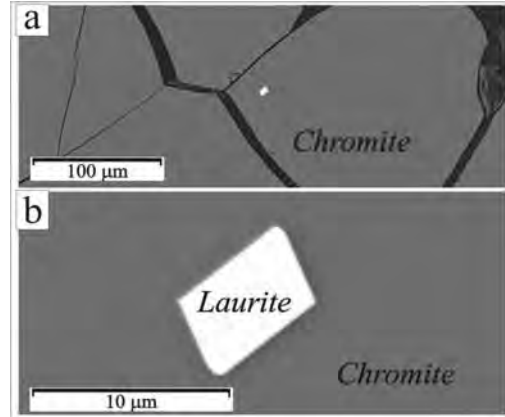


Fig. 2. Backscatter electron images of a laurite grain included within a chromite from Stillwater chromitite H. b) enlargement of transient LA-ICPMS signal shown in a).

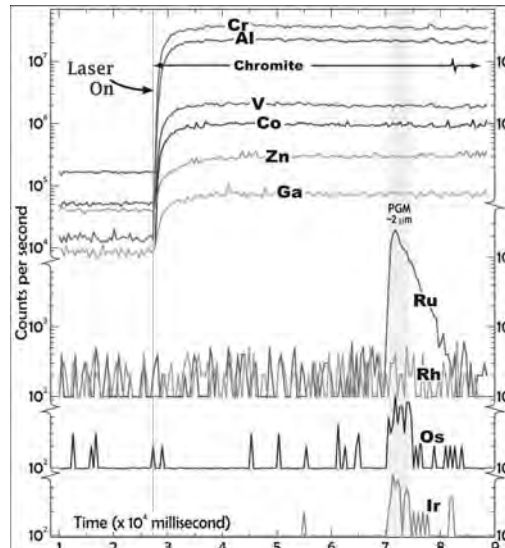


Fig. 3. Graph showing Cr, Al, V, Co, Zn, Ga, Ru, Rh, Os, and Ir profiles from a laser ablation analysis of chromite with counts per second vs time. Apart from a small Ru (±Os, ±Ir)-bearing PGM inclusion (diameter ~2 µm), the chromites do not contain IPGE. Chromite sample is from a podiform chromitite from TMO.

calculated the weight fraction of chromite (F_{Chr}) in samples using the concentration of Cr_2O_3 in the whole-rock and in the chromite. Then, we evaluated the weight fraction of the different elements i from the whole rock that is present in the chromite and controlled by it using the equation:

$$F_{Chr}^i = 100 * (C_{Chr}^i * F_{Chr}) / C_{WR}^i \quad (1)$$

where F_{Chr}^i = % of element i in the whole-rock accounted for by the chromite, C_{Chr}^i = concentration of element i in the chromite, and C_{WR}^i = concentration of element i in the whole-rock (Table 1). Since IPGE were found to be less than detection levels, we used our LLD as the maximum IPGE content in the chromite. The calculations show that IPGE are not controlled by chromite.

In view of the presence of laurite and/or alloys, it can be concluded that these phases control IPGE abundance in chromitites.

DISCUSSION

One explanation to explain why IPGE are not detectable in chromite from plutonic rocks could be that the IPGE exsolve from chromite to form discrete PGM (now included within the chromite). However, if this were the case, it does not account for the source of sulphur found in the PGM (e.g., laurite). Nor does it explain the presence of Pt-bearing PGM, or composite PGM+silicate inclusions within chromite. Furthermore, if the IPGE are not detectable in chromite from plutonic rocks because of their exsolution to form PGM, they should be detectable in chromite from lavas but are not. It is most likely that the IPGE, at realistic oxygen fugacities, do not enter the chromite structure. This invalidates the results obtained from high oxygen fugacity partitioning experiments. Calculated oxygen fugacities from olivine-chromite pairs (Ballhaus *et al.* 1990) range from $0.61 < FMQ < +1.92$ for Stillwater chromitites, and from $-0.74 < FMQ < -0.05$ for TMO chromitites; these values are well below those reported from experiments that studied IPGE partitioning into chromite.

Chromite crystallization from a melt, or its re-equilibration with a melt, creates an even more reduced boundary layer at the crystal-melt interface as a consequence of the incorporation of Cr^{3+} and Fe^{3+} relative to divalent ions. The reduced conditions trigger the precipitation of IPGE minerals on the surface of crystallizing chromite that can be later on entrapped during chromite growth (Finnigan *et al.* 2008).

Table 1. Maximum proportion in % of WR IPGE accounted for by the chromite.

	Os	Ir	Ru	Rh	F_{Chr}
<i>Stillwater stratiform chromitites (n = 29)</i>					
Min	2.5	1.8	5.2	4.4	8.3
Max	27.0	19.0	29.0	49.7	97.3
Ave	11.0	7.9	15.6	22.4	65.7
<i>TMO podiform chromitites (n = 9)</i>					
Min	1.7	1.2	3.6	74.8	37.9
Max	61.2	17.4	40.2	133	86.7
Ave	24.0	7.6	20.2	111	62.6
<i>Various lavas</i>					
MORB	-	5.8	85.8	40.9	0.72
BONb	-	-	15.7	7.7	0.48
TMOb	-	9.8	33.1	10.2	0.36

CONCLUSIONS

We have evaluated the IPGE (Os, Ir, Ru, ± Rh) content of chromite grains from chromitites and lavas in various tectonic settings using LA-ICPMS.

- (1) The concentrations of these elements in chromite are below detection limits. This cannot be attributed to the exsolution of IPGE from chromite to form PGM in slow cooling environments since similar results are obtained from chromite in rapidly cooled lavas.
- (2) Consideration of whole rock and chromite IPGE analyses, when combined in a mass balance calculation, shows that chromite does not control the IPGE budget.
- (3) IPGE solubility in chromite is favoured only at unrealistically high oxygen fugacity. In natural systems, chromite crystallization creates a reduction front that seems to trigger the precipitation of IPGE-bearing minerals on the chromite surface, in the boundary layer between the growing chromite and the surrounding melt (Finnigan *et al.* 2008).

ACKNOWLEDGEMENTS

J.H. Bédard, J.-M. Schroetter, A. Tremblay, and V. Bécu (INRS-ETE) are thanked for their help with mapping, and collecting samples during PP's PhD. P.L. Bédard, D. Savard and R.A. Cox (UQAC) are also thanked for their assistance with

the laboratory work and laser analysis. This work was funded by the Canadian Research Chair in Magmatic Metallogeny.

REFERENCES

- BALLHAUS, C., BERRY, R.F., & GREEN, D.H. 1990. Oxygen fugacity controls in the Earth's upper mantle. *Nature*, **348**, 437-440.
- CAPOBIANCO, C.H. & DRAKE, M. 1990. Partitioning of ruthenium, rhodium, and palladium between spinel and silicate melt and implications for platinum-group element fractionation trends, *Geochimica et Cosmochimica Acta*, **54**, 869-874.
- CAPOBIANCO, C.H., HERVIG, R.L., DRAKE, M. 1994. Experiments on crystal/liquid partitioning of Ru, Rh and Pd for magnetite and hematite solid solutions crystallised from silicate melt. *Chemical Geology*, **113**, 23-43.
- FINNIGAN, C.S., BRENNAN, J.M., MUNGALL, J.E., & McDONOUGH, W.F. 2008. Experiments and Models Bearing on the Role of Chromite as a Collector of Platinum Group Minerals by Local Reduction. *Journal of Petrology*, **49**, 1647-1665.
- HOMOLOVA, V., BRENNAN, J.M., McDONOUGH, W.F., & ASH, R. 2008. Olivine- and spinel-silicate melt partitioning of platinum group elements (PGEs) as a function of oxygen fugacity. *Geological Association of Canada / Mineralogical Association of Canada, Abstracts with program*, 74 p.
- PAGÉ, P. 2001. *L'origine de la distribution des teneurs en EGP dans les faciès mantelliques océaniques et ophiolitiques (exemples de la Faille Transformante Garrett, Pacifique sud et du massif de North Arm Mountain, Complexe Ophiolitique de Bay of Islands, Terre-Neuve, Canada)* M.Sc. thesis, Laval University, Québec, 414 p.
- PAGÉ, P. 2006. *Pétrogenèse de l'ophiolite de Theftford Mines, Québec, Canada, avec un accent particulier sur les roches du manteau et les chromitites*. Ph.D. thesis, Institut National de la Recherche Scientifique, Québec, PQ, Canada, 282 p.
- PAGE, N.J., CASSARD, D., & HAFFTY, J. 1982a. Palladium, Platinum, Rhodium, Ruthenium, and Iridium in chromitites from the Massif du Sud and Tiébaghi Massif, New Caledonia. *Economic Geology*, **77**, 1571-1577.
- PAGE N.J., PALLISTER J.S., BROWN M.A., SMEWING, J.D., & HAFFTY, J. 1982b. Palladium, platinum, rhodium, ruthenium and iridium in chromite-rich rocks from the Semail ophiolite, Oman. *Canadian Mineralogist*, **20**, 537-548.
- PRICHARD, H.M., POTTS, P.J., & NEARY, C.R. 1981. Platinum group element minerals in the Unst chromite, Shetland Isles. *Transaction of the Institution of Mining and Metallurgy (section B: Applied Earth Sciences)*, **90**, B186-B188.
- RIGHTER, K., CAMPBELL, A.J., HUMAYUN, M., & HERVIG, R.L. 2004. Partitioning of Ru, Rh, Pd, Re, Ir, and Au between Cr-bearing spinel, olivine, pyroxene and silicate melts. *Geochimica et Cosmochimica Acta*, **68**, 867-880.
- STOCKMAN, H.W. & HLAVA, P.F. 1984. Platinum-group minerals in Alpine chromitites from south-westren Oregon. *Economic Geology*, **79**, 491-508.

Aplitic dykes at the world-class Cantung tungsten skarn deposit: indicators of fluid flow and mineralizing processes

Kirsten L. Rasmussen¹, David Lentz², & Hendrik Falck³

¹University of British Columbia, 6339 Stores Road, Vancouver, BC, V6T 1Z4 CANADA
(e-mail: krasmusse@eos.ubc.ca)

²University of New Brunswick, 2 Bailey Drive, Box 4400, Fredericton, NB, E3B 5A3 CANADA

³Northwest Territories Geoscience Office, 4601-B 52nd Ave, P.O. Box 1500, Yellowknife, NT, X1A 2R3 CANADA

ABSTRACT: The Cantung mine (NWT) is one of the world's highest grade tungsten skarn deposits. At least six episodes of magmatism are evident underground: two unaltered and differentiated plutonic phases; three sets of highly differentiated felsic dykes emplaced mainly sub-parallel to folded bedding and affected by sporadic potassic ± white mica alteration; and a late set of extremely differentiated aplites that are pervasively calcic-metasomatized ± late white-mica alteration, and emplaced parallel to sub-vertical normal faults. Elevated grades of tungsten are empirically related to the aplite dykes. These late dykes originated from residual melt enriched in incompatible elements that evolved in a large, inwardly-crystallizing magma chamber. Due to an increase in volatile concentration with magma evolution, magmatic overpressuring initiated and propagated sub-vertical fractures into overlying rocks. Melt crystallized along the fractures by pressure-quenching and metal-rich magmatic fluid was brought into contact with reactive calcareous wallrocks to form tungsten skarn and a calcic magmatic fluid gradient that led to pervasive calcic metasomatism of the late aplites. The evolved and altered nature of the aplites reveals the existence of a large magmatic system at depth and provides information on the processes responsible for mineralization. These distinct aplites may be a useful tool for exploration.

KEYWORDS: *tungsten, skarn, aplite, Cantung, Cordillera*

INTRODUCTION

The northern Canadian Cordillera is one of the most well-endowed (richest) tungsten districts in the world (e.g., Dick & Hodgson 1982). The highest grade tungsten deposit in this district is the Cantung mine, a world-class tungsten skarn with recent reserve estimates of 2.9 Mt at 1.21%WO₃ indicated and 0.73 Mt at 0.74%WO₃ inferred (Clow *et al.* 2006), and over 4.6 Mt at 1.6%WO₃ removed prior to temporary mine shut-down in 2003 (Rasmussen 2004).

During mine operation from 1962-1986, researchers and mine geologists noted an empirical relationship between felsic dykes, or "aplites" and the localization of higher grade ore; this observation led to the hypothesis that the dykes may have played an important role in the formation of the deposit and perhaps could be used for exploration as indicators of tungsten-bearing fluid pathways (Atkinson 1984). However, this idea was not tested until

2003, due to a 15-year mine closure from 1986 to 2001.

GEOLOGICAL SETTING

Regional Geology

All of the significant tungsten deposits in the northern Cordillera are associated with intermediate to felsic, sub-alkaline plutons and batholiths of mid-Cretaceous age (e.g., Hart *et al.* 2004). This magmatism was emplaced well inboard of the ancestral North American margin, in a late- to post-collisional environment undergoing decompression-assisted partial melting of continental crust (e.g., Mair *et al.* 2006). Most of the intrusions associated with tungsten are very small, weakly to moderately peraluminous, K-feldspar-phyric to megacrystic, ilmenite- and biotite-bearing monzogranites (e.g., Hart *et al.* 2004). The Cretaceous magmatic rocks have intruded a thin veneer of Paleozoic, passive continental margin rocks, underlain by a thick

package of Proterozoic extension- or rift-related sediments that are in turn believed to be resting on thinned North American Archean to Paleoproterozoic basement.

Local Geology

Country rocks in the Cantung mine area consist of rocks typical of the Selwyn Basin, including turbiditic sandstone, deepwater limestone, chert, shale, and dolostone. Two ore-bearing calcareous units of the Sekwi Formation are bound by argillaceous rocks. In mine terminology, the “Swiss Cheese Limestone” (SCL) is a calcareous siltstone with chert nodules. The “Ore Limestone” (OL) conformably overlies the SCL, and is a pure, coarsely crystalline marble up to 50m thick.

Local strata were folded into a large NW-SE-trending syncline, and then refolded into a smaller, NE-SW trending overturned anticline that gently plunges to the northeast (Armstrong *et al.* 1983). Figure 1 is a generalized NW-SE section through the local geology. Five mine-scale, steeply dipping, brittle, NE-trending faults with small displacements cut the country rocks, intrusions, and skarn (Cummings & Bruce 1977).

Intrusive rocks at Cantung consist of the “Mine Stock”: a laterally extensive and flat-topped, biotite monzogranite with a fine-grained apical phase underlying the mineralization and local apophyses (inset; Fig. 1). The Mine Stock and country rock are cut by several pulses of aplitic to pegmatitic dykes. Although large quartz feldspar porphyry dykes are seen at the surface, the focus here is on dykes found underground. Quartz ± minor scheelite-chalcocopyrite-biotite-tourmaline-powellite veins are sporadically exposed underground as sub-horizontal or bedding-concordant veins; a series of high-grade tungsten-mineralized, en-echelon quartz veins are exposed cutting the SCL in the floor of the Open Pit. Late lamprophyre dikes cut all the intrusions and the skarn.

Tungsten mineralization at Cantung is developed in two zones (Fig. 1). The Open Pit hosts anhydrous garnet-diopside skarn in the domed upper limb of the

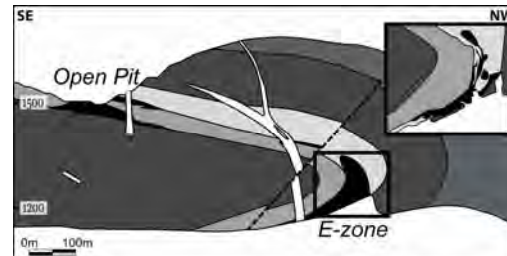


Fig. 1. General cross-section through the Cantung mine with upper right inset detailing typical E-zone geometry; ore zones are black and intrusive phases (including the underlying Mine Stock) are white (modified after Hodgson 2000).

recumbent fold (e.g., Crawford 1963). The underground E-zone ore is hosted within the OL in the hinge zone and the lower limb of the recumbent fold (Fig. 1). Although both anhydrous and hydrous skarn facies are found in the E-zone, the highest tungsten grades are associated with amphibole-pyrrhotite and biotite skarns. Skarn geometry in both zones includes irregularly shaped massive pods or lenticular wavy bands, is controlled by fractures, faults, and bedding planes, and is focused along the contacts of the OL.

Felsic Magmatic Episodes

There are six main textural, mineralogical, and morphological variations of felsic intrusions underground at Cantung:

- 1) medium-grained, K-feldspar megacrystic, hypidiomorphic-granular, biotite monzogranite (distal to skarn);
- 2) apical, fine- to medium-grained, sparsely K-feldspar-phyric, hypidiomorphic-granular, biotite monzogranite with minor secondary muscovite (proximal to skarn);
- 3) shallowly dipping, <20cm thick, fine-grained, sparsely K-feldspar megacrystic, biotite-rich monzogranite dykes with foliated biotite;
- 4) moderately dipping, <0.5m thick, fine-grained, biotite-poor, hypidiomorphic-equigranular monzo- to syeno-granite dykes;
- 5) moderately-dipping, <0.5m thick, fine-grained and foliated to pegmatitic, leucocratic, tourmaline-muscovite-garnet bearing, leucocratic dykes; and

6) syn-mineralization, steeply dipping, <0.25m thick, white, aplite dykes with tonalitic to dioritic chemistry.

All dyke sets are present as marginal phases to the Mine Stock proximal to skarn. Phase 6 dykes crosscut all other felsic dyke phases.

Structure

There are a few main structural trends that the underground dykes follow: (a) emplacement of phases 3, 4, and 5 predominantly sub-parallel to folded bedding planes near the apical Mine Stock (phase 2), or upper portions of the mine; (b) 115°-295°: emplacement of phases 4 and 5 sub-parallel to bedding in the lower recumbent fold limb (Fig. 2), or lower portions of the mine; and (c) 040°-220°: emplacement of phase 6 sub-parallel to the 5 mine-scale normal faults (Fig. 2), throughout the mine near the Mine Stock margins. Phase 6 dykes also offset other dykes and bedding in a normal sense.

Alteration

Several types of alteration in the intrusive phases are apparent from sample staining, petrography, geochemistry, and electron-probe microanalytical work. The main intrusive phases (1 & 2) are essentially unaltered, but phase 2 contains minor secondary muscovite; anorthite content in plagioclase is An₄₁₋₄₅, but approaches An₄₉₋₅₅ (phase 2). Dyke phase 3 is similarly unaltered (An₄₄), except for cm-wide, bleached margins consisting of plagioclase (An₅₆) and quartz. Dyke phase 4 has been affected by early patchy to pervasive potassic alteration resulting in very fine-grained consertal and intergranular K-feldspar, and rare pale brown biotite veinlets or ragged grains. Several examples of dyke phases 4 and 5 also have very fine-grained, secondary white-green mica veins and plagioclase pseudomorphs.

Tonalitic phase 6 dykes are quartz- and plagioclase-rich (An₄₃₋₄₉; up to An₉₆₋₉₈ near skarn), and have undergone calcic metasomatism with replacement of K-feldspar by plagioclase and destruction of biotite. Dioritic phase 6 dykes are quartz

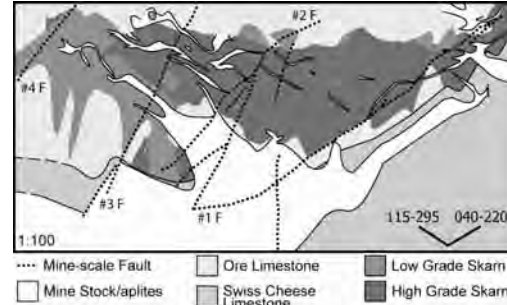


Fig. 2. Level plan showing the empirical relationship between high-grade skarn and dykes; two dominant trends of dykes, apophyses, and faults are apparent (Cantung Internal Files, 1981).

poor (<10%) and have also undergone pervasive calcic metasomatism, resulting in alteration of plagioclase (90-100%) to a range of compositions on the intra-grain scale (An₃₉₋₉₈), destruction of K-feldspar and biotite, and formation of minor epidote-group minerals, titanite, and apatite. The dioritic dykes are mineralized with calcite-titanite-pyrrhotite-chalcopryrite veinlets ± disseminated scheelite (5-90%) ± disseminated pyrrhotite (up to 40%). White-mica and calcite overprint the calcic mineral assemblage in all dioritic dykes.

Differentiation

Relatively low Ti/Zr ratios for the Mine Stock (~14-15) indicate a well-differentiated magma source. However, even lower Ti/Zr (~7-13) in the dykes, particularly phase 6, suggests that they originated from more evolved magmas. This differentiation is interpreted to have occurred gradually from normal magma crystallization processes.

INTERPRETATION

The felsic intrusive phases at Cantung provide information on a large and evolving magmatic system at depth. A highly differentiated, sub-horizontal magma body (phase 1) was emplaced into recumbently folded sedimentary rocks, accompanied by a finer-grained apical phase (phase 2) located near the fold hinge zone. A deeper source magma continued to evolve, crystallizing inward to form increasingly differentiated melts

enriched in incompatible elements, which were mainly emplaced sub-parallel to folded beds (phases 3, 4, & 5). Bleaching along the phase 3 dyke margins is due to interaction with calcic country rocks, and potassic alteration affecting phases 4 and 5 dykes is explained by pulses of hot magmatic fluids along the relatively permeable dykes. Extreme differentiation in the residual melt, due to a high degree of crystallization in the magma source region, led to an increase in fluid pressure. The resultant magma overpressuring resulted in the initiation and propagation of sub-vertical fractures and subsequent injection of highly differentiated melt and metal-rich magmatic fluid. A calcic fluid gradient developed between the aplite melt (phase 6) crystallizing by pressure-quenching, and calcareous country rocks reacting with magmatic fluid to form tungsten skarn, leading to pervasive calcic metasomatism of the aplites. Late white-green mica +/- calcite alteration affecting most dyke phases could be the result of interaction between the calcic fluids and minor influx of the last magmatic fluids.

The emplacement of extremely differentiated melts in association with high-grade tungsten skarn necessitates the existence of a large magmatic system at depth, capable of sequestering incompatible elements through normal crystallization processes prior to the main mineralization event. The aplites represent the most evolved melt extruded from the source magma, and as such their recognition has the potential to be a powerful tool in future exploration for tungsten mineralization at Cantung.

ACKNOWLEDGEMENTS

We thank North American Tungsten Corp., Dave Tenney, Bill Mann, Dan Kontak, and David Pattison for assistance. Funding for this project was provided by

the NWT Geoscience Office, the Aurora Research Institute Research Assistant Program, and the University of Calgary.

REFERENCES

- ATKINSON, D. 1984. Comments and observations on Cantung geology with comparison to Mactung based on March 19-22, 1984 mine visit. *Amex Northwest Mining Company Ltd. Inter-office memorandum*, 6 p.
- ARMSTRONG, D.W., HARRIS, F.R., KERRIGAN, J.E., KIEHN, O.A., & JOHNSON, R.E. 1983. Technological Assessment Report of Canada Tungsten Mining Corporation Ltd., Tungsten, NWT, Canada. *Amex engineering and management services company*, 184p.
- CRAWFORD, W.J.P. 1963. *Geology of the Canada Tungsten Mine, SW District of Mackenzie, Canada*. MSc thesis, University of Washington, Seattle, Washington.
- CUMMINGS, W.W. & BRUCE, D.E. 1977. Canada Tungsten - Change to underground mining and description of mine-mill procedures. *CIM Bulletin*, **70**, 94-101.
- DICK, L.A. & HODGSON, C.J. 1982. The MacTung W-Cu(Zn) contact metasomatic and related deposits of the northeastern Canadian Cordillera. *Economic Geology*, **77**, 845-867.
- HART, C.J.R., MAIR, J.L., GOLDFARB, R.J., & GROVES, D.I. 2004. Source and redox controls on metallogenic variations in intrusion-related ore systems, Tombstone-Tungsten Belt, Yukon Territory, Canada. *Transactions of the Royal Society of Edinburgh: Earth Sciences*, **95**, 339-356.
- HODGSON, C.J. 2000. Exploration potential at Cantung Mine, District of Mackenzie, NWT. *Andean Engineering*, 26p.
- MAIR, J.L., HART, C.J.R., & STEPHENS, J.R. 2006. Deformation history of the northwestern Selwyn Basin, Yukon, Canada: implications for orogen evolution and mid-Cretaceous magmatism. *GSA Bulletin*, **118**, 304-323.
- RASMUSSEN, K.L. 2004. The aplitic dykes of the Cantung Mine: petrography, geochemistry, and implications for the mineralization process. *University of Calgary, Calgary, Alberta*.

Geochemistry and genesis of a mafic-ultramafic hosted VMS occurrence, Marathon, Ontario

Marc L. Rinne¹, Peter N. Hollings¹, & Aubrey J. Eveleigh²

¹Department of Geology, Lakehead University, Thunder Bay, ON, P7B 5E1 CANADA
(e-mail: mrinne1@lakeheadu.ca)

¹Department of Geology, Lakehead University, Thunder Bay, ON, P7B 5E1 CANADA

²MetalCORP Ltd., 129 W. Frederica Street, Thunder Bay, ON, P7E 3V8 CANADA

ABSTRACT: The Big Lake volcanogenic massive sulphide (VMS) occurrence in the Schreiber-Hemlo belt of the Superior Province near Marathon, Ontario was discovered in March 2006. It is hosted in a mafic-ultramafic metavolcanic sequence lacking felsic volcanic or volcanoclastic rocks, as a surface of mineralisation and hydrothermal alteration currently defined over a plan area of approximately 0.5x0.5 km, subparallel to and 5-50 m below the base of a large ultramafic cumulate complex. Several arguments point to an overturned sequence, where VMS sulphides are stratigraphically above the ultramafic cumulates. Among other possibilities, a genetic relationship between these cumulates and the VMS is implied.

KEYWORDS: *volcanogenic massive sulphide, Superior Province, ultramafic, exploration geochemistry, Schreiber-Hemlo greenstone belt*

INTRODUCTION

The Big Lake Cu-Zn-Ag-Au volcanogenic massive sulphide (VMS) occurrence is hosted in mafic-ultramafic strata of the Schreiber-Hemlo greenstone belt near Marathon, Ontario (Fig. 1). This VMS is unusual in that it is one of a few documented VMS occurrences in sequences lacking felsic volcanic or volcanoclastic rock.

Three dimensional modeling and interpretation of whole-rock geochemical data were used to describe the setting and genesis of the occurrence, with the aim of clarifying how VMS mineralisation can occur in settings lacking felsic volcanic rock. Results of these models and geochemical data are presented here.

GEOLOGICAL SETTING

Regional Geology

The Wawa subprovince is a volcano-plutonic assemblage of 2.88-2.72 Ga rocks (Percival *et al.* 2006) accreted to the southern part of the Superior Province during the end of the Kenoran Orogeny, ca. 2.69 Ga. Extending approximately 1000 km from NE Minnesota to just south of James Bay, the Superior Province is

bounded to the north by the metasedimentary Quetico Subprovince and to the southeast by the Kapuskasing Structural Zone.

Local Geology

The Heron Bay assemblage is located in the southeast portion of the Schreiber-Hemlo Greenstone Belt of the Wawa Subprovince, south of the Hemlo Fault Zone and east of the Coldwell alkalic complex (Fig. 1). Mafic to ultramafic metavolcanic rocks of the Pulpwood-Playter Harbours sequence, located between the Pukaskwa and Heron Bay plutons, are host to the Big Lake VMS occurrence. The recently identified Big Lake Ultramafic Complex (BLUC) forms a prominent part of this host sequence, as an E-W striking sill-like body comprising laterally continuous sequences of ultramafic cumulates 200-350 m thick. The Big Lake VMS occurrence underlies the eastern margin of the BLUC (Fig. 1).

METHODS AND RESULTS

Scale of Study

Leapfrog software was used to generate lithological contacts and chemical

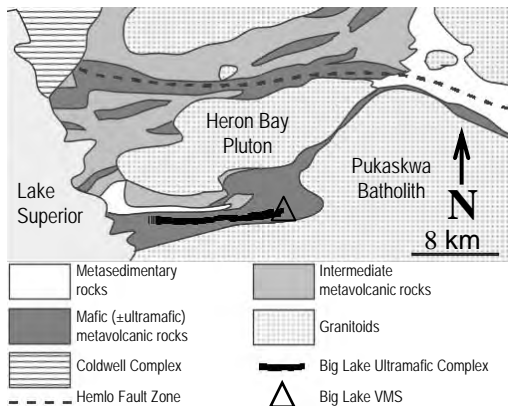


Fig. 1. Part of the Schreiber-Hemlo Greenstone Belt, showing the location of study. Modified after Polat *et al.* (1998).

distributions of the Big Lake VMS occurrence. Most modeling was restricted to 53 diamond drill holes over a plan area approximately 500 x 500 m and 400 m deep. Data used were compiled from MetalCORP assay and whole-rock sampling data, including 99 whole-rock metavolcanic samples and 60 whole-rock ultramafic cumulate samples.

Mineralisation and Lithostratigraphy

VMS mineralisation at Big Lake consists of stringer-textured to semi-massive pyrrhotite, chalcopyrite, and sphalerite, in decreasing order of abundance, at up to 80% sulphides by volume over a few metres. Best-mineralised intervals contain ~6 % Cu and ~2 % Zn weighted over five to ten metres, with significant enrichment in Au, Ag, and other metals.

The VMS sulphides define a broadly conformable sheet 5-50 m below the base of the BLUC. This synformal surface of mineralisation generally coincides with the transition from ultramafic cumulates and strongly foliated metavolcanic rocks to an underlying sequence of metavolcanic rocks and interflow metawacke and metasilstone rocks (Fig. 2). Sphalerite-pyrrhotite mineralisation in hydrothermal veins was also observed within the BLUC several km west of this study area.

Hydrothermal Alteration

Hydrothermal alteration, as defined by

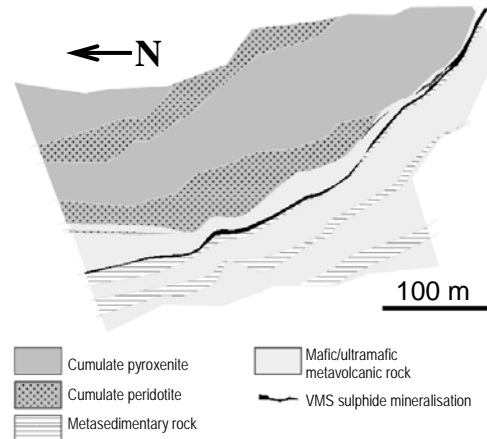


Fig. 2. Representative lithological section through the Big Lake Ultramafic Complex and Big Lake VMS occurrence.

chemical alteration indices or visual estimation in hand sample, is restricted to a few metres above visible sulphide mineralisation and may be a function of limited permeability in a flow-dominated setting, or some degree of tectonic shortening. The alteration mineral assemblages consist of chlorite, biotite, and anthophyllite, in decreasing order of abundance, and lack an appreciable zoning or strict relationship to metal contents. Veined talc was observed in some intensely altered intervals, though this may be of regional metamorphic origin.

Least-altered metavolcanic samples have Na₂O and MgO contents of 1.8-4.0 wt. % and 4-25 wt. %, respectively, whereas strongly altered samples (having greater than 30% hydrothermal minerals by volume, in dense net-textured veins, in places obscuring primary textures) contain less than 1.5 wt. % Na₂O and 11-23 wt. % MgO.

Whole-Rock Geochemistry

All samples plot in the basalt to alkaline basalt fields of the Zr/TiO₂ vs. Nb/Y diagram of Pearce (1996) (Fig. 3). The Nb/Y ratios define two distinct groups: (1) tholeiitic metavolcanic rocks structurally underlying VMS mineralisation; and (2) more alkaline ultramafic cumulates and metavolcanic rocks above VMS

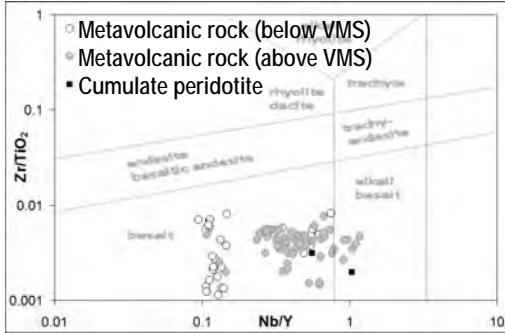


Fig. 3. Zr/TiO₂ vs. Nb/Y in rocks of the Big Lake VMS host sequence. Note two distinct sample populations. Fields are from Pearce (1996) after Winchester & Floyd (1977).

mineralisation.

Trace element patterns also differ between these two groups (Fig. 4). Samples above the VMS have weakly fractionated REE (La/Yb_{cn}=2-8), unlike underlying rocks with a nearly flat REE profile (La/Yb_{cn}= 1-2). Though absolute Nb concentrations are similar in both sample sets, structurally underlying rocks show weak negative Nb anomalies (Nb/Nb* = 0.4-0.9), and generally undepleted Th, Zr, and Hf, whereas overlying rocks show relatively undepleted Nb (Nb/Nb* = 0.6-1.3) and have relative depletions in the other HFSE.

The trace element patterns in Figure 4 are similar to komatiites of the Kidd-Munro assemblage, whose negative HFSE were interpreted by Wyman (1999) to be a result of contamination by other HFSE-depleted rock. If Big Lake volcanic rocks are plume-derived, their negative HFSE depletions could similarly be explained by country arc rock contamination in lavas or parent magma chambers.

Deposit Models

Given that olivine-compatible elements such as Mg or Co are likely to be most concentrated in the first olivine crystals to form an olivine cumulate, assays through two cumulate peridotite units of the BLUC reveal trends that are consistent with a downward younging direction (Fig. 5).

We did not encounter any evidence for assimilation of VMS sulphides by the BLUC. Given an overturned sequence, it

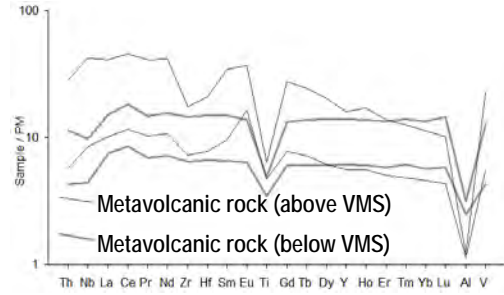


Fig. 4. Representative primitive mantle normalised trace element patterns of metavolcanic rocks structurally above and below VMS mineralisation. Normalising values are from Sun and McDonough (1989).

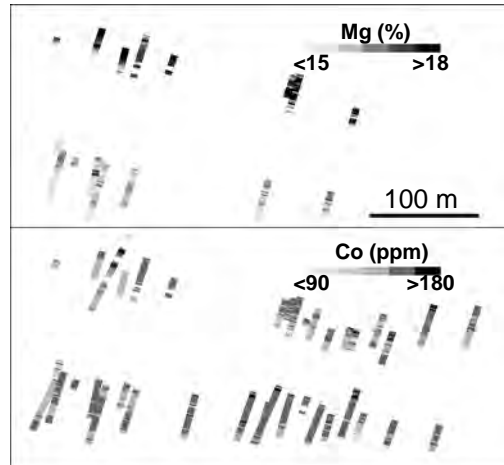


Fig. 5. View along strike of cumulate peridotites at Big Lake shows Mg and Co contents are highest at tops and gradually decrease down hole.

is possible that the BLUC is a shallow heat source directly responsible for VMS mineralisation, as was suggested by Barrie *et al.* (2001) for the Empire cumulate komatiite flow and Terminus VMS occurrence of the Kidd-Munro assemblage. This model is supported by the spatial relationship between VMS sulphides and the lower surface (stratigraphic top) of the BLUC, and by the occurrence of VMS sulphides within the BLUC several km west of the study area, implying a genetic relationship between the BLUC and VMS.

CONCLUSIONS

The Big Lake VMS occurrence is hosted in mafic-ultramafic metavolcanic rocks of

the Schreiber-Hemlo Greenstone Belt, in a setting lacking felsic volcanic or volcanoclastic rock. Modeling of lithology and chemical distributions yields the following conclusions:

- (1) The VMS sulphides define an anastomosing sheet subparallel to and 5-50 m below of the base of the BLUC;
- (2) Hydrothermal alteration involved Na depletion and Mg addition, and visibly altered rock is restricted to within a few metres above visible sulphide mineralisation, but not below;
- (3) BLUC peridotite chemostratigraphy, downward-fining cumulate flows, and asymmetry of hydrothermal alteration suggest the local host sequence to the VMS is overturned;
- (4) A plausible model for the Big Lake occurrence involves a genetic relationship between BLUC cumulates and VMS sulphides, similar to VMS occurrences of the Kidd-Munro assemblage summarized by Barrie *et al.* (2001). This would be the first such documented occurrence outside of the Abitibi subprovince, and illustrates the potential for similar occurrences above large ponded cumulates.

ACKNOWLEDGEMENTS

We thank MetalCORP Ltd. and the Ontario Centres of Excellence for their continued support of this project. The study was also supported by a Society of

Economic Geologists student research grant and an NSERC PGS-M scholarship.

REFERENCES

- Barrie, C., Erendi, A., & Cathles, L. 2001. Paleosea-floor volcanic-associated massive sulfide mineralization related to a cooling komatiite flow, Abitibi Subprovince, Canada. *Economic Geology*, 96, 1695-1700.
- Percival, J., McNicoll, V., & Bailes, A. 2006. Strike-slip juxtaposition of ca. 2.72 Ga juvenile arc and >2.98 Ga continent margin sequences and its implications for Archean terrane accretion, western Superior Province, Canada. *Canadian Journal of Earth Sciences*, 43, 895-927.
- Polat, A., Kerrich, R., & Wyman, D. 1998. The late Archean Schreiber-Hemlo and White River-Dayohessarah greenstone belts, Superior Province: collages of oceanic plateaus, oceanic arcs, and subduction-accretion complexes. *Tectonophysics*, 289, 295-326.
- Sun, S. & McDonough, W. 1989. Chemical and isotopic systematics of oceanic basalts: implications for mantle composition and processes. In: Saunders, A. & Norry, M. (ed.), *Magmatism in the Ocean Basins*. Geological Society Special Publication, 313-345.
- Wyman, D. 1999. A 2.7 Ga komatiite, low Ti tholeiite, arc tholeiite transition, and inferred proto-arc geodynamic setting of the Kidd Creek deposit: evidence from precise trace element data. *Economic Geology Monograph*, 10, 511-528.

The Middle River Gold deposit, NE New Brunswick, Canada: an example of an orogenic style gold system in the Brunswick Subduction Complex

Sabine Schwarz¹, David Lentz¹, & James Walker²

¹ University of New Brunswick, Department of Geology, Fredericton, NB, E3B 5A3 CANADA
(email: s.vetter@unb.ca)

² Geological Surveys Branch, Department of Natural Resources-Minerals, Bathurst, NB, E2A 3Z1 CANADA

ABSTRACT: The Middle River Gold (MRG) deposit is the largest of several genetically related Au-Sb-As occurrences hosted within the Brunswick Subduction Complex (BSC), NB (Canada). Mineralization and related alteration at MRG is localized in a shear zone cutting Middle Ordovician grey shale, siltstone, chert, and subalkaline to alkaline basalts. Mineralizing hydrothermal fluids were localized along late tectonic ductile to brittle shear zones that formed auriferous sulfide-bearing quartz-carbonate veins. Sulfide mineralization can be divided into three types; a) arsenopyrite-pyrite, b) sphalerite-galena-tetrahedrite-bismuthinite-chalcocopyrite, and c) Hg-argentite-electrum. Early sulfides consist of euhedral arsenopyrite and pyrite, which exhibit deformation textures. The cores of pyrite (<3 mm) exhibit dissolution, whereas the rims are faceted; data obtained by EPMA show four zones of variable gold content at constant As values. Arsenopyrite shows similar characteristics with only three different zones (core and rim are Au-rich). Fractures within arsenopyrite and pyrite are filled with sphalerite, galena, bismuthinite, chalcocopyrite, and tetrahedrite. Later Hg-Au-Ag-bearing fluids are responsible for mineralized quartz veins along microfractures. Sulfur isotopic data of arsenopyrite and pyrite have an average $\delta^{34}\text{S}$ of 8.0 ± 0.4 ‰ and one pyrite grain with -3.3 ‰ $\delta^{34}\text{S}$; the higher values are similar to the sulfides hosted within the California Lake Nappe (BSC).

KEYWORDS: *sulfides, Brunswick Subduction Complex, hydrothermal, orogenic gold, Northern Miramichi Highlands*

INTRODUCTION

The Brunswick Subduction Complex (BSC) is best known as the host sequence to world class, syngenetic volcanogenic massive sulfide deposits of the Bathurst Mining Camp (BMC) hosting deposits such as the giant Brunswick No. 12 VMS deposit (>300 Mt of massive sulfides). Less well known are the syntectonic, precious-metal breccia and (or) vein deposits/occurrences in the BSC. The shear zone-hosted Middle River gold deposit (MRG) is the most significant of these and has returned assays of up to 7.44 g/t Au over 6.5 m (DDH MR-05-06).

Gold mineralization at MGR has been delineated by trenching and diamond drilling over a strike length of >500 m and is open below 276 m. Visible gold has not been observed, so it is assumed that Au occurs as submicroscopic inclusions and (or) as refractory gold in sulfides.

Several stages of mineralization have

been recognized, all of which can be related to the tectonic evolution of the BSC (van Staal 1994). Repeated hydrofracturing during episodic tectonic events resulted in the development of multi-stage veins and alteration.

The purpose of this paper is to describe the gold-bearing sulfide-carbonate-quartz veins of the MRG in order to compare this deposit with similar styles of gold mineralization in the region.

GEOLOGICAL SETTING

The MRG area is within the BMC and characterized by three thrust-bound nappes, each containing rocks assigned to different stratigraphic units, specifically: the Miramichi Group, the Tetagouche Group (Tomogonops and Little River formations), and the California Lake Group (Boucher Brook Formation). The Miramichi Group consists of upward-fining sedimentary rocks that are in (dis-)

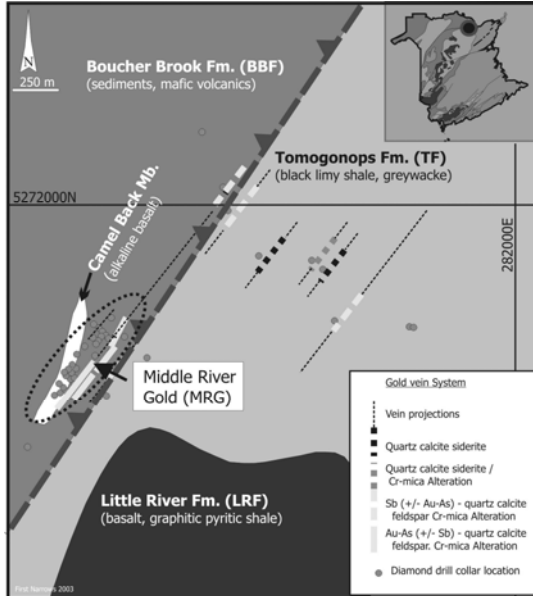


Fig. 1. Geological map of the Middle River Gold (MRG) deposit, including the characterization of the veins projected to the surface from drill data (Gummer 2004).

conformable contact with the overlying Tetagouche Group. The Tetagouche Group is divided into four formations of which only the Little River (LRF) and the Tomogonops formations (TF) are present in the MRG deposit area (Fig. 1). The LRF is characterized by dark grey to black shale, siltstone, and chert that are interlayered with subalkaline to alkaline pillow basalts (Camel Back Member). The TF consists of a coarsening-upward grey, thin- to medium-bedded, calcareous siltstone, shale, lithic (quartz) wacke, and non-calcareous coarse-grained sandstone and conglomerate (Langton 1996).

The Boucher Brook Formation is the upper-most unit in the California Lake Group and consists of grey shale, siltstone, chert, alkalic basalt, and minor peralkaline felsic volcanic rocks including the alkaline basalt of the Camel Back Member (Fig. 1).

The BSC (part of the Dunnage tectonic Zone) formed in Late Ordovician to Early Silurian (i.e., during the Salinic Orogeny), and contains the accreted and subducted remnants of the Middle to Late Ordovician Tetagouche–Exploits back-arc basin. Consequently, the rocks of the BSC have

undergone poly-phase brittle- to ductile deformation resulting in intense thrust tectonics prevalent in this type of setting. Exhumation of the BSC began during the main stage Salinic Orogeny (Early Silurian) and led to the deposition of Silurian sedimentary rocks. The ongoing orogenesis resulted in a polyphase deformed and regionally developed lower- to middle-greenschist grade metamorphism followed by exhumation to near the current structural level.

METHODS AND RESULTS

This investigation relied on petrographic analysis of polished sections using reflected light and the scanning electron microscopy (SEM) and electron microprobe (EPMA) analyses to identify minerals and to document the distribution of gold. The mineralized zone is coincident with a distinct bleached alteration zone that contains fine- to coarse-grained, subhedral arsenopyrite and pyrite in quartz-carbonate veins.

In the MRG deposit, five vein types are recognized (Types I through V). Type II arsenopyrite-pyrite-gold veins are linked to D₁ deformation via sericitization (⁴⁰Ar/³⁹Ar age date 435±3Ma, unpublished data) and carbonatization of the mafic volcanic and adjacent sedimentary host rocks. This mineralization is manifested by increasing Fe₂O₃* and a relative decrease in SiO₂, K₂O, and Al₂O₃ in whole-rock analyses. The color change of the rocks, from a dark grey-green to a beige-yellow, is coincident with the mineralization.

The five vein phases, three of which are sulfide-bearing, can be differentiated into: Type I - early quartz-carbonate, Type II - arsenopyrite-pyrite-quartz-carbonate, Type III - sphalerite-galena-tetrahedrite-bismuthinite-chalcocopyrite, Type IV - Hg-argentite-electrum, and Type V – late, metal-barren quartz-carbonate veins.

Type I veins are folded, off set and are the earliest vein type, as they are cut by all other veins. Type II veins, 1-5 cm width with arsenopyrite and pyrite (90%) in a quartz-calcite gangue, are associated with the main stage of sulfide-electrum mineralization. Type III and Type IV veins

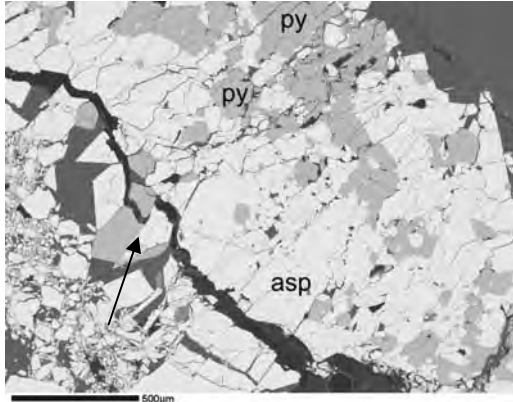


Fig. 2. SEM backscattered electron image of a Type II vein containing euhedral to cataclastically brecciated arsenopyrite (asp), pyrite (py), quartz, and calcite. A thin Type IV quartz vein showed a SEM-EDAX analysis of a very fine-grained mineral mass rich in Hg-Au-As vein (arrow).

occur as microfractures in arsenopyrite and pyrite (Type II), and their relative paragenetic relationship is uncertain. Type V quartz-carbonate veins are the youngest vein type, as they cut all other vein types. Type V veins have no recognizable associated alteration and they offset the foliation, as well as all earlier vein types (I to IV).

This study focused on the sulfide-bearing, types II to IV veins (0.5-2cm wide) and on the fine- to coarse-grained disseminated sulfides in the host rocks.

In Type II veins arsenopyrite is situated along the walls of the vein, with pyrite overgrowths and as vein fill. Wider veins contain angular to subrounded host rock fragments. These veins contain euhedral arsenopyrite (≤ 4 mm) and pyrite (≤ 3 mm) (Fig. 3). Both minerals have Au enriched rims and cores with an intermediate zone devoid of detectable Au.

Microfractures cutting sulfides of Type II veins are cored with anhedral galena, sphalerite, bismuthinite, tetrahedrite, and chalcopryrite in a quartz-calcite gangue. Tetrahedrite also occurs as thin coatings on arsenopyrite and pyrite. These grains and their coatings are too small to be analyzed by EPMA. The microveins (Type IV) appear in sulfides of Type II veins and consist of small (0.1-0.5 mm) anhedral

grains of argentite, electrum, and an undeterminable Hg mineral, in a quartz gangue. SEM-EDAX analyses of these fine grains show element peaks for Hg, Au, and Ag, but the grains are too small for precise determination of the mineral phase.

Sulfur Isotopes

Sulfide grains sampled from the Type II veins in the high gold zones from two drill cores were prepared for sulfur isotope analysis. Pyrite samples (n=5) have average $\delta^{34}\text{S}$ of 8.0 ± 0.5 ‰ and a range of 7.6 - 8.3 ‰, whereas arsenopyrite (n=4) averages 7.9 ± 0.5 ‰ and ranges between 7.3 - 8.4 ‰ (Fig. 3).

One sample of euhedral pyrite collected from a zone of disseminated sulfide coincident with a high-grade gold zone gave a $\delta^{34}\text{S}$ value of -3.3 ‰ (Fig. 3). Similar S isotope data have been reported from the BB Formation, Caribou mine, and other base-metal deposits in the area (Fig. 3).

CONCLUSIONS

The MRG mineralization can be related to the orogenic gold deposit model summarized by Groves *et al.* (2005):

- (1) Type II vein sulfides (arsenopyrite and

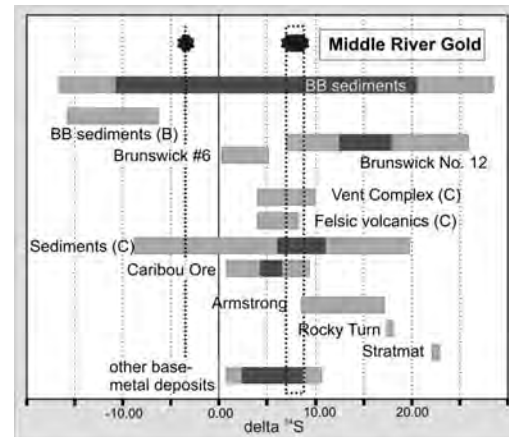


Fig. 3. Sulfur isotopic data for the MRG deposit compared to published data for sedimentary rocks and base-metal and gold deposits in the BSC. (BB=Boucher Brook Fm, B=Brunswick Mine area, C=Caribou Mine, data from Tupper 1960; Lentz *et al.* 1996; Goodfellow & McCutcheon 2003).

pyrite) have Au-rich cores and rims separated by an Au-poor zone. The Au zoning is interpreted to equate to hypozonal As-Au mineralization. At MRG this mineralization occurred during the main phase of the Salinic Orogeny.

(2) Microfractures cutting arsenopyrite and pyrite in Type II veins are infilled by base-metal sulfides (galena, sphalerite, bismuthinite, tetrahedrite, and chalcopyrite). The Cu, Bi, Zn, and Pb that formed these phases were likely scavenged from the VMS bodies and associate sulfide-bearing rocks in the area. The sulfide phases in Type III veins are characteristic of assemblages in orogenic epizonal Sb-Au mineralization.

(3) Mercury-Au-Ag rich (Type IV) veins are interpreted to represent epithermal, near surface mineralization subsequent to the orogenic mineralization and probably formed during the exhumation of the Brunswick Subduction Complex.

(4) The $\delta^{34}\text{S}$ values for arsenopyrite and pyrite in Type II veins might be linked to the strataform VMS deposits of the BSC. In particular, the $\delta^{34}\text{S}$ values are similar to those for the Caribou Mine (located in the California Lake Group [Spruce Lake Formation] above a felsic intrusion). The negative $\delta^{34}\text{S}$ value returned from one pyrite probably reflects biogenic S or reduced seawater sulfate from the Iapetus back-arc basin (Lentz *et al.* 1996).

4) Based on dating ($^{40}\text{Ar}/^{39}\text{Ar}$) of alteration-related sericite at 435 ± 3 Ma, the MRG mineralization is inferred to be associated with and, therefore, generated during the D₁ deformation of the BSC accretionary wedge system. Thus, mineralization at MGR can be described as being similar to the metamorphogenic orogenic gold style.

ACKNOWLEDGEMENTS

We thank the Department of Natural Resources for the funding of this project and their staff for research support. Additional funding was provided with a NSERC Discovery grant to DL.

REFERENCES

- GOODFELLOW, W.D. & McCUTCHEON, S.R. 2003. Geologic and genetic attributes of volcanic sediment-hosted massive sulfide deposits of the Bathurst mining camp, northern New Brunswick; a synthesis. *Economic Geology Monograph*, **11**, 245-301.
- GROVES, D.I., GOLDFARB, R.J., ROBERT, F., & HART, C.J.R. 2003. Gold deposits in metamorphic belts; overview of current understanding, outstanding problems, future research, and exploration. *Economic Geology*, **98**, 1-29.
- GUMMER, P. 2004. http://www.uno.ca/middle_river/.
- LANGTON, J.P. 1996. Relative age, stratigraphic position, and provenance of new sedimentary formations in the eastern Bathurst Camp, New Brunswick. In: CARROLL, B.M.W., (ed.), *New Brunswick Department of Natural Resources and Energy - Current Research*, **96-1**, 61-71.
- LENTZ, D.R., Goodfellow, W.D., & Brooks, E. 1996. Chemostratigraphy and depositional environment of an Ordovician sedimentary section across the Miramichi Group-Tetagouche Group contact, northeastern New Brunswick. *Atlantic Geology*, **32**, 101-122.
- TUPPER, W.M. 1960. Sulfur Isotopes and the origin of the Sulfide Deposits of the Bathurst-Newcastle Area of Northern New Brunswick. *Economic Geology*, **55**, 1676-1707.
- VAN STAAL, C.R. 1994. Brunswick subduction complex in the Canadian Appalachians; record of the Late Ordovician to Late Silurian collision between Laurentia and the Gander margin of Avalon. *Tectonics*, **13**, 946-962.

Gold mineralization in the Kakagi-Rowan Lake greenstone belt: a study of the Angel Hill Gold Zone

Scott Secord¹ & Pete Hollings¹

¹Lakehead University, 955 Oliver Rd. Thunder Bay ON, P7B 3W2 CANADA (e-mail: ssecord@lakeheadu.ca)

ABSTRACT: The Angel Hill Gold Zone is a recent discovery in Houston Lake Mining's West Cedartree Gold Project near Sioux Narrows, Ontario. The mineralised zone spans the contact between the ultramafic and gabbroic units of the Kakagi Gabbro Sill. Highest gold values occur in a zone of alteration up to 20 m either side of a 5 cm wide fault which runs parallel to the contact between the ultramafic and gabbro units of the sill. The gold zone was studied using petrographic techniques and SEM-EDS to assess the nature of mineralization and alteration, whereas down-hole geochemistry was used to determine mobility and fluid characteristics. Gold occurs as micron-size free gold, but predominantly as sylvanite and petzite within and rimming pyrite grains. However, not all pyrite contains gold, as both barren and fertile phases have been identified, suggesting a multistage fluid evolution. Alteration within the gold zone consists of serpentinite, carbonate, fuchsite and quartz, thus involving aqueous-carbonic fluids. Results to date have helped to define and characterise similar areas of mineralization determined through field mapping at the property-scale.

KEYWORDS: Archean, lode-gold, Superior Province, alteration, fuchsite

INTRODUCTION

The Kenora Mining District has historically been one of Ontario's leading gold producing areas. Houston Lake Mining Inc. has discovered a new gold occurrence, the Angel Hill Gold Zone (AHGZ), at their West Cedartree Gold Project (WCGP) near the township of Sioux Narrows, Ontario, near Lake of the Woods. The AHGZ is one of four known gold occurrences within the WCGP and is hosted in an altered peridotite at its contact with a gabbro of the Kakagi Gabbro Sill. The AHGZ has been exposed over 300 metres by mechanical trenching along a roughly north north-west trending zone. The AHGZ is considered to represent an example of Archean lode gold or mesothermal vein-type mineralisation. This project will analyze in detail the alteration associated with gold mineralization in order to help define a continuation of the zone.

GEOLOGICAL SETTING

Regional Geology

The WCGP is located in the western arm of the Savant Lake-Crow Lake greenstone

belt of the Wabigoon subprovince of the Superior Province (Card & Ciesielski 1986).

Local Geology

The WCGP is dominated by three main lithologies (Fig. 1): the Snake Bay formation of the Rowan Lake Group, the Emm Bay formation of the Kakagi Lake Group, and the Kakagi Sill (a gabbro and ultramafic intrusion). The Snake Bay formation conformably underlies the Emm Bay formation and is composed of greenschist grade mafic metavolcanic rocks and comprise interlayered massive, pillowed and porphyritic flows as well as tuff and lapilli tuff. The rocks are fine- to medium-grained and composed of plagioclase feldspar, chlorite, amphibole (tremolite and hornblende), quartz, muscovite, carbonate (calcite and ankerite) and talc. The Emm Bay formation is composed of intermediate to felsic lapilli tuffs, pyroclastic debris flows and lapilli tuffs. The rocks have a fine-grained texture and are composed chiefly of chlorite, plagioclase, quartz, and muscovite. Intruding these two volcanic suites is the Kakagi Gabbro Sill. The

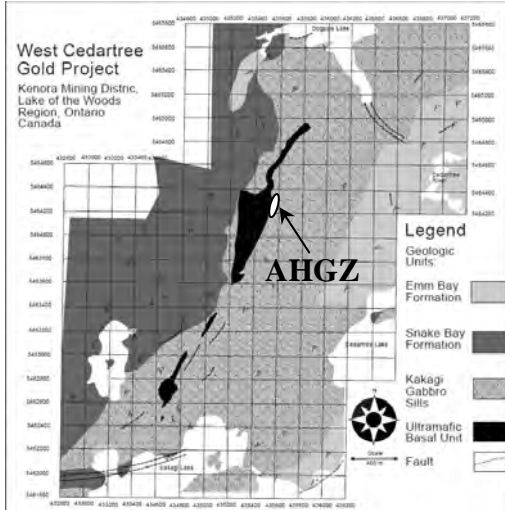


Fig. 1. Property map of the WCGP with outline of the AHGZ indicated.

intrusive contact is somewhat variable, but is generally sharp with well-defined margins. The sill is composed of an ultramafic basal unit that grades upwards into a differentiated gabbro away from the contact with Snake Bay formation. The ultramafic unit is an altered peridotite composed primarily of chlorite altered clino- (augite) and ortho- (hypersthene) pyroxene and highly serpentinised olivine with minor carbonate. The gabbro is composed chiefly of amphibole (tremolite with minor hornblende), plagioclase (albite), pyroxene (augite with minor hypersthene), mica (muscovite with minor biotite), chlorite, and quartz.

Methods

Field mapping at the property scale was performed over two summers at the WCGP (Fig. 1). Sampling was conducted throughout the property, across the gold zone and also from diamond drill holes. Scanning electron microscopy was performed at Lakehead University using an SEM-EDS JEOL 5900 equipped with an Oxford energy dispersion system with a resolution of 139eV. The backscatter electron detector (BSE) was used in order to locate and analyze gold phases and gangue phases associated with the mineralisation. Analyses were done using the following operating condition:

accelerating voltage of 20kV, a beam current of 0.475 pA and a beam width of less than 0.2 micrometres. Standardization was done using samples from the Lakehead University Instruments Lab's standard library. Whole-rock geochemical data was obtained using X-ray fluorescence and inductively coupled plasma mass spectrometry at the Geoscience Laboratory at GeoLabs in Sudbury, Ontario. Trace elements, including the REE and HFSE, were analyzed at the Geoscience Laboratories using a Perkin-Elmer Elan 9000 ICP-MS following a variation on the protocol described by Burnham & Schweyer (2004) and Tomlinson *et al.* (1998).

The Angel Hill Gold Zone

Drilling of the AHGZ has outlined a resources estimate of 106,400 tonnes grading 2.97 g/t (Cutting & Anthony 2005). The mineralised zone straddles the contact between the gabbro hanging wall and ultramafic footwall, which are separated by a zone of brittle deformation about 5 cm wide. The fault zone is filled with quartz and carbonate and a zone of alteration extends about 20 metres into the hangingwall and footwall. Footwall alteration is characterised by intense carbonatization with augite altered to carbonate and chlorite, hypersthene altered to chlorite and minor carbonate, olivine altered to serpentine and magnetite, and interstitial feldspars altered to muscovite. Slight silicification has occurred with a concomitant increase in the abundance of sulfides, chiefly pyrite with minor pyrrhotite. Hanging wall alteration, also characterized by intense carbonatization, consists of plagioclase extensively altered to mica and minor chlorite, augite altered to carbonate, and hypersthene altered to chlorite and carbonate. The secondary amphibole present is predominantly tremolite. Quartz flooding is evident, as well as an increase of matrix carbonate.

The main zone, as mentioned above, is a fault with quartz veining. The zone occurs in the ultramafic suite of the intrusion, as reflected by its texture and

events: (1) alteration of mafic phases to carbonate and felsic phases to micas; (2) influx of quartz and carbonate with the associated formation of fuchshite and deposition of gold +/- sulfides; (5) The nature of the gold mineralization suggests a protracted history of veining and alteration.

ACKNOWLEDGEMENTS

I would to thank Grayme Anthony and Dean Cutting at Houston Lake Mining Inc for their generous time and support. I would like to also thank NSERC for their generous support as well.

REFERENCES

BURNHAM, O.M. & SCHWYER, J. 2004. Trace

Element Analysis of Geological Samples by ICP-MS at the Geoscience Laboratories: Revised Capabilities Due to Improvements to Instrumentation. In: *Summary of Field Work and Other Activities 2004*. Ontario Geological Survey Open File Report **6145**, 54-1 to 54-20.

CARD, K.D. & CIESIELSKI, A. 1986. Subdivisions of the Superior Province of the Canadian Shield. *Geoscience Canada*, **13**, 5-13.

CUTTING D. & ANTHONY, E.G. 2005. Exploration summary and mineral resource estimate for the Angel Hill Gold Zone: West Cedartree Gold Project. Houston Lake Mining, 495 p.

TOMLINSON, K.Y. *et al.* 1998. Refinement of Hafnium (Hf) and Zirconium (Zr) analysis by improvement in the sample digestion procedure. *Ontario Geologic Survey, Miscellaneous Paper*, **169**, 189-192.

Rhenium in Canadian mineral deposits

W. David Sinclair¹, Ian R. Jonasson¹, Rod V. Kirkham², & Art E. Soregaroli³

¹Geological Survey of Canada, 601 Booth Street, Ottawa, ON, K1A 0E8 CANADA
(e-mail: sinclair@nrcan.gc.ca)

²1786 Golf Club Drive, Delta, BC, V4M 4E2 CANADA

³1376 West 26th Avenue, Vancouver, BC, V6H 2B1 CANADA

ABSTRACT: Rhenium is one of the most widely dispersed elements in the earth's crust and minerals in which rhenium is a major constituent are rare. It is similar geochemically to molybdenum and is concentrated primarily in molybdenite in granite-related deposits, particularly porphyry deposits, which are the principal industrial source of rhenium. Molybdenites from porphyry Cu and Cu-Au deposits have the highest contents of rhenium, typically ranging from 200 to 2000 ppm Re, although some (e.g., Ajax West, Mitchell) contain more than 3000 ppm Re. Molybdenites from porphyry Mo deposits generally contain much less rhenium, on the order of 100 ppm Re or less. Elevated contents of rhenium, ranging from 0.5 to 100 ppm, are also present in sediment-hosted Cu deposits, which are the second most important source of rhenium. Our data indicate that sediment-hosted Cu deposits in Canada, such as Redstone (NWT), have comparable rhenium contents and represent significant rhenium resources.

KEYWORDS: *rhenium, molybdenite, porphyry copper, sediment-hosted copper, Canada*

INTRODUCTION

Rhenium is a rare metal with total world production in 2007 estimated at about 50 tonnes. The principal industrial applications of rhenium are in high-temperature alloys used in jet engines and in platinum-rhenium catalysts used in the petroleum industry. In recent years, the demand for rhenium has increased and prices have risen to more than US\$10,000 per kg. In late 2008, rhenium was the sixth most expensive traded element (www.lipmann.co.uk/facts/expensive.html)

Rhenium abundance in most rocks is measured in parts per billion or less and minerals in which it is a major constituent are rare. It is similar geochemically to molybdenum, which it commonly accompanies through magmatic and related hydrothermal stages, and is concentrated in molybdenite associated with various types of granite-related deposits. Molybdenites with some of the highest concentrations of rhenium are associated with porphyry Cu and Cu-Au deposits, which are the primary industrial source of rhenium. Rhenium can also be concentrated by low-temperature

hydrothermal and diagenetic processes. Elevated levels of rhenium are present in sediment-hosted Cu deposits at Dzhezkazgan in Kazakhstan and in the Kupferschiefer of Poland and Germany, and these deposits are the second most important source of rhenium production. Rhenium is also recovered as a byproduct from in situ leaching of sandstone-hosted uranium deposits in Uzbekistan.

Rhenium in molybdenite has been studied by various authors (e.g., Giles & Schilling 1972; Stein *et al.* 2001; Berzina *et al.* 2005). Rhenium data in this paper are from a study of more than 150 Canadian and some foreign deposits (Jonasson *et al.* in prep.).

RHENIUM IN PORPHYRY DEPOSITS

Rhenium content of molybdenite from porphyry deposits varies widely and appears to be inversely related to the molybdenum content (Fig. 1). Molybdenites from porphyry Cu-Au deposits have the highest Re contents, typically on the order of thousands of ppm Re and ranging as high as 8170 ppm Re (Mitchell) and 4609 ppm Re (Kemess South). Re-in-

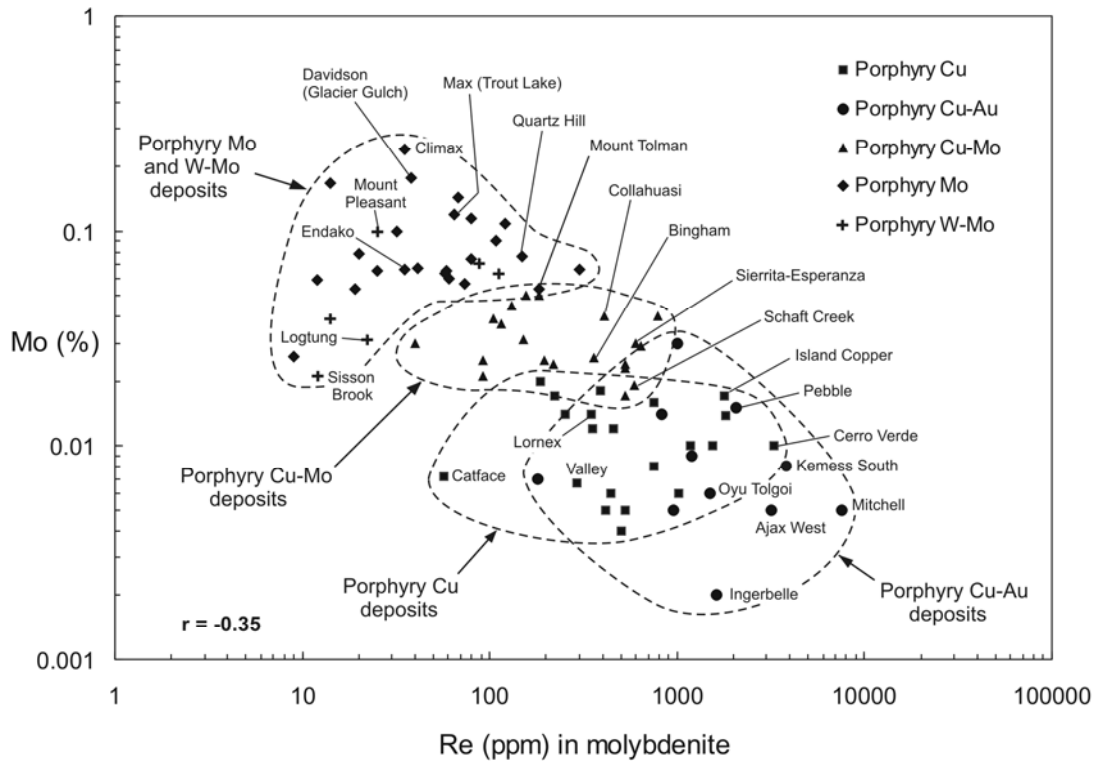


Fig. 1. Rhenium content of molybdenite versus Mo grade of Canadian and selected foreign porphyry deposits.

molybdenite contents of foreign porphyry Cu-Au deposits are also high, averaging about 1500 ppm at Oyu Tolgoi in Mongolia and as much as 2070 ppm Re in the Pebble deposit in Alaska.

Molybdenites from porphyry Cu deposits have Re contents that range from 59 ppm (Catface) to as high as 1863 ppm in the Island Copper deposit. The latter is notable for its rhenium production; during its operation from 1971 to 1994, the Island Copper mine produced about 27 t Re (Perelló *et al.* 1995). In foreign porphyry Cu deposits, the rhenium content of molybdenite is as high as 3200 ppm Re (e.g., Cerro Verde, Peru).

Re-in-molybdenite contents from Canadian porphyry Cu-Mo deposits range from 13 ppm Re (Whiting Creek) to 590 ppm Re (Schaft Creek). In foreign deposits, Re contents in molybdenites from most porphyry Cu-Mo deposits, excluding anomalous occurrences in northern Greece, are on the order of 200

to 800 ppm Re, e.g., Bingham, Utah (360 ppm Re), Sierrita-Esperanza, Arizona (600 ppm Re) and Collahuasi, Chile (410 ppm Re). Molybdenites from some porphyry-type Cu-Mo occurrences in northern Greece (Kirki, Melitena and Maronia) have exceptionally high Re contents that range from 7260 ppm to 42,100 ppm (Melfos *et al.* 2001). Such high contents of Re in molybdenite are atypical for porphyry deposits.

Rhenium contents in molybdenites from Canadian porphyry Mo and W-Mo deposits typically fall in the range of 10 to 100 ppm Re, e.g., Endako (35 ppm Re), Max-Trout Lake (65 ppm Re), Sisson Brook (12 ppm Re). Rhenium contents in molybdenites from foreign deposits are similar, e.g., Climax, Colorado (35 ppm Re), although they range as high as 149 at Quartz Hill, Alaska and 182 ppm Re at Mount Tolmin, Washington.

RHENIUM IN SEDIMENT-HOSTED COPPER DEPOSITS

Sediment-hosted copper deposits are the second most important source of rhenium after porphyry deposits. The rhenium content of deposits at Dzhezkazgan (Kazakhstan) averages 1.4 ppm Re (Hitzman *et al.* 2005), and the Lubin and Mansfeld-Sangerhausen deposits in the Kupferschiefer of Poland and Germany average 1.1 and 21 ppm Re, respectively. The mineralogy of rhenium in these deposits is not well understood, but Re appears to be concentrated in sulfide- and organic-rich sections that also carry elevated levels of Mo and PGEs. Average values of samples analyzed by us from sediment-hosted copper deposits and occurrences in Canada include 32 ppm Re in the Redstone deposit, NWT, 35 ppm at Lochaber Lake, NS and 29 ppm Re at Cape Dorchester, NB.

GRADE-TONNAGE CHARACTERISTICS OF RHENIUM-BEARING DEPOSITS

Rhenium grades of molybdenite-bearing deposits have been calculated based on the MoS₂ content of each deposit and assuming that Re is contained primarily in molybdenite. Calculated Re grades versus tonnages of Canadian and selected foreign deposits are plotted in Figure 2. Rhenium grades for porphyry deposits fall mainly in the range of 0.01 to 0.3 g/t Re, although a few deposits have higher grades ranging up to more than 0.6 g/t Re. The highest grades are in porphyry Cu deposits such as Cerro Verde (0.55 g/t Re) and porphyry Cu-Au deposits such as Mitchell (0.63 g/t Re) and Pebble (0.52 g/t Re); the lowest grades are in porphyry W-Mo deposits such as Logtung (0.01 g/t Re) and Sisson Brook (0.003 g/t Re). Rhenium grades of most porphyry Mo deposits are are.

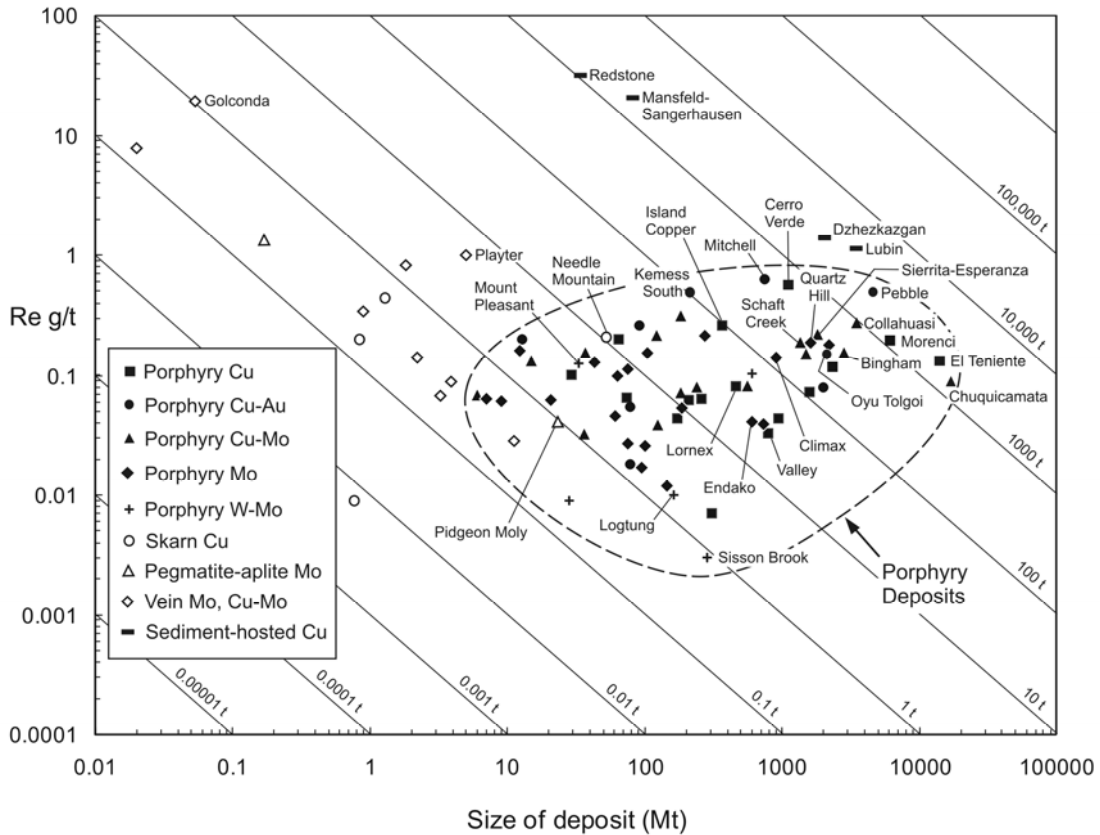


Fig. 2. Rhenium grade versus tonnage for Canadian and selected foreign deposits. Diagonal lines represent tonnes of contained rhenium.

within the range of 0.02 to 0.2 g/t Re, and are indistinguishable from Re grades of other types of porphyry deposits. This suggests that no appreciable differences exist between the overall rhenium contents of Mo-dominant porphyry deposits and Cu-dominant porphyry deposits of comparable tonnage. Variations in Re content of molybdenite in porphyry deposits are due primarily to simple mass balance phenomena; because all the Re in a deposit is taken up by molybdenite, the less molybdenite in a deposit, the higher its Re content, and vice versa.

Because of the large size of porphyry deposits, their total Re contents can be considerable, e.g., Pebble contains as much as 4000 t Re. Only large sediment-hosted Cu deposits such as in the Kupferschiefer and at Dzhezkazgan contain larger resources of rhenium.

Lesser but in some cases significant amounts of rhenium are present in other types of deposits such as skarn deposits (e.g., Needle Mountain-Gaspé Copper), pegmatite-aplite deposits (e.g., Pidgeon Moly) and vein deposits (e.g., Playter, Golconda).

CONCLUSION

Although porphyry Cu and Cu-Au deposits are likely the most important potential source of rhenium in Canada, other types of deposits including sediment-hosted Cu deposits and some vein deposits also represent potential sources.

ACKNOWLEDGEMENTS

Numerous colleagues assisted with sample collection and analysis. Bob Anderson contributed funds for sample

analysis through the GSC's Targeted Geoscience Initiative (TGI-3). Holly Stein (AIRIE) provided unpublished data on the Oyu Tolgoi deposit.

REFERENCES

- BERZINA, A.N., SOTNIKOV, V.I., ECONOMOU-ELIOPOULOS, M. & ELIOPOULOS, D.G. 2005. Distribution of rhenium in molybdenite from porphyry Cu-Mo and Mo-Cu deposits of Russia (Siberia) and Mongolia. *Ore Geology Reviews*, **26**, 91-113.
- GILES, D.L. & SCHILLING, J.H. 1972. Variation in rhenium content of molybdenite. *Report of the 24th Session, International Geological Congress*, **24**, (10), 145-152.
- HITZMAN, M., KIRKHAM, R., BROUGHTON, D., THORSON, J., & SELLEY, D. 2005. The sediment-hosted stratiform copper ore system. *Economic Geology 100th Anniversary Volume*, 609-642.
- JONASSON, I.R., SINCLAIR, W.D., KIRKHAM, R.V., & SOREGAROLI, A.E. (in prep.). Rhenium in Canadian mineral deposits. *Geological Survey of Canada*, Open File.
- MELFOS, V., VOUDOURIS, P., ARIKAS, K., & VAVELIDIS, M. 2001. Rhenium-rich molybdenites in Thracian porphyry Cu±Mo occurrences, NE Greece: *Bulletin of the Geological Society of Greece*, **34**, 1015-1022 (in Greek with English abstract).
- PERELLÓ, J.A., FLEMING, J.A., O'KANE, K.P., BURT, P.D., CLARKE, G.A., HIMES, M.D., & REEVES, A.T. 1995. Porphyry copper-gold-molybdenum deposits in the Island Copper cluster, northern Vancouver Island, British Columbia. In: SCHROETER, T.G. (ed.), *Porphyry Deposits of the Northwestern Cordillera of North America*. Canadian Institute of Mining, Metallurgy and Petroleum, Special Volume **46**, 214-238.
- STEIN, H.J., MARKEY, R.J., MORGAN, J.W., HANNAH, J.L., & SCHERSTEN, A. 2001. The remarkable Re-Os chronometer in molybdenite: how and why it works. *Terra Nova*, **13**(6), 479-486.

Getting the scale right: links between metallogenesis, planetary degassing and the redox state of Earth's oceans?

John L. Walshe¹

¹CSIRO Exploration and Mining, PO Box 1130, Bentley, WA 6102 AUSTRALIA (e-mail: john.walshe@csiro.au)

ABSTRACT: The mineral systems that created the major mineral deposits and provinces of Earth were thermo-chemical engines with roots deep in the mantle if not to the core. Anhydrous fluids, both strongly oxidizing and strongly reducing, are intrinsic, originate in the deep-Earth, and may be linked to Earth degassing. The chemical evolution of mineral systems within the crust reflects interactions of deep-Earth anhydrous fluids with the Earth's hydrous outer layers. These interactions generated the chemical gradients required to promote/sustain metal transport and/or deposition within the crust. To appreciate the size of these systems it is necessary to integrate information across a wide range of scales within mineral provinces and consider links with other Earth phenomena, particularly redox related phenomena of the Earth's mantle, crust, hydrosphere and atmosphere. Potential links between gold mineralization at ~ 2.7 to 2.63 Ga and the evolution of the hydrosphere are explored.

KEYWORDS: *mineral systems, mantle fluids, chemical gradients*

INTRODUCTION

Metal deposits within the Earth are rare and accumulations of high grade, large tonnage deposits are much more so. In contrast, models of formation of metal deposits are based on relatively common processes that operate within the middle to upper crust, hydro- and bio-sphere; metamorphism, basin dewatering, devolatilization of magmas, sea floor metamorphism, and meteoric fluid circulation. So why are metal deposits rare? Here it is argued that metal deposits and provinces are a product of thermo-chemical systems that have their roots in the deep mantle if not the core. Production of metal deposits and provinces through Earth history reflects the constraints of deep-Earth degassing, the trans-crustal and mantle architecture that controlled fluid release, the nature of the crustal interactions and tectonic controls on fluid focusing mechanisms in the mid to upper crust. Planetary degassing links mineral systems to many other Earth redox - related phenomena of the mantle, crust, hydrosphere and atmosphere. Understanding the crust - mantle links is the key to developing mineral systems models that are independent of commodity or traditional classification

schemes and provide robust explanations of the spatial and temporal distribution of deposits and provinces.

WHY METALLOGENIC PROVINCES AND EPOCHS?

The extant models provide little guide to understanding why some arcs of the circum Pacific are well endowed with Cu and Au deposits and others are not or why some Proterozoic basins of the Australian Craton are well endowed with base metal deposits but most are not. Why are quartz veins in Paleozoic slate belts mostly barren but a few richly endowed with gold? Existing models provide little guide as to why the porphyry Cu deposits of Chile formed in a few short pulses of a few million years despite the existence of an active convergent margin over 100s of millions of years.

Does the rarity of major metal accumulations in both space and time reflect the low probability of certain combinations of common processes of the crust including processes of preservation /denudation of the crust? Is it possible that we yet to understand some key elements of mineral systems that operate at length scales and time scales yet to be

appreciated?

**THE ROOTS OF MINERAL SYSTEMS:
HOW DEEP?**

The commonly observed spatial association of mineral deposits and provinces with old cratonic margins, cross-arc structures or tears in slabs and association of metallogenesis with times of plate re-orientation, slab-rollback and slab-faulting are important architectural and dynamic factors that suggest at least some fluids in mineral systems may originate at depths much greater than 10s of kilometres commonly assumed.

Au provinces are associated with crustal-penetrating structures, commonly traceable for 1000s kilometres across the Earth's surface. In the Eastern Yilgarn, Western Australia tomographic studies have identified "architecture" at depths >100 km that may have provided pathways for deep-Earth fluids. Given that aspect ratios (length to depth) of systems can be expected to be of the order of 1:1 then the depth of mineral systems could conceivably be 100s to 1000s of kilometres (Fig. 1). The distance from the surface of the Earth to the core is approximately 3000 km making it conceivable that some components in mineral systems originate in the lower mantle, if not the core of the Earth. Mantle tomography studies (e.g., van der Hilst & K arason 1999) have identified structures in the lower mantle that may provide pathways for fluids to migrate from the lower mantle/core to the Earth's outer layers.

CHARACTERISTICS OF DEEP - EARTH ANHYDROUS FLUIDS: LEARNINGS FROM ARCHEAN AU DEPOSITS

Studies of ~2.65 Ga gold systems in the Yilgarn Craton, Western Australia, have emphasised the interaction of intrinsically reduced ($\text{CH}_4 \pm \text{H}_2 \pm \text{N}_2 \pm \text{HCl}$) and oxidized ($\text{CO}_2 \pm \text{SO}_2$) anhydrous fluids as well as hydrous fluids in deposit formation. Carbonate veins have $\delta^{13}\text{C}$ between -4 and -6 ‰, typical of mantle values and primary sulfate have $\delta^{34}\text{S}$ of ~ 8 to 12 ‰,

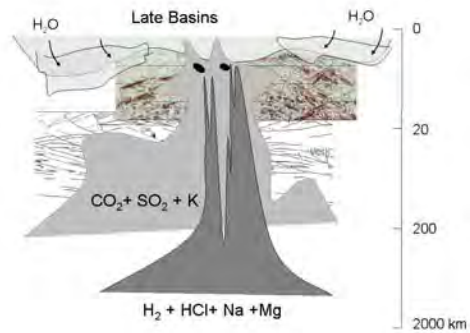


Fig. 1. Anhydrous fluids, oxidized and reduced, are intrinsic to mineral systems, originating in the deep-Earth.

consistent with precipitation from mantle/magmatic $\text{SO}_2 - \text{CO}_2$ fluids with mantle S ($\delta^{34}\text{S} \text{ SO}_{2(\text{g})} \sim 0 \text{ ‰}$). The noble gas signature of CO_2 - rich fluids confirms the involvement of magmatic fluids that contained a mantle component ($^{40}\text{Ar}/^{36}\text{Ar} \leq 21000$ and $^{20}\text{Ne}/^{22}\text{Ne}$ of 7- 11). In contrast CH_4 - dominated fluid inclusions have much lower ^{36}Ar concentrations (sub-ppb) and exceptional noble gas signatures ($^{40}\text{Ar}/^{36}\text{Ar}$ of $\leq 50,000$; $^{20}\text{Ne}/^{22}\text{Ne} = 8.5 - 10$ and $^{21}\text{Ne}/^{22}\text{Ne}$ of ≤ 0.55), that indicate a deep-Earth abiogenic origin (Walshe & Kendrick 2009).

The ultimate source of $\text{CO}_2 \pm \text{SO}_2$ fluids was probably the sub-continental lithosphere as evidenced by the SO_2 discharge during island arc volcanism. The occurrence of oxidized fluids in late Archean gold deposits similar in character to oxidized fluids in magmatic - hydrothermal deposits of the circum-Pacific is consistent with argument that the upper mantle has been oxidized through much of Earth history. Possible sources of reduced fluids include serpentinisation reactions in the deep crust or mantle wedge. Thermodynamic studies, and inclusion mineralogy of diamondiferous kimberlites and lamproites suggest hydric fluids could dominate in the Earth at depths greater than 300 - 400 km. The Earth's core may well be the dominant reservoir of hydrogen (Williams & Hemley 2001). A core-mantle involvement in metallo-genesis, possibly linked to mantle overturn and plumes of

hydric fluids from the D^{II}- layer, provides an attractive explanation for the large-scale temporal pattern of metallogenic epochs.

THE ROLE OF MANTLE VOLATILES IN METALLOGENESIS

Metal transport and deposition capacities of mineral systems are closely linked to propagation of redox and related physico-chemical gradients (pH, aH₂, aHCl, aH₂S, aSO₂, aCO₂, aCH₄, aH₂O, etc) within mineral systems. For metals transported in solution, the rate of mineralization is a product of 3 factors (see Fig. 2);

1. Fluid(s) velocity
2. Changes in metal solubility with respect to physico-chemical parameters controlling solubility: P, T, redox, etc
3. Gradients in physico-chemical parameters (change with respect to distance)

Redox gradients in Au systems of the Yilgarn Craton, Western Australia have been mapped across gold lodes and at camp to district scales using C and S isotopes combined with alteration studies. These gradients can be related to the interplay of oxidized and reduced anhydrous fluids sourced from the mantle or lower crust (Fig. 1), as defined by stable and radiogenic isotopes, with aqueous fluids of crustal origin. Chemically contrasting fluids, particular fluids of contrasting redox state appear intrinsic to productive mineral systems.

LINKS BETWEEN EARTH DEGASSING, GOLD AND THE REDOX STATE OF LATE ARCHEAN OCEANS

One implication of Earth – degassing models of metallogenesis is that there should be links between the formation of the Earth’s resources, secular changes in architecture and geochemistry of the planet over some 4.5 billion years of evolution and phenomena such as mass extinction events, global anoxia, and atmospheric evolution.

The variation of δ¹³C, Δ³³S in sedimentary sulfides and phenomena

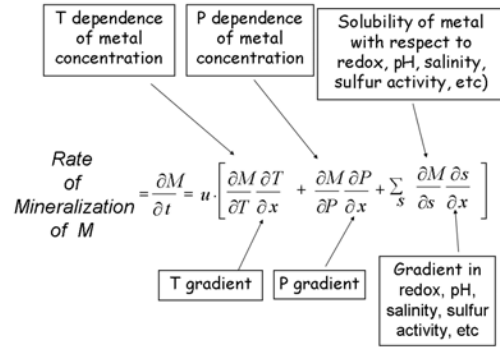


Fig. 2. Mathematical description of mineralization (after Phillips 1990).

such as banded iron formation are sensitive indicators of redox variations in the Earth’s hydrosphere and atmosphere and may be used to map the impact of deep-Earth degassing on Earth’s outer layers. From Figure 3 the levels of CH₄ ± H₂ and CO₂ ± SO₂ fluctuated in the hydrosphere/atmosphere prior to ~ 2.7 with H₂ dominating post ~ 2.5 Ga. Formation of Late Archean Au deposits, at ~ 2.7 to 2.63 Ga, can be interpreted as one manifestation of planetary degassing of highly reduced volatiles that impacted on the hydrosphere and atmosphere from ~ 2.7 to ~ 2.5 Ga as evidenced by a decline in BIF deposition after ~ 2.7 Ga and an excursion in Δ³³S. Peaks in deposition of BIFs prior to ~ 2.7 Ga could be taken as times of higher ratio of SO₂ - CO₂ / CH₄ - H₂ in the volatile flux. Increasing δ³⁴S of seawater in the Late Archean from near zero to ~ +10 ‰ at 2.5 Ga could reflect hydrothermal recycling of SO₂ from mantle de-volatilization fixed in the crust as sulphate.

The rate of H₂ escape from the upper atmosphere and thus oxygenation from decomposition of H₂O vapour is directly dependent on the density of H₂ at the critical level of escape. It may be that the Great Oxidation Event from ~ 2.4 Ga to ~ 2.0 Ga reflects elevated H₂ in the hydrosphere / atmosphere during much of this period.

CONCLUSIONS

Major mineral deposits and provinces may

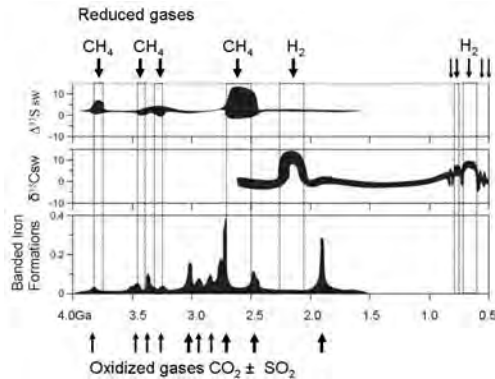


Fig. 3. Indicators of redox variations in the Earth's hydrosphere and atmosphere. Dominance of $\text{CH}_4 \pm \text{H}_2$ defined from $\Delta^{33}\text{S}$ anomalies, H_2 from $\delta^{13}\text{C}$ anomalies and $\text{CO}_2 \pm \text{SO}_2$ from banded iron formations. Data from Canfield (2005), Holland (2005), & Melezhik *et al.* (2005).

be considered one manifestation of planetary degassing and products of thermo-chemical engines with roots in the deep mantle. Studies of Yilgarn gold deposits, Western Australia, are providing insights into the nature of deep-Earth fluids and possible links to the evolution of the Late Archean hydrosphere and atmosphere.

ACKNOWLEDGEMENTS

The study of Archean gold deposits was financially supported by the Predictive Mineral Discovery Cooperative Research Centre (pmd^{*}CRC) and MERIWA (Mineral and Energy Research Institute of Western Australia), Projects 358 and 377. The

support of SIGMC (Gold Fields) is acknowledged and the contributions of Peter Neumayr, Klaus Petersen and Tony Roache. Many friends and colleagues have contributed to the broader conversation re Earth degassing and mineral systems.

REFERENCES

- CANFIELD, D.E. 2005. The early history of atmospheric oxygen: Homage to Robert M. Garrels. *Annual Reviews Earth Planetary Science*, **33**, 1-36.
- HOLLAND, H.D. 2005. Sedimentary mineral deposits and the evolution of Earth's near-surface environments. *Economic Geology*, **100**, 1489-1509.
- MELEZHNIK, V.A., FALICK, A.E., HANSKI, E.J., KUMP, L.R., LEPLAND, A., PRAVE, A.R., & STRAUSS, H. 2005. Emergence of the aerobic biosphere during the Archean-Paleoproterozoic transition: Challenges of future research. *GSA Today*, **15**, 4-11.
- PHILLIPS, O.M. 1990. Flow controlled reactions in rock fabrics. *Journal of Fluid Mechanics*, **212**, 263-278.
- VAN DER HILST, R.D. & KÁRASON, H. 1999. Compositional heterogeneity in the bottom 1000 kilometers of Earth's mantle: Toward a hybrid convection model. *Science*, **283**, 1885-1888.
- WALSHE, J.L. & KENDRICK, M.A. 2009. Links between planetary degassing, gold and the redox state of Late Archean Oceans? 19th V.M. Goldschmidt Conference - Challenges to Our Volatile Planet, 2009.
- WILLIAMS, Q. & HEMLEY, R.J. 2001. Hydrogen in the deep Earth. *Annual Reviews Earth Planetary Science*, **29**, 365-418.

⁴⁰Ar-³⁹Ar geochronological constraints of the ore-bearing ductile shear zones at Hukeng tungsten deposit, Jiangxi Province

Zhang Wei¹, Chen Maohong^{1,2}, Ye Huishou², & Yang Zongxi¹

¹China University of Geosciences, Beijing, 100083 CHINA (email: zhangwei-china@live.cn)

²Institute of Mineral Resources, Chinese Academy of Geological Science, Beijing, 100037 CHINA

ABSTRACT: The Hukeng tungsten deposit is a large-scale quartz vein-type tungsten deposit, which is located at Wugong Mountain, west Jiangxi Province. Massive structure and banded structures occur widely in the ore-bearing quartz veins. Detailed field work and petrographic research reveal that these banded quartz veins are actually ductile shear zones, with quartzitic mylonite reflecting plastic deformation microstructures. ⁴⁰Ar/³⁹Ar dating of neoform sericite folia from mylonite in the EW- and NW-trending shear zones yield a plateau age of 144.1±1.5 Ma and 140.3±1.0 Ma, respectively and yield an isochron age of 144.6±3.6 Ma and 139.6±2.4 Ma, respectively. The Ar-Ar dating reveals that ductile shear deformation occurred after vein petrogenesis. The banded quartz veins were formed by the ductile shear of massive quartz veins. The formation mechanism of the ductile shear may be related to sidelong intrusion of the later magmatic emplacement.

KEYWORDS: Quartzs-veins-type tungsten deposit; banded structure; ductile shear zone; ⁴⁰Ar-³⁹Ar dating; Hukeng, Jiangxi

INTRODUCTION

The Hukeng tungsten deposit is a large-scale quartz vein-type tungsten deposit, which was discovered in 1950. At that time it was considered a small-scale deposit according to the proven reserves. After 50 years of mining and exploration, it is now recognized as a large-scale tungsten deposit. It didn't attract many researchers' attention, so there has been minimal research on it (Liu *et al.* 2004). In order to offer some useful information to direct exploration at depth and outside part of the ore deposit, we examined the mechanisms of formation of the ductily sheared quartz veins in terms of geological characters and chronology.

Regional Geology

The Hukeng Tungsten deposit is located at Wugong Mountain, which is situated along the central part of the north margin of the South China Caledonian fold belt (Tang *et al.* 1991). The Wugong Mountain area experienced multiple stages of magmatism and tectonic activity, therefore it possesses a unique rock association with a complicated structure style.

A great deal of research indicates that

the Wugong Mountain area is a typical Mesozoic metamorphic core complex (Lou *et al.* 2002), which consists of three-layers model: the baseottom is metamorphism-magma nuclear and ductile shear detachment zone; the middle part is shear fold zone; the top part is an unmetamorphic cover sequence.. Studies about its formation mechanism indicated that plate collision caused granite remelting, strong magmatic diapirism resulted in crustal uplift and formation of an extensional gliding nappe (Liu *et al.* 2003).

Local Geology

The research area consists of mica schist, mica-quartz schist, phyllitic quartz schist, gneiss, and granulite, which belong to Sinian Laohutang and Likeng formations. The overall sequence is inclined to S-SE with dips of 25° to 40°. In the main mining area, strata occur parallel to the contact between strata and intrusion, such that the interface formed a good geochemical barrier; this lead to the ore-bearing fluid enrichment and participation in the original joints (ore-hosting structure).

The ore-bearing rock body is the

Hukeng granite stock, which was the product of third stage Yanshanian intrusions that were invasion of early Yanshanian epoch covered by the Laohutang Formation rock. This muscovite granite's outcrop area is 14 km² and the stock's shape is irregular in space. The lithology of rock mass is muscovite granite. WO₃ in rock mass ranges from with a content of 160 to 1100 ppm, with $\times 10^{-6}$ and the average of level is $563 \text{ ppm} \times 10^{-6}$, which is 75 times the compared with average WO₃ content of granite from the Yanshanian Period. Thus we believe that this specialized granite is the source of the ore-bearing fluid.

The Hukeng granite stock was predominated by S-type granites which was enriched in SiO₂ and K, ascribed to K-high calc-alkaline series. The trace elements and REE analysis show that the intrusion has undergone full evolutionary differentiation. The fluids were participated in the forming process of the Hukeng granite intrusion, and the siliceous melts severely interacted with fluids enrich in volatile, which can provide conditions for the migration and enrichment of the ore-forming elements (Liu *et al.* 2008).

A fine-grained muscovite granite dyke with EW strike direction intruded into the Hukeng granite stock. It is gray with a fine-grained texture and massive structure. Constituent minerals consist of quartz, potassium feldspar, plagioclase, and muscovite. Accessory minerals contain garnet, fluorite, pyrite etc. Alteration in the fine-grained muscovite granite include greisenization and silicification.

Main faults in the area include the NE striking Hukeng-Zhangzhuang fault, the Xijialong-Yashan fault and the NW-trending Hukeng-Xijialong fault (Fig.1). The Hukeng tungsten deposit doesn't have the typical five layers model which is common in other tungsten deposit in south Jiangxi Province. The width of the single ore-bearing quartz veins is about dozens of centimetres and the average grade of WO₃ is lower than 1%. Constituent minerals in the quartz veins consist of wolframite, scheelite, pyrite. Accessory minerals contain sphalerite, copper pyrites,

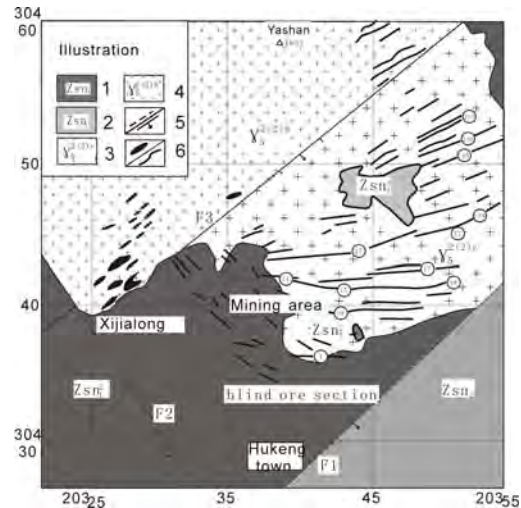


Fig. 1. General geological map of the Hukeng tungsten deposit, South China. 1-Schist, gneiss, and migmatite of Sinian Laohutang Formation; 2-Schist and gneiss of the Sinian Likeng Formation; 3-Third-stage Early Yanshanian muscovite granite; 4-Second-stage Early Yanshanian muscovite granite; 5-inferred large fault(s); 6- network and large vein structure of tungsten quartz veins.

molybdenite.

⁴⁰Ar-³⁹Ar age dating

Field and laboratory work suggests that banded quartz veins are actually the results of ductile shear movement and accordingly, the banded ores are quartzitic mylonite. The banded quartz veins have the typical character of mylonite, minerals' grain diameter become smaller (from normal 1-5cm to 20-30 μ m), i.e., grain-size reduction. Transposition foliations and lineations were generated during deformation. Heterogeneous ductile shearing of the granite occurred next to quartz veins. In order to confine the age of the ductile shear activity, sericite generated by the shearing were sampled. Results of our analysis appear below (Figs.2, 3). The sericite was generated by the ductile shear activity, so they don't contain any radiogenic Ar from the granite or hydrothermal muscovite, which were formed during earlier mineralizing episode. The age of sericite (140.3-144.1 Ma) indicates the blocking temperature age of shear deformation. The age difference between the two samples may

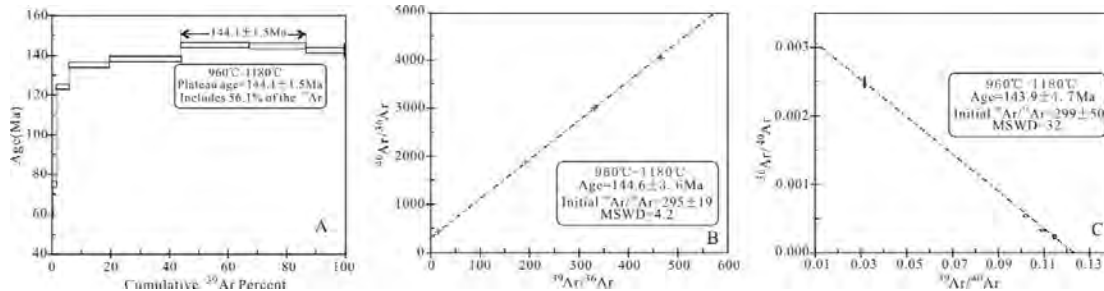


Fig. 2. The step heating Ar-Ar plateau age (A), isochron age (B), and inverse isochron age (C) for sericite folia from mylonite of the EW-trending ductile shear zone.

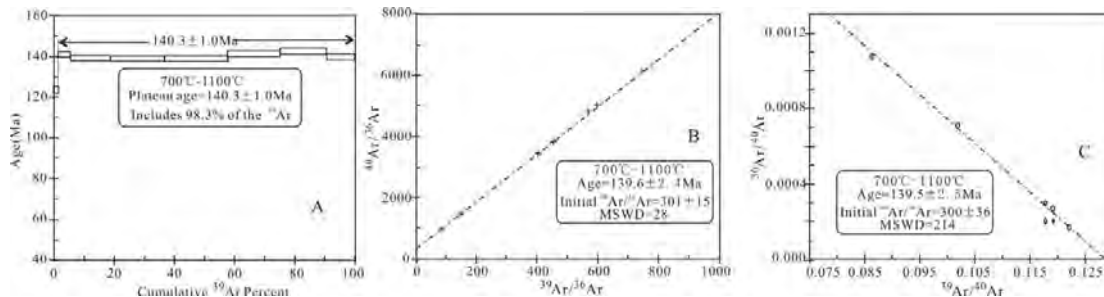


Fig. 3. The step heating Ar-Ar plateau age (A), isochron age (B), and inverse isochron age (C) for sericite folia from mylonite of NW-trending ductile shear zone.

only reflect the error difference, but also relate to the character of inhomogenous cooling in shear zone.

DISCUSSION

Time sequence between diagenesis, mineralisation and ductile shear activity. According to our field observations, the ductile shear zone is mainly developed in the ore-bearing quartz veins and seldom appear in the granite. This phenomenon indicates that the quartz veins, also the original joints, are the zone of relative weakness. The degree of shear deformation intensifies from the quartz veins' centre to both margins. In additionally ore minerals in the quartz veins are disaggregated and locally elongated in the stretching direction. All the macroscopic vein formation and growth features reveal that mineralisation happened before ductile shear activity.

The age of sericite ($^{40}\text{Ar}/^{39}\text{Ar}$, 140-144 Ma) also illustrates that the ductile shear activity was later than ore genesis (Zircon SHRIMP U-Pb, 152 Ma) (Liu *et al.* 2008) and mineralisation (Re-Os, 147-150 Ma) (Liu *et al.* 2008). It offers indirect and

complementary information to infer the later age of ductile shearing.

Mechanism of Ductile Shear Movement

The formation of the ductile shear is probably related to the extensional deformation of Wugong mountain metamorphic core complex. Wu *et al.* (2001) found that the Hukeng super-unit rock intrude along the south part of the shear detachment zone of the Wugong mountain metamorphic core complex. It indicates that the magmatic emplacement happened after the detachment movement. Liu *et al.* (2008) obtained the zircon SHRIMP U-Pb age from the medium- to coarse-grained muscovite granite, which belongs to the Hukeng super-unit rock. It is about 151.1 Ma, which means that extensional detachment preceded emplacement. So the later vein-parallel ductile shearing is unrelated to the earlier episode of extensional deformation.

Comparing the kinematic characteristics of the ductile shear zone and main fault zone in the mining area, there is a genetic relationship. Field mapping reveals that there was another intrusive episode after the ore-bearing granite was emplaced. It

may account for the ductile deformation. In addition, the direction of magmatic emplacement can be resolved mathematically into two components. This is a perfect kinematic model that explains the orientations of ore-bearing quartz veins in different directions (NW, EW) with both having left-lateral shear sense. Therefore, the ductile shear movement was likely the result of later magma emplacement.

Evolutionary Series of Metallogenic Structure

Based on the geological character, kinematic model, and formation age of ductily sheared, ore-bearing quartz veins, we can establish the petrogenetic evolutionary of the metallogenic structure: emplacement of medium- to coarse-grained muscovite granite (152 Ma) massive quartz veins formed along original joints (main mineralization period, 147 to 150 Ma) fine- to coarse-grained felsic dyke emplacement. Massive quartz veins suffered from ductile shearing resulting in heterogeneously deformed, banded quartz veins (140 to 144 Ma) second period of massive quartz precipitated in brecciated fault zone overprinting the former banded quartz veins with brittle fragments of the quartz veins.

ACKNOWLEDGEMENTS

The project is sponsored by the National

Major Fundamental Research Program of China (Grant No.2007CB411407; No.2007CB411405). Thanks are due to Tong Fusheng, Liu Zhiping and Qin Jianyun for providing supports in the field. I thank David Lentz for constructive comments and suggestions.

REFERENCES

- LIU, J. *et al.* 2008. Re-Os dating of molybdenite from the Hukeng tungsten deposit in Wugongshan area, Jiangxi Province, and its geological implications[J]. *Acta Geologica Sinica*, **82**(11), 1576-1583.
- LIU, J. *et al.* 2008. Zircon LA-ICPMS U-Pb dating of Hukeng granite in Wugongshan area, Jiangxi Province and its geochemical characteristics[J]. *Acta Petrologica Sinica*, **24**(8), 1813-1822.
- LIU, X. 2003. Discussion of the structure problem in Wugongshan Region in Western Jiangxi province[J]. *Journal of East China Geological Institute*, **26**(3), 249-253.
- LIU, ZH.P. 2004. The occurrence law of the big vein belt and deep exploring direction in Hukeng Tungsten mine[J]. *China Tungsten Industry*, **19**(6), 30-33.
- LOU, F. SH. *et al.* 2002. The Mesozoic Wugongshan granitic domal extensional tectonics and petro-geochemistry[J]. *Geological Bulletin of China*, **21**(4/5), 264-269.
- TANG, J.F. *et al.* 1991. *Tectonic deformation and geological survey of Wugongshan metamorphic terrane*[M]. Wuhang: China University of Geosciences Press, 1-24.
- WU, F.J. *et al.* 2001. Basic features and age of the extensional gliding nappe structure of Wugongshan magmatic thermal dome in Jiangxi[J]. *Jiangxi Geology*, **15**(3), 161-165.



Sponsors



Symposium bags sponsor



Platinum sponsors



**ANGLO
AMERICAN**

Gold sponsors



Silver sponsors



Bronze sponsors

